

VALOR DUNE Joint Oscillation and Systematics Constraint Fit

(Version 2016a v2)

Costas Andreopoulos^{1,2}, Andy Chappell³, Christopher Barry¹, Francis Bench¹, Thomas Dealtry⁴, Steve Dennis¹, Lorena Escudero Sánchez⁵, Rhiannon Jones¹, Nick Grant³, Marco Roda¹, Davide Sgalaberna⁶, and Raj Shah^{2,7}

¹University of Liverpool, Physics Department, Liverpool, L69 7ZE, UK

²STFC Rutherford Appleton Laboratory, Harwell Oxford Campus, OX11 0QX, UK

³University of Warwick, Physics Department, Coventry, CV4 7AL, UK

⁴Lancaster University, Physics Department, Lancaster, LA1 4YB, UK

⁵University of Cambridge, Cavendish Laboratory, Cambridge CB3 0HE, UK

⁶University of Geneva, Departement de physique nucleaire et corpusculaire, 1211 Geneve, Switzerland

⁷University of Oxford, Subdepartment of Particle Physics, Oxford, OX1 3RH, UK

(The VALOR group)

June 15, 2016

Abstract

An end-to-end simulation, reconstruction and analysis chain for DUNE is under development. The chain is being incrementally improved and tested in a series of end-to-end "pass-throughs" with an increasing physics content. A short-term objective of this effort is to develop a chain of sufficient sophistication for a physics-driven evaluation and optimization of proposed DUNE Near Detector designs. A Near Detector Task Force has been charged with delivering a report early in 2017.

VALOR¹ is an established neutrino fitting group which led several T2K oscillation analyses and contributed to most published T2K oscillation papers. The existence of a powerful, flexible, well-validated, and optimised analysis and software framework, enabled the VALOR group to adapt its advanced analysis procedures on several other experiments. Results from the VALOR analysis is a major deliverable of the DUNE Near Detector Evaluation WG towards the Task Force's goal of producing a complete and sophisticated DUNE analysis by the end of 2016.

The VALOR group is providing a DUNE oscillation analysis through a simultaneous fit to O(50) Near and Far detector samples. In this preliminary VALOR DUNE technical note we present a general description of the analysis and its present status, and we report the results of the 2016a VALOR DUNE analysis used for the 2nd Near Detector Task Force pass-through. The 2016a version is an intermediate step towards the implementation of the full DUNE fit, and it provides a systematics constraint, via the joint fit of O(150) neutrino flux and neutrino interaction parameters to O(20) Near Detector event samples. Preliminary results were obtained using simulated and reconstructed samples from all 3 proposed Near Detector designs. Details of the 2016a analysis, as well as preliminary validation and physics sensitivity results are presented. The 2016a analysis already includes a realistic flux error model (taken from MINERvA/NuMI) and a newly-produced neutrino interaction error model developed by the VALOR group and discussed in detail in this note. A work-plan towards the 2016b VALOR DUNE analysis (for the 3rd pass-through) is also presented.

¹<https://valor.pp.rl.ac.uk>

Contents

1	Introduction	3
2	General description of the VALOR DUNE Oscillation and Systematics Constraint Fit	5
2.1	Overview of the VALOR analysis for a <i>single</i> LBL neutrino experiment	5
2.2	Fit spectra predictions	5
2.3	Toy experiment generation	6
2.4	Applying neutrino oscillations	7
2.4.1	3-flavour neutrino oscillation probabilities	7
2.4.2	Inputs to the 3-flavour neutrino oscillation probability calculations	9
2.4.3	Validation of the 3-flavour oscillation probabilities	10
2.4.4	Accuracy of the 3-flavour oscillation probabilities	11
2.4.5	Beyond the standard 3-flavour framework	12
2.5	Parameter estimation	13
2.5.1	Construction of likelihood	13
2.5.2	Parameter elimination through profiling or marginalization	14
2.5.3	Calculation of best-fit spectra with marginalized nuisance parameters	15
2.5.4	Construction of confidence intervals	16
3	Specifics of the 2016a VALOR DUNE analysis	17
3.1	Choice of fit samples	17
3.2	Choice of kinematical distributions, and of kinematical variable binning / modes	17
3.3	Nominal predictions	18
3.4	Systematic uncertainties	25
3.4.1	Flux uncertainties (MINERvA/NuMI flux error assignments)	25
3.4.2	Neutrino interaction uncertainties (2016a VALOR/GENIE error assignments)	25
3.4.3	Detector acceptance uncertainties (tentative)	32
3.4.4	Synopsis of systematic parameters and assigned uncertainties	34
3.5	Effect of systematic uncertainties on event spectra	38
3.6	Fit parameters and parameter ranges	43
4	Improvements/changes planned for 2016b VALOR DUNE analysis	45
4.1	Implementation of joint 3-flavour oscillation fit with marginalization of O(400) systematics	45
4.2	Addition of 26 Near Detector samples	45
4.3	Enabling option for multiple Near Detector samples for a given observed final state	47
4.4	Addition of 4 high-resolution and 4 low-resolution Far Detector samples	47
4.5	Improved neutrino interaction errors (2016b VALOR/GENIE error assignments)	47
4.6	Realistic detector acceptance and leptonic/hadronic energy scale errors	47
5	2016a systematics constraint fit results	48
5.1	Example fits to systematically-varied datasets	48
5.2	Pull studies	49
5.3	Fits to Asimov datasets for all 3 DUNE Near Detector options	49
6	Summary	51
Appendix A	2016a VALOR/GENIE error model: Supporting GENIE / data comparisons	64
Appendix B	Applying VALOR systematics to MC templates: Full specification	167

1 Introduction

An end-to-end simulation, reconstruction and analysis chain for DUNE is being developed. The chain is being incrementally improved and tested in a series of end-to-end "pass-throughs" with an increasing physics content. A short-term objective of this effort is to develop a chain of sufficient sophistication for a physics-driven evaluation and optimization of proposed DUNE Near Detector designs. A Near Detector Task Force has been charged with delivering a report early in 2017.

VALOR [1] is an established neutrino fitting group which led several T2K oscillation analyses [2] [3] [4] [5] [6] [7] [8] [9] [10] [11] [12] and contributed to most published T2K oscillation papers. The existence of a powerful, flexible, well-validated, and optimised analysis and software framework, enabled the VALOR group to setup advanced analysis procedures for several other experiments. Today the group also plays an important role in physics sensitivity and design optimisation studies for the DUNE and HyperK experiments. The group is increasingly active in preparations for the physics exploitation of the Fermilab SBN programme, and in the development of global multi-experiment neutrino oscillation fits with proper treatment of correlated systematic uncertainties.

Results from the VALOR analysis with all 3 proposed DUNE Near Detector designs (Fine Grained Tracker, High pressure Gas Argon TPC, Liquid Argon TPC), or hybrids, is a major deliverable of the DUNE Near Detector Evaluation WG towards the Task Force's goal of producing a complete and sophisticated DUNE analysis by the end of 2016.

VALOR provides a sensitive DUNE oscillation analysis and oscillation sensitivity simulation. This joint oscillation and systematics constraint fit is currently being validated in preparation of the 2016b version of the VALOR DUNE analysis to be used in the next (3rd) Near Detector Task Force pass-through. The 2016b VALOR DUNE analysis is a simultaneous fit of oscillation and O(400) systematic parameters to O(50) Near and Far Detector samples described in Secs. 4.2 and 4.4. A powerful and flexible software framework developed to position VALOR for global multi-experiment fits, and tested in a long series of T2K oscillation analyses, allows such complex fits to be setup with relative ease, and to be run reliably and efficiently. VALOR constructs its nominal predictions using Monte Carlo (MC) templates, as explained in Sec. 2.2. The observable distributions included in the fit for each sample are flexibly defined, and all desired intra-sample and inter-sample systematic parameter correlations are taken into account.

Analyses are typically performed in a full 3-flavour framework including matter effects in constant density matter, but options exist to perform analyses in frameworks with additional sterile neutrinos (3+1, 3+2, 1+3+1 models) and to include Non-Standard Interaction effects. Details are presented in Sec. 2.4.

A binned likelihood-ratio method is typically used by VALOR. Several options exist for eliminating the nuisance parameters. Profile likelihood was, historically, the main method used by the VALOR group. However, the main method adopted by the VALOR group in its recent T2K oscillation analyses is a hybrid Bayesian-frequentist method: The parameters of interest are maximized with respect to the likelihood distribution, but the nuisance parameters are marginalised. The marginalization procedure yields the so-called marginal likelihood that depends only on the parameters of interest. A description of the statistical treatment used by VALOR is presented in Sec. 2.5.

The 2016a version of the VALOR DUNE analysis is an intermediate point in the development of the full fit. The 2016a analysis provides a first implementation of a DUNE Near Detector systematics constraint, and a Near to Far extrapolation method, and underpins the development of the joint fit. 156 systematic parameters (104 neutrino flux parameters, 43 neutrino interaction parameters, and 9 detector parameters - see Sec. 3.4) are constrained through a fit to 18 Near Detector samples, while the best-fit values of the neutrino flux and interaction parameters provide a Near to Far extrapolation. These systematic parameters are applied as specified in the Appendix B. The effect of prior uncertainties on the reconstructed (or visible) energy projection of each fit sample is summarised in Sec. 3.5.

Prior uncertainties on VALOR DUNE systematic parameters are obtained largely from comprehensive comparisons of models to external data. For the prior flux uncertainties, VALOR uses the NuMI flux error analysis from MINERvA [14] as a realistic model for the LBNF flux uncertainties. Errors and covariances between different bins, corresponding to different DUNE detector locations, beam configurations, neutrino species, and true energy ranges were provided by L.Fields [15]. Since 2016a provides only a systematic

constraint fit to Near Detector samples, only the errors and covariances between Near Detector bins are considered. The full matrix and correlations between the Near and Far detector bins will be considered in the 2016b joint analysis. The input covariance matrix used in the present analysis is shown in Sec. 3.4.1.

For the present analysis, a fairly comprehensive set of neutrino interaction systematics were implemented, and appropriately conservative prior uncertainties were calculated by the VALOR group, using tools provided by GENIE [16]. Largely model-independent neutrino interaction systematics were used. This choice will enable us to easily move the VALOR DUNE analysis from the present version of GENIE to the retuned version of GENIE (v3.0.0) once it becomes available later this year. The VALOR GENIE error assignments are shown in Sec. 3.4.2. Several GENIE comparisons with external data were performed in collaboration with the GENIE group, in support of the systematic error assignments used in the VALOR DUNE analysis. Some of these comparisons are shown in Appendix A. The GENIE systematic error assignments and the supporting GENIE/data comparisons will be revised in each iteration of the VALOR DUNE analysis. Improvements will be underpinned by the rapidly expanding GENIE arsenal of data/MC comparison tools and error analyses.

For the 2016a analysis, simplistic and tentative detector acceptance parameters and uncertainties were used. They are described in Sec. 3.4.3. To date, no better input is provided by the proponents of specific Near Detector design options. Detector uncertainty assignments should come from detailed studies using the actual simulation, reconstruction and event selection chain used by each detector group. The VALOR group will adopt the recommendations of each detector group, and has no plans to perform own studies to inform the detector systematic assignments used. However, in absence of such studies and recommendations, the VALOR group could produce its results for a range of detector performance characteristics (provided by the detector groups) in order to establish performance thresholds for meeting the DUNE oscillation sensitivity targets.

After the 2016a VALOR DUNE fit, best-fit values and correlations between all constrained systematic parameters are obtained. Since the Near Detector provides an event rate constraint, constrained flux and cross-section parameter become anti-correlated. The main output of the 2016a analysis is a 156×156 covariance matrix. As the number of systematic parameters grows, concerns exist over the accuracy with which that large covariance matrix is being computed. Some evidence exists that the level of accuracy is not sufficient for the power of the systematic constraint that can be derived from DUNE. Although this will be investigated further, in the 2016b analysis the need for such an intermediate covariance matrix will be eliminated by a simultaneous Near and Far Detector fit where all nuisance parameters will be integrated out and a marginal likelihood will be constructed (see Sec. 2.5.2). The full list of improvements to be installed in the 2016b analysis is outlined in Sec. 4.

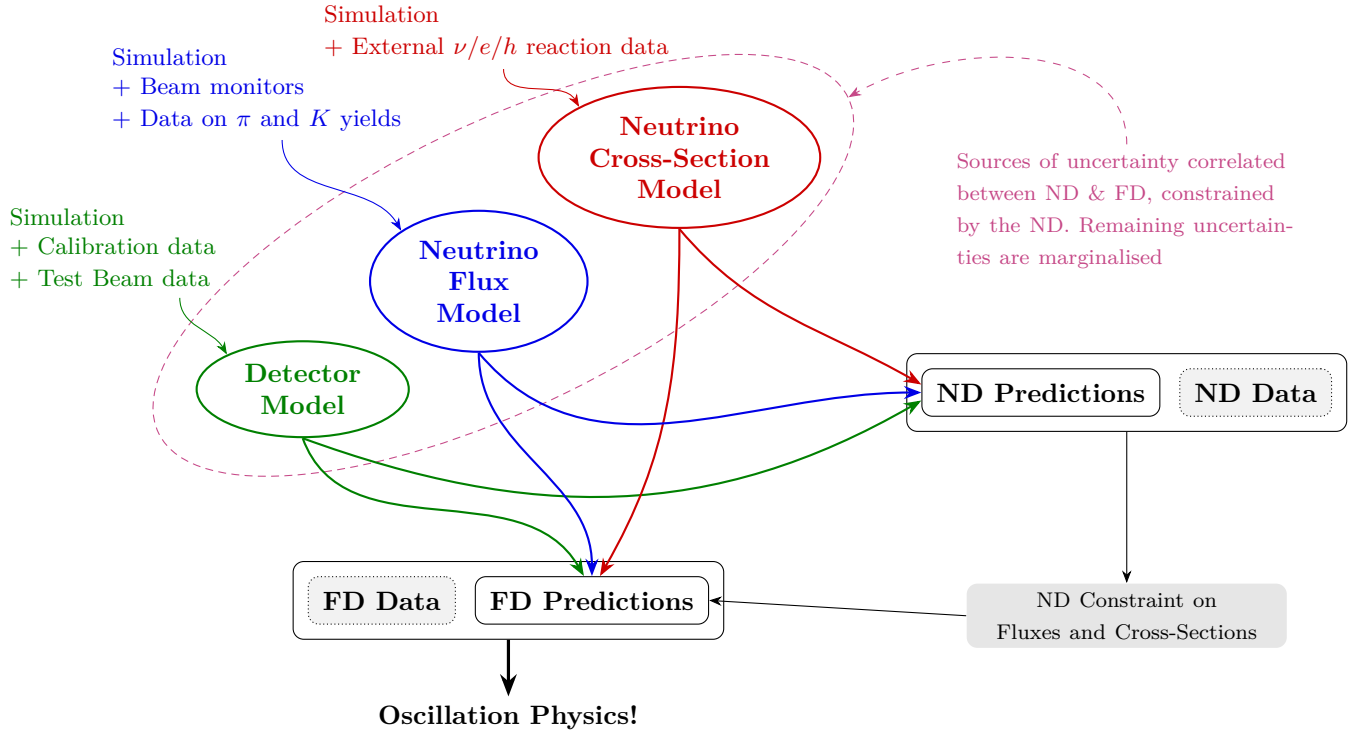
The main 2016a results are presented in Sec. 5. Fits to single toy experiments and pull studies shown in Secs. 5.1 and 5.2 suggest that the fit works as expected. Several physics studies were attempted, envisioning situations that may challenge the fit. However, the quality of the inputs was prohibitive. Generally, very low statistics samples were produced. Mock-up reconstruction and truth-based selections were used, and, when not missing, several event samples were unrealistically pure. Out-of-fiducial beam-related backgrounds were largely neglected. Not only the fit was unchallenged, but it produced unreasonably strong constraints that were a mere reflection of the shortcuts taken in producing the input samples. Overall, **the physics content of the 2nd pass-through was still low and studies are not suitable for any physics conclusion**. Results to Asimov [31] datasets produced for all 3 detector options are shown in Sec. 5.3, and a rather naive comparison between the 3 detector options is made, if nothing else as a proof of the significant challenges that detector groups should overcome in order to bring more realism to the event samples and, eventually, make an apples-to-apples comparison possible.

A summary is provided in Sec. 6.

2 General description of the VALOR DUNE Oscillation and Systematics Constraint Fit

2.1 Overview of the VALOR analysis for a *single* LBL neutrino experiment

The VALOR DUNE analysis uses an ‘indirect’ extrapolation method, and a systematics constraint derived from a joint fit of flux and cross-section parameters to several Near Detector event samples (outlined below).



2.2 Fit spectra predictions

In the VALOR framework an arbitrary number of samples, each corresponding to a given i) detector (or sub-detector region), ii) beam configuration, iii) observed final state, and iv) kinematical phase space, can be fit jointly to determine the parameters of a physics hypothesis in the presence of uncertainties.

A nominal prediction needs to be calculated for each fit sample. Predictions are constructed from Monte Carlo (MC) templates T , which represent the number of MC events (after event reconstruction and analysis cuts were applied) as function of several reconstructed and true quantities. Separate MC templates are constructed for each detector d , beam configuration b , and sample s . Each MC template contains information on how the number of events is distributed in the same N_r -dimensional space K_r of reconstructed kinematical variables chosen for the fit samples. The same reconstructed kinematical variable binning scheme is used both for the MC templates and the fit distributions. The MC templates provide a mapping between reconstructed and true information. Separate templates are constructed for different true reaction modes m , and each template contains information on how the number of events, for each individual reconstructed bin, is distributed in a chosen N_t -dimensional space K_t of true kinematical variables. The true reaction modes, the true kinematic variables, and the kinematical variable binning schemes are defined so that the intended flavour dependencies, reaction mode dependencies and kinematical dependencies of systematics and/or of considered physics hypotheses can be taken into account. Therefore, summarizing all MC template dependencies, we can write

$$T = T_{d;b;s;m}(r, t) \quad (1)$$

where r is a bin in the K_r space of reconstructed kinematical variables, and t is a bin in the K_t space of true kinematical variables. A MC template $T_{d;b;s;m}$ is constructed from a MC sample corresponding to an exposure of $e_{d;b}^{MC}$ and then used to predict observations, or fit data, corresponding to an exposure of $e_{d;b}^{data}$. Here, we will assume that a scaling factor $e_{d;b}^{data} / e_{d;b}^{MC}$ is absorbed in the definition of $T_{d;b;s;m}$.

Using MC templates, the predicted number of events $n_{d;b;s}^{pred}(r; \vec{\theta}; \vec{f})$ in a N_r -dimensional reconstructed kinematical bin r , for a specific sample s , seen in a detector d exposed in a beam configuration b , and for a particular set of M physics parameters $\vec{\theta} = (\theta_0, \theta_1, \dots, \theta_{M-1})$ and N nuisance (systematic) parameters $\vec{f} = (f_0, f_1, \dots, f_{N-1})$, is computed as

$$n_{d;b;s}^{pred}(r; \vec{\theta}; \vec{f}) = \sum_m \sum_t P_{d;b;m}(t; \vec{\theta}) \cdot R_{d;b;s;m}(r, t; \vec{f}) \cdot T_{d;b;s;m}(r, t) \quad (2)$$

where $P_{d;b;m}(t; \vec{\theta})$ encapsulates the effect of a physics hypothesis (e.g. neutrino oscillations in a 3-flavour framework), and $R_{d;b;s;m}(r, t; \vec{f})$ parameterizes the response of a template bin to systematic variations. In principle, the range of m values in the above sum depends on the sample s . In addition, the number, type and dimensionality of true bins t is a function of both s and m . The above will be assumed implicitly and not written explicitly.

The term $P_{d;b;m}(t; \vec{\theta})$ is naturally only a function of true kinematical variables and of neutrino flavour and/or true reaction mode (both of which are encapsulated in m). For multi-detector fits, the dependence on d and b reflects the dependence of P on the appropriate baseline (or on the distribution of baselines in SBL oscillation variants of the VALOR analysis). The 2016a version VALOR DUNE analysis provides a systematic constraint fit to Near Detector samples, and therefore $P_{d;b;m}(t; \vec{\theta}) = 1$. A joint 3-flavour oscillation and systematic constraint fit considering several Near and Far Detector samples will be implemented in the 2016b version of the VALOR DUNE analysis. The construction of $P_{d;b;m}(t; \vec{\theta})$ in a full 3-flavour framework considering matter-effects in constant density matter, and in different physics frameworks, is described in Sec. 2.4.

Typically, but not always, the response $R_{d;b;s;m}(r, t; \vec{f})$ factorises and it can be written as

$$R_{d;b;s;m}(r, t; \vec{f}) = \prod_{i=0}^{N-1} R_{d;b;s;m}^i(r, t; f_i) \quad (3)$$

For several systematics the response is linear and, therefore,

$$R_{d;b;s;m}^i(r, t; f_i) \propto f_i \quad (4)$$

For non linear systematics, the response function $R_{d;b;s;m}^i(r, t; f_i)$ is pre-computed in the $[-5\sigma, +5\sigma]$ range of the parameter f_i and it is represented internally using a cubic spline. Values of systematic parameters that give a negative predicted number of events in any reconstructed bin in any interaction mode are not allowed.

In VALOR, not only the fit samples and the reconstructed kinematical information used for each sample, but also types of MC templates chosen to construct the predictions for each sample, and the true kinematical information recorded in each MC template are all very flexibly defined.

2.3 Toy experiment generation

A toy experiment, for a set of physics parameters $\vec{\theta}$ and systematic parameters \vec{f} , is generated by calculating all $n_{d;b;s}^{pred}(r; \vec{\theta}; \vec{f})$ values and then drawing random numbers $n_{d;b;s}^{obs;toy}(r)$, each from a Poisson distribution with a mean value equal to $n_{d;b;s}^{pred}(r; \vec{\theta}; \vec{f})$. The above procedure is correct when the MC templates are constructed from MC samples generated for an exposure $e_{d;b}^{MC}$ which is far larger than the corresponding experimental $e_{d;b}^{data}$. In the opposite case, a second statistical fluctuation due to finite MC statistics is taken into account in the calculation of $n_{d;b;s}^{pred}(r; \vec{\theta}; \vec{f})$ by appropriately fluctuating the all bin contents of all MC templates $T_{d;b;s;m}(r, t)$.

During the analysis, ensembles of toy experiments with randomized subsets of the physics parameters $\vec{\theta}$ and systematic parameters \vec{f} need to be generated. The procedure for generating toy experiment ensembles should respect the correlations that may exist between the randomized parameters. In VALOR, this is accomplished with a special type of LU decomposition called the *Cholesky* decomposition.

The LU decomposition is a well-known factorization of a matrix C as a product of a lower triangular matrix L and an upper triangular matrix U . The LU decomposition has several applications in scientific computing [29]. Let C be a square, symmetric, positive-definite² matrix. Under the stated conditions, there exists a special factorization of C , the Cholesky decomposition, which is significantly *more efficient* than the generic LU decomposition. Rather than factorizing C as the product of two independent matrices L and U , the Cholesky method factorizes C as the product of a lower triangular matrix L and its transpose matrix:

$$C = L \cdot L^T \quad (5)$$

The Cholesky decomposition algorithm can be found in [29].

The Cholesky decomposition is commonly used for Monte Carlo simulation of systems with correlated variables. Let S_N be such a system whose dimensionality is N and let C be the $N \times N$ matrix which describes the covariance of the N simulated variables. The covariance matrix C is decomposed to obtain the lower triangular matrix L . Let \vec{u} be a N -dimensional vector of uncorrelated variables; each vector element u_i can be randomly generated from a Gaussian distribution with a mean of 0 and a standard deviation of 1. The vector

$$\vec{x} = L \cdot \vec{u} \quad (6)$$

has the covariance properties of S_N .

2.4 Applying neutrino oscillations

VALOR uses bespoke oscillation probability calculation code. Oscillation probabilities can be calculated both in vacuum and matter within the standard 3-flavour framework and in extensions to it, including the 3+2, 1+3+1 and 3+1 models.

The method of calculation of the 3-flavour oscillation probabilities is given in Sec. 2.4.1. Inputs to the 3-flavour oscillation probability code are described in Sec. 2.4.2 and validation of it in Sec. 2.4.3. An estimate of the accuracy of the 3-flavour oscillation probabilities in matter is given in Sec. 2.4.4. Finally, the calculation of VALOR oscillation probabilities for models beyond the standard 3-flavour framework is described in Sec. 2.4.5.

2.4.1 3-flavour neutrino oscillation probabilities

The 3-flavour neutrino oscillation probabilities in vacuum are calculated from Eq. 11 in [19]:

$$P(\nu_\alpha \rightarrow \nu_\beta) = \delta_{\alpha\beta} - 4 \sum_{i>j} \text{Re}(U_{\alpha i}^* U_{\beta i} U_{\alpha j} U_{\beta j}^*) \sin^2 \left(\frac{\Delta m_{ij}^2 L}{4E} \right) + 2 \sum_{i>j} \text{Im}(U_{\alpha i}^* U_{\beta i} U_{\alpha j} U_{\beta j}^*) \sin \left(\frac{\Delta m_{ij}^2 L}{2E} \right) \quad (7)$$

In equation 7, $\Delta m_{ij}^2 = m_j^2 - m_i^2$, L is the distance from the neutrino target to the far detector, E is the neutrino energy, and U is the PMNS matrix in vacuum:

$$U = \begin{pmatrix} c_{12}c_{13} & c_{13}s_{12} & s_{13}e^{-i\delta} \\ -c_{23}s_{12} - s_{13}s_{23}c_{12}e^{i\delta} & c_{12}c_{23} - s_{12}s_{13}s_{23}e^{i\delta} & c_{13}s_{23} \\ s_{12}s_{23} - s_{13}c_{12}c_{23}e^{i\delta} & -s_{23}c_{12} - s_{12}c_{23}s_{13}e^{i\delta} & c_{13}c_{23} \end{pmatrix} \quad (8)$$

² $\vec{v}^T \cdot C \cdot \vec{v} > 0$ for every vector \vec{v} .

with $s_{12} = \sin(\theta_{12})$, $c_{12} = \cos(\theta_{12})$, etc. $P(\bar{\nu}_\alpha \rightarrow \bar{\nu}_\beta)$ is calculated by changing the sign of the third term in Eq. 7 (this assumes that CPT is conserved).

All three neutrino flavours undergo neutral-current interactions with protons, neutrons and electrons in matter. These neutral-current interactions have identical amplitudes for all three flavours, and they produce no observable effects on the probabilities of oscillation between one flavour and another. However the oscillation probabilities are changed by coherent forward scattering of electron neutrinos in charged-current interactions with electrons in matter [19].

Using natural units with $\hbar = c = 1$, the time evolution of neutrino flavour states in vacuum is described by the Schrödinger equation:

$$i \frac{\partial \psi}{\partial t} = H_F \psi \quad (9)$$

where

$$\psi = \begin{pmatrix} \psi_e \\ \psi_\mu \\ \psi_\tau \end{pmatrix} \quad (10)$$

and H_F is the effective Hamiltonian in the flavour-state basis

$$H_F = \frac{1}{2E} U M U^\dagger \quad (11)$$

with M defined by

$$M = \begin{pmatrix} 0 & 0 & 0 \\ 0 & \Delta m_{21}^2 & 0 \\ 0 & 0 & \Delta m_{31}^2 \end{pmatrix} \quad (12)$$

The calculation of oscillation probabilities requires neutrino flight time to be converted to distance travelled, and this conversion assumes that neutrinos are highly relativistic. In this calculation, $U M U^\dagger$ is used for neutrinos, but its complex conjugate is used for antineutrinos. For neutrinos, the effects of the charged-current interactions between electron neutrinos and electrons are taken into account by adding the potential $2E\sqrt{2G_F N_e}$ to the real part of the first diagonal element of $U M U^\dagger$, where E is the neutrino energy, G_F is the Fermi coupling constant, and N_e is the number density of electrons in matter. For antineutrinos, this potential is subtracted from the real part of the first diagonal element of the complex conjugate of $U M U^\dagger$ (for further details see section 9.2 in [20]).

After the addition or subtraction of this potential, $U M U^\dagger$ (or its complex conjugate) is diagonalised. The eigenvalues of a Hermitian matrix are always real; they are calculated by solving the (cubic) characteristic equation using the method of del Ferro, Tartaglia and Cardano as described in [22]. The differences between the eigenvalues are the effective mass-squared differences in matter. The eigenvectors are calculated using an algebraic method: one of the components is set to be 1.0 (real), and the other two components are calculated using two of the three simultaneous equations in $U M U^\dagger - \lambda I = 0$, where the λ are the eigenvalues. After being normalised, the three eigenvectors become the columns of the effective mixing matrix in matter.

The initial flavour state of the neutrino is represented by a 1×3 column vector whose entries are complex; if, for example, the initial flavour state is a muon neutrino, this column vector is

$$\begin{pmatrix} 0 \\ 1 \\ 0 \end{pmatrix}$$

The vector representing the initial flavour state is then multiplied by the Hermitian conjugate of the matter mixing matrix to convert it to another 1×3 complex column vector representing the initial mass states. These mass states are propagated to the far detector by multiplying the j th initial mass state by $\exp\left(\frac{-i\Delta m_{j1}^2 L}{2E}\right)$, where the Δm_{j1}^2 are the mass-squared differences in matter, i.e. the differences between the eigenvalues of $U M U^\dagger$. This gives a new 1×3 complex column vector representing the final mass states, and these

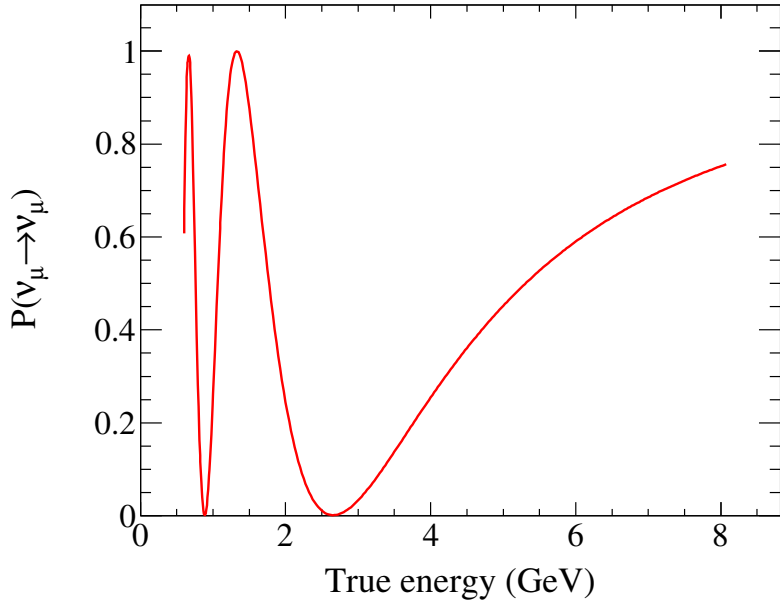


Figure 1: $P(\nu_\mu \rightarrow \nu_\mu)$ in matter as a function of true neutrino energy for a baseline of 1300 km; the oscillation parameters are $\sin^2(\theta_{12}) = 0.3$, $\sin^2(\theta_{13}) = 0.025$, $\sin^2(\theta_{23}) = 0.5$, $\Delta m_{21}^2 = 7.5 \times 10^{-5}$ eV $^2/c^4$, $\Delta m_{32}^2 = 2.5 \times 10^{-3}$ eV $^2/c^4$, $\delta_{CP} = 0$, normal mass hierarchy, Earth matter density = 2.7 g/cm 3 .

are converted to the final flavour states by multiplying by the matter mixing matrix. The entries of the resulting 1×3 complex column vector represent the amplitudes of each flavour at the far detector, and the corresponding oscillation probabilities are calculated as the moduli squared of these amplitudes.

The 3-flavour $P(\nu_\mu \rightarrow \nu_\mu)$ in matter is shown for a baseline of 1300 km in Fig. 1, and $P(\nu_\mu \rightarrow \nu_e)$ in matter is shown for the same baseline and for four different values of δ_{CP} in Fig. 2. A comparison of $P(\nu_\mu \rightarrow \nu_e)$ against $P(\bar{\nu}_\mu \rightarrow \bar{\nu}_e)$ for the normal and inverted mass hierarchies is shown in Fig. 3; this comparison is in matter for a baseline of 1300 km and for different values of δ_{CP} .

2.4.2 Inputs to the 3-flavour neutrino oscillation probability calculations

When calculating the 3-flavour oscillation probabilities, the mixing angles can be input either in the form $\sin^2(2\theta_{ij})$ or as $\sin^2(\theta_{ij})$. $\sin(\theta_{ij})$ and $\cos(\theta_{ij})$ are calculated from the input values, and these are used in turn to calculate the elements of U . The “solar” mass-squared difference is input as Δm_{21}^2 , and this is > 0 for both mass hierarchies. The “atmospheric” mass-squared difference is input either as $|\Delta m_{32}^2|$ or using a definition introduced by G. Fogli, E. Lisi et al. in [18]:

$$\Delta m_{FL}^2 = m_3^2 - \frac{m_2^2 + m_1^2}{2} \quad (13)$$

The quantity denoted Δm_{FL}^2 is useful since its absolute value is the same for both mass hierarchies, and only its sign changes. If the atmospheric mass-squared difference is input as Δm_{32}^2 , the mass hierarchy is set using the sign of Δm_{32}^2 ; this is positive for the normal mass hierarchy (NH) and negative for the inverted mass hierarchy (IH). In this case, Δm_{31}^2 is not input but is calculated as $\Delta m_{31}^2 = \Delta m_{21}^2 + \Delta m_{32}^2$ for both hierarchies. If the atmospheric mass-squared difference is input as Δm_{FL}^2 , the mass hierarchy is set using the sign of Δm_{FL}^2 . Then Δm_{32}^2 and Δm_{31}^2 are calculated from the input values of Δm_{FL}^2 and Δm_{21}^2 .

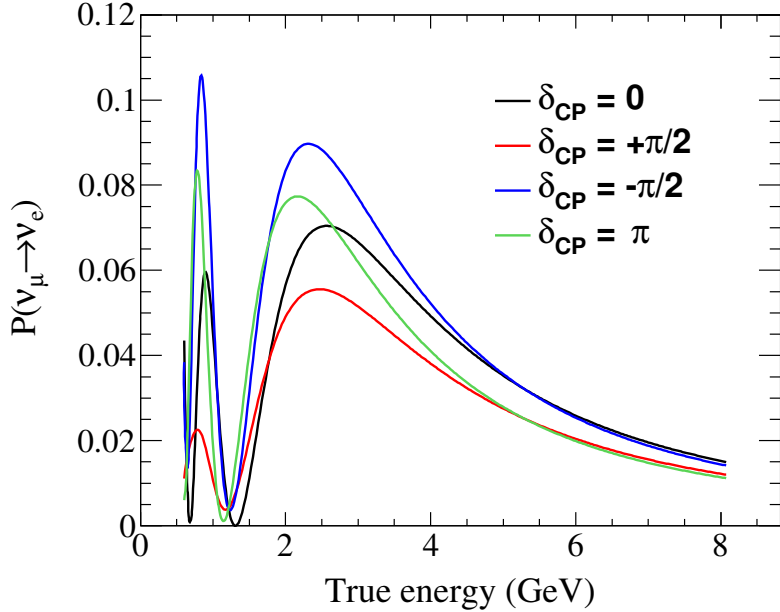


Figure 2: $P(\nu_\mu \rightarrow \nu_e)$ in matter as a function of true neutrino energy for a baseline of 1300 km and for four different values of δ_{CP} : 0 (black), $+\pi/2$ (red), $-\pi/2$ (blue), and π (green); the other oscillation parameters are $\sin^2(\theta_{12}) = 0.3$, $\sin^2(\theta_{13}) = 0.025$, $\sin^2(\theta_{23}) = 0.5$, $\Delta m_{21}^2 = 7.5 \times 10^{-5} \text{ eV}^2/\text{c}^4$, $\Delta m_{32}^2 = 2.5 \times 10^{-3} \text{ eV}^2/\text{c}^4$, normal mass hierarchy, Earth matter density = 2.7 g/cm^3 .

2.4.3 Validation of the 3-flavour oscillation probabilities

The 3-flavour oscillation probabilities in vacuum were checked using an alternative formulation in Eq. 13.13 and 13.14 in the PDG review [21]:

$$P(\nu_\alpha \rightarrow \nu_\beta) = \sum_j |U_{\beta j}|^2 |U_{\alpha j}|^2 + 2 \sum_{j > k} |U_{\beta j} U_{\alpha j}^* U_{\alpha k} U_{\beta k}^*| \cos \left(\frac{\Delta m_{jk}^2 L}{2E} - \phi_{\beta\alpha;jk} \right) \quad (14)$$

where $\phi_{\beta\alpha;jk} = \arg(U_{\beta j} U_{\alpha j}^* U_{\alpha k} U_{\beta k}^*)$. $P(\bar{\nu}_\alpha \rightarrow \bar{\nu}_\beta)$ is calculated by changing the sign of $\phi_{\beta\alpha;jk}$ in the argument of the cosine. The probabilities calculated from Eq. 14 agreed with those calculated from Eq. 7 to 14 significant figures.

Several checks of the oscillation probabilities in constant density matter are written into the code that calculates them:

1. The eigenvalues of $U M U^\dagger$ are checked by comparing their sum with the trace of the matrix.
2. Each normalised eigenvector is multiplied in turn by each of the 3 matrices formed by subtracting the eigenvalues from the real parts of the diagonal elements of $U M U^\dagger$, and a check is made of the differences between these products and a zero vector.
3. A check is made that the normalised eigenvectors of $U M U^\dagger$ are orthogonal by calculating the scalar product between them (the scalar product of two complex vectors is the product of the first vector with the complex conjugate of the second vector).
4. A check is also made that the Hermitian conjugate of the mixing matrix in matter is equal to the inverse of the matrix. This is done by multiplying the mixing matrix in matter by its Hermitian conjugate, and checking the differences between the product and an identity matrix.

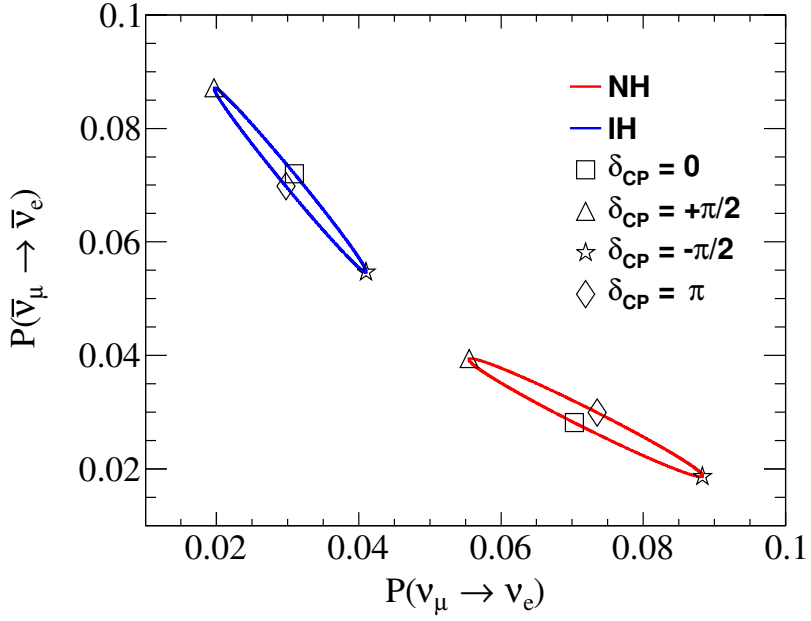


Figure 3: $P(\nu_\mu \rightarrow \nu_e)$ against $P(\bar{\nu}_\mu \rightarrow \bar{\nu}_e)$ in matter for a baseline of 1300 km and for the normal mass hierarchy (red) and the inverted mass hierarchy (blue); the red and blue ellipses are produced by changing the value of δ_{CP} , with four values of δ_{CP} being shown on each ellipse. The true energy is 2.5 GeV and the other oscillation parameters are $\sin^2(\theta_{12}) = 0.3$, $\sin^2(\theta_{13}) = 0.025$, $\sin^2(\theta_{23}) = 0.5$, $\Delta m_{21}^2 = 7.5 \times 10^{-5} \text{ eV}^2/\text{c}^4$, $\Delta m_{32}^2 = 2.5 \times 10^{-3} \text{ eV}^2/\text{c}^4$, Earth matter density = 2.7 g/cm^3 .

The values of the oscillation probabilities in constant density matter were checked by comparing them with equivalent probabilities calculated by an independently-written Fortran program [23]. This Fortran program uses different algorithms, and calculates numerically the eigenvalues and eigenvectors of UMU^\dagger . Nevertheless there was very good agreement between the two calculations of the probabilities, with the fractional differences being $\approx 2 \times 10^{-6}$.

The values of the matter oscillation probabilities were also compared with those given by Prob3++ [24], and the fractional differences were $\approx 1-5 \times 10^{-4}$.

2.4.4 Accuracy of the 3-flavour oscillation probabilities

As stated in section 2.4.3, the 3-flavour oscillation probabilities in vacuum agreed to 14 significant figures between the two formulations.

An estimate of the accuracy of the 3-flavour oscillation probabilities in constant density matter was made in three separate ways:

1. The matter probabilities for zero density were compared with the vacuum probabilities; there was good agreement, with the fractional differences being $\approx 2-5 \times 10^{-6}$.
2. The probabilities given when calculating the eigenvectors with simultaneous equations 1 and 2 in $\text{UMU}^\dagger - \lambda I = 0$ were compared with the probabilities given when calculating the eigenvectors with simultaneous equations 2 and 3. The fractional differences between these two calculations were again $\approx 2-5 \times 10^{-6}$.
3. The sum of three matter probabilities, for example $P(\nu_\mu \rightarrow \nu_e) + P(\nu_\mu \rightarrow \nu_\mu) + P(\nu_\mu \rightarrow \nu_\tau)$, was compared with 1.0; again there was good agreement, and the differences were $\approx 2 \times 10^{-6}$.

This means that the matter oscillation probabilities should be considered to be accurate to 5 decimal places. The accuracy of the matter probabilities is less than that of the vacuum probabilities due to the method of calculation of the eigenvectors. This involves calculations of the form

$$\frac{(ab - cd)}{(ef - gh)}$$

where a, b, c, etc. are elements of $UMU^\dagger - \lambda I$. Frequently ab is close in value to cd, which means that (ab - cd) is much smaller than ab or cd, and the same applies to (ef - gh). However the advantage of the method of calculation of the eigenvectors is that it allows the worst of these cancellation errors to be avoided; this can be done by calculating the eigenvectors using different pairs of simultaneous equations in $UMU^\dagger - \lambda I = 0$ for different combinations of the oscillation parameters. In practice, the eigenvectors are nearly always calculated using equations 1 and 2 in $UMU^\dagger - \lambda I = 0$, but equations 2 and 3 are used when $3.10 < \delta_{CP} < 3.18$ and $\sin^2(2\theta_{13}) > 10^{-8}$ in order to avoid such cancellation errors.

2.4.5 Beyond the standard 3-flavour framework

VALOR can also calculate oscillation probabilities for more than 3 neutrinos using the 3+2, 1+3+1 and 3+1 models. In the 3+2 model, m_4^2 and m_5^2 are both $>$ than m_1^2 , m_2^2 and m_3^2 while in the 1+3+1 model $m_4^2 < m_1^2$, m_2^2 and m_3^2 with $m_5^2 > m_1^2$, m_2^2 and m_3^2 .

In order to obtain these probabilities, the 5-flavour vacuum PMNS matrix is needed. This is calculated by multiplying the 2D rotation matrices 35, 34, 25, 24, 23, 15, 14, 13 and 12; two examples of these rotation matrices (12 and 13) are shown in Eq. 15 and 16 respectively:

$$\begin{pmatrix} \cos \theta_{12} & \sin \theta_{12} & 0 & 0 & 0 \\ -\sin \theta_{12} & \cos \theta_{12} & 0 & 0 & 0 \\ 0 & 0 & 1 & 0 & 0 \\ 0 & 0 & 0 & 1 & 0 \\ 0 & 0 & 0 & 0 & 1 \end{pmatrix} \quad (15)$$

$$\begin{pmatrix} \cos \theta_{13} & 0 & \sin \theta_{13} & 0 & 0 \\ 0 & 1 & 0 & 0 & 0 \\ -\sin \theta_{13} & 0 & \cos \theta_{13} & 0 & 0 \\ 0 & 0 & 0 & 1 & 0 \\ 0 & 0 & 0 & 0 & 1 \end{pmatrix} \quad (16)$$

In general, rotation matrix 45 should also be included in the matrix product. This represents oscillations between the two sterile flavours ν_{S4} and ν_{S5} , but these produce no observable effects. For this reason, matrix 45 is not included in the product (this is equivalent to setting $\theta_{45} = 0$). It is also necessary to choose a convention for including the 5 complex phases (δ_{ij}) in the 5-flavour PMNS matrix; VALOR uses the convention in [25] in which these phases are contained in rotation matrices 12, 13, 24, 25 and 35. This is done by multiplying the positive sin term by $e^{-i\delta_{ij}}$ and the negative sin term by $e^{i\delta_{ij}}$ in those matrices. These complex phases are included in the 5-flavour PMNS matrix by including them in the product of the rotation matrices.

There are 4 independent mass-squared differences, namely Δm_{21}^2 , Δm_{31}^2 , Δm_{41}^2 and Δm_{51}^2 , and the other mass-squared differences are calculated from them. In the VALOR code, it is simple to switch between the 3+2 and the 1+3+1 models by setting a parameter. It is also straightforward to change to the 3+1 model by setting θ_{15} , θ_{25} and θ_{35} to zero. The 3-flavour mass hierarchy can also be set as described in Sec. 2.4.2.

The 5-flavour oscillation probabilities in vacuum are given by Eq. 7, but now U is the 5-flavour vacuum PMNS matrix and the sums are from $j=1-4$ and $i>j$, i. e. $ij = 21, 31, 41, 51, 32, 42, 52, 43, 53$ and 54. To obtain the oscillation probabilities in constant-density matter, UMU^\dagger is again calculated, but now U is the 5-flavour vacuum PMNS matrix and

$$M = \begin{pmatrix} 0 & 0 & 0 & 0 & 0 \\ 0 & \Delta m_{21}^2 & 0 & 0 & 0 \\ 0 & 0 & \Delta m_{31}^2 & 0 & 0 \\ 0 & 0 & 0 & \Delta m_{41}^2 & 0 \\ 0 & 0 & 0 & 0 & \Delta m_{51}^2 \end{pmatrix} \quad (17)$$

Again UMU^\dagger is used for neutrinos and its complex conjugate for antineutrinos. The potential $2E\sqrt{2G_F}N_e$ due to CC interactions of electrons with matter is added for neutrinos (or subtracted for antineutrinos) to the real part of the first diagonal element of UMU^\dagger as described in Sec. 2.4.1. For 5 flavours, however, the potential $E\sqrt{2G_F}N_n$ due to NC interactions of protons, neutrons and electrons with matter must also be subtracted for neutrinos (or added for antineutrinos) to the real parts of the first 3 diagonal elements of UMU^\dagger . N_n is the number density of neutrons in matter which is assumed to be equal to the number density of electrons. N_n is used since couplings of the Z boson to protons and electrons are equal and opposite at zero momentum transfer, i. e. the proton and electron contributions to NC coherent forward scattering cancel each other.

After adding or subtracting these potentials, UMU^\dagger or its complex conjugate is diagonalised using the complex form of symmetric bidiagonalisation and QR reduction in the GNU scientific library [26]. The 5-flavour oscillation probabilities are then calculated as described for 3 flavours in Sec. 2.4.1 except that a 1×5 complex column vector is used instead of a 1×3 vector.

The 5-flavour oscillation probabilities have been validated in 4 ways:

- The same checks are made during the calculation of the oscillation probabilities as for the 3-flavour probabilities.
- The matter probabilities for zero density were compared with the vacuum probabilities, and there was agreement to 14 decimal places.
- The sum of $P(\nu_\mu \rightarrow \nu_e) + P(\nu_\mu \rightarrow \nu_\mu) + P(\nu_\mu \rightarrow \nu_\tau) + P(\nu_\mu \rightarrow \nu_{S4}) + P(\nu_\mu \rightarrow \nu_{S5})$ was compared with 1.0, and there was agreement to 14 decimal places for both the matter and vacuum probabilities.
- The oscillation probabilities were compared with those given by GLoBES [27], and there was agreement to 3 decimal places. The small differences between the VALOR and GLoBES probabilities are understood, and are due to VALOR and GLoBES using slightly different values of the dimensional constant in the $\left(\frac{\Delta m^2 L}{E}\right)$ terms. This was checked by recalculating the VALOR probabilities using the GLoBES value of the dimensional constant; in this case, the vacuum probabilities agreed with those of GLoBES to 6 decimal places and the matter probabilities to 5 decimal places.

2.5 Parameter estimation

2.5.1 Construction of likelihood

Measurements of a set of physics parameters $\vec{\theta} = (\theta_0, \theta_1, \dots, \theta_{M-1})$ in the presence of several systematic parameters $\vec{f} = (f_0, f_1, \dots, f_{N-1})$ are obtained by comparing the observed and expected reconstructed kinematical distributions (in an N_r -dimensional space K_r) for a series of samples.

A binned likelihood-ratio method is typically used by VALOR. The following log-likelihood function is constructed for each sample s, recorded in a detector d and exposed to a beam configuration b:

$$\ln \lambda_{d;b;s}(\vec{\theta}; \vec{f}) = - \sum_r \left\{ \left(n_{d;b;s}^{\text{pred}}(r; \vec{\theta}; \vec{f}) - n_{d;b;s}^{\text{obs}}(r) \right) + n_{d;b;s}^{\text{obs}}(r) \cdot \ln \frac{n_{d;b;s}^{\text{obs}}(r)}{n_{d;b;s}^{\text{pred}}(r; \vec{\theta}; \vec{f})} \right\} \quad (18)$$

Here, using the same notation introduced earlier, r is a bin in a multi-dimensional reconstructed kinematical space (which, in principle, can be different for each sample). The observed number of events in bin r is given by $n_{d;b;s}^{\text{obs}}(r)$, whereas $n_{d;b;s}^{\text{pred}}(r; \vec{\theta}; \vec{f})$ is the predicted number of events constructed as shown in Eq. 2. The following quantity is constructed in the VALOR DUNE analysis by summing up the contributions from all fit samples:

$$\lambda_{DUNE}(\vec{\theta}; \vec{f}) = \prod_d \prod_b \prod_s \lambda_{d;b;s}(\vec{\theta}; \vec{f}) \quad (19)$$

The above is the general expression used for the 2016b version of the VALOR DUNE analysis where a joint oscillation and systematic constraint fit using both DUNE Near and Far detector samples is performed.

In the reported 2016a version of the analysis where VALOR provides a systematic constraint using only Near detector samples, the above equation becomes:

$$\lambda_{DUNE/ND}(\vec{f}) = \prod_b \prod_s \lambda_{DUNE/ND;b;s}(\vec{f}) \quad (20)$$

Most physics and systematic parameters in the VALOR fit come with prior constraints from external data. The following Gaussian penalty term is computed:

$$\ln \lambda_{prior}(\vec{\theta}; \vec{f}) = -\frac{1}{2} \left\{ (\vec{\theta} - \vec{\theta}_0)^T C_\theta^{-1} (\vec{\theta} - \vec{\theta}_0) + (\vec{f} - \vec{f}_0)^T C_f^{-1} (\vec{f} - \vec{f}_0) \right\} \quad (21)$$

where C_θ is an $M \times M$ physics parameter covariance matrix, C_f is an $N \times N$ systematic parameter covariance matrix, $\vec{\theta}_0$ is a vector with the nominal values of the measured physics parameter, and \vec{f}_0 is a vector with the nominal values of the systematic parameters. Typically, depending on the details of the analysis and the actual physics framework used, we choose to ignore most of the contribution from the first term in Eq. 21. For example, in the VALOR DUNE 3-flavour analysis, prior (external) constraints on θ_{12} and Δm_{21}^2 are always used, prior constraints on θ_{13} may or may not be used, and, typically, prior constraints on δ_{CP} , θ_{23} and Δm_{32}^2 (for the Normal hierarchy, or Δm_{13}^2 for the Inverted hierarchy) are not used. The prior constraints on the systematic parameters are almost always used but, a successfully designed Near detector and analysis procedure should ensure that the determination of these parameters is not driven by the prior constraints. In the present 2016a version of the VALOR DUNE analysis, C_f is a 156×156 covariance matrix obtained by adding diagonally the 104×104 flux covariance matrix, the 43×43 neutrino interaction covariance matrix, and the 9×9 detector covariance matrix.

Best-fit values are obtained by maximizing:

$$\lambda(\vec{\theta}; \vec{f}) = \lambda_{DUNE}(\vec{\theta}; \vec{f}) \cdot \lambda_{prior}(\vec{\theta}; \vec{f}) \quad (22)$$

The advantage of the likelihood ratio method is that, in the large-sample limit, the quantity $-2\ln\lambda(\vec{\theta}; \vec{f})$ has a χ^2 distribution and it can therefore be used as a goodness-of-fit test.

2.5.2 Parameter elimination through profiling or marginalization

Several of the parameters in $\vec{\theta}$ and \vec{f} need to be eliminated, while the parameters of interest are measured. In a typical analysis, all parameters in \vec{f} and a set of parameters in $\vec{\theta}$ will be eliminated. For example, all (flux, cross-section and detector) systematics in \vec{f} , as well as all squared-mass splittings and mixing angles in $\vec{\theta}$ may be elicited in a 3-flavour analysis for measuring the CP-invariance violating phase δ_{CP} . The presently reported VALOR DUNE Near detector analysis (2016a), as a intermediate step towards the VALOR joint DUNE Near and Far detector analysis (2016b), is somewhat unusual in that all parameters are systematics. Only detector systematics need to be eliminated, as they are not correlated between the Near and Far detectors, whereas the flux and cross-section systematics are taken to be the parameters of interest (only to be eliminated at a subsequent step where an oscillation fit is performed to Far detector data only). Concerns over the robustness of the two-step implementation and the accuracy of the very large covariance matrix produced by the fit to the Near detector data only dictate the development of the joint Near and Far detector analysis.

Whereas the actual treatment of systematics parameters will be altered significantly between versions 2016a and 2016b, a generic description of the methodology used can be made. Any set from the union of the $\vec{\theta}$ and \vec{f} parameters can be designated as parameters of interest. Let $\vec{\theta}'$ be that set, while \vec{f}' is the complementary set of parameters (nuisance parameters) that needs to be eliminated. The $\vec{\theta}'$ parameters are maximized with respect to the likelihood distribution, but for the elimination of the \vec{f}' parameters several different strategies exist. Historically VALOR group was using the typical frequentist approach for Gaussian parameters, and the nuisance parameters were profiled [32]. Whereas this possibility still exists and, in fact, profiling was used in the 2016a VALOR DUNE analysis, the main method adopted by the VALOR group in

its recent T2K oscillation analyses is a hybrid Bayesian-frequentist method. The parameters of interest are maximized with respect to the likelihood distribution, but the nuisance parameters are marginalised [33]. The marginalization procedure yields the so-called marginal likelihood that depends only on the parameters of interest, $\vec{\theta}'$.

The marginal likelihood is derived using the following equation:

$$\lambda_{marg}(\vec{\theta}') = \int \lambda(\vec{\theta}'; \vec{f}') \pi(\vec{f}') d\vec{f}' \quad (23)$$

where $\pi(\vec{f}')$ is the prior of the parameters to be eliminated.

The marginal likelihood can be approximated numerically by generating toy MC experiments. Let n be the number of toy experiments produced. Then the marginal likelihood can be written as:

$$\lambda_{marg}(\vec{\theta}') \approx \frac{1}{n} \sum_{i=0}^{n-1} \lambda(\vec{\theta}'; \vec{f}'_i) \quad (24)$$

where \vec{f}'_i represents the single set of nuisance parameters generated for the i^{th} toy experiment. Many experiments need to be generated in order to effectively sample the nuisance parameter space. The number of toy experiments depends on the number of nuisance parameters, as well as the precision that is required by the measurement.

It is important to note that this numerical integration is a weighted average of the likelihood evaluated at the n throws, not a weighted average of the log-likelihood. During the marginalization process, random values of the nuisance parameters are drawn from the $\pi(\vec{f}')$ distribution which encapsulates the prior knowledge on these parameters. Therefore, each throw is already weighted based on the prior information, and as a result a penalty term for \vec{f}' should not be used. However, it may be the case that some of the parameters of interest, $\vec{\theta}'$, which are not marginalised, are constrained by a penalty term. In this case, Eq. 24 can be written as:

$$-2\ln\lambda_{marg}(\vec{\theta}') \approx -2\ln\left\{\frac{1}{n} \sum_{i=0}^{n-1} \lambda(\vec{\theta}'; \vec{f}'_i)\right\} + (\vec{\theta}' - \vec{\theta}'_0)^T C_{\theta'}^{-1} (\vec{\theta}' - \vec{\theta}'_0) \quad (25)$$

2.5.3 Calculation of best-fit spectra with marginalized nuisance parameters

When the nuisance parameters $\vec{\theta}'$ are eliminated by profiling, the best-fit spectra are unambiguously defined by the MC prediction that gives the largest likelihood value. However, if the nuisance parameters are marginalised, there does not exist a single set of parameters which corresponds to the best fit. Therefore, a new method has been developed to represent the best fit spectra.

From each toy experiment, i , used to marginalise the nuisance parameters, a different predicted spectrum $n_{d;b;s}^{pred}(r; \vec{\theta}'_{bf}; \vec{f}'_i)$ is produced, as well as a different likelihood value $\lambda(\vec{\theta}'_{bf}; \vec{f}'_i)$, where $\vec{\theta}'_{bf}$ is the vector of best-fit values of the parameters of interest.

The best-fit number of events in the multi-dimensional reconstructed kinematical bin r is calculated as:

$$\langle n_{d;b;s}^{pred}(r) \rangle_{bf;marg} = \frac{\sum_{i=0}^{n-1} \lambda(\vec{\theta}'_{bf}; \vec{f}'_i) \cdot n_{d;b;s}^{pred}(r; \vec{\theta}'_{bf}; \vec{f}'_i)}{\sum_{i=0}^{n-1} \lambda(\vec{\theta}'_{bf}; \vec{f}'_i)} \quad (26)$$

One can easily find a relation between the profiled and marginalised best-fit spectra. In the limit of infinite number of toy experiments, the marginal likelihood can be written as:

$$\lambda_{marg}(\vec{\theta}'_{bf}) = \frac{1}{n} \sum_{i=0, i \neq bf}^{n-1} [\lambda(\vec{\theta}'_{bf}; \vec{f}'_i) + \lambda_{prof}] \quad (27)$$

where $\lambda_{prof} = \lambda(\vec{\theta}'_{bf}; \vec{f}'_{bf})$ is the profiled best-fit likelihood. If we denote as $\langle n_{d;b;s}^{pred}(r) \rangle_{bf;prof}$ the best-fit number of events obtained using the profiling method for the multi-dimensional reconstructed kinematical bin r

$$\langle n_{d;b;s}^{pred}(r) \rangle_{bf;prof} = n_{d;b;s}^{pred}(r; \vec{\theta}'_{bf}; \vec{f}'_{bf}) \quad (28)$$

then the Eq. 29 can be written as:

$$\langle n_{d;b;s}^{pred}(r) \rangle_{bf;marg} = \frac{\sum_{i=0, i \neq bf}^{n-1} \lambda(\vec{\theta}'_{bf}; \vec{f}'_i) \cdot n_{d;b;s}^{pred}(r; \vec{\theta}'_{bf}; \vec{f}'_i) + \lambda_{prof} \cdot \langle n_{d;b;s}^{pred}(r) \rangle_{bf;prof}}{\sum_{i=0}^{n-1} \lambda(\vec{\theta}'_{bf}; \vec{f}'_i)} \quad (29)$$

2.5.4 Construction of confidence intervals

After the fit is completed, the full χ^2 distribution is then shifted with respect to $\chi^2(\vec{\theta}_{bf})$:

$$\Delta\chi^2(\vec{\theta}) = \chi^2(\vec{\theta}) - \chi^2(\vec{\theta}_{bf}) \quad (30)$$

Confidence intervals are set on $\Delta\chi^2(\vec{\theta})$. If

$$\Delta\chi^2(\vec{\theta}) > \Delta\chi^2_{crit} \quad (31)$$

where $\Delta\chi^2_{crit}$ is the critical value for a certain confidence level $X\%$ (CL), that value of $\vec{\theta}$ is excluded at the $X\%$ CL. In the Gaussian approximation constant values of $\Delta\chi^2_{crit}$ can be used. It will be called “constant $\Delta\chi^2$ method”.

However in some cases the Gaussian approximation is not reliable and the “Feldman-Cousins method” [34] must be used. In this method a different critical value for each point of the $\vec{\theta}$ grid $\Delta\chi^2(\vec{\theta})_{crit}$ is calculated. The procedure consists of the following steps:

1. many toys MC (e.g. 10k) are produced assuming the oscillation hypothesis of the grid point $\vec{\theta}$ and taking into account both the statistical and systematic uncertainties;
2. for each toy first $\chi^2(\vec{\theta}_{fix})$ is obtained by minimizing $\chi^2(\vec{\theta})$ where the oscillation parameters $\vec{\theta}$ are kept fixed to the values corresponding to the grid point and the nuisance parameters are marginalised. Then $\chi^2(\vec{\theta})$ is minimized, leaving the oscillation parameters $\vec{\theta}$ as free and $\chi^2(\vec{\theta}_{bf})$ is obtained.
3. The steps 2 and 3 are repeated for each toy MC and a distribution of $\Delta\chi^2(\vec{\theta})$ ($f(\Delta\chi^2)$) is obtained.
4. The critical value for $X\%$ CL, $\Delta\chi^2(\vec{\theta})_{crit}$, can be defined as:

$$\Delta\chi^2_{crit} : \int_{-\infty}^{\Delta\chi^2_{crit}} f(\Delta\chi^2) d(\Delta\chi^2) = X\% \quad (32)$$

5. This procedure is repeated for all the points of the $\vec{\theta}$ grid and several critical values are computed

Once a critical value, $\Delta\chi^2(\vec{\theta})_{crit}$, is computed for each oscillation hypothesis in the $\vec{\theta}$ grid, the confidence intervals are set by the condition of Eq. 31.

3 Specifics of the 2016a VALOR DUNE analysis

3.1 Choice of fit samples

For the 2016a implementation of the VALOR DUNE analysis we have selected 18 Near Detector event samples (9 event samples in each of two LBNF beam configurations). The following 9 samples are currently included for the FHC (neutrino-enhanced) beam configuration (final state shown in the parenthesis):

- ν_μ CC
 - 1. 1-track QE enhanced (μ^- only)
 - 2. 2-track QE enhanced ($\mu^- + p$)
 - 3. $1\pi^\pm (\mu^- + 1\pi^\pm + X)$
 - 4. $1\pi^0 (\mu^- + 1\pi^0 + X)$
 - 5. $1\pi^\pm + 1\pi^0 (\mu^- + 1\pi^\pm + 1\pi^0 + X)$
 - 6. Other
- Wrong-sign ν_μ CC
 - 7. Inclusive ($\mu^+ + X$)
- ν_e CC
 - 8. Inclusive ($e^- + X$)
- NC
 - 9. Inclusive

and a similar set of 9 samples is included for the RHC (antineutrino-enhanced) beam configuration.

3.2 Choice of kinematical distributions, and of kinematical variable binning / modes

Within VALOR, a different reconstructed kinematical distribution can be fitted for each sample. For the 2016a analysis, we have chosen to fit 2-dimensional (E_{reco}, y_{reco}) distributions for all CC-like samples and 1-dimensional E_{vis} for all NC-like samples, where E_{reco} is the reconstructed neutrino energy, y_{reco} is the reconstructed inelasticity, and E_{vis} is the reconstructed visible energy.

The following binning of reconstructed kinematical variables is used:

- 10 E_{reco} (E_{vis}) bins defined by the following bin edges:
(0, 1.0, 1.4, 2.0, 3.0, 4.0, 5.0, 7.0, 10.0, 15.0, 1000) GeV
- 8 y_{reco} bins for CC-like samples defined by the following bin edges:
(0, 0.02, 0.05, 0.1, 0.2, 0.3, 0.5, 0.7, 1)
- 1 y_{reco} bins for NC-like samples.

As it was explained in the earlier sections, MC templates provide a mapping between reconstructed and true information. Separate templates are constructed for different true reaction modes m , and each template contains information on how the number of events, for each individual reconstructed bin, is distributed in a chosen N_t -dimensional space K_t of true kinematical variables. Within VALOR, not only the fit samples and the reconstructed kinematical information used for each sample, but also types of MC templates chosen

to construct the predictions for each sample, and the true kinematical information recorded in each MC template are all very flexibly defined.

In the 2016a analysis, 52 MC templates corresponding to the true reaction modes shown in Tab. 1 are constructed for each of the 18 fit samples. All ν_μ , $\bar{\nu}_\mu$, ν_e and $\bar{\nu}_e$ contributions, however small, are kept track of for each sample. This makes 936 (18×52) MC templates in all. The choice of these specific modes was driven mainly by the systematic parameter choices (see Sec. 3.4 and Appendix B). For simplicity and consistency in the application of systematic variations across different samples, the same set of models is used for all samples. Unless CPU-intensity becomes a major limitation, this choice will be maintained in subsequent revisions of this analysis.

Table 1: For each fit sample in the 2016a analysis, MC templates are constructed for the following true reaction modes.

1. ν_μ CC QE	14. $\bar{\nu}_\mu$ CC QE	27. ν_e CC QE	40. $\bar{\nu}_e$ CC QE
2. ν_μ CC MEC	15. $\bar{\nu}_\mu$ CC MEC	28. ν_e CC MEC	41. $\bar{\nu}_e$ CC MEC
3. ν_μ CC $1\pi^\pm$	16. $\bar{\nu}_\mu$ CC $1\pi^\pm$	29. ν_e CC $1\pi^\pm$	42. $\bar{\nu}_e$ CC $1\pi^\pm$
4. ν_μ CC $1\pi^0$	17. $\bar{\nu}_\mu$ CC $1\pi^0$	30. ν_e CC $1\pi^0$	43. $\bar{\nu}_e$ CC $1\pi^0$
5. ν_μ CC $2\pi^\pm$	18. $\bar{\nu}_\mu$ CC $2\pi^\pm$	31. ν_e CC $2\pi^\pm$	44. $\bar{\nu}_e$ CC $2\pi^\pm$
6. ν_μ CC $2\pi^0$	19. $\bar{\nu}_\mu$ CC $2\pi^0$	32. ν_e CC $2\pi^0$	45. $\bar{\nu}_e$ CC $2\pi^0$
7. ν_μ CC $1\pi^\pm + 1\pi^0$	20. $\bar{\nu}_\mu$ CC $1\pi^\pm + 1\pi^0$	33. ν_e CC $1\pi^\pm + 1\pi^0$	46. $\bar{\nu}_e$ CC $1\pi^\pm + 1\pi^0$
8. ν_μ CC coherent	21. $\bar{\nu}_\mu$ CC coherent	34. ν_e CC coherent	47. $\bar{\nu}_e$ CC coherent
9. ν_μ CC other	22. $\bar{\nu}_\mu$ CC other	35. ν_e CC other	48. $\bar{\nu}_e$ CC other
10. ν_μ NC $1\pi^\pm$	23. $\bar{\nu}_\mu$ NC $1\pi^\pm$	36. ν_e NC $1\pi^\pm$	49. $\bar{\nu}_e$ NC $1\pi^\pm$
11. ν_μ NC $1\pi^0$	24. $\bar{\nu}_\mu$ NC $1\pi^0$	37. ν_e NC $1\pi^0$	50. $\bar{\nu}_e$ NC $1\pi^0$
12. ν_μ NC coherent	25. $\bar{\nu}_\mu$ NC coherent	38. ν_e NC coherent	51. $\bar{\nu}_e$ NC coherent
13. ν_μ NC other	26. $\bar{\nu}_\mu$ NC other	39. ν_e NC other	52. $\bar{\nu}_e$ NC other

For each of the above MC templates, and for each multi-dimensional reconstructed kinematical bin in these templates, VALOR keeps track of the distribution in several true kinematical variables. For the 2016a analysis, VALOR stores the distribution in the (E_{true}, Q_{true}^2) space of the events in each reconstructed kinematical bin. The following true kinematical variable binning is used:

- 19 E_{true} bins defined by the following bin edges:
 $(0, 0.5, 1.0, 1.5, 2.0, 2.5, 3.0, 3.5, 4.0, 4.5, 5.0, 5.5, 6.0, 7.0, 8.0, 12.0, 16.0, 20.0, 40.0, 1000)$ GeV
- A number of Q_{true}^2 bins depending on the true reaction mode:
 - For neutrino and anti-neutrino CCQE, 3 Q_{true}^2 bins defined by the following bin edges:
 $(0, 0.20, 0.55, 1000)$ GeV 2
 - For neutrino and anti-neutrino CC $1\pi^\pm$, 3 Q_{true}^2 bins defined by the following bin edges:
 $(0, 0.30, 0.80, 1000)$ GeV 2
 - For neutrino and anti-neutrino CC $1\pi^0$, 3 Q_{true}^2 bins defined by the following bin edges:
 $(0, 0.35, 0.90, 1000)$ GeV 2
 - For all other reaction modes, 1 Q_{true}^2 bin.

3.3 Nominal predictions

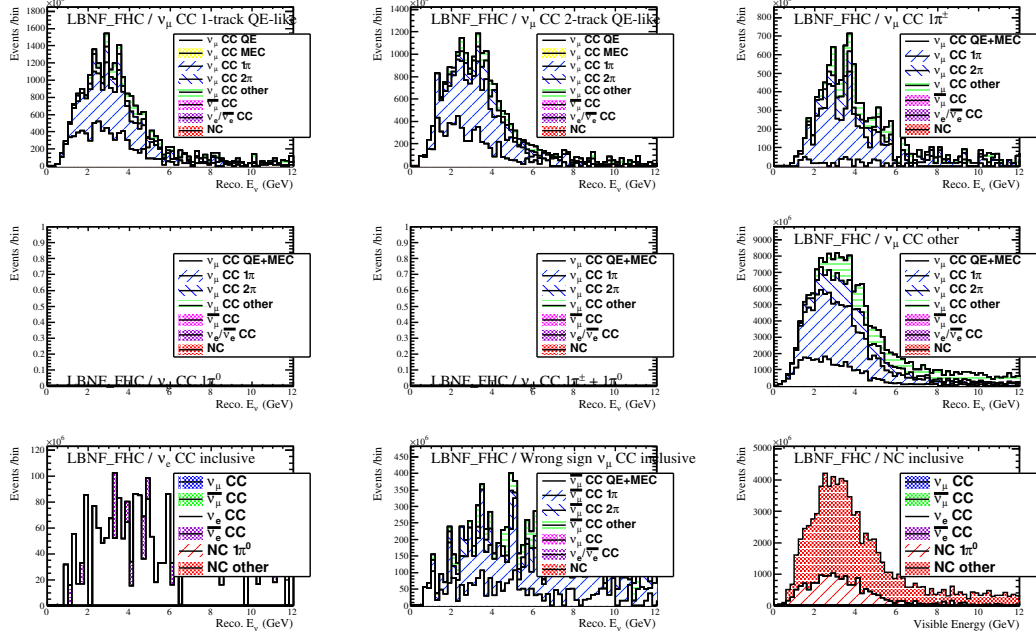


Figure 4: Reconstructed (or visible) energy spectra of all 9 FHC ND event samples of the 2016a analysis. The contribution to each spectrum from few broadly defined true event categories is shown. The plot is shown for the FGT detector, using the simulation, reconstruction and analysis cuts of the FGT group.

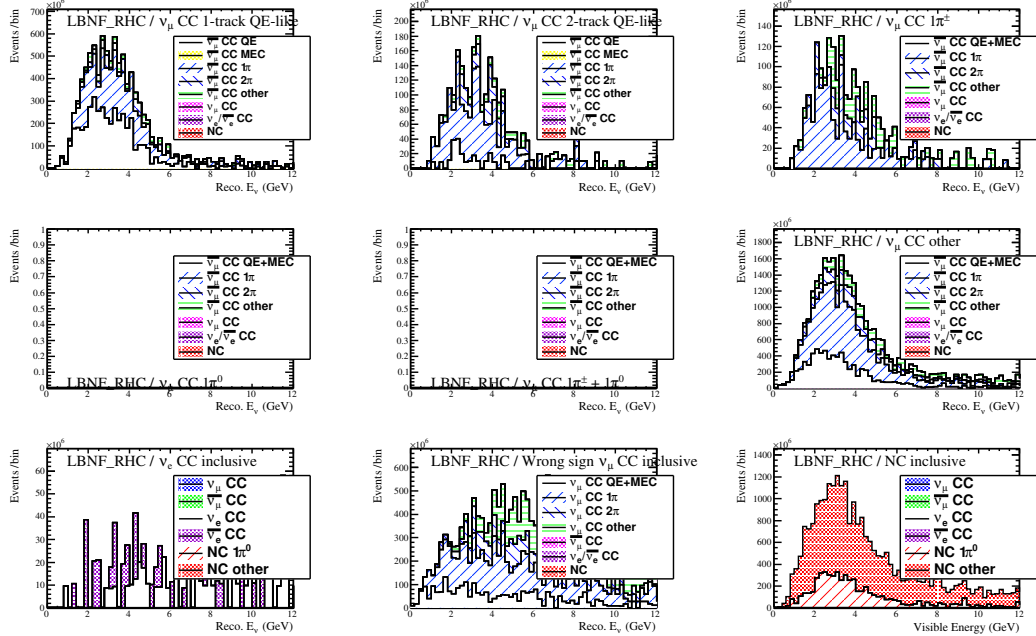


Figure 5: As in Fig. 4, but for RHC.

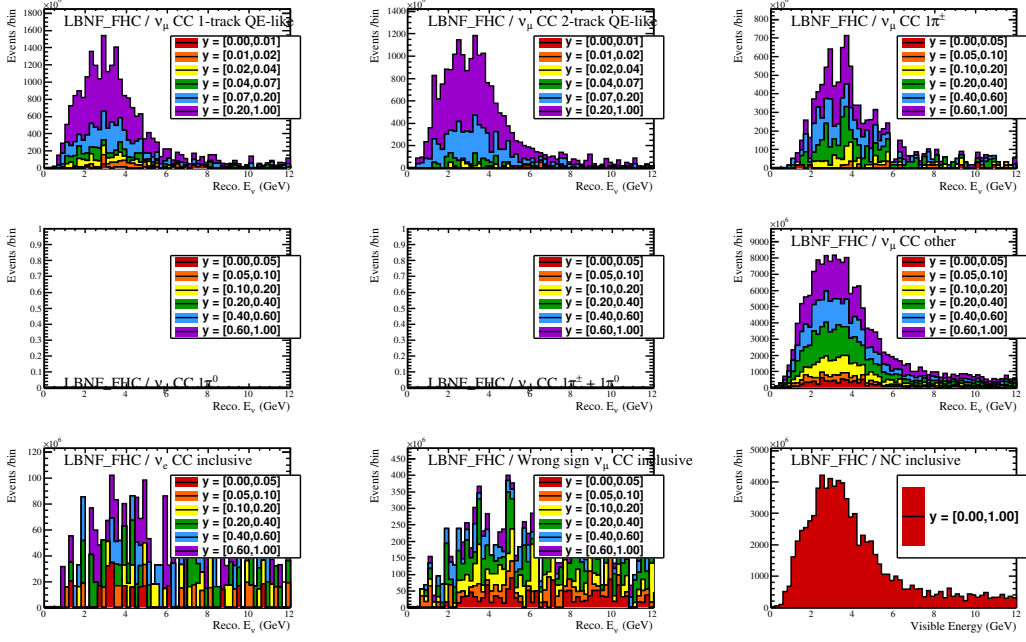


Figure 6: Reconstructed (or visible) energy spectra of all 9 FHC ND event samples of the 2016a analysis. The contribution from different reconstructed inelasticity ranges is shown. The plot is shown for the FGT detector, using the simulation, reconstruction and analysis cuts of the FGT group.

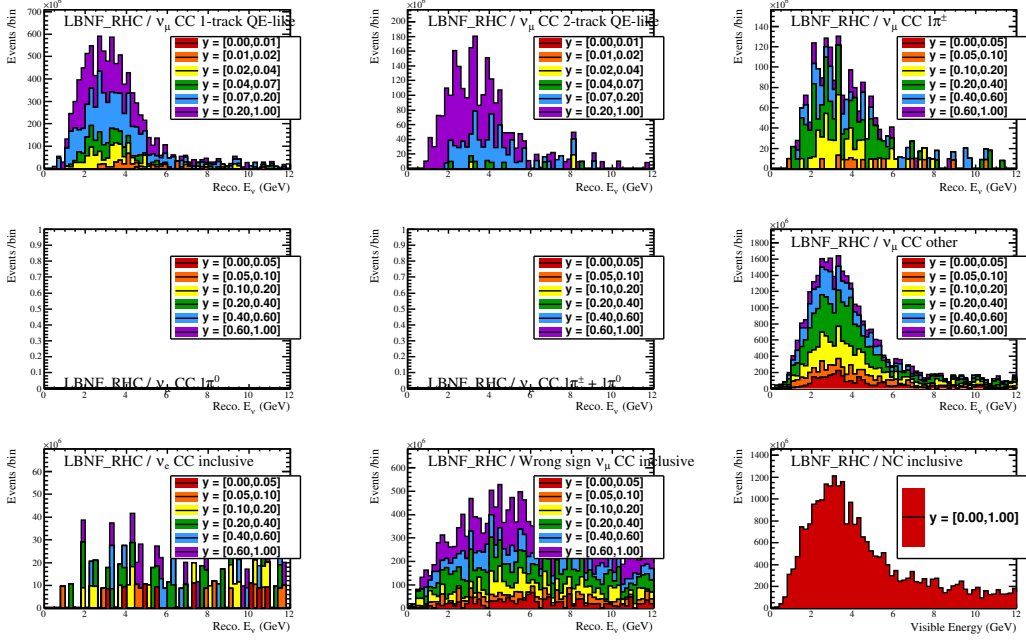


Figure 7: As in Fig. 6, but for RHC.

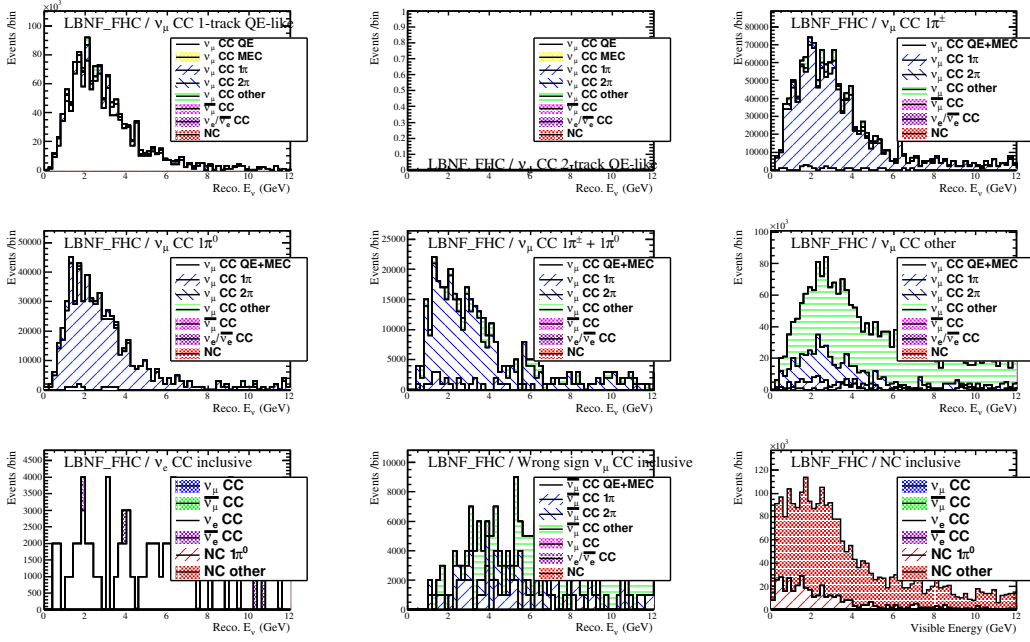


Figure 8: Reconstructed (or visible) energy spectra of all 9 FHC ND event samples of the 2016a analysis. The contribution to each spectrum from few broadly defined true event categories is shown. The plot is shown for the GArTPC detector, using the simulation, reconstruction and analysis cuts of the GArTPC group.

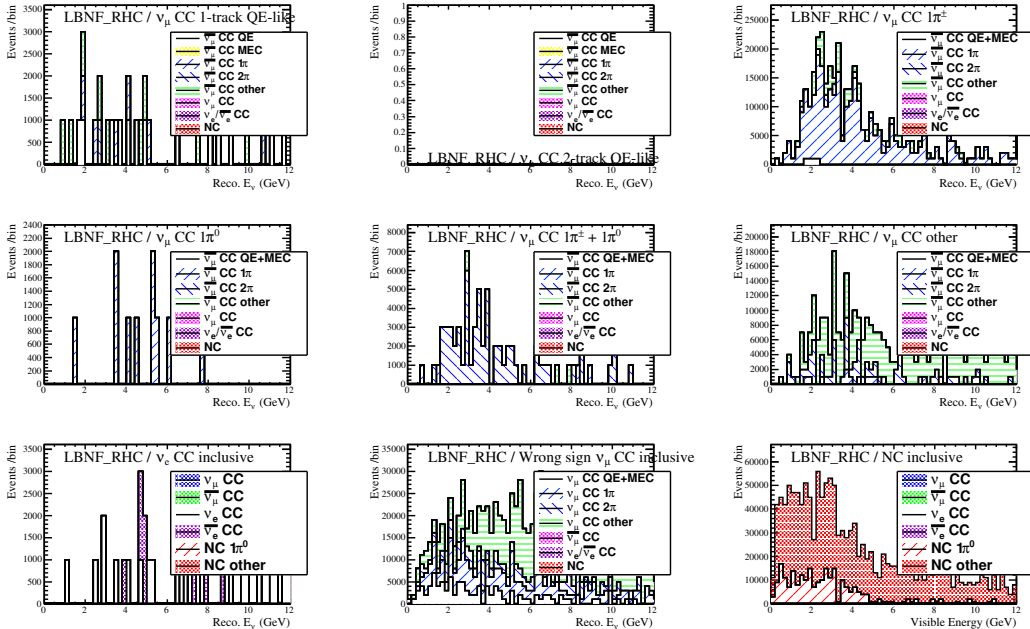


Figure 9: As in Fig. 8, but for RHC.

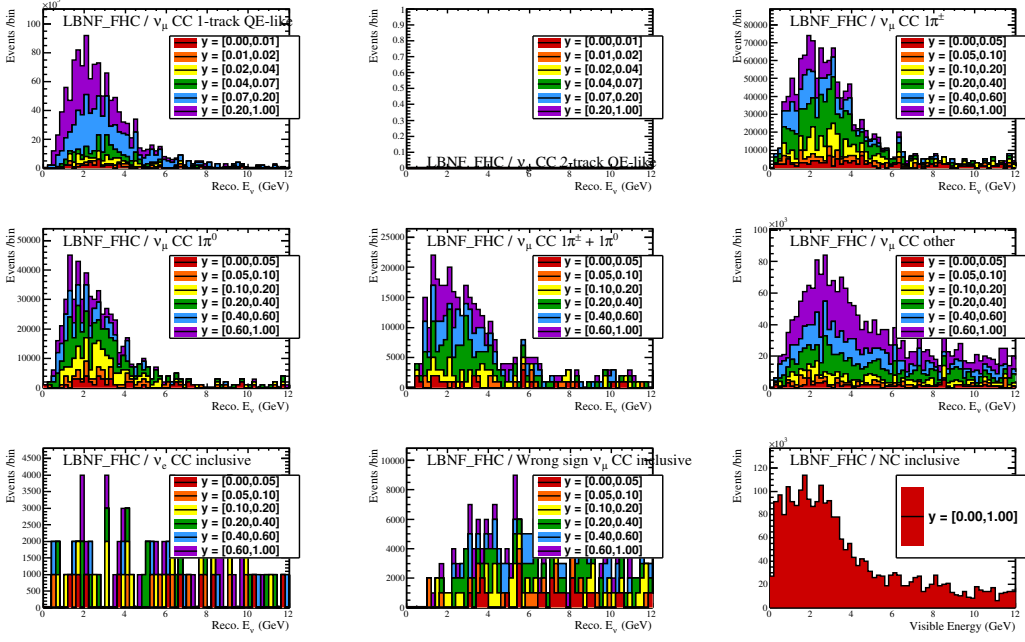


Figure 10: Reconstructed (or visible) energy spectra of all 9 FHC ND event samples of the 2016a analysis. The contribution from different reconstructed inelasticity ranges is shown. The plot is shown for the GArTPC detector, using the simulation, reconstruction and analysis cuts of the GArTPC group.

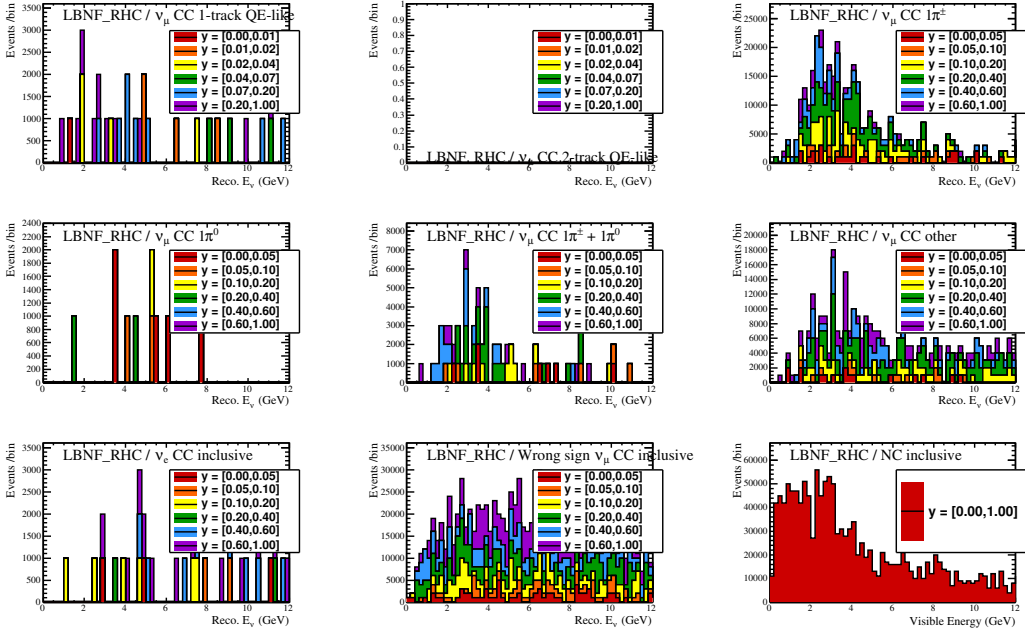


Figure 11: As in Fig. 10, but for RHC.

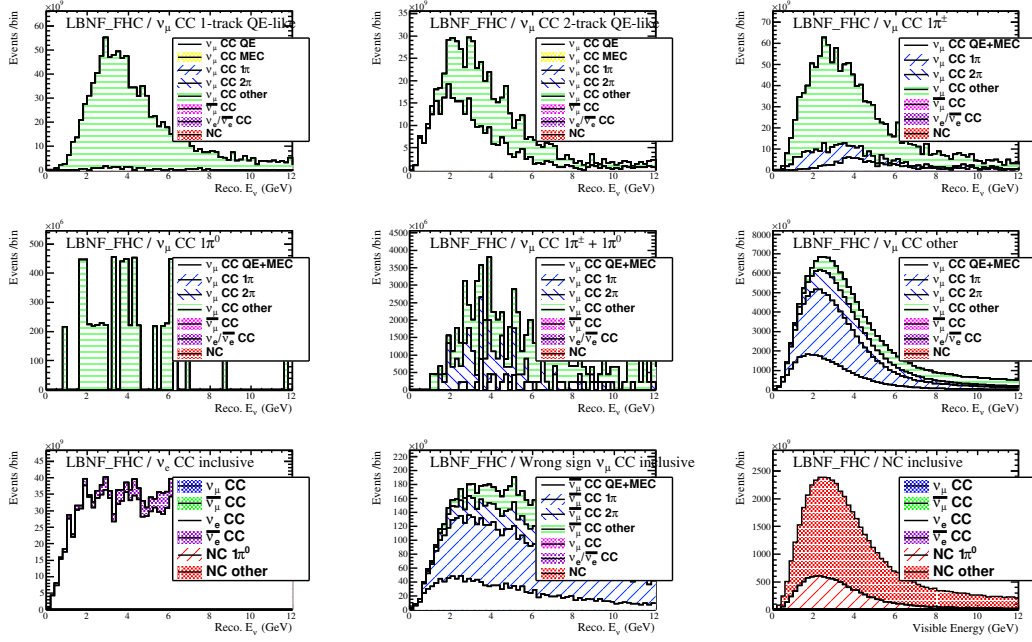


Figure 12: Reconstructed (or visible) energy spectra of all 9 FHC ND event samples of the 2016a analysis. The contribution to each spectrum from few broadly defined true event categories is shown. The plot is shown for the LArTPC detector, using the simulation, reconstruction and analysis cuts of the LArTPC group.

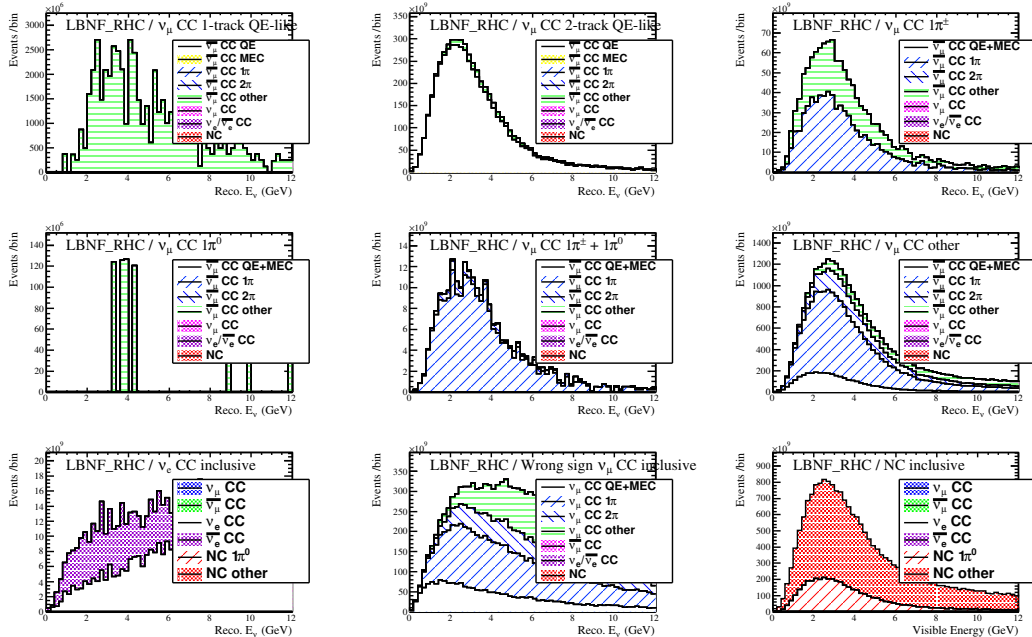


Figure 13: As in Fig. 12, but for RHC.

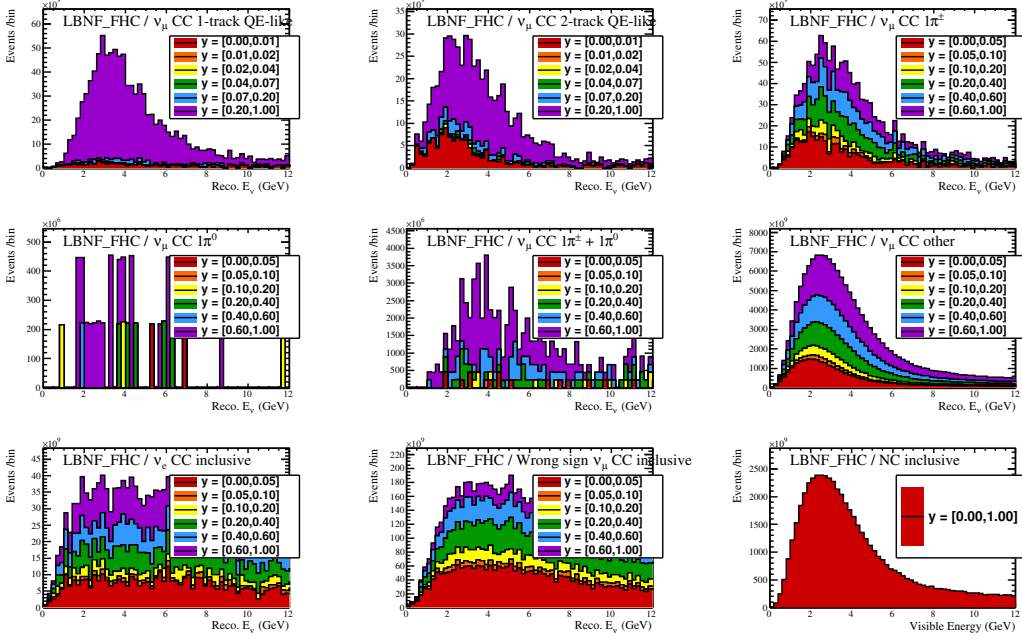


Figure 14: Reconstructed (or visible) energy spectra of all 9 FHC ND event samples of the 2016a analysis. The contribution from different reconstructed inelasticity ranges is shown. The plot is shown for the LArTPC detector, using the simulation, reconstruction and analysis cuts of the LArTPC group.

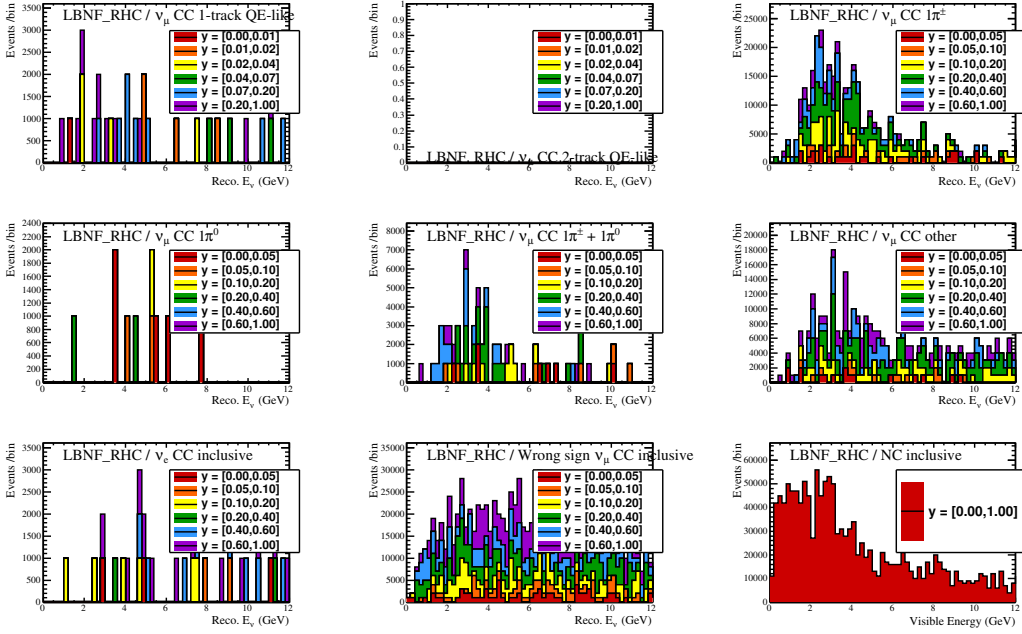


Figure 15: As in Fig. 14, but for RHC.

3.4 Systematic uncertainties

3.4.1 Flux uncertainties (MINERvA/NuMI flux error assignments)

For the prior flux uncertainties, VALOR uses the NuMI flux error analysis from MINERvA [14] as a realistic model for the LBNF flux uncertainties. Errors and covariances between different bins, corresponding to different DUNE detector locations, beam configurations, neutrino species, and true energy ranges were provided by L.Fields [15]. The following 208 linear systematic parameters were used:

- 19 ν_μ FHC Near Detector flux systematics (0 - 18)
- 19 $\bar{\nu}_\mu$ FHC Near Detector flux systematics (19 - 37)
- 7 ν_μ FHC Near Detector flux systematics (38 - 44)
- 7 $\bar{\nu}_\mu$ FHC Near Detector flux systematics (45 - 51)
- 19 ν_μ RHC Near Detector flux systematics (52 - 70)
- 19 $\bar{\nu}_\mu$ RHC Near Detector flux systematics (71 - 89)
- 7 ν_μ RHC Near Detector flux systematics (90 - 96)
- 7 $\bar{\nu}_\mu$ RHC Near Detector flux systematics (97 - 103)
- 19 ν_μ FHC Far Detector flux systematics (104 - 122)
- 19 $\bar{\nu}_\mu$ FHC Far Detector flux systematics (123 - 129)
- 7 ν_μ FHC Far Detector flux systematics (130 - 136)
- 7 $\bar{\nu}_\mu$ FHC Far Detector flux systematics (137 - 155)
- 19 ν_μ RHC Far Detector flux systematics (156 - 174)
- 19 $\bar{\nu}_\mu$ RHC Far Detector flux systematics (175 - 193)
- 7 ν_μ RHC Far Detector flux systematics (194 - 200)
- 7 $\bar{\nu}_\mu$ RHC Far Detector flux systematics (201 - 207)

Each systematic corresponds to a true neutrino energy range. The following vector of bin edges defines the 19 ν_μ / $\bar{\nu}_\mu$ bins: (0.0, 0.5, 1.0, 1.5, 2.0, 2.5, 3.0, 3.5, 4.0, 4.5, 5.0, 5.5, 6.0, 7.0, 8.0, 12.0, 16.0, 20.0, 40.0, 100.0) GeV. The following bin edges defines the 7 ν_e / $\bar{\nu}_e$ bins: (0.0, 2.0, 4.0, 6.0, 8.0, 10.0, 20.0, 100.0) GeV. The corresponding 208×208 covariance matrix is shown in Fig. 16.

In the 2016a VALOR DUNE analysis, where only Near Detector samples are included in a systematics constraint fit, only the first 104×104 block of that covariance matrix relevant to the Near Detector flux is used. The full matrix is implemented and will be used for the joint oscillation and systematics constraint fit of the 2016b VALOR DUNE analysis.

3.4.2 Neutrino interaction uncertainties (2016a VALOR/GENIE error assignments)

For the 2016a analysis, we considered 43 neutrino interaction systematics (2016a VALOR GENIE systematics) parameterizing the uncertainties on a wide range of neutrino interaction modelling aspects relevant to DUNE. Only 6 systematics were used in the previous pass-through, so the 2016a VALOR GENIE set is a marked improvement providing several new neutrino interaction physics handles. The chosen set of neutrino interaction systematics is not final (studies are ongoing). This set was judged to be sufficient for the purposes and the physics content of the 2nd pass-through and it represents a well-judged incremental upgrade of the VALOR DUNE fit. A further incremental upgrade will be installed in the 2016b analysis, in preparation for

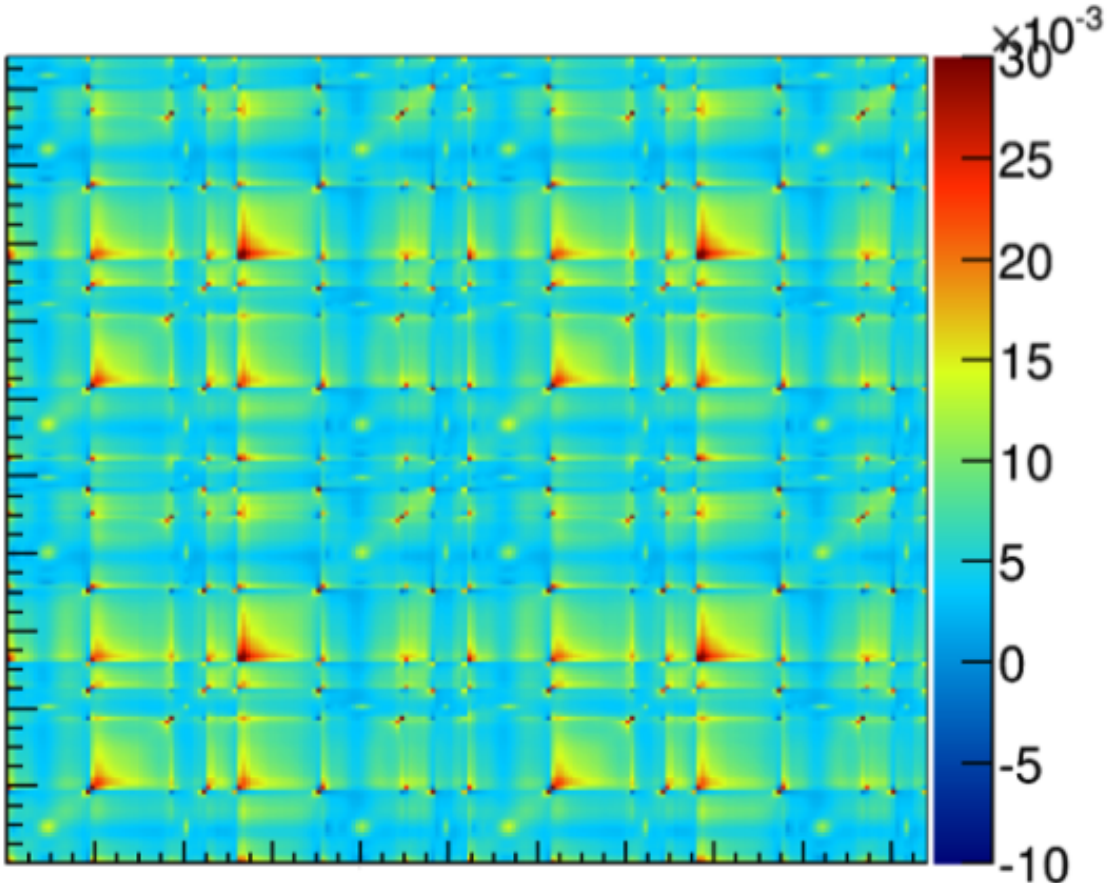


Figure 16: Graphical representation of the 208×208 LBNF flux correlation matrix [15] used in the VALOR DUNE analysis. See main text for description of the 208 bins.

the 3rd pass-through. This upgrade will be informed by the progress towards the release of GENIE v3.0.0, as well as by the validation and understanding of the present VALOR DUNE fit performance and by VALOR DUNE physics studies. Largely model-independent neutrino interaction systematics were used. This choice will enable us to easily move the VALOR DUNE analysis from the present version of GENIE to the retuned version of GENIE (v3.0.0) once it becomes available later this year.

For the DUNE oscillation sensitivity simulation and Near Detector optimization task, we want to give the VALOR fit sufficient freedom to vary the cross-section model and, also, ensure that it is the Near Detector data and not the priors that drive the DUNE systematics constraint. Therefore, all assigned uncertainties should be manifestly amply conservative. Appropriately conservative prior uncertainties were calculated by the VALOR group, using the GENIE event re-weighting tools. Several comparisons with external data were performed in collaboration with the GENIE group, in support of the systematic error assignments used in this analysis. Some of these data/MC comparisons are shown in Appendix A. The GENIE systematic error assignments and the supporting comparisons against external data will be revised in each iteration of the VALOR DUNE analysis. Improvements will be underpinned by the rapidly expanding GENIE arsenal of data/MC comparison and error analysis tools.

The following neutrino interaction systematic parameters were included in the 2016a analysis:

- 3 ν_μ CCQE systematics (0-2) for the following true kinematical bins:

- i) $Q^2 < 0.2 \text{ GeV}^2$, ii) $0.2 \text{ GeV}^2 < Q^2 < 0.55 \text{ GeV}^2$, iii) $Q^2 > 0.55 \text{ GeV}^2$
- 3 $\bar{\nu}_\mu$ CCQE systematics (3-5) for the following true kinematical bins:
i) $Q^2 < 0.2 \text{ GeV}^2$, ii) $0.2 \text{ GeV}^2 < Q^2 < 0.55 \text{ GeV}^2$, iii) $Q^2 > 0.55 \text{ GeV}^2$
- 1 ν_μ CC MEC systematic (6)
- 1 $\bar{\nu}_\mu$ CC MEC systematic (7)
- 3 ν_μ CC $1\pi^\pm$ systematics (8-10) for the following true kinematical bins:
i) $Q^2 < 0.3 \text{ GeV}^2$, ii) $0.3 \text{ GeV}^2 < Q^2 < 0.8 \text{ GeV}^2$, iii) $Q^2 > 0.8 \text{ GeV}^2$
- 3 $\bar{\nu}_\mu$ CC $1\pi^\pm$ systematics (11-13) for the following true kinematical bins:
i) $Q^2 < 0.3 \text{ GeV}^2$, ii) $0.3 \text{ GeV}^2 < Q^2 < 0.8 \text{ GeV}^2$, iii) $Q^2 > 0.8 \text{ GeV}^2$
- 3 ν_μ CC $1\pi^0$ systematics (14-16) for the following true kinematical bins:
i) $Q^2 < 0.35 \text{ GeV}^2$, ii) $0.35 \text{ GeV}^2 < Q^2 < 0.9 \text{ GeV}^2$, iii) $Q^2 > 0.9 \text{ GeV}^2$
- 3 $\bar{\nu}_\mu$ CC $1\pi^0$ systematics (17-19) for the following true kinematical bins:
i) $Q^2 < 0.35 \text{ GeV}^2$, ii) $0.35 \text{ GeV}^2 < Q^2 < 0.9 \text{ GeV}^2$, iii) $Q^2 > 0.9 \text{ GeV}^2$
- 1 ν_μ CC 2π systematic (20)
- 1 $\bar{\nu}_\mu$ CC 2π systematic (21)
- 3 ν_μ CC DIS systematics (22-24) for the following true kinematical bins:
i) $E_\nu < 7.5 \text{ GeV}$, ii) $7.5 \text{ GeV} < E_\nu < 15 \text{ GeV}$, iii) $E_\nu > 15 \text{ GeV}$
- 3 $\bar{\nu}_\mu$ CC DIS systematics (25-27) for the following true kinematical bins:
i) $E_\nu < 7.5 \text{ GeV}$, ii) $7.5 \text{ GeV} < E_\nu < 15 \text{ GeV}$, iii) $E_\nu > 15 \text{ GeV}$
- 1 ν_μ CC coherent systematic (28)
- 1 $\bar{\nu}_\mu$ CC coherent systematic (29)
- 1 ν_μ NC systematic (30)
- 1 $\bar{\nu}_\mu$ NC systematic (31)
- 1 ν_e/ν_μ cross-section ratio systematic (32)
- 10 final state re-interaction (FSI) systematics (33-42):
 - pion mean free path, controlling the pions re-interaction rate (33)
 - nucleon mean free path, controlling the nucleon re-interaction rate (34)
 - fraction of rescattered pions in charge exchange channels (35)
 - fraction of rescattered pions in inelastic channels (36)
 - fraction of rescattered pions in absorption channels (37)
 - fraction of rescattered pions in pion production channels (38)
 - fraction of rescattered nucleons in charge exchange channels (39)
 - fraction of rescattered nucleons in inelastic channels (40)
 - fraction of rescattered nucleons in absorption channels (41)
 - fraction of rescattered nucleons in pion production channels (42)

The first 33 parameters describe the uncertainty in the cross-section for the corresponding process in the *absence* of FSI effects. They are linear systematics (see Sec. 2.2) and they are applied in the appropriate kinematical range of MC templates corresponding to the appropriate true reaction mode as shown in Appendix B. The last 10 systematic parameters parameterize FSI effects. They are non-linear systematics and they are applied to every single multi-dimensional kinematical bin, of each one of the 52 MC templates used for each one of the 18 fit samples of the present analysis. The response of each individual bin to each of the 10 FSI systematics was pre-computed for a range of values of each systematic. Using the pre-computed values, the response of each bin was parameterized using cubic splines (68,400 cubic splines were used for the 2016a analysis, and they are interrogated during the process of producing any single set of VALOR DUNE predictions). Separate response functions were calculated for each of the 3 detector options, using the outputs of the corresponding simulation chain. The kinematical ranges listed above were chosen to ensure sufficient statistics in each bin, but will be further informed by studies of the kinematical dependence of GENIE error envelopes.

Initially, a covariance matrix for the first 32 systematic parameters listed above was computed. The procedure itself is largely model agnostic, and translates it the effect of several model-dependent parameters to an appropriately chosen set of primarily linear model-independent ones. A sample of 100k ν_μ and 100k $\bar{\nu}_\mu$ events was generated using GENIE v2.10.6 and the LBNF flux used for the 2015 Conceptual Design Report (CDR) [35] (which is available at [36]). The 80 GeV, 204 x 4 m DP version of the Reference Beam was used. Using reweighting tools available in GENIE v2.10.6 [17], these event samples were reweighted by tweaking physics modelling parameters (listed in Tab. 2) specific to the v2.10.6 default model and tune. Two different methods were used to construct the covariance matrix that was then input to the VALOR DUNE fit.

Method A:

Firstly, in order to obtain the most conservative prior errors possible to construct our covariance matrix, we calculate the effect of the 1σ variation of each GENIE model parameter listed in Tab. 2. In this method, each GENIE model parameter is varied to $\pm 1\sigma$ independently (with the exception of those taken to be covariant as stated in Tab. 2, which are varied together), avoiding therefore potential cancellations that may occur when several of parameters affecting the same bins are tweaked at the same time. However, since this method is varying model parameters independently, it does not allow to obtain all the correlations between the different bins (e.g. between CCQE and CC1 π bins). Thus, another complementary method will be necessary in order to obtain all the correlations between the bins of our covariance matrix, and it will be described later.

By varying each model parameter, we can calculate the tweaked number of events in each bin as the sum of event weights, and compute the usual covariance matrix elements for each GENIE model parameter. Notice that in this first method only the computation of the diagonal elements of the covariance matrix is necessary, since the correlations will be calculated with the second method. Let n_i^p be the number of events in the i^{th} bin when varying the systematic parameter p . The diagonal element of the covariance matrix for one model parameter p is then computed as:

$$(C_{ii}^{(A)})_p = (n_i^p - n_i^{nom})^2 \quad (33)$$

where n_i^{nom} is the nominal number of events, i.e. the number of events in the i^{th} bin when no variations of the parameters are done, and they remain to their default values. The total covariance matrix taking into account the effect of all the GENIE model parameters would be then calculated as the sum in quadrature of all the independent elements described above:

$$C_{ii}^{(A)} = \sum_{p=1}^{N_{params}} (C_{ii}^{(A)})_p = \sum_{p=1}^{N_{params}} (n_i^p - n_i^{nom})^2 \quad (34)$$

And the fractional covariance matrix elements are:

$$C_{ii,frac}^{(A)} = \frac{C_{ij}^A}{n_i^{nom} \cdot n_j^{nom}} \quad (35)$$

which allow us to obtain the 1σ error in each bin simply as:

$$\sigma_i^{(A)} = \sqrt{C_{ii,frac}^{(A)}} \quad (36)$$

This method was followed for $+1\sigma$ and -1σ variations of the GENIE model parameters, and the final matrix was constructed using the maximum $\sigma_i^{(A)}$ produced. The comparison of the $\sigma_i^{(A)}$ elements using $+1\sigma$ and -1σ variations of the GENIE model parameters will be illustrated in Fig. 17.

Method B:

In order to obtain the correlations between all the parameters in our covariance matrix, we implemented another method in which all GENIE model parameter listed in Tab. 2 were varied simultaneously. Each parameter was drawn from a normal distribution, centred at the nominal value, with the 1σ error recommended by the GENIE group [17]. For each randomly drawn set of GENIE model parameters, the number of the events (i.e. the sum of event weights) belonging in each of the 32 “bins” (i.e. the true primary reaction type and kinematical variable range corresponding to the first 32 model-independent parameters) was calculated. Let n_i^k be the number of events in the i^{th} bin as computed at the k^{th} randomly drawn set of GENIE model parameters. The (i,j) element of the covariance matrix $C^{(A)}$ was calculated as:

$$C_{ij}^{(B)} = \frac{\sum_{k=1}^N (n_i^k - n_i^{nom})(n_j^k - n_j^{nom})}{N} \quad (37)$$

where n_i^{nom} is the nominal value corresponding to the i^{th} bin no parameters varied. Typically, in this analysis, N is of the order of 20k. The fractional covariance matrix is then calculated by:

$$C_{ij,frac}^{(B)} = \frac{C_{ij}^B}{n_i^{nom} \cdot n_j^{nom}} \quad (38)$$

This (fractional) covariance matrix gives us the correlations between all bins when tweaking all the GENIE model parameters at the same time. These correlations are used to build the final matrix in combination with the errors obtained with the previous method, and they are calculated as follows:

$$Cor_{ij}^{(B)} = \frac{C_{ij}^B}{C_{ii}^B \cdot C_{jj}^B} \quad (39)$$

Combination of methods A and B:

To build the final covariance matrix, we can combine the errors calculated avoiding cancellations by following method A, i.e. $\sigma_i^{(A)}$, with the correlations obtained tweaking all the GENIE model parameters at the same time in method B. The final (fractional) covariance matrix is then calculated as follows:

$$C_{ij} = Cor_{ij}^{(B)} \cdot \sqrt{(C_{ii}^{(A)} \cdot C_{jj}^{(A)})} \quad (40)$$

$$C_{ij,frac} = \frac{C_{ij}}{n_i^{nom} \cdot n_j^{nom}} \quad (41)$$

Table 2: GENIE v2.10.6 parameters x_P (each affecting the physics quantity P) varied for the calculation of the 32×32 covariance matrix (see text).

x_P	Description of P	GENIE R/W param	Frac. Err
$x_{M_A^{NCEL}}$	Axial mass for NC elastic; It affects $d\sigma(NCEL)/dQ^2$ both in shape and normalization	kXSecTwkDial.MaNCEL, taken to be covariant with kXSecTwkDial.MaCCQE	$\pm 25\%$
$x_{\eta^{NCEL}}$	Strange axial form factor η NC elastic; It affects $d\sigma(NCEL)/dQ^2$ both in shape and normalization	kXSecTwkDial.EtaNCEL	$\pm 30\%$
$x_{M_A^{CCQE}}$	Axial mass for CC quasi-elastic; It affects $d\sigma(CCQE)/dQ^2$ both in shape and normalization	kXSecTwkDial.MaCCQE	$-15\% + 25\%$
$x_{M_A^{CCRES}}$	Axial mass for CC resonance neutrino production; It affects $d^2\sigma(CCRES)/dWdQ^2$ both in shape and normalization	kXSecTwkDial.MaCCRES	$\pm 20\%$
$x_{M_V^{CCRES}}$	Vector mass for CC resonance neutrino production; It affects $d^2\sigma(CCRES)/dWdQ^2$ both in shape and normalization	kXSecTwkDial.MvCCRES	$\pm 10\%$
$x_{M_A^{CCRES}}$	Axial mass for NC resonance neutrino production; It affects $d^2\sigma(CCRES)/dWdQ^2$ both in shape and normalization	kXSecTwkDial.MaNCRES, taken to be covariant with kXSecTwkDial.MaCCRES	$\pm 20\%$
$x_{M_V^{CCRES}}$	Vector mass for NC resonance neutrino production; It affects $d^2\sigma(CCRES)/dWdQ^2$ both in shape and normalization	kXSecTwkDial.MvNCRES, taken to be covariant with kXSecTwkDial.MvCCRES	$\pm 10\%$
$x_{R_{bkg}^{\nu p, CC1\pi}}$	Non-resonance background in the νp CC1 π channel	kXSecTwkDial.RvpCC1pi	$\pm 50\%$
$x_{R_{bkg}^{\nu p, CC2\pi}}$	Non-resonance background in the νp CC2 π channel	kXSecTwkDial.RvpCC2pi	$\pm 50\%$
$x_{R_{bkg}^{\nu p, NC1\pi}}$	Non-resonance background in the νp NC1 π channel	kXSecTwkDial.RvpNC1pi	$\pm 50\%$
$x_{R_{bkg}^{\nu p, NC2\pi}}$	Non-resonance background in the νp NC2 π channel	kXSecTwkDial.RvpNC2pi	$\pm 50\%$
$x_{R_{bkg}^{\nu n, CC1\pi}}$	Non-resonance background in the νn CC1 π channel	kXSecTwkDial.RvnCC1pi	$\pm 50\%$
$x_{R_{bkg}^{\nu n, CC2\pi}}$	Non-resonance background in the νn CC2 π channel	kXSecTwkDial.RvnCC2pi	$\pm 50\%$
$x_{R_{bkg}^{\nu n, NC1\pi}}$	Non-resonance background in the νn NC1 π channel	kXSecTwkDial.RvnNC1pi	$\pm 50\%$
$x_{R_{bkg}^{\nu n, NC2\pi}}$	Non-resonance background in the νn NC2 π channel	kXSecTwkDial.RvnNC2pi	$\pm 50\%$
$x_{R_{bkg}^{\bar{\nu} p, CC1\pi}}$	Non-resonance background in the $\bar{\nu} p$ CC1 π channel	kXSecTwkDial.RvbarpCC1pi	$\pm 50\%$
$x_{R_{bkg}^{\bar{\nu} p, CC2\pi}}$	Non-resonance background in the $\bar{\nu} p$ CC2 π channel	kXSecTwkDial.RvbarpCC2pi	$\pm 50\%$
$x_{R_{bkg}^{\bar{\nu} p, NC1\pi}}$	Non-resonance background in the $\bar{\nu} p$ NC1 π channel	kXSecTwkDial.RvbarpNC1pi	$\pm 50\%$
$x_{R_{bkg}^{\bar{\nu} p, NC2\pi}}$	Non-resonance background in the $\bar{\nu} p$ NC2 π channel	kXSecTwkDial.RvbarpNC2pi	$\pm 50\%$
$x_{R_{bkg}^{\bar{\nu} n, CC1\pi}}$	Non-resonance background in the $\bar{\nu} n$ CC1 π channel	kXSecTwkDial.RvbarnCC1pi	$\pm 50\%$
$x_{R_{bkg}^{\bar{\nu} n, CC2\pi}}$	Non-resonance background in the $\bar{\nu} n$ CC2 π channel	kXSecTwkDial.RvbarnCC2pi	$\pm 50\%$
$x_{R_{bkg}^{\bar{\nu} n, NC1\pi}}$	Non-resonance background in the $\bar{\nu} n$ NC1 π channel	kXSecTwkDial.RvbarnNC1pi	$\pm 50\%$
$x_{R_{bkg}^{\bar{\nu} n, NC2\pi}}$	Non-resonance background in the $\bar{\nu} n$ NC2 π channel	kXSecTwkDial.RvbarnNC2pi	$\pm 50\%$
$x_{A_{HT}^{BY}}$	A_{HT} higher-twist parameter in scaling variable ξ_w	kXSecTwkDial.AhtBY	$\pm 25\%$
$x_{B_{HT}^{BY}}$	B_{HT} higher-twist parameter in scaling variable ξ_w	kXSecTwkDial.BhtBY	$\pm 25\%$
$x_{C_{V1u}^{BY}}$	C_{V1u} u valence GRV98LO PDF correction parameter	kXSecTwkDial.CV1uBY	$\pm 30\%$
$x_{C_{V2u}^{BY}}$	C_{V2u} u valence GRV98LO PDF correction parameter	kXSecTwkDial.CV2uBY	$\pm 40\%$
$x_{M_A^{COH\pi}}$	Axial mass for NC and CC coherent production of pions; It affects $d\sigma(Coh)/dxdy$ both in shape and normalization	kXSecTwkDial.MaCOHpi	$\pm 50\%$
$x_{R_0^{COH\pi}}$	Nuclear size parameter controlling π absorption in NC and CC coherent production of pions; It affects $d\sigma(Coh)/dxdy$ both in shape and normalization	kXSecTwkDial.R0COHpi	$\pm 10\%$

$x_{BR}^{R \rightarrow X + \gamma}$	Branching ratio for radiative resonance decays (e.g. $\Delta^+(1232) \rightarrow p + \gamma$)	kRDcyTwkDial_BR1gamma	$\pm 50\%$
$x_{BR}^{R \rightarrow X + \eta}$	Branching ratio for singe- η resonance decays (e.g. $N^+(1440) \rightarrow p + \eta$)	kRDcyTwkDial_BR1eta	$\pm 50\%$

With 43 neutrino interaction systematic parameters defined, the VALOR DUNE fit expects a 43×43 neutrino interaction covariance matrix, which is then used to construct a block-diagonal matrix of all VALOR DUNE flux, interaction and detector systematics. The larger neutrino interaction covariance matrix is constructed from the 32×32 one by adding the remaining 11 elements in the diagonal. Element 33 is a ν_e/ν_μ cross-section ratio systematic which is assumed to be 3% and is taken to be uncorrelated with all other systematics. The 10 elements 34-42 are the FSI systematics described above. Although in the covariance matrix the FSI parameters (mean free paths, and fraction of rescattered hadrons in different channels) are taken to be uncorrelated with other systematic parameters, *correlations between all kinematical bins used in the 2016a analysis are taken into account*. Indeed, as it was mentioned above, all 10 FSI systematics are non-linear ones and response functions were pre-computed for each multi-dimensional kinematical bin.

These response functions were computed using the GENIE event reweighting. Each of the GENIE model parameters listed in Tab. 3 was set to 11 uniformly distributed values in the -5σ to $+5\sigma$ range. For each value, the number of events in each kinematic bin was calculated and recorded for the construction of the response functions. As it can be noted, there is one-to-one correspondence between the VALOR FSI systematics 33-42 and the 10 GENIE FSI model (INTRANUKE/hA) parameters listed in Tab. 3. However, these INTRANUKE/hA parameters are evidently model-independent and, in principle, they could be defined for any intranuclear cascade Monte Carlo. Readers familiar with the GENIE physics simulations may notice that from the 5 “hadron fates” defined by INTRANUKE/hA for each type of hadron, only 4 are used below. Indeed, the GENIE parameters x_{el}^h ($h = \pi, N$) controlling the fraction of elastically rescattered hadrons is not set explicitly during the construction of the response functions, and there is not corresponding VALOR systematic. However, this parameter is always allowed to float internally and it acts as a *cushion* term (for details, see [17]) ensuring unitarity of the reweighted simulations, i.e. that the sum, over all channels, of the fraction of rescattered hadrons is always 1.

Table 3: GENIE v2.10.6 parameters x_P (each affecting the physics quantity P) varied for the calculation of the FSI systematic response functions for each kinematic bin (see text).

x_P	Description of P	GENIE R/W param	Frac. Err
x_{mfp}^π	Pion mean free path; It affects the total pion rescattering probability	kINukeTwkDial_MFP_pi	$\pm 20\%$
x_{mfp}^N	Nucleon mean free path; It affects the total nucleon rescattering probability	kINukeTwkDial_MFP_N	$\pm 20\%$
x_{cex}^π	Fraction of rescattered pions in charge exchange channels	kINukeTwkDial_FrCEEx_pi	$\pm 50\%$
x_{inel}^π	Fraction of rescattered pions in inelastic channels	kINukeTwkDial_FrInel_pi	$\pm 40\%$
x_{abs}^π	Fraction of rescattered pions in absorption channels	kINukeTwkDial_FrAbs_pi	$\pm 30\%$
x_{abs}^π	Fraction of rescattered pions in pion production channels	kINukeTwkDial_FrPiProd_pi	$\pm 20\%$
x_{cex}^N	Fraction of rescattered nucleons in charge exchange channels	kINukeTwkDial_FrCEEx_N	$\pm 50\%$
x_{inel}^N	Fraction of rescattered nucleons in inelastic channels	kINukeTwkDial_FrInel_N	$\pm 40\%$
x_{abs}^N	Fraction of rescattered nucleons in absorption channels	kINukeTwkDial_FrAbs_N	$\pm 20\%$
x_{abs}^N	Fraction of rescattered nucleons in pion production channels	kINukeTwkDial_FrPiProd_N	$\pm 20\%$

The result for the fractional covariance matrix and correlation matrix are illustrated in Figs. 18 and 19 respectively.

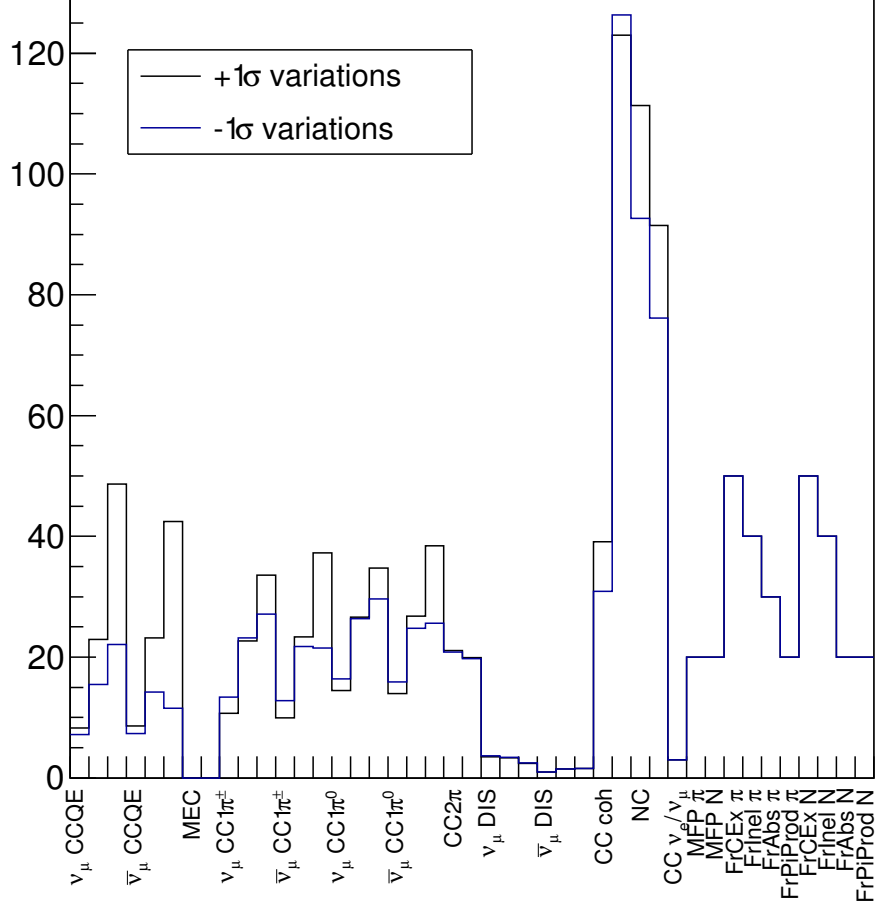


Figure 17: Comparison of the $\sigma_i^{(A)}$ elements using $+1\sigma$ and -1σ variations of the GENIE model parameters in the construction of the covariance matrix (method A). The maximum values of $\sigma_i^{(A)}$ between the ones calculated for $+1\sigma$ and -1σ variations will be used for the final covariance matrix.

3.4.3 Detector acceptance uncertainties (tentative)

For the 2016a analysis, simplistic and tentative detector acceptance parameters and uncertainties were used. When more realistic detector uncertainties are available from detailed studies using the actual simulation, reconstruction and event selection chain by each detector group, the VALOR group will adopt the recommendations of each detector group. For this analysis, as no better input has been provided, a simple 10% efficiency is assumed for the 9 efficiencies included in this analysis. Those efficiencies are the ones for the different samples, which are defined by the final state topologies. Specifically, they are:

- ν_μ CC / 1-track QE enhanced sample efficiency

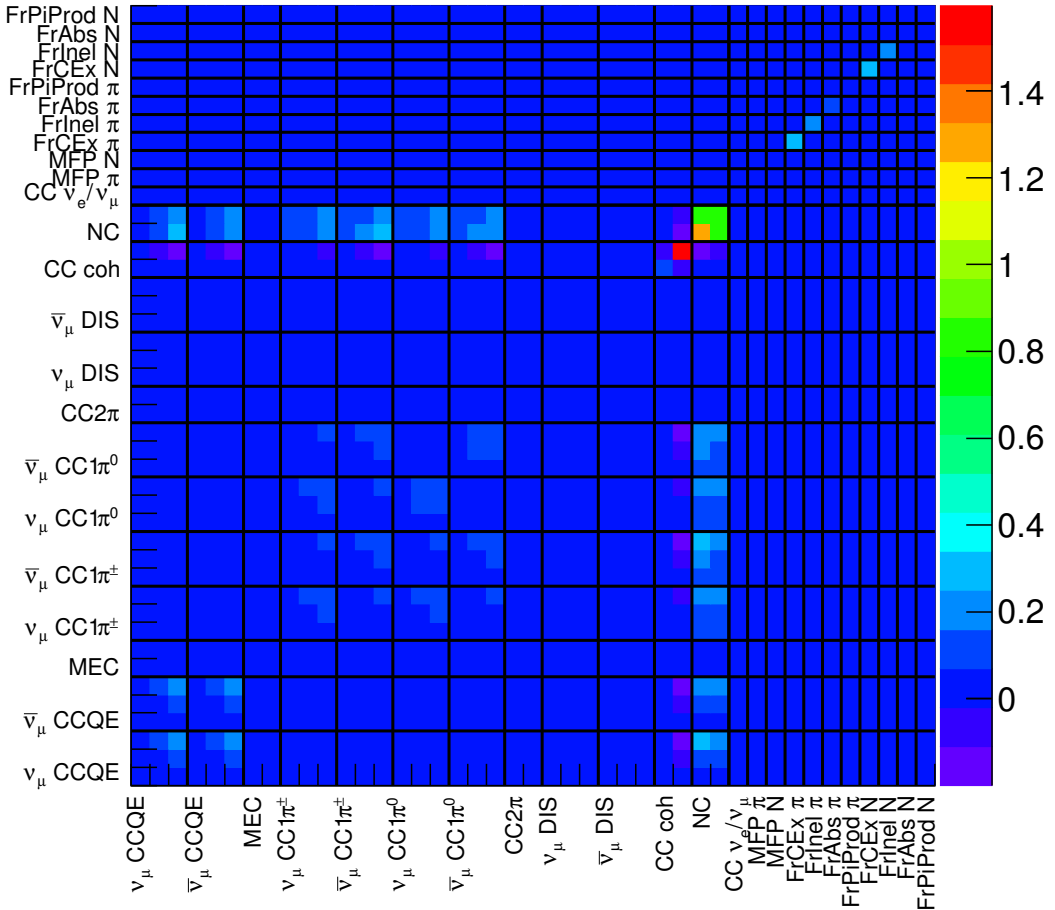


Figure 18: Graphical representation of the VALOR 2016a neutrino interaction fractional covariance matrix computed using GENIE v2.10.6 [16].

- ν_μ CC / 2-track QE enhanced sample efficiency
- ν_μ CC / $1\pi^\pm$ sample efficiency
- ν_μ CC / $1\pi^0$ sample efficiency
- ν_μ CC / $1\pi^\pm + 1\pi^0$ sample efficiency
- ν_μ CC / Other sample efficiency
- ν_e CC inclusive sample efficiency
- Wrong-sign ν_μ CC inclusive sample efficiency
- NC inclusive sample efficiency

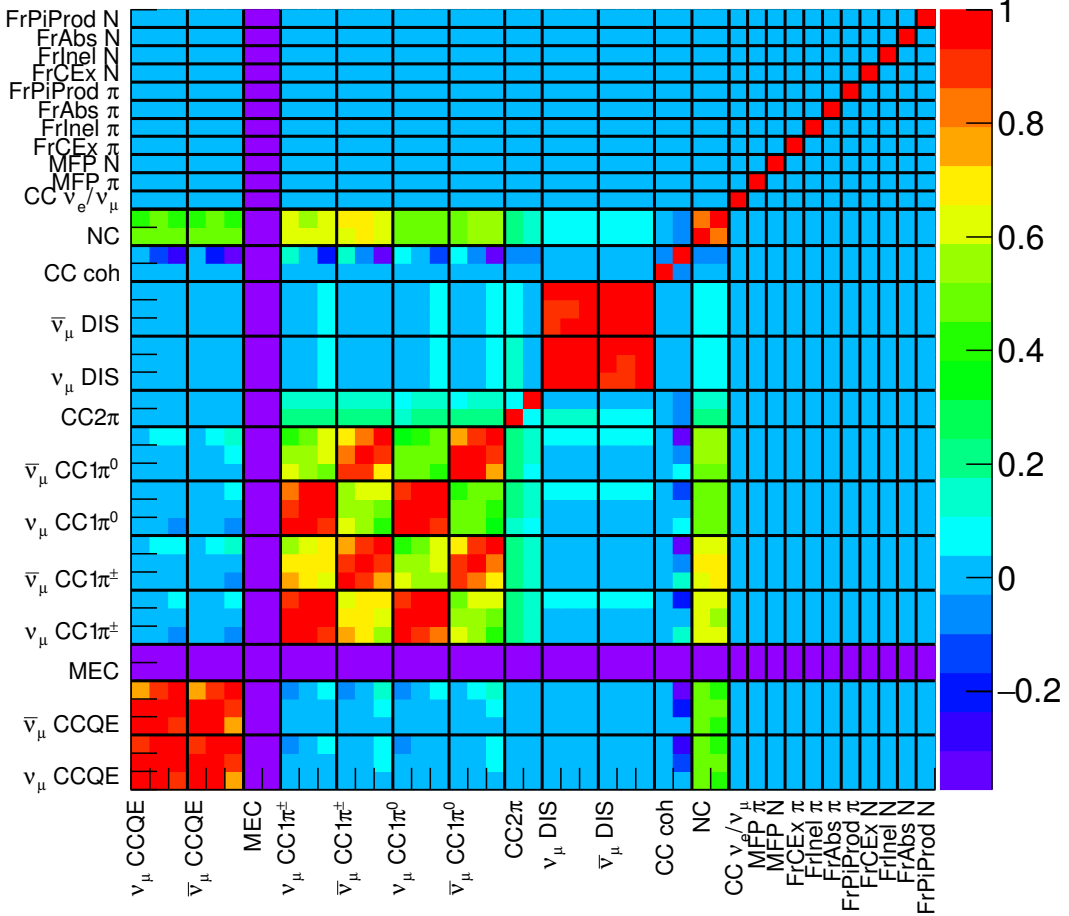


Figure 19: Graphical representation of the VALOR 2016a neutrino interaction correlation matrix computed using GENIE v2.10.6 [16].

3.4.4 Synopsis of systematic parameters and assigned uncertainties

A summary of the systematic parameters included in the 2016a analysis is given in Tab. 4. The analysis considers 156 systematics parameters: 104 parameters from the MINERvA/NuMI flux error model adopted for the present DUNE sensitivity studies, 43 parameters from the 2016a VALOR/GENIE neutrino interaction error model, and 9 parameters from a tentative detector error model (further input is required from the proponents of each ND design).

Table 4: Systematic parameters in VALOR 2016a DUNE analysis. All parameters are allowed to float in the fit

Idx	Name	Nom	Pre-fit 1σ err	Cor	N/L	Physics quantity controlled by the fit parameter
0	$f_{FHC;\nu_\mu;00}$	1	15.78 %	✓		FHC ν_μ ND flux in $E_\nu = [0, 0.5]$ GeV
1	$f_{FHC;\nu_\mu;01}$	1	11.18 %	✓		FHC ν_μ ND flux in $E_\nu = [0.5, 1.0]$ GeV

2	$f_{FHC;\nu_\mu;02}$	1	8.28 %	✓	FHC ν_μ ND flux in $E_\nu = [1.0, 1.5]$ GeV
3	$f_{FHC;\nu_\mu;03}$	1	7.98 %	✓	FHC ν_μ ND flux in $E_\nu = [1.5, 2.0]$ GeV
4	$f_{FHC;\nu_\mu;04}$	1	8.07 %	✓	FHC ν_μ ND flux in $E_\nu = [2.0, 2.5]$ GeV
5	$f_{FHC;\nu_\mu;05}$	1	7.77 %	✓	FHC ν_μ ND flux in $E_\nu = [2.5, 3.0]$ GeV
6	$f_{FHC;\nu_\mu;06}$	1	7.39 %	✓	FHC ν_μ ND flux in $E_\nu = [3.0, 3.5]$ GeV
7	$f_{FHC;\nu_\mu;07}$	1	8.13 %	✓	FHC ν_μ ND flux in $E_\nu = [3.5, 4.0]$ GeV
8	$f_{FHC;\nu_\mu;08}$	1	10.72 %	✓	FHC ν_μ ND flux in $E_\nu = [4.0, 4.5]$ GeV
9	$f_{FHC;\nu_\mu;09}$	1	12.01 %	✓	FHC ν_μ ND flux in $E_\nu = [4.5, 5.0]$ GeV
10	$f_{FHC;\nu_\mu;10}$	1	10.32 %	✓	FHC ν_μ ND flux in $E_\nu = [5.0, 5.5]$ GeV
11	$f_{FHC;\nu_\mu;11}$	1	9.12 %	✓	FHC ν_μ ND flux in $E_\nu = [5.5, 6.0]$ GeV
12	$f_{FHC;\nu_\mu;12}$	1	9.12 %	✓	FHC ν_μ ND flux in $E_\nu = [6.0, 7.0]$ GeV
13	$f_{FHC;\nu_\mu;13}$	1	9.35 %	✓	FHC ν_μ ND flux in $E_\nu = [7.0, 8.0]$ GeV
14	$f_{FHC;\nu_\mu;14}$	1	9.11 %	✓	FHC ν_μ ND flux in $E_\nu = [8.0, 12.0]$ GeV
15	$f_{FHC;\nu_\mu;15}$	1	8.66 %	✓	FHC ν_μ ND flux in $E_\nu = [12.0, 16.0]$ GeV
16	$f_{FHC;\nu_\mu;16}$	1	8.69 %	✓	FHC ν_μ ND flux in $E_\nu = [16.0, 20.0]$ GeV
17	$f_{FHC;\nu_\mu;17}$	1	10.93 %	✓	FHC ν_μ ND flux in $E_\nu = [20.0, 40.0]$ GeV
18	$f_{FHC;\nu_\mu;18}$	1	20.42 %	✓	FHC ν_μ ND flux in $E_\nu > 40.0$ GeV
19	$f_{FHC;\bar{\nu}_\mu;00}$	1	18.05 %	✓	FHC $\bar{\nu}_\mu$ ND flux in $E_\nu = [0, 0.5]$ GeV
20	$f_{FHC;\bar{\nu}_\mu;01}$	1	15.49 %	✓	FHC $\bar{\nu}_\mu$ ND flux in $E_\nu = [0.5, 1.0]$ GeV
21	$f_{FHC;\bar{\nu}_\mu;02}$	1	14.50 %	✓	FHC $\bar{\nu}_\mu$ ND flux in $E_\nu = [1.0, 1.5]$ GeV
22	$f_{FHC;\bar{\nu}_\mu;03}$	1	12.94 %	✓	FHC $\bar{\nu}_\mu$ ND flux in $E_\nu = [1.5, 2.0]$ GeV
23	$f_{FHC;\bar{\nu}_\mu;04}$	1	12.15 %	✓	FHC $\bar{\nu}_\mu$ ND flux in $E_\nu = [2.0, 2.5]$ GeV
24	$f_{FHC;\bar{\nu}_\mu;05}$	1	11.48 %	✓	FHC $\bar{\nu}_\mu$ ND flux in $E_\nu = [2.5, 3.0]$ GeV
25	$f_{FHC;\bar{\nu}_\mu;06}$	1	11.12 %	✓	FHC $\bar{\nu}_\mu$ ND flux in $E_\nu = [3.0, 3.5]$ GeV
26	$f_{FHC;\bar{\nu}_\mu;07}$	1	10.80 %	✓	FHC $\bar{\nu}_\mu$ ND flux in $E_\nu = [3.5, 4.0]$ GeV
27	$f_{FHC;\bar{\nu}_\mu;08}$	1	10.56 %	✓	FHC $\bar{\nu}_\mu$ ND flux in $E_\nu = [4.0, 4.5]$ GeV
28	$f_{FHC;\bar{\nu}_\mu;09}$	1	10.14 %	✓	FHC $\bar{\nu}_\mu$ ND flux in $E_\nu = [4.5, 5.0]$ GeV
29	$f_{FHC;\bar{\nu}_\mu;10}$	1	9.99 %	✓	FHC $\bar{\nu}_\mu$ ND flux in $E_\nu = [5.0, 5.5]$ GeV
30	$f_{FHC;\bar{\nu}_\mu;11}$	1	9.44 %	✓	FHC $\bar{\nu}_\mu$ ND flux in $E_\nu = [5.5, 6.0]$ GeV
31	$f_{FHC;\bar{\nu}_\mu;12}$	1	9.02 %	✓	FHC $\bar{\nu}_\mu$ ND flux in $E_\nu = [6.0, 7.0]$ GeV
32	$f_{FHC;\bar{\nu}_\mu;13}$	1	8.83 %	✓	FHC $\bar{\nu}_\mu$ ND flux in $E_\nu = [7.0, 8.0]$ GeV
33	$f_{FHC;\bar{\nu}_\mu;14}$	1	8.91 %	✓	FHC $\bar{\nu}_\mu$ ND flux in $E_\nu = [8.0, 12.0]$ GeV
34	$f_{FHC;\bar{\nu}_\mu;15}$	1	9.13 %	✓	FHC $\bar{\nu}_\mu$ ND flux in $E_\nu = [12.0, 16.0]$ GeV
35	$f_{FHC;\bar{\nu}_\mu;16}$	1	10.59 %	✓	FHC $\bar{\nu}_\mu$ ND flux in $E_\nu = [16.0, 20.0]$ GeV
36	$f_{FHC;\bar{\nu}_\mu;17}$	1	15.64 %	✓	FHC $\bar{\nu}_\mu$ ND flux in $E_\nu = [20.0, 40.0]$ GeV
37	$f_{FHC;\bar{\nu}_\mu;18}$	1	24.93 %	✓	FHC $\bar{\nu}_\mu$ ND flux in $E_\nu > 40.0$ GeV
38	$f_{FHC;\nu_e;00}$	1	8.00 %	✓	FHC ν_e ND flux in $E_\nu = [0, 2.0]$ GeV
39	$f_{FHC;\nu_e;01}$	1	7.12 %	✓	FHC ν_e ND flux in $E_\nu = [2.0, 4.0]$ GeV
40	$f_{FHC;\nu_e;02}$	1	9.84 %	✓	FHC ν_e ND flux in $E_\nu = [4.0, 6.0]$ GeV
41	$f_{FHC;\nu_e;03}$	1	6.36 %	✓	FHC ν_e ND flux in $E_\nu = [6.0, 8.0]$ GeV
42	$f_{FHC;\nu_e;04}$	1	7.40 %	✓	FHC ν_e ND flux in $E_\nu = [8.0, 10.0]$ GeV
43	$f_{FHC;\nu_e;05}$	1	9.60 %	✓	FHC ν_e ND flux in $E_\nu = [10.0, 20.0]$ GeV
44	$f_{FHC;\nu_e;06}$	1	14.97 %	✓	FHC ν_e ND flux in $E_\nu > 20.0$ GeV
45	$f_{FHC;\bar{\nu}_e;00}$	1	15.11 %	✓	FHC $\bar{\nu}_e$ ND flux in $E_\nu = [0, 2.0]$ GeV
46	$f_{FHC;\bar{\nu}_e;01}$	1	12.10 %	✓	FHC $\bar{\nu}_e$ ND flux in $E_\nu = [2.0, 4.0]$ GeV
47	$f_{FHC;\bar{\nu}_e;02}$	1	10.58 %	✓	FHC $\bar{\nu}_e$ ND flux in $E_\nu = [4.0, 6.0]$ GeV
48	$f_{FHC;\bar{\nu}_e;03}$	1	10.85 %	✓	FHC $\bar{\nu}_e$ ND flux in $E_\nu = [6.0, 8.0]$ GeV
49	$f_{FHC;\bar{\nu}_e;04}$	1	10.22 %	✓	FHC $\bar{\nu}_e$ ND flux in $E_\nu = [8.0, 10.0]$ GeV
50	$f_{FHC;\bar{\nu}_e;05}$	1	10.06 %	✓	FHC $\bar{\nu}_e$ ND flux in $E_\nu = [10.0, 20.0]$ GeV
51	$f_{FHC;\bar{\nu}_e;06}$	1	12.19 %	✓	FHC $\bar{\nu}_e$ ND flux in $E_\nu > 20.0$ GeV
52	$f_{RHC;\nu_\mu;00}$	1	18.33 %	✓	RHC ν_μ ND flux in $E_\nu = [0, 0.5]$ GeV
53	$f_{RHC;\nu_\mu;01}$	1	18.12 %	✓	RHC ν_μ ND flux in $E_\nu = [0.5, 1.0]$ GeV
54	$f_{RHC;\nu_\mu;02}$	1	15.44 %	✓	RHC ν_μ ND flux in $E_\nu = [1.0, 1.5]$ GeV

55	$f_{RHC;\nu_\mu;03}$	1	13.59 %	✓	RHC ν_μ ND flux in $E_\nu = [1.5, 2.0]$ GeV
56	$f_{RHC;\nu_\mu;04}$	1	12.94 %	✓	RHC ν_μ ND flux in $E_\nu = [2.0, 2.5]$ GeV
57	$f_{RHC;\nu_\mu;05}$	1	12.33 %	✓	RHC ν_μ ND flux in $E_\nu = [2.5, 3.0]$ GeV
58	$f_{RHC;\nu_\mu;06}$	1	11.60 %	✓	RHC ν_μ ND flux in $E_\nu = [3.0, 3.5]$ GeV
59	$f_{RHC;\nu_\mu;07}$	1	10.99 %	✓	RHC ν_μ ND flux in $E_\nu = [3.5, 4.0]$ GeV
60	$f_{RHC;\nu_\mu;08}$	1	10.86 %	✓	RHC ν_μ ND flux in $E_\nu = [4.0, 4.5]$ GeV
61	$f_{RHC;\nu_\mu;09}$	1	10.54 %	✓	RHC ν_μ ND flux in $E_\nu = [4.5, 5.0]$ GeV
62	$f_{RHC;\nu_\mu;10}$	1	10.40 %	✓	RHC ν_μ ND flux in $E_\nu = [5.0, 5.5]$ GeV
63	$f_{RHC;\nu_\mu;11}$	1	10.18 %	✓	RHC ν_μ ND flux in $E_\nu = [5.5, 6.0]$ GeV
64	$f_{RHC;\nu_\mu;12}$	1	10.11 %	✓	RHC ν_μ ND flux in $E_\nu = [6.0, 7.0]$ GeV
65	$f_{RHC;\nu_\mu;13}$	1	9.76 %	✓	RHC ν_μ ND flux in $E_\nu = [7.0, 8.0]$ GeV
66	$f_{RHC;\nu_\mu;14}$	1	9.48 %	✓	RHC ν_μ ND flux in $E_\nu = [8.0, 12.0]$ GeV
67	$f_{RHC;\nu_\mu;15}$	1	9.10 %	✓	RHC ν_μ ND flux in $E_\nu = [12.0, 16.0]$ GeV
68	$f_{RHC;\nu_\mu;16}$	1	9.16 %	✓	RHC ν_μ ND flux in $E_\nu = [16.0, 20.0]$ GeV
69	$f_{RHC;\nu_\mu;17}$	1	11.34 %	✓	RHC ν_μ ND flux in $E_\nu = [20.0, 40.0]$ GeV
70	$f_{RHC;\nu_\mu;18}$	1	21.11 %	✓	RHC ν_μ ND flux in $E_\nu > 40.0$ GeV
71	$f_{RHC;\bar{\nu}_\mu;00}$	1	15.16 %	✓	RHC $\bar{\nu}_\mu$ ND flux in $E_\nu = [0, 0.5]$ GeV
72	$f_{RHC;\bar{\nu}_\mu;01}$	1	9.79 %	✓	RHC $\bar{\nu}_\mu$ ND flux in $E_\nu = [0.5, 1.0]$ GeV
73	$f_{RHC;\bar{\nu}_\mu;02}$	1	7.57 %	✓	RHC $\bar{\nu}_\mu$ ND flux in $E_\nu = [1.0, 1.5]$ GeV
74	$f_{RHC;\bar{\nu}_\mu;03}$	1	7.53 %	✓	RHC $\bar{\nu}_\mu$ ND flux in $E_\nu = [1.5, 2.0]$ GeV
75	$f_{RHC;\bar{\nu}_\mu;04}$	1	7.48 %	✓	RHC $\bar{\nu}_\mu$ ND flux in $E_\nu = [2.0, 2.5]$ GeV
76	$f_{RHC;\bar{\nu}_\mu;05}$	1	7.14 %	✓	RHC $\bar{\nu}_\mu$ ND flux in $E_\nu = [2.5, 3.0]$ GeV
77	$f_{RHC;\bar{\nu}_\mu;06}$	1	6.59 %	✓	RHC $\bar{\nu}_\mu$ ND flux in $E_\nu = [3.0, 3.5]$ GeV
78	$f_{RHC;\bar{\nu}_\mu;07}$	1	7.42 %	✓	RHC $\bar{\nu}_\mu$ ND flux in $E_\nu = [3.5, 4.0]$ GeV
79	$f_{RHC;\bar{\nu}_\mu;08}$	1	10.17 %	✓	RHC $\bar{\nu}_\mu$ ND flux in $E_\nu = [4.0, 4.5]$ GeV
80	$f_{RHC;\bar{\nu}_\mu;09}$	1	11.50 %	✓	RHC $\bar{\nu}_\mu$ ND flux in $E_\nu = [4.5, 5.0]$ GeV
81	$f_{RHC;\bar{\nu}_\mu;10}$	1	9.72 %	✓	RHC $\bar{\nu}_\mu$ ND flux in $E_\nu = [5.0, 5.5]$ GeV
82	$f_{RHC;\bar{\nu}_\mu;11}$	1	8.31 %	✓	RHC $\bar{\nu}_\mu$ ND flux in $E_\nu = [5.5, 6.0]$ GeV
83	$f_{RHC;\bar{\nu}_\mu;12}$	1	8.19 %	✓	RHC $\bar{\nu}_\mu$ ND flux in $E_\nu = [6.0, 7.0]$ GeV
84	$f_{RHC;\bar{\nu}_\mu;13}$	1	8.40 %	✓	RHC $\bar{\nu}_\mu$ ND flux in $E_\nu = [7.0, 8.0]$ GeV
85	$f_{RHC;\bar{\nu}_\mu;14}$	1	8.38 %	✓	RHC $\bar{\nu}_\mu$ ND flux in $E_\nu = [8.0, 12.0]$ GeV
86	$f_{RHC;\bar{\nu}_\mu;15}$	1	8.47 %	✓	RHC $\bar{\nu}_\mu$ ND flux in $E_\nu = [12.0, 16.0]$ GeV
87	$f_{RHC;\bar{\nu}_\mu;16}$	1	9.59 %	✓	RHC $\bar{\nu}_\mu$ ND flux in $E_\nu = [16.0, 20.0]$ GeV
88	$f_{RHC;\bar{\nu}_\mu;17}$	1	14.55 %	✓	RHC $\bar{\nu}_\mu$ ND flux in $E_\nu = [20.0, 40.0]$ GeV
89	$f_{RHC;\bar{\nu}_\mu;18}$	1	23.70 %	✓	RHC $\bar{\nu}_\mu$ ND flux in $E_\nu > 40.0$ GeV
90	$f_{RHC;\nu_e;00}$	1	14.29 %	✓	RHC ν_e ND flux in $E_\nu = [0, 2.0]$ GeV
91	$f_{RHC;\nu_e;01}$	1	10.70 %	✓	RHC ν_e ND flux in $E_\nu = [2.0, 4.0]$ GeV
92	$f_{RHC;\nu_e;02}$	1	10.21 %	✓	RHC ν_e ND flux in $E_\nu = [4.0, 6.0]$ GeV
93	$f_{RHC;\nu_e;03}$	1	10.07 %	✓	RHC ν_e ND flux in $E_\nu = [6.0, 8.0]$ GeV
94	$f_{RHC;\nu_e;04}$	1	10.51 %	✓	RHC ν_e ND flux in $E_\nu = [8.0, 10.0]$ GeV
95	$f_{RHC;\nu_e;05}$	1	10.83 %	✓	RHC ν_e ND flux in $E_\nu = [10.0, 20.0]$ GeV
96	$f_{RHC;\nu_e;06}$	1	15.12 %	✓	RHC ν_e ND flux in $E_\nu > 20.0$ GeV
97	$f_{RHC;\bar{\nu}_e;00}$	1	7.20 %	✓	RHC $\bar{\nu}_e$ ND flux in $E_\nu = [0, 2.0]$ GeV
98	$f_{RHC;\bar{\nu}_e;01}$	1	6.70 %	✓	RHC $\bar{\nu}_e$ ND flux in $E_\nu = [2.0, 4.0]$ GeV
99	$f_{RHC;\bar{\nu}_e;02}$	1	9.71 %	✓	RHC $\bar{\nu}_e$ ND flux in $E_\nu = [4.0, 6.0]$ GeV
100	$f_{RHC;\bar{\nu}_e;03}$	1	5.94 %	✓	RHC $\bar{\nu}_e$ ND flux in $E_\nu = [6.0, 8.0]$ GeV
101	$f_{RHC;\bar{\nu}_e;04}$	1	7.58 %	✓	RHC $\bar{\nu}_e$ ND flux in $E_\nu = [8.0, 10.0]$ GeV
102	$f_{RHC;\bar{\nu}_e;05}$	1	8.86 %	✓	RHC $\bar{\nu}_e$ ND flux in $E_\nu = [10.0, 20.0]$ GeV
103	$f_{RHC;\bar{\nu}_e;06}$	1	11.57 %	✓	RHC $\bar{\nu}_e$ ND flux in $E_\nu > 20.0$ GeV
104	$f_{\nu CCQE;1}$	1	8.25 %	✓	ν CCQE cross-section in $Q^2 = [0, 0.20]$ GeV 2
105	$f_{\nu CCQE;2}$	1	22.97 %	✓	ν CCQE cross-section in $Q^2 = [0.20, 0.55]$ GeV 2
106	$f_{\nu CCQE;3}$	1	48.66 %	✓	ν CCQE cross-section in $Q^2 > 0.55$ GeV 2
107	$f_{\bar{\nu} CCQE;1}$	1	8.62 %	✓	$\bar{\nu}$ CCQE cross-section in $Q^2 = [0, 0.20]$ GeV 2

108	$f_{\nu CCQE;2}$	1	23.17 %	✓		ν CCQE cross-section in $Q^2 = [0.20, 0.55] \text{ GeV}^2$
109	$f_{\bar{\nu} CCQE;3}$	1	42.46 %	✓		$\bar{\nu}$ CCQE cross-section in $Q^2 > 0.55 \text{ GeV}^2$
110	$f_{\nu CCMEC}$	1	0.00 %	✓		ν CCMEC cross-section
111	$f_{\bar{\nu} CCMEC}$	1	0.00 %	✓		$\bar{\nu}$ CCMEC cross-section
112	$f_{\nu CC1\pi^0;1}$	1	13.35 %	✓		ν CC1 π^0 cross-section in $Q^2 = [0, 0.35] \text{ GeV}^2$
113	$f_{\nu CC1\pi^0;2}$	1	23.18 %	✓		ν CC1 π^0 cross-section in $Q^2 = [0.35, 0.90] \text{ GeV}^2$
114	$f_{\nu CC1\pi^0;3}$	1	33.60 %	✓		ν CC1 π^0 cross-section in $Q^2 > 0.90 \text{ GeV}^2$
115	$f_{\nu CC1\pi^\pm;1}$	1	12.83 %	✓		ν CC1 π^\pm cross-section in $Q^2 = [0, 0.30] \text{ GeV}^2$
116	$f_{\nu CC1\pi^\pm;2}$	1	23.36 %	✓		ν CC1 π^\pm cross-section in $Q^2 = [0.30, 0.80] \text{ GeV}^2$
117	$f_{\nu CC1\pi^\pm;3}$	1	37.27 %	✓		ν CC1 π^\pm cross-section in $Q^2 > 0.80 \text{ GeV}^2$
118	$f_{\bar{\nu} CC1\pi^0;1}$	1	16.42 %	✓		$\bar{\nu}$ CC1 π^0 cross-section in $Q^2 = [0, 0.35] \text{ GeV}^2$
119	$f_{\bar{\nu} CC1\pi^0;2}$	1	26.60 %	✓		$\bar{\nu}$ CC1 π^0 cross-section in $Q^2 = [0.35, 0.90] \text{ GeV}^2$
120	$f_{\bar{\nu} CC1\pi^0;3}$	1	34.78 %	✓		$\bar{\nu}$ CC1 π^0 cross-section in $Q^2 > 0.90 \text{ GeV}^2$
121	$f_{\bar{\nu} CC1\pi^\pm;1}$	1	15.87 %	✓		$\bar{\nu}$ CC1 π^\pm cross-section in $Q^2 = [0, 0.30] \text{ GeV}^2$
122	$f_{\bar{\nu} CC1\pi^\pm;2}$	1	26.81 %	✓		$\bar{\nu}$ CC1 π^\pm cross-section in $Q^2 = [0.30, 0.80] \text{ GeV}^2$
123	$f_{\bar{\nu} CC1\pi^\pm;3}$	1	38.43 %	✓		$\bar{\nu}$ CC1 π^\pm cross-section in $Q^2 > 0.80 \text{ GeV}^2$
124	$f_{\nu CC2\pi}$	1	21.08 %	✓		ν CC2 π cross-section
125	$f_{\bar{\nu} CC2\pi}$	1	19.96 %	✓		$\bar{\nu}$ CC2 π cross-section
126	$f_{\nu CCDIS;1}$	1	3.66 %	✓		ν CCDIS ($> 2\pi$) cross-section in $E_\nu = [0, 7.5] \text{ GeV}$
127	$f_{\nu CCDIS;2}$	1	3.40 %	✓		ν CCDIS ($> 2\pi$) cross-section in $E_\nu = [7.5, 15.0] \text{ GeV}$
128	$f_{\nu CCDIS;3}$	1	2.46 %	✓		ν CCDIS ($> 2\pi$) cross-section in $E_\nu > 15.0 \text{ GeV}$
129	$f_{\bar{\nu} CCDIS;1}$	1	1.00 %	✓		$\bar{\nu}$ CCDIS ($> 2\pi$) cross-section in $E_\nu = [0, 7.5] \text{ GeV}$
130	$f_{\bar{\nu} CCDIS;2}$	1	1.52 %	✓		$\bar{\nu}$ CCDIS ($> 2\pi$) cross-section in $E_\nu = [7.5, 15.0] \text{ GeV}$
131	$f_{\bar{\nu} CCDIS;3}$	1	1.58 %	✓		$\bar{\nu}$ CCDIS ($> 2\pi$) cross-section in $E_\nu > 15.0 \text{ GeV}$
132	$f_{\nu CCCoh}$	1	39.08 %	✓		ν CC coherent π production cross-section
133	$f_{\bar{\nu} CCCoh}$	1	126.35 %	✓		$\bar{\nu}$ CC coherent π production cross-section
134	$f_{\nu NC}$	1	111.35 %	✓		ν NC inclusive cross-section
135	$f_{\bar{\nu} NC}$	1	91.46 %	✓		$\bar{\nu}$ NC inclusive cross-section
136	f_{ν_e/ν_μ}	1	3.00 %	✓		ν_e/ν_μ cross-section ratio
137	$f_{FSI;\pi;MFP}$	1	20.00 %		✓	π mean free path in nucleus
138	$f_{FSI;N;MFP}$	1	20.00 %		✓	nucleon mean free path in nucleus
139	$f_{FSI;\pi;CEx}$	1	50.00 %		✓	π -nucleus charge exchange cross-section fraction
140	$f_{FSI;\pi;Inel}$	1	40.00 %		✓	π -nucleus inelastic cross-section fraction
141	$f_{FSI;\pi;Abs}$	1	30.00 %		✓	π -nucleus absorption cross-section fraction
142	$f_{FSI;\pi;\pi Prod}$	1	20.00 %		✓	π -nucleus π production cross-section fraction
143	$f_{FSI;N;CEx}$	1	50.00 %		✓	nucleon-nucleus charge exchange cross-section fraction
144	$f_{FSI;N;Inel}$	1	40.00 %		✓	nucleon-nucleus inelastic cross-section fraction
145	$f_{FSI;N;Abs}$	1	20.00 %		✓	nucleon-nucleus absorption cross-section fraction
146	$f_{FSI;N;\pi Prod}$	1	20.00 %		✓	nucleon-nucleus π production cross-section fraction
147	$f_{eff;\nu_\mu CC;1trkQE}$	1	10.00 %			ν_μ CC / 1-track QE enhanced sample efficiency
148	$f_{eff;\nu_\mu CC;2trkQE}$	1	10.00 %			ν_μ CC / 2-track QE enhanced sample efficiency
149	$f_{eff;\nu_\mu CC;1\pi^\pm}$	1	10.00 %			ν_μ CC / $1\pi^\pm$ sample efficiency
150	$f_{eff;\nu_\mu CC;1\pi^0}$	1	10.00 %			ν_μ CC / $1\pi^0$ sample efficiency
151	$f_{eff;\nu_\mu CC;1\pi^\pm 1\pi^0}$	1	10.00 %			ν_μ CC / $1\pi^\pm + 1\pi^0$ sample efficiency
152	$f_{eff;\nu_\mu CC;other}$	1	10.00 %			ν_μ CC / Other sample efficiency
153	$f_{eff;\nu_e CC}$	1	10.00 %			ν_e CC inclusive sample efficiency
154	$f_{eff;\nu_\mu CC;wsgn}$	1	10.00 %			Wrong-sign ν_μ CC inclusive sample efficiency
155	$f_{eff;NC}$	1	10.00 %			NC inclusive sample efficiency

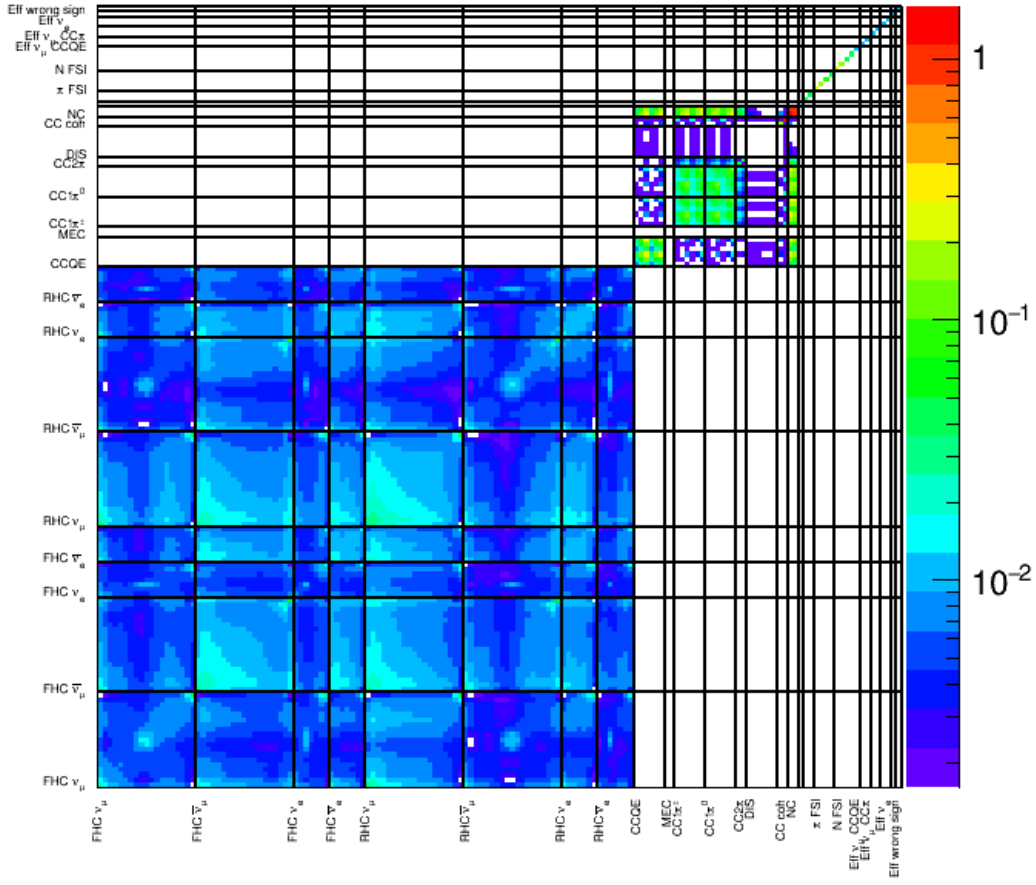


Figure 20: Combined 156×156 systematic pre-fit covariance matrix used in the 2016a VALOR DUNE analysis.

3.5 Effect of systematic uncertainties on event spectra

Combined pre-fit error envelopes are presented in Figs. 21 - 26. for all fit samples of all Near Detector options considered in 2016a.

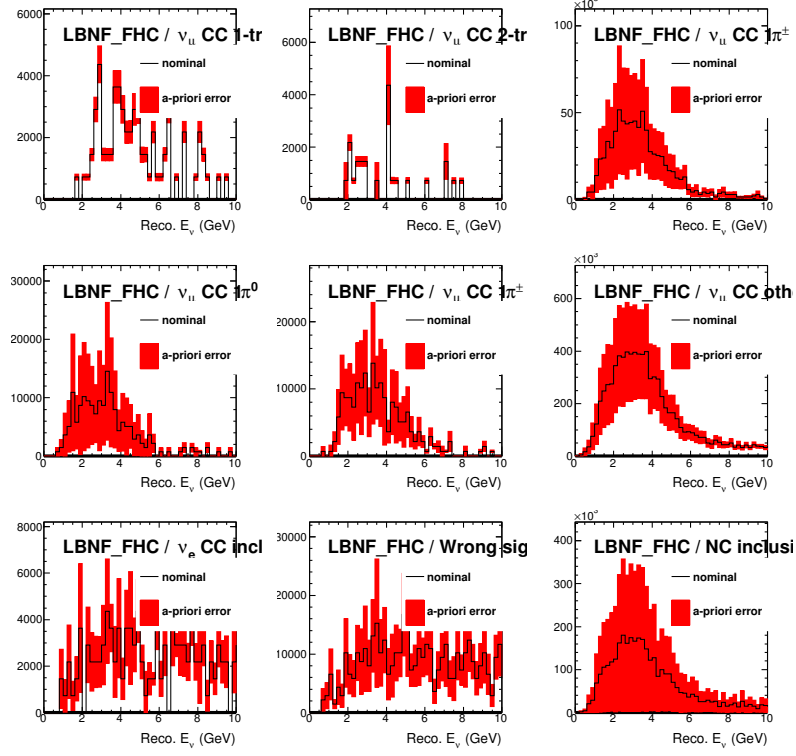


Figure 21: Error envelopes for the reconstructed (or visible) energy spectra of all 9 FHC FGT event samples of the 2016a analysis. The total error due to the flux (104 systematic parameters) and neutrino interaction (43 systematic parameters) uncertainties considered in this analysis is shown. The contributions to the error envelope coming only from the flux and only from the neutrino interaction systematics is also shown. Contributions due to the tentatively assigned detector error model are ignored. In each case 10k toy-MC experiments are generated with randomised (correlated) systematics using the input / pre-fit systematic parameter covariance matrix and the 1σ spread of bin contents is calculated.

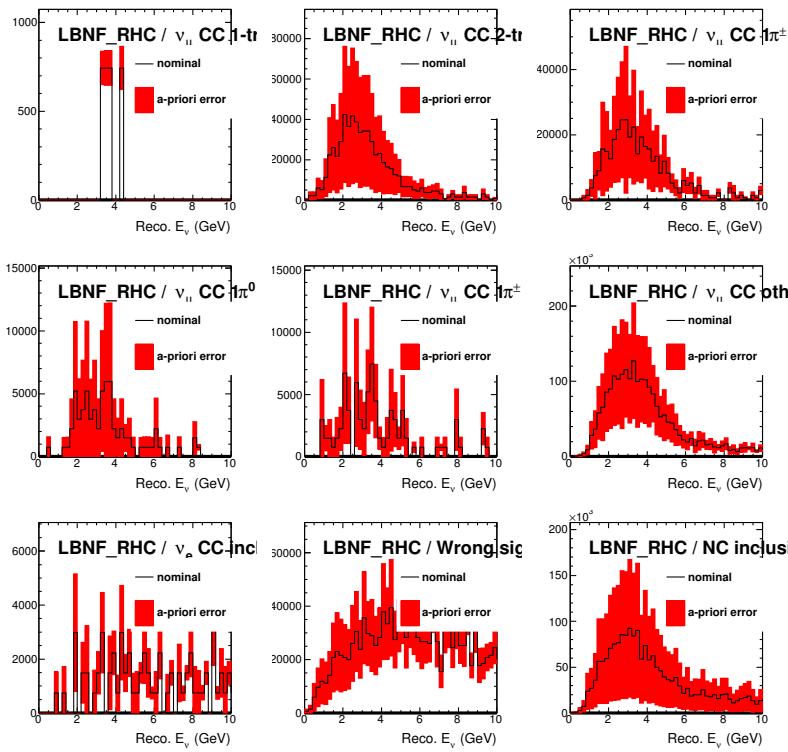


Figure 22: As in Fig. 21, but for the 9 RHC FGT samples of the 2016a analysis.

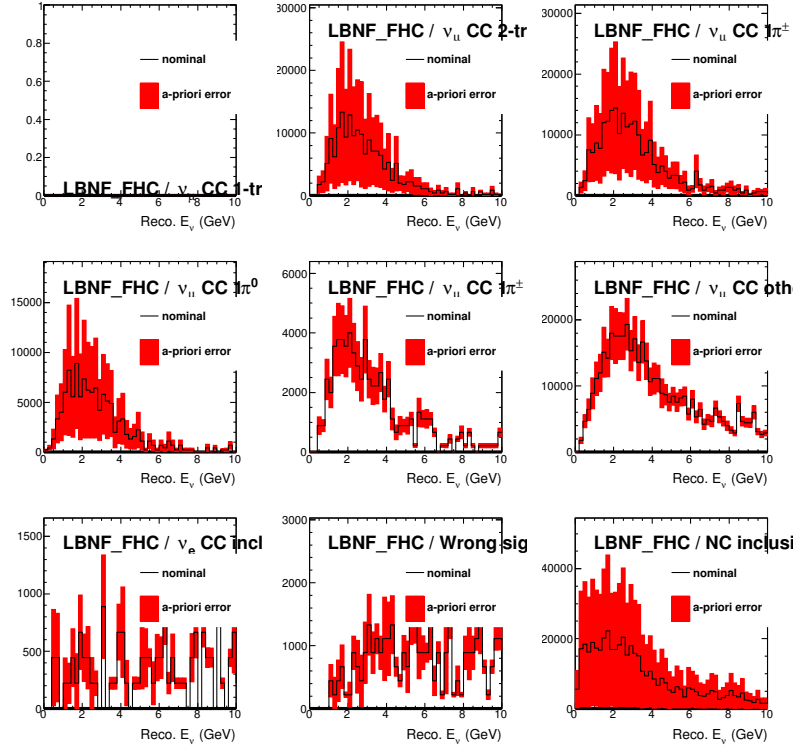


Figure 23: Error envelopes for the reconstructed (or visible) energy spectra of all 9 FHC GArTPC event samples of the 2016a analysis. The total error due to the flux (104 systematic parameters) and neutrino interaction (43 systematic parameters) uncertainties considered in this analysis is shown. The contributions to the error envelope coming only from the flux and only from the neutrino interaction systematics is also shown. Contributions due to the tentatively assigned detector error model are ignored. In each case 10k toy-MC experiments are generated with randomised (correlated) systematics using the input / pre-fit systematic parameter covariance matrix and the 1σ spread of bin contents is calculated.

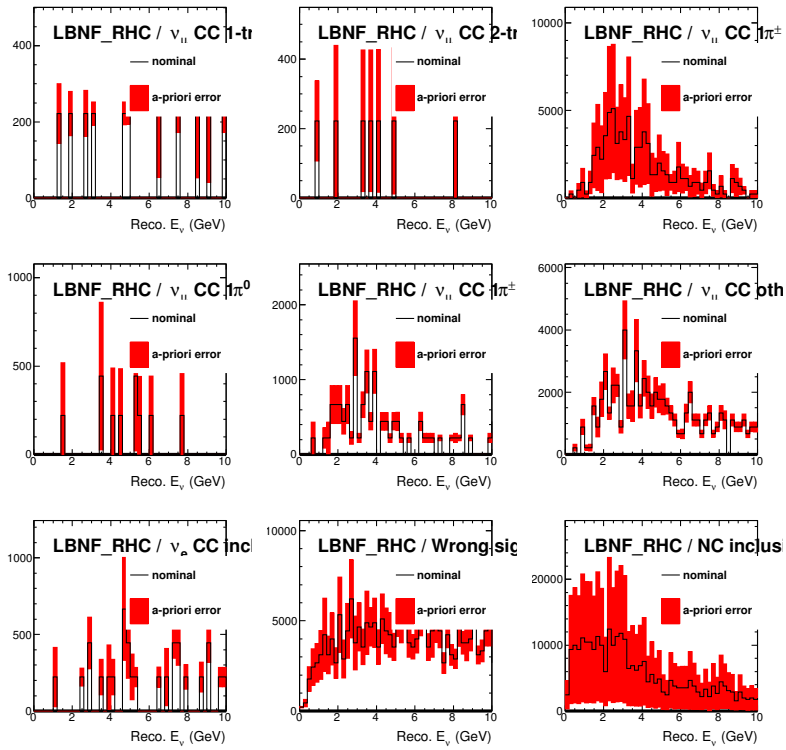


Figure 24: As in Fig. 23, but for the 9 RHC GArTPC samples of the 2016a analysis.

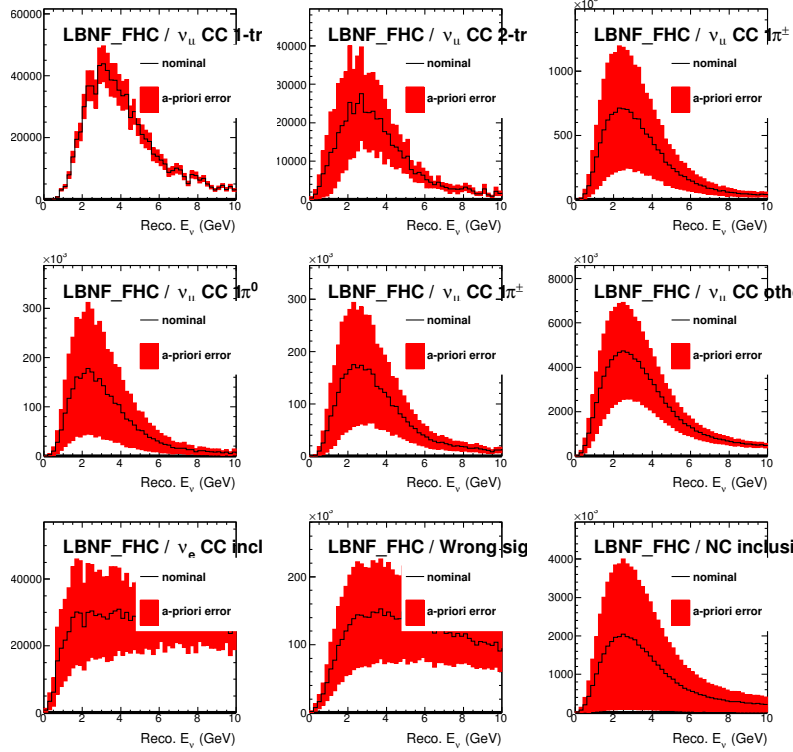


Figure 25: Error envelopes for the reconstructed (or visible) energy spectra of all 9 FHC LArTPC event samples of the 2016a analysis. The total error due to the flux (104 systematic parameters) and neutrino interaction (43 systematic parameters) uncertainties considered in this analysis is shown. The contributions to the error envelope coming only from the flux and only from the neutrino interaction systematics is also shown. Contributions due to the tentatively assigned detector error model are ignored. In each case 10k toy-MC experiments are generated with randomised (correlated) systematics using the input / pre-fit systematic parameter covariance matrix and the 1σ spread of bin contents is calculated.

3.6 Fit parameters and parameter ranges

From the 156 systematic parameters in Tab. 4, 154 parameters were allowed to float in the 2016a fit. Parameters $f_{\nu CCMEC}$ (110) and $f_{\bar{\nu} CCMEC}$ (111) were fixed to their nominal values (=1) since the input MC samples (produced with the default model in GENIE v2.10.6) used for constructing the VALOR MC templates contained no MEC component. All linear systematic parameters allowed to float in the fit, were limited in the [0,2] range (where a value of 0 causes a vanishing contribution from the MC templates where that systematic is applied, and a value of 2 causes a 100% increase in the contribution from the corresponding MC templates). For the non-linear parameters a range of [-2,2] was used (corresponding to a $[-2\sigma, 2\sigma]$ range). All non-linear parameters in the 2016a fit are related to FSI modelling. For these parameters, variations much larger than 2σ can become problematic due to inherent limitations of corresponding event reweighting schemes used for the construction of the systematic response functions. By extrapolating the response function it is possible to relax this limit and use a wider range ($[-5\sigma, 5\sigma]$). However this has no impact on the fit and it was not the method chosen for 2016a.

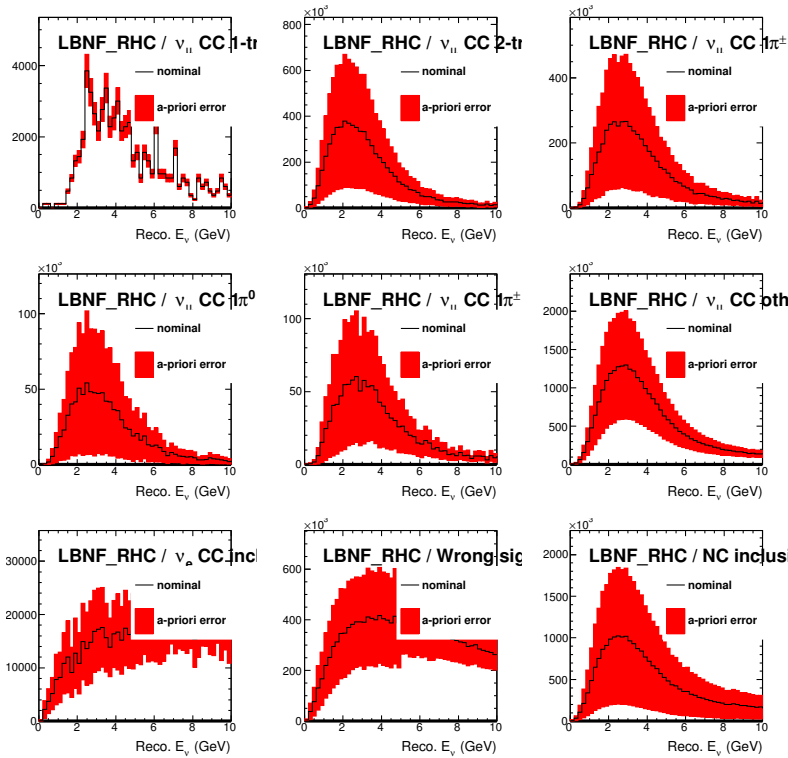


Figure 26: As in Fig. 25, but for the 9 RHC LArTPC samples of the 2016a analysis.

4 Improvements/changes planned for 2016b VALOR DUNE analysis

4.1 Implementation of joint 3-flavour oscillation fit with marginalization of O(400) systematics

For the 2nd pass-through the VALOR Near Detector systematics constraint was fed to an external Far Detector oscillation fitter. This two-step procedure is sub-optimal and there is evidence that very large systematic parameter covariance matrix produced by MINUIT is not sufficiently accurate. By performing a joint fit of Near and Far Detector samples the need for such an intermediate covariance matrix is eliminated. This joint fit will be available in the 2016b version of the VALOR / DUNE analysis. In this analysis all flux and cross-section systematic parameters, in addition to the detector systematics parameters, will be marginalized during the oscillation fit (see Sec. 2.5.2).

4.2 Addition of 26 Near Detector samples

26 additional samples (13 for each of the two beam configurations) were already included by further splitting the ‘other’ or inclusive samples included in the present 2016a analysis:

- Added N-track ν_μ CC 0π (QE enhanced) to complement the existing 1-track and 2-track CC QE enhanced samples.
- Split ν_μ CC 3-track Δ -enhanced out of ν_μ CC Other.
- Added $\nu + e^-$ elastic.
- Added inverse muon decay $\nu_\mu + e^- \rightarrow \mu^- + \nu_e$ (including the annihilation channel $\bar{\nu}_e + e^- \rightarrow \mu^- + \bar{\nu}_\mu$).
- Split each of the wrong-sign ν_μ CC inclusive, ν_e CC inclusive and NC inclusive to 0π (QE enhanced), $1\pi^\pm$, $1\pi^0$ and Other samples.

The extended VALOR fit is currently being tested and will be deployed for the next round of processing. It is expected that the 2016b version of the VALOR DUNE analysis will fit jointly the following 23 samples for the FHC (neutrino-enhanced) beam configuration:

- ν_μ CC

1. 1-track 0π (μ^- only)
2. 2-track 0π (μ^- + nucleon)
3. N-track 0π (μ^- + (>1) nucleons)
4. 3-track Δ -enhanced ($\mu^- + \pi^+ + p$, with $W_{reco} \approx 1.2$ GeV)
5. $1\pi^\pm$ ($\mu^- + 1\pi^\pm + X$)
6. $1\pi^0$ ($\mu^- + 1\pi^0 + X$)
7. $1\pi^\pm + 1\pi^0$ ($\mu^- + 1\pi^\pm + 1\pi^0 + X$)
8. Other

- Wrong-sign ν_μ CC

9. 0π ($\mu^+ + X$)
10. $1\pi^\pm$ ($\mu^+ + \pi^\pm + X$)
11. $1\pi^0$ ($\mu^+ + \pi^0 + X$)
12. Other

- ν_e CC

13. 0π ($e^- + X$)
14. $1\pi^\pm$ ($e^- + \pi^\pm + X$)
15. $1\pi^0$ ($e^- + \pi^0 + X$)
16. Other

- Wrong-sign ν_e CC

17. Wrong-sign ν_e CC inclusive ($e^+ + X$)

- NC

18. 0π (nucleon(s))
19. $1\pi^\pm$ ($\pi^\pm + X$)
20. $1\pi^0$ ($\pi^0 + X$)
21. Other

- ν_e

22. $\nu + e^-$ elastic
23. Inverse muon decay $\nu_\mu + e^- \rightarrow \mu^- + \nu_e$ (including the annihilation channel $\bar{\nu}_e + e^- \rightarrow \mu^- + \bar{\nu}_\mu$).

and a similar set of 23 samples is included for the RHC (antineutrino-enhanced) beam configuration.

4.3 Enabling option for multiple Near Detector samples for a given observed final state

The present analysis considers a single sample per final state. The possibility exists to further extend the analysis to fit jointly samples that correspond to the same final state, but originate from different detector regions with different nuclear targets, to accommodate inhomogeneous or hybrid detectors. For example, two separate ν_μ CC 3-track Δ -enhanced samples may be installed with different systematics: A sample for interactions in an Argon target volume, and sample for interactions in a non-Argon target volume. This option will be investigated in 2016b and it will be fully deployed in 2016c.

4.4 Addition of 4 high-resolution and 4 low-resolution Far Detector samples

To implement the joint oscillation and systematics constraint fit, ν_μ CC and ν_e CC samples will be added for the FHC configuration and $\bar{\nu}_\mu$ CC and $\bar{\nu}_e$ CC samples for the RHC configuration. Each will be split into CC0 π (high energy resolution) and CC Other (low energy resolution) sample (8 Far Detector samples in total). The exact definition / topology of the high energy resolution sample is to be determined.

4.5 Improved neutrino interaction errors (2016b VALOR/GENIE error assignments)

The VALOR/GENIE systematic error studies will be repeated with the imminent GENIE v2.12.0, and a constellation of new physics models that will underpin the retuned GENIE v3.0.0.

The supporting data/MC comparisons and systematic studies shown in this technical note (Appendix A) will be improved and extended in collaboration with the GENIE group.

The effect of hadronization systematics, absent from 2016b, will also be studied, parameterized and included in the VALOR DUNE analysis. Some R&D will be required to develop such a parameterization that captures the hadronization uncertainties in a practical and CPU efficient manner for inclusion in the complex VALOR DUNE fit.

4.6 Realistic detector acceptance and leptonic/hadronic energy scale errors

Adding realistic detector acceptance and energy scale errors is an area that requires a substantial improvement.

Leptonic and hadronic energy scale errors will be included in 2016b. This will be implemented using the same technique employed for energy scale errors in the VALOR T2K analysis: By scaling the E_{reco} and y_{reco} bin edges of the MC templates and calculating the number of events gained from / lost to neighbouring bins, under the assumption of uniform distribution of events within each bin.

There is no plan to further improve on the current detector acceptance / efficiency errors. Much further study and input is needed from the detector groups. Ideally, reweighting functions will be developed by each group to handle systematics specific to their detector technology, reconstruction and event selection. When this becomes available, the VALOR group will parameterize the effect of these systematics, similarly to what was done for the neutrino interaction systematics, so that they can be applied in the joint VALOR analysis in an efficient and detector-agnostic manner.

5 2016a systematics constraint fit results

5.1 Example fits to systematically-varied datasets

Fits to several toy experiments with randomized systematics or special systematic tweaks were performed for testing purposes. Several examples are shown in Figs. 27 - 32. The true input and best-fit systematic parameters for each toy experiment is shown. The 1σ pre-fit and post-fit uncertainties are also shown, although the postfit may be difficult to see due to its small scale.

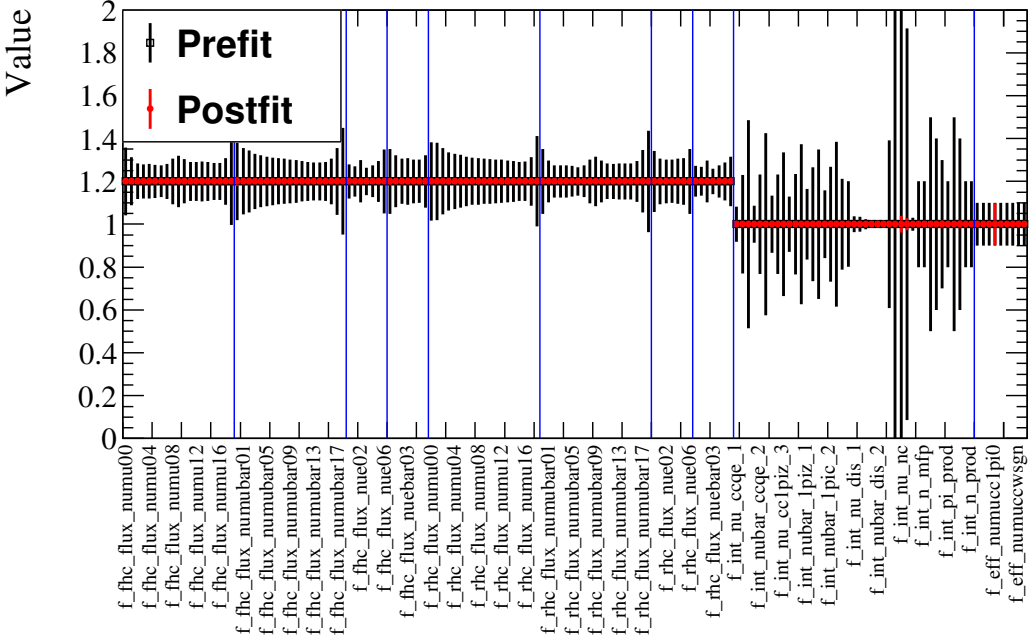


Figure 27: True input and best-fit systematic parameters for the toy experiment #1. This fit has the flux parameters increased by 20% and uses the GArTPC Monte Carlo. The 1σ pre-fit and post-fit uncertainties are also shown, although the postfit may be difficult to see due to its small scale.

5.2 Pull studies

We validated the 2016a fit by testing parameter pulls. For a constrained parameter the pull is defines as

$$\text{Pull} = \frac{p_{\text{bestfit}} - p_{\text{nominal}}}{\sqrt{\sigma_{\text{prior}}^2 - \sigma_{\text{postfit}}^2}} \quad (42)$$

where p is the parameter and σ its uncertainty. The distributions of these parameter pulls should be Gaussian with mean 0 and standard deviation 1 [30]. This was checked by generating 500 toy experiments as outlined in Sec. 2.3. All systematics were randomized using the prior uncertainties and statistical fluctuations were taken into account. The means and standard deviations of Gaussian fits of the pull distributions are shown in Figs. 33 and 34 for the FGT and the HPTPC respectively. Due to MIGRAD reporting bad error matrix status for a majority of LArTPC fits the pull distribution for this detector is not included here.

The standard deviations of the fits represent our tendency to over- or under-estimate our errors. These are generally close to one, showing that our calculated errors are indeed an accurate result from the dataset fitted, even though they may seem unrealistic.

The difference between zero and the mean of the pull distributions shows the bias on our best-fit values. It should be noted that the these biases are large compared to the fitted error, providing a strong motivation for a joint near-to-far oscillation fit, in which these parameters are fully marginalised out.

5.3 Fits to Asimov datasets for all 3 DUNE Near Detector options

Results to Asimov [31] datasets produced for all 3 detector options are shown in this section. They were the main VALOR deliverable for the 2nd pass-through. In the current 2-step fitting process folowed in the 2nd pass-through results from these fits are passed to an external oscillation fitter, but subsequent pass-throughs the main deliverable will be in the form of oscillation sensitivity results from a joint oscillation and

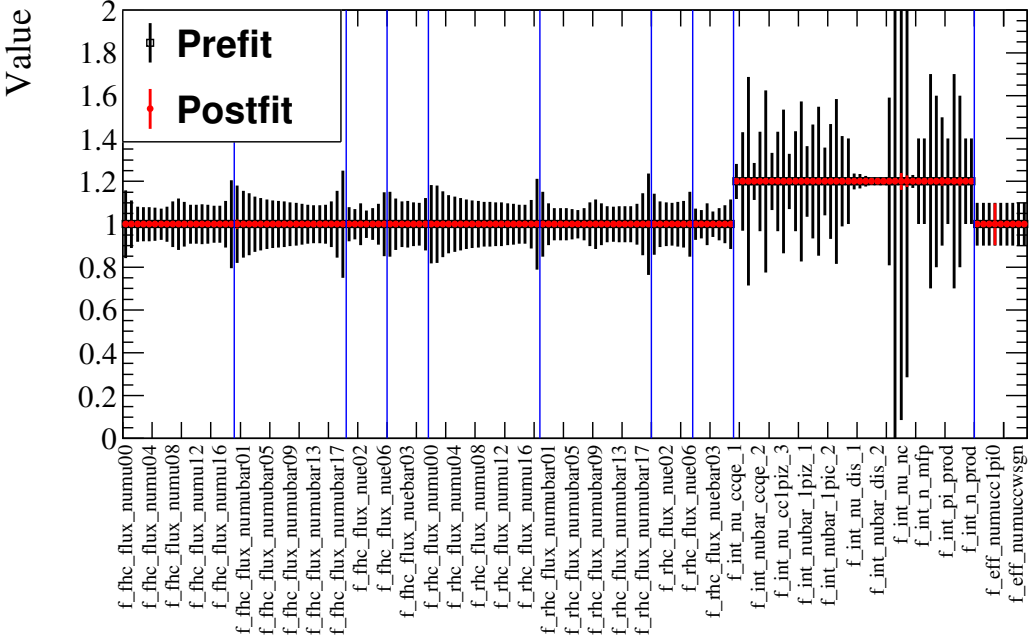


Figure 28: True input and best-fit systematic parameters for the toy experiment #2. This fit has the interaction parameters increased by 20% and uses the GArTPC Monte Carlo. The 1σ pre-fit and post-fit uncertainties are also shown, although the postfit may be difficult to see due to its small scale.

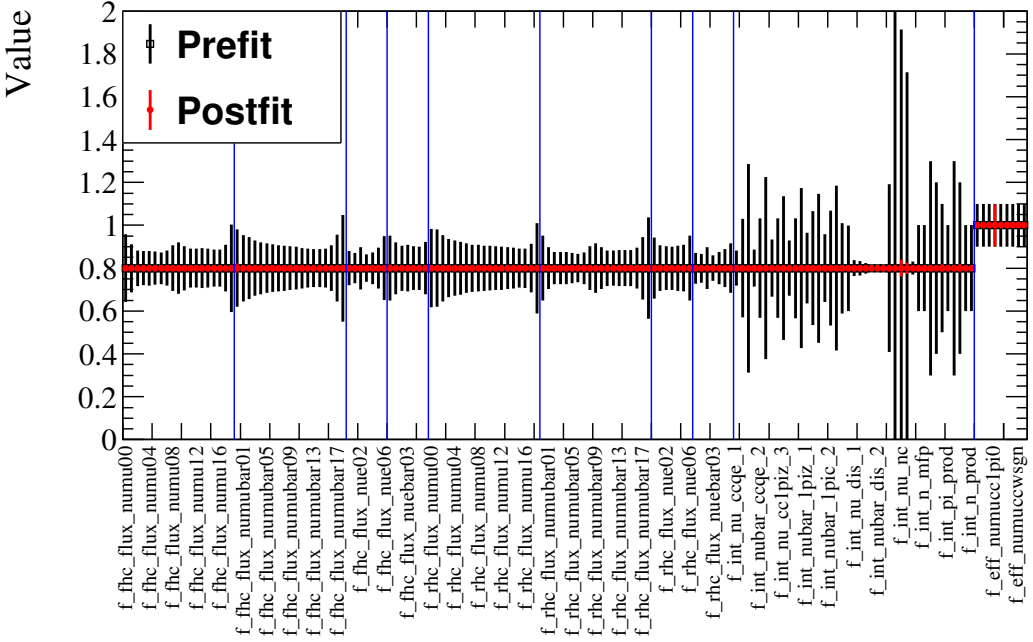


Figure 29: True input and best-fit systematic parameters for the toy experiment #3. This fit has the flux and interaction parameters decreased by 20% and uses the GArTPC Monte Carlo. The 1σ pre-fit and post-fit uncertainties are also shown, although the postfit may be difficult to see due to its small scale.

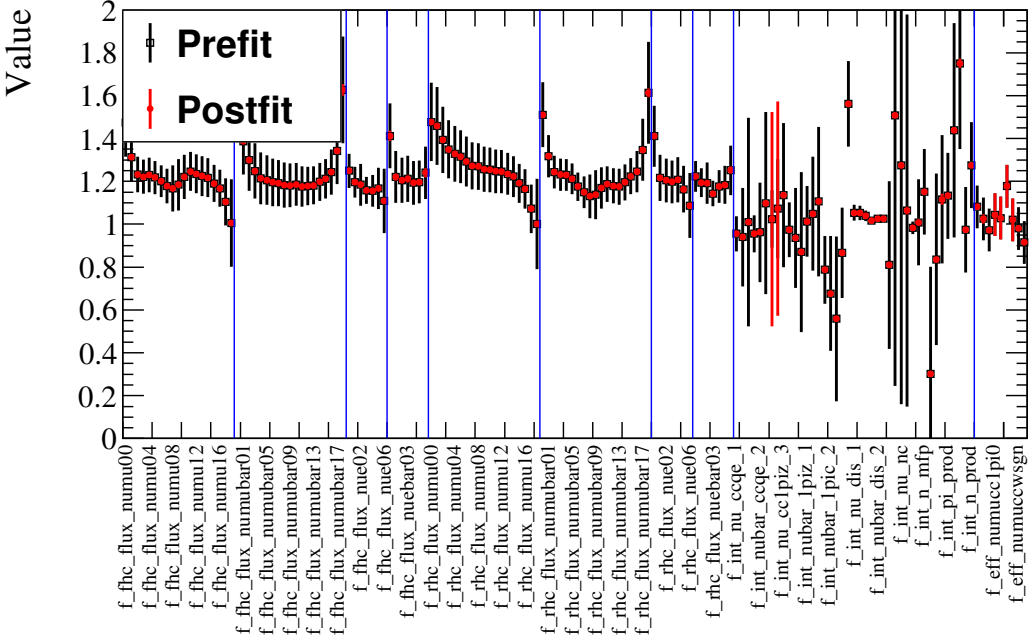


Figure 30: True input and best-fit systematic parameters for the toy experiment #4. This fit has systematic parameterised randomised according to their prior uncertainties and correlations, and uses the FGT Monte Carlo. The 1σ pre-fit and post-fit uncertainties are also shown, although the postfit may be difficult to see due to its small scale.

systematics constraint fit. Results for FGT are shown in Figs. 35, 36. They show the true input and best-fit systematic parameters, along with the the 1σ pre-fit and post-fit uncertainties. The complete covariance matrix provided by VALOR to external oscillation fitters is also shown. The covariance matrix for GArTPC is shown in Fig. 37 wheres for LArTPC in Fig. 38. A comparison between the 3 detector options is shown in Fig. 39. It should be observed that there are significant differences in per-parameter Asimov errors for each detector, although given the differing levels of ‘cheating’ in the reconstruction and selection code for each design no significant conclusions should be drawn from these constraints at this stage. Using the error envelope methodology used in Sec. 3.5 the overall effect of the systematic parameters on the event rate was calculated for each detector, and these can be seen in Tab. 5.

6 Summary

An end-to-end simulation, reconstruction and analysis chain for DUNE is under development. The chain is being incrementally improved and tested in a series of end-to-end “pass-throughs” with an increasing physics content. Results from the VALOR analysis is a major deliverable of the DUNE Near Detector Evaluation WG towards the Task Force’s goal of producing a complete and sophisticated DUNE analysis by the end of 2016. The VALOR group is providing a DUNE oscillation analysis through a simultaneous fit to O(50) Near and Far detector samples. In this preliminary VALOR DUNE technical note, a general description of the analysis and its present status were reported. The present (2016a) version of the VALOR DUNE analysis is an intermediate point in the development of the full fit (2016b) currently being validated for deployment in the next pass-through. The 2016a analysis provides a first implementation of a DUNE Near Detector systematics constraint, and a Near to Far extrapolation method, and underpins the development of the joint fit. A major upgrade of the present analysis, discussed in detail in this technical note, was the inclusion of a fairly comprehensive set of neutrino interaction systematics, and appropriately conservative

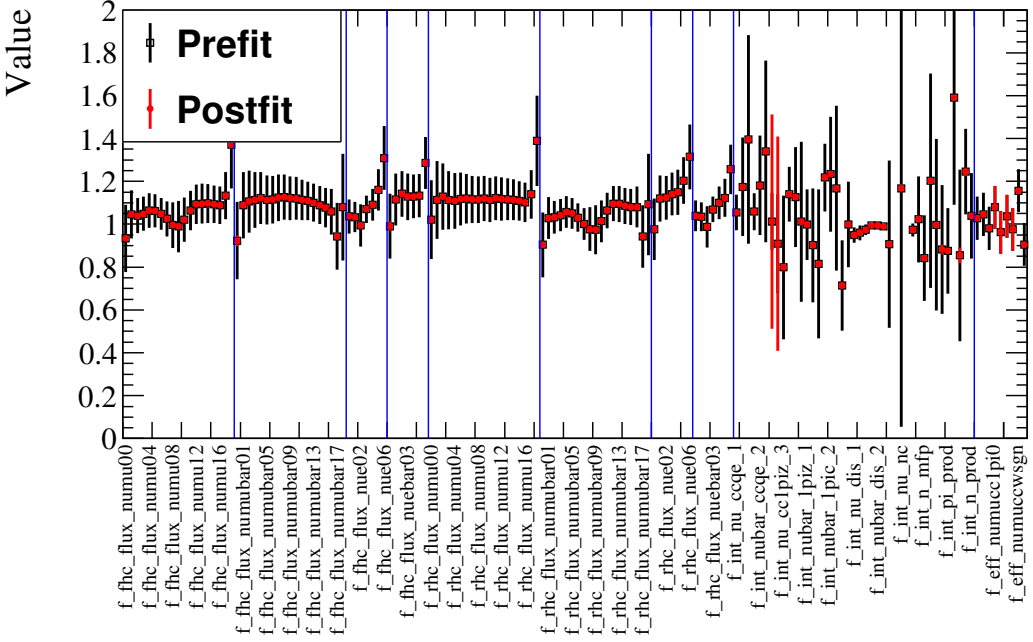


Figure 31: True input and best-fit systematic parameters for the toy experiment #5. This fit has systematic parameterised randomised according to their prior uncertainties and correlations, and uses the FGT Monte Carlo. The 1σ pre-fit and post-fit uncertainties are also shown, although the postfit may be difficult to see due to its small scale.

prior uncertainties supported by a range of data/MC comparisons. The improvements expected to be deployed over the next few weeks were outlined. Results from fits to toy experiments were performed, largely as a validation of technical aspects and of the readiness of the tools. The physics content of the 2nd pass-through was relatively low, and the available event samples can not yet underpin detailed physics studies. Going forward towards the 3rd pass-through, it is clear much more effort needs to be invested in event reconstruction, selections based on reconstructed objects rather than MC truth, and in a first-pass evaluation of acceptance and energy scale errors.

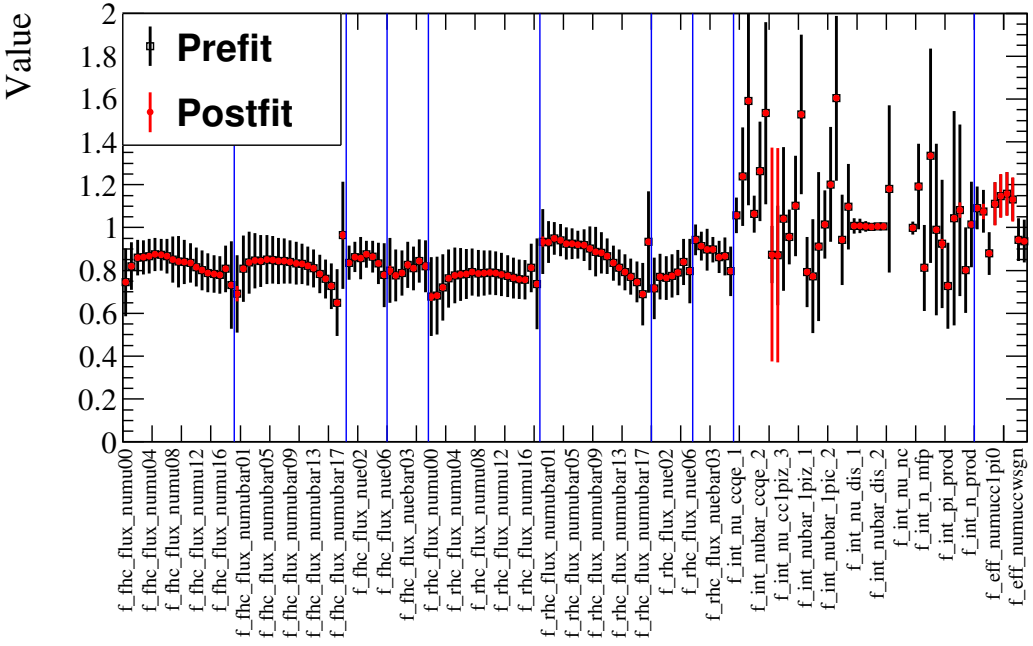


Figure 32: True input and best-fit systematic parameters for the toy experiment #6. This fit has systematic parameterised randomised according to their prior uncertainties and correlations, and uses the FGT Monte Carlo. The 1σ pre-fit and post-fit uncertainties are also shown, although the postfit may be difficult to see due to its small scale.

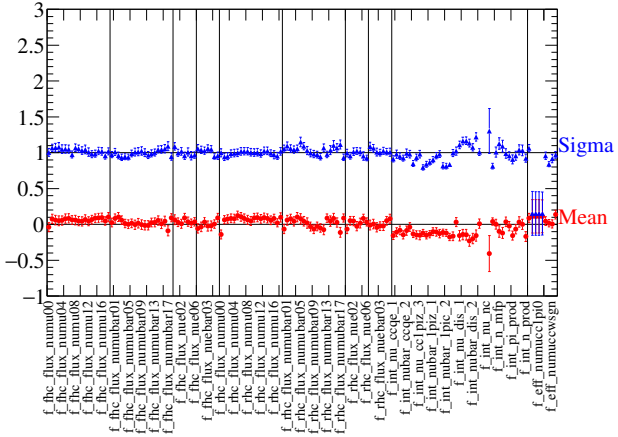


Figure 33: Distributions of parameter pulls for the Fine Grained Tracker. These distributions are from the fits of 500 toy experiments in which systematics were randomized and statistical fluctuations were taken into account. A Gaussian is fitted to each pull histogram. The deviation of the fitted mean (red) from zero represents the bias in the fit. The deviation of the fitted width (blue) from one represents the tendency to over or underestimate the fitted errors.

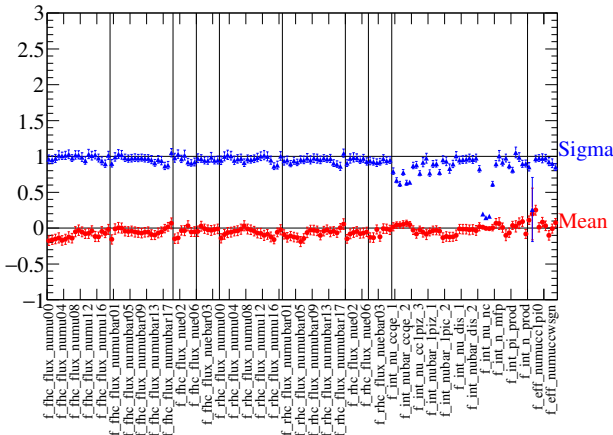


Figure 34: Distributions of parameter pulls for the HPTPC. These distributions are from the fits of 500 toy experiments in which systematics were randomized and statistical fluctuations were taken into account. A Gaussian is fitted to each pull histogram. The deviation of the fitted mean (red) from zero represents the bias in the fit. The deviation of the fitted width (blue) from one represents the tendency to over or underestimate the fitted errors.

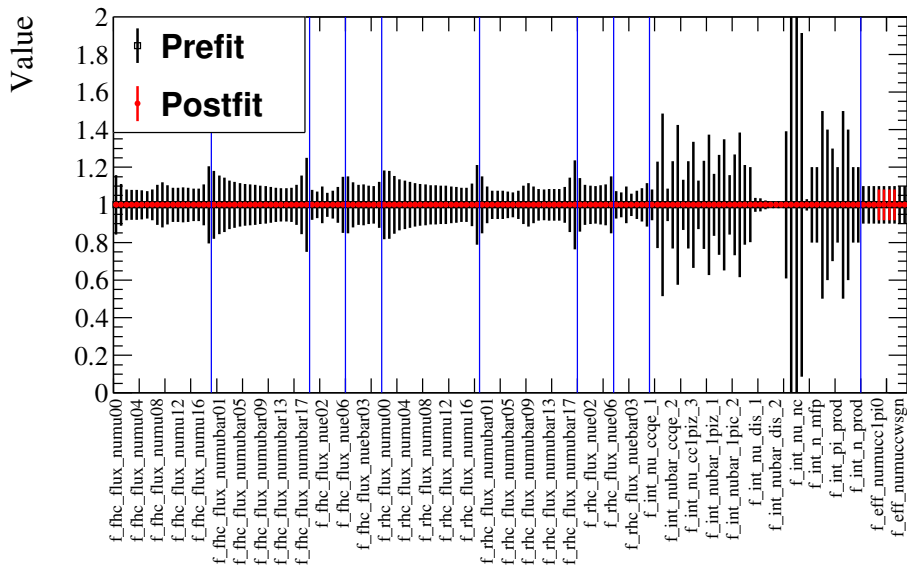


Figure 35: True input and best-fit systematic parameters for a fit to the FGT Asimov dataset. The 1σ pre-fit and post-fit uncertainties are also shown.

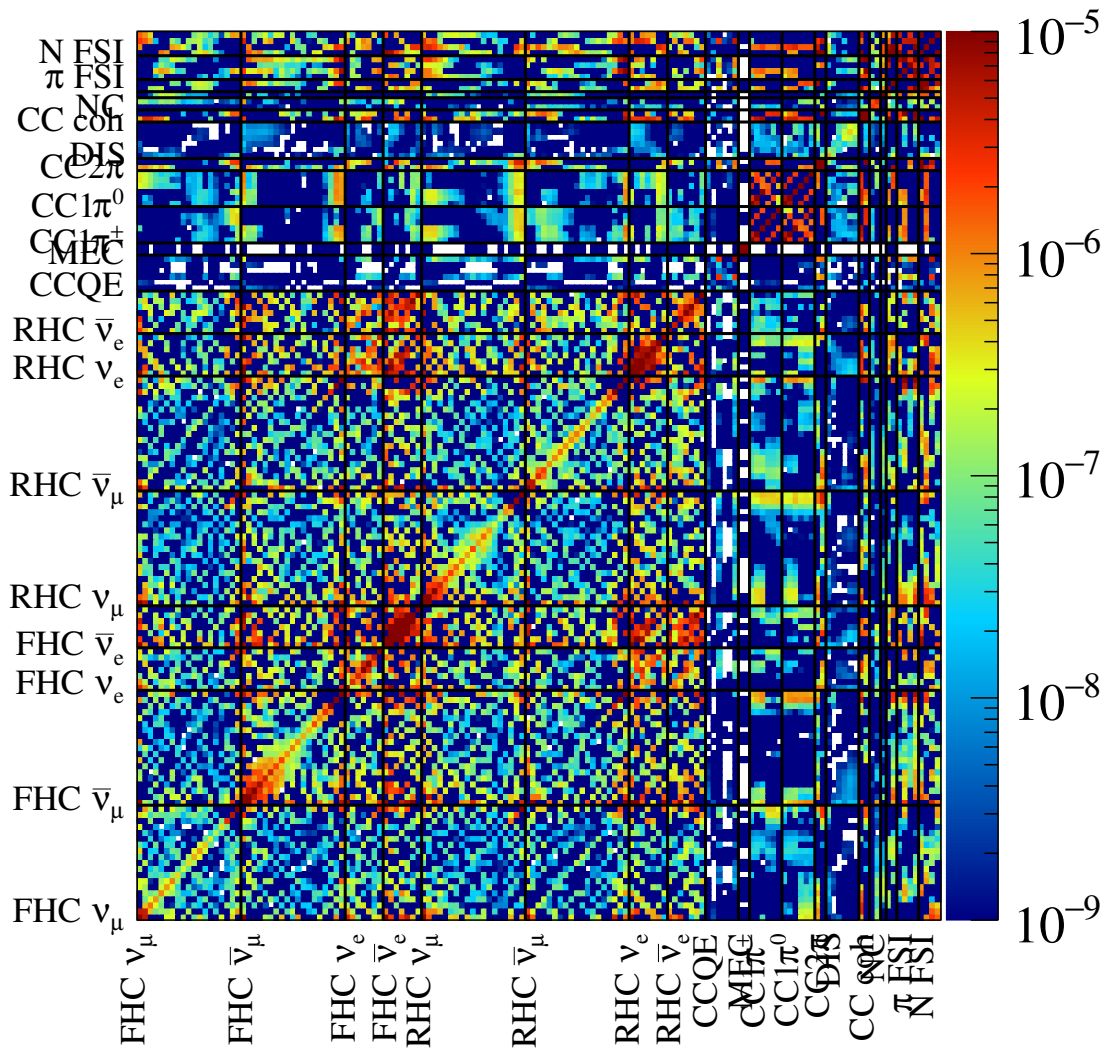


Figure 36: The complete covariance matrix for the VALOR fit to the FGT Asimov dataset.

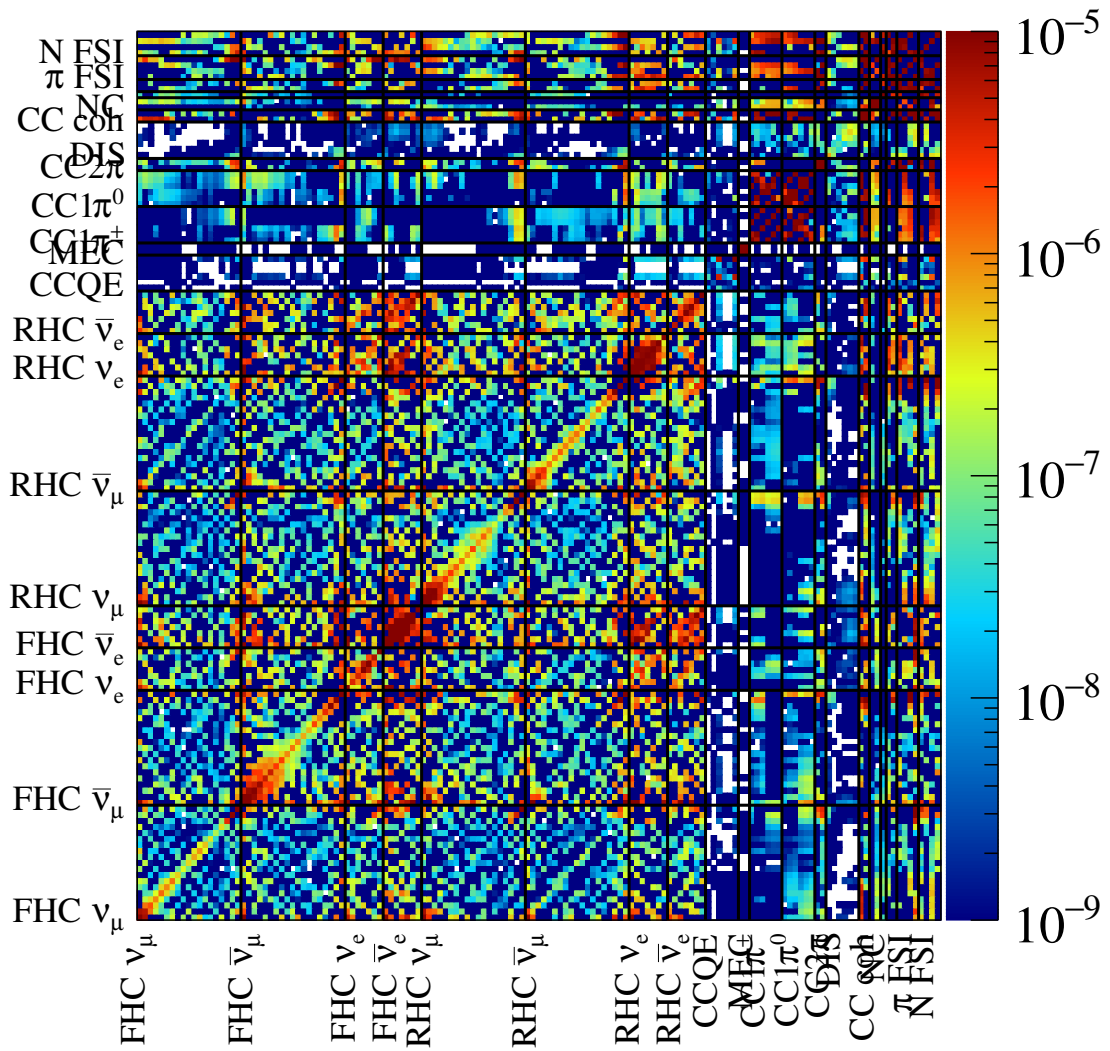


Figure 37: The complete covariance matrix for the VALOR fit to the GArTPC Asimov dataset.

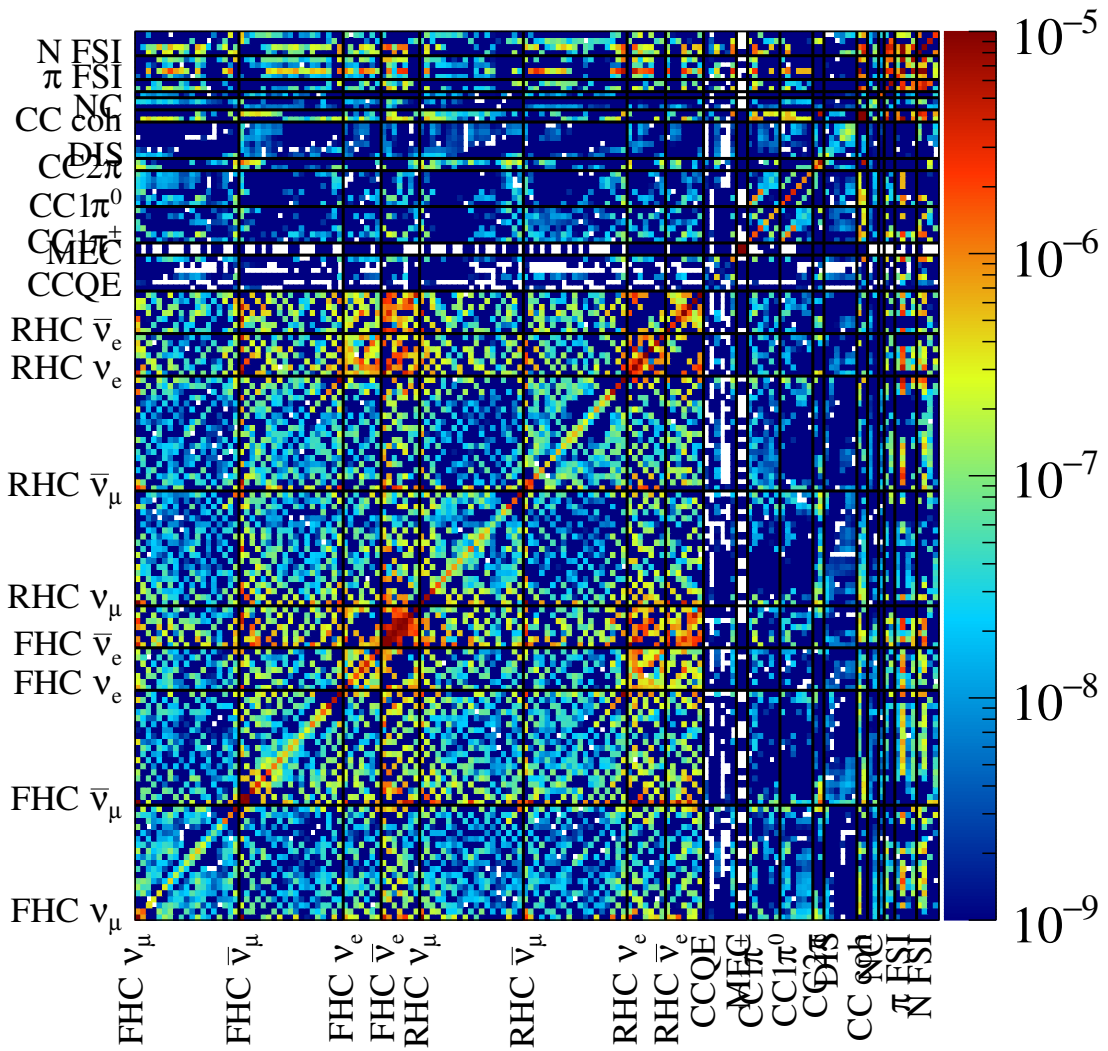


Figure 38: The complete covariance matrix for the VALOR fit to the LArTPC Asimov dataset.

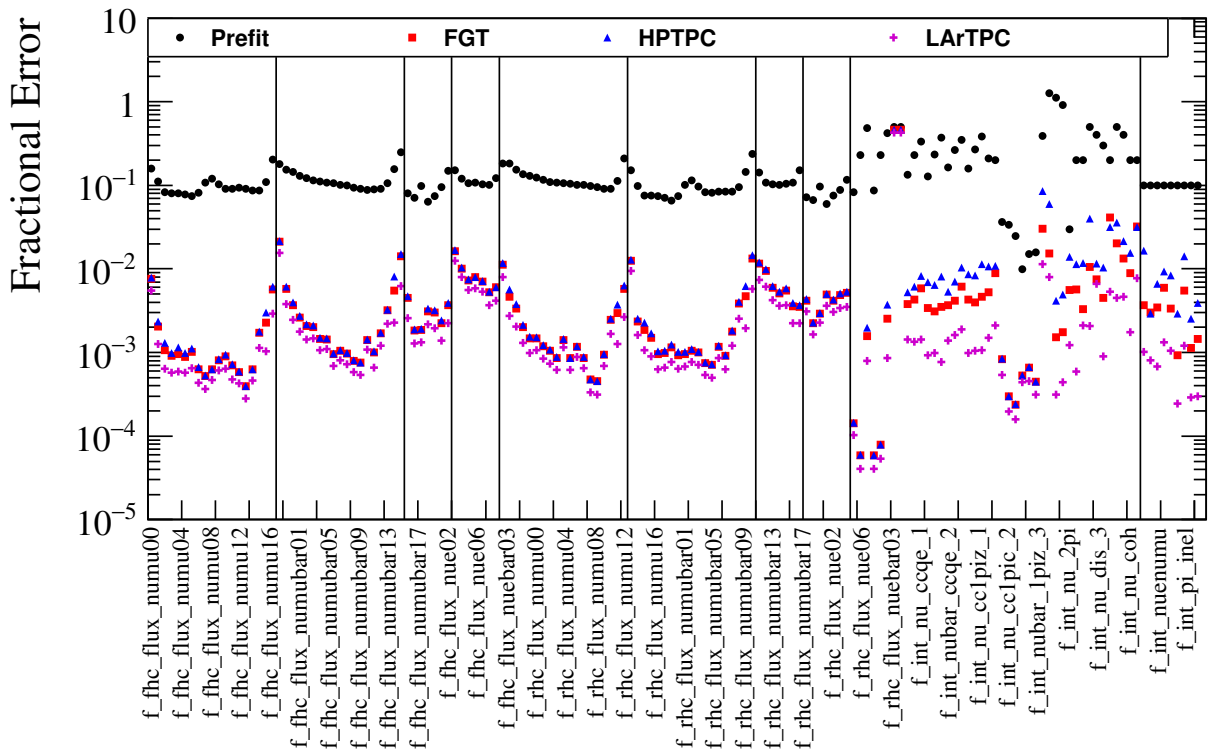


Figure 39: The final fitted errors from each simulated near detector using Asimov dataset for the PT2 Monte Carlo. For PT2, the very large differences in sensitivity are primarily driven by the differences in the ersatz selection and reconstruction between the three detector designs.

Beam	Selection	FGT Postfit (Prefit)	HPTPC Postfit (Prefit)	LArTPC Postfit (Prefit)
FHC	ν_μ CC 1-track QE-like	0.38% (14.99%)	1.63% (18.15%)	0.10% (13.84%)
FHC	ν_μ CC 2-track QE-like	0.42% (26.49%)	0.28% (80.36%)	0.12% (47.29%)
FHC	ν_μ CC $1\pi^\pm$	0.25% (61.53%)	0.50% (68.11%)	0.03% (62.41%)
FHC	ν_μ CC $1\pi^0$	0.31% (85.41%)	0.44% (74.46%)	0.06% (73.87%)
FHC	ν_μ CC $1\pi^\pm + 1\pi^0$	0.34% (58.44%)	0.60% (27.71%)	0.05% (60.00%)
FHC	ν_μ CC other	0.09% (39.17%)	0.20% (18.28%)	0.02% (36.73%)
FHC	ν_e CC inclusive	0.43% (38.03%)	0.96% (37.36%)	0.12% (29.40%)
FHC	Wrong sign ν_μ CC inclusive	0.26% (38.29%)	0.63% (29.57%)	0.07% (35.87%)
FHC	NC inclusive	0.09% (95.74%)	0.19% (95.66%)	0.02% (93.66%)
RHC	ν_μ CC 1-track QE-like	0.41% (13.81%)	1.61% (48.30%)	0.12% (12.91%)
RHC	ν_μ CC 2-track QE-like	0.18% (79.45%)	1.66% (81.96%)	0.05% (73.94%)
RHC	ν_μ CC $1\pi^\pm$	0.31% (72.66%)	0.83% (75.30%)	0.05% (73.81%)
RHC	ν_μ CC $1\pi^0$	0.48% (101.93%)	2.26% (102.94%)	0.10% (85.04%)
RHC	ν_μ CC $1\pi^\pm + 1\pi^0$	0.49% (78.96%)	0.93% (31.66%)	0.07% (69.95%)
RHC	ν_μ CC other	0.19% (49.71%)	0.47% (20.44%)	0.04% (51.46%)
RHC	ν_e CC inclusive	0.52% (37.68%)	0.95% (30.65%)	0.14% (28.77%)
RHC	Wrong sign ν_μ CC inclusive	0.15% (28.36%)	0.29% (22.45%)	0.04% (31.87%)
RHC	NC inclusive	0.11% (84.09%)	0.25% (89.21%)	0.03% (82.53%)

Table 5: Prefit and postfit uncertainties on the total event rate for each selection. In each case 1k toy-MC experiments are generated with randomised (correlated) systematics using the prefit or postfit systematic parameter covariance matrix and the 1σ spread of bin contents is calculated.

References

- [1] Costas Andreopoulos, Christopher Barry, Francis Bench, Andrew Chappell, Thomas Dealtry, Steve Dennis, Lorena Escudero, Rhiannon Jones, Nick Grant, Marco Roda, Davide Sgalaberna and Raj Shah (The VALOR group), <https://valor.pp.rl.ac.uk>
- [2] C.Andreopoulos et al. (The VALOR group), T2K 3.23×10^{19} -POT Muon-Neutrino Disappearance Analysis, T2K internal note T2K-TN-036(v4), <http://www.t2k.org/docs/technotes/036>
- [3] C.Andreopoulos et al. (The VALOR group), T2K 1.431×10^{20} -POT Muon-Neutrino Disappearance Analysis T2K internal note T2K-TN-064(v3), <http://www.t2k.org/docs/technotes/064>
- [4] C.Andreopoulos et al. (The VALOR group), T2K 1.431×10^{20} -POT 3-Flavour Muon-Neutrino Disappearance Analysis T2K internal note T2K-TN-087(v1), <http://www.t2k.org/docs/technotes/087>
- [5] C.Andreopoulos et al. (The VALOR group), T2K 3.010×10^{20} -POT 3-Flavour Muon-Neutrino Disappearance Analysis T2K internal note T2K-TN-141(v10), <http://www.t2k.org/docs/technotes/141>
- [6] C.Andreopoulos et al. (The VALOR group), T2K 6.3933×10^{20} -POT 3-Flavour Muon-Neutrino Disappearance Analysis T2K internal note T2K-TN-155(v2), <http://www.t2k.org/docs/technotes/155>
- [7] C.Andreopoulos et al. (The VALOR group), T2K 6.57×10^{20} -POT 3-Flavour Muon-Neutrino Disappearance Analysis T2K internal note T2K-TN-183(v3), <http://www.t2k.org/docs/technotes/183>
- [8] C.Andreopoulos et al. (The VALOR group), T2K 3.010×10^{20} -POT Joint 3-Flavour Oscillation Analysis T2K internal note T2K-TN-154(v3), <http://www.t2k.org/docs/technotes/154>
- [9] C.Andreopoulos et al. (The VALOR group), T2K 6.57×10^{20} -POT Joint 3-Flavour Oscillation Analysis T2K internal note T2K-TN-175, <http://www.t2k.org/docs/technotes/175>
- [10] C.Andreopoulos et al. (The VALOR group), T2K 4.011×10^{20} -POT 3-Flavour Muon-Antineutrino Disappearance Analysis T2K internal note T2K-TN-243(v5), <http://www.t2k.org/docs/technotes/243>
- [11] C.Andreopoulos et al. (The VALOR group), T2K 4.0108×10^{20} -POT 3-Flavour Electron-Antineutrino Appearance Analysis T2K internal note T2K-TN-252(v2.3), <http://www.t2k.org/docs/technotes/252>
- [12] C.Andreopoulos et al. (The VALOR group), T2K 6.914×10^{20} -POT Neutrino T2K 4.011×10^{20} -POT Anti-Neutrino 3-Flavour Joint Analysis T2K internal note T2K-TN-266, <http://www.t2k.org/docs/technotes/266>
- [13] Description of the 2nd Run Through of the Processing Chain for the Near Detector Task Force, <https://docs.google.com/document/d/1CNEO8xW06ooCEG3YG0AKtUdvLFuWO3GN-wGLEwdetO0>
- [14] Leonidas Aliaga Soplin, FERMILAB-THESIS-2016-03, <http://inspirehep.net/record/1450751?ln=en>
- [15] Laura Fields, DUNE DocDB-893, <http://docs.dunescience.org:8080/cgi-bin>ShowDocument?docid=893>
- [16] C.Andreopoulos, A.Bell, D.Bhattacharya, F.Cavanna, J.Dobson, S.Dytman, H.Gallagher, P.Guzowski, R.Hatcher, P.Kehayias, A.Meregaglia, D.Naples, G.Pearce, A.Rubbia, M.Whalley and T.Yang, The GENIE Neutrino Monte Carlo Generator, Nucl.Instrum.Meth.A614 (2010) 87-104
- [17] C.Andreopoulos, C.Barry, S.Dytman, H.Gallagher, T.Golan, R.Hatcher, G.Perdue and J.Yarba The GENIE Neutrino Monte Carlo Generator: Physics and User Manual, arXiv:1510.05494[hep-ph]
- [18] G.L.Fogli, E.Lisi et al., Evidence of theta(13)>0 from global neutrino data analysis, arXiv:1106.6028 [hep-ph]
- [19] B. Kayser (2005), Neutrino physics, hep-ph 0506165

- [20] C Giunti and C.W. Kim (2007) Fundamentals of neutrino physics and astrophysics, Oxford University Press
- [21] K. Nakamura and S.T. Petcov (2014) Neutrino mass, mixing and oscillations, <http://pdg.lbl.gov/2015/reviews/rpp2015-rev-neutrino-mixing.pdf>
- [22] J. Kopp (2006), Efficient numerical diagonalisation of Hermitian 3x3 matrices, arXiv:physics/0610206
- [23] T. Sloan, private communication (June-July 2011)
- [24] <http://www.phy.duke.edu/~raw22/public/Prob3++>
- [25] J. Kopp et al. (2014), Sterile neutrino oscillations: the global picture, <http://arxiv.org/pdf/1303.3011v3.pdf>
- [26] GNU scientific library, <http://www.gnu.org/software/gsl/>
- [27] General long-baseline experiment simulator (GLoBES), <https://www.mpi-hd.mpg.de/personalhomes/globes/>
- [28] F.James, M.Roos (1975) Minuit: A System for Function Minimization and Analysis of the Parameter Errors and Correlations, Comput.Phys.Commun. 10:343
- [29] Numerical Recipes: The art of scientific computing, Cambridge University Press, 3rd Edition, ISBN 978-0-521-88068-0, pp. 100-102.
- [30] L. Demortier and L. Lyons (2002), Everything you always wanted to know about pulls, http://physics.rockefeller.edu/luc/technical_reports/cdf5776_pulls.pdf
- [31] G.Cowan, K.Cranmer, E.Gross, O.Vitells, Asymptotic formulae for likelihood-based tests of new physics, arXiv:1007.1727v2
- [32] J. Stuart, A. Ord and S.Arnold, Kendall's Advanced Theory of Statistics, Vol 2A (6th Ed.), Oxford University Press, New York, 1994.
- [33] R.D. Cousins and V.L.Highland, Nucl.Instrum.Meth.A320 (1992) 331035
- [34] G.J. Feldman and R.D. Cousins, A Unified approach to the classical statistical analysis of small signals, Phys.Rev.D57:3873-3889,1998; physics/9711021
- [35] Long-Baseline Neutrino Facility (LBNF) and Deep Underground Neutrino Experiment (DUNE). Conceptual Design Report (2015) <http://docs.dunescience.org/>
- [36] <http://home.fnal.gov/~ljf26/DUNE2015CDRFluxes/>
- [37] <http://hepdata.cedar.ac.uk/review/f2/> ad references there-in.
- [38] Barish et al. (ANL 12-ft Bubble Chamber Collaboration), Phys.Lett.B66:291 (1977)
- [39] Barish et al. (ANL 12-ft Bubble Chamber Collaboration), Phys.Rev.D19:2521 (1979)
- [40] Mann et al. (ANL 12-ft Bubble Chamber Collaboration), Phys.Rev.Lett.31:844 (1973)
- [41] Barish et al. (ANL 12-ft Bubble Chamber Collaboration), Phys.Rev.D16:3103 (1977)
- [42] Campbell et al. (ANL 12-ft Bubble Chamber Collaboration), Phys.Rev.Lett.30:335(1973)
- [43] Radecky et al. (ANL 12-ft Bubble Chamber Collaboration), Phys.Rev.D25:1161 (1982)
- [44] Day et al. (ANL 12-ft Bubble Chamber Collaboration), Phys.Rev.D28:2714 (1983);

- [45] Bossetti et al. (BEBC Collaboration), Phys.Lett.B70:273 (1977)
- [46] Bossetti et al. (BEBC Collaboration), Phys.Lett.B110:167 (1982)
- [47] Colley et al. (BEBC Collaboration), Zeit.Phys.C2:187 (1979)
- [48] Bosetti et al. (BEBC Collaboration), Phys.Lett.B110:167 (1982)
- [49] Parker et al. (BEBC Collaboration), Nucl.Phys.B232:1 (1984)
- [50] Allasia et al. (BEBC Collaboration), Nucl.Phys.B343:285 (1990)
- [51] Allen et al. (BEBC Collaboration), Nucl.Phys.B176:269 (1980);
- [52] Allen et al. (BEBC Collaboration), Nucl.Phys.B264:221 (1986);
- [53] Baltay et al. (BNL 7-ft Bubble Chamber Collaboration), Phys.Rev.Lett.44:916 (1980)
- [54] Baker et al. (BNL 7-ft Bubble Chamber Collaboration), Phys.Rev.D25:617 (1982)
- [55] Fanourakis et al. (BNL 7-ft Bubble Chamber Collaboration), Phys.Rev.D21:562 (1980)
- [56] Baker et al. (BNL 7-ft Bubble Chamber Collaboration), Phys.Rev.D23:2499 (1981)
- [57] Kitagaki et al. (BNL 7-ft Bubble Chamber Collaboration), Phys.Rev.D34:2554 (1986);
- [58] Seligman et al. (CCFR Collaboration), Nevis Report 292 (1996)
- [59] MacFarlane et al. (CCFRR Collaboration), Zeit.Phys.C26:1 (1984)
- [60] Jonker et al. (CHARM Collaboration), Phys.Lett.B99:265 (1981)
- [61] Allaby et al. (CHARM Collaboration), Zeit.Phys.C38:403 (1988)
- [62] Kitagaki et al. (FNAL 15-ft Bubble Chamber Collaboration), Phys.Rev.Lett.49:98 (1982)
- [63] Baker et al. (FNAL 15-ft Bubble Chamber Collaboration), Phys.Rev.Lett.51:735 (1983)
- [64] Taylor et al. (FNAL 15-ft Bubble Chamber Collaboration), Phys.Rev.Lett.51:739 (1983)
- [65] Asratyan et al. (FNAL 15-ft Bubble Chamber Collaboration), Phys.Lett.B137:122 (1984)
- [66] Bell et al. (FNAL 15-ft Bubble Chamber Collaboration), Phys.Rev.Lett.41:1008 (1978);
- [67] Eichten et al. (Gargamelle Collaboration), Phys.Lett.B46:274 (1973)
- [68] Ciampolillo et al. (Gargamelle Collaboration), Phys.Lett.B84:281 (1979)
- [69] Morfin et al. (Gargamelle Collaboration), Phys.Lett.B104:235 (1981)
- [70] Erriquez et al. (Gargamelle Collaboration), Phys.Lett.B80:309 (1979)
- [71] Lerche et al. (Gargamelle Collaboration), Phys.Lett.B78:510 (1978);
- [72] Asratyan et al. (IHEP/ITEP), Phys.Lett.B76:239 (1978)
- [73] Vovenko et al. (IHEP/ITEP), Sov.J.Nucl.Phys.30:528 (1979)
- [74] Anikeev et al. (IHEP/JINR), Zeit.Phys.C70:39 (1996)
- [75] Baranov et al. (SKAT Collaboration), Phys.Rev.B81 255 (1979)
- [76] Ammosov et al. (SKAT Collaboration), Sov.J.Nucl.Phys.50:67 (1988);

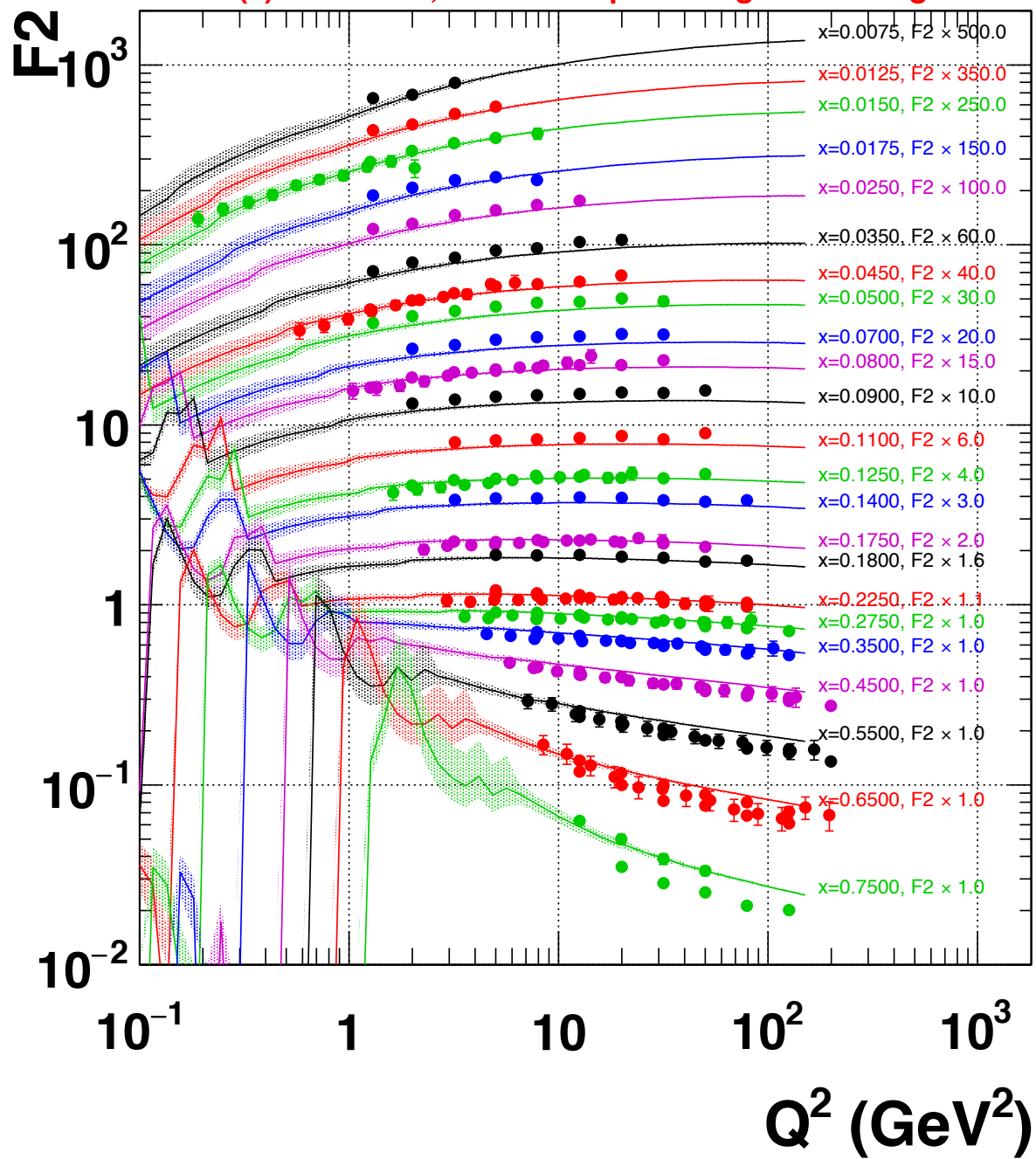
- [77] Grabosch et al. (SKAT Collaboration), *Zeit.Phys.C*41:527 (1988)
- [78] Adamson et al. (MINOS Collaboration), *Phys.Rev.D*81:072002 (2010)
- [79] Nakajima et al. (SciBooNE Collaboration), *Phys.Rev.D*83:012005 (2011)
- [80] A.A. Aguilar-Arevalo et al. (The MiniBooNE Collaboration), *Phys. Rev. D*81 (2010) 092005
2010 Neutrino CCQE data release, http://www-boone.fnal.gov/for_physicists/data_release/ccqe
- [81] A.A. Aguilar-Arevalo et al. (The MiniBooNE Collaboration), *Phys. Rev. D*88 (2013) 032001
2013 Anti-neutrino CCQE data release, http://www-boone.fnal.gov/for_physicists/data_release/ccqe_nubar
- [82] A.A. Aguilar-Arevalo et al. (The MiniBooNE Collaboration), *Phys. Rev. D*83 (2011) 052007
2011 Neutrino CC1pi+ data release, http://www-boone.fnal.gov/for_physicists/data_release/ccpip
- [83] A.A. Aguilar-Arevalo et al. (The MiniBooNE Collaboration), *Phys. Rev. D*83 (2011) 092009
2010 Neutrino CC1pi0 data release, http://www-boone.fnal.gov/for_physicists/data_release/ccpi0
- [84] A.A. Aguilar-Arevalo et al. (The MiniBooNE Collaboration), *Phys. Rev. D*81 (2010) 013005
2010 Neutrino and Anti-neutrino NC1pi0 data release,
http://www-boone.fnal.gov/for_physicists/data_release/ncpi0
- [85] A.A. Aguilar-Arevalo et al. (The MiniBooNE Collaboration), *Phys. Rev. D*82 (2010) 092005
2010 Neutrino NCEL data release, http://www-boone.fnal.gov/for_physicists/data_release/ncel
- [86] A.A. Aguilar-Arevalo et al. (The MiniBooNE Collaboration), *Phys. Rev. D*91 (2015) 012004
2015 Anti-neutrino NCEL data release, http://www-boone.fnal.gov/for_physicists/data_release/ncel_nubar
- [87] K.Abe et al. (The T2K Collaboration), Measurement of double-differential muon neutrino charged-current interactions on C8H8 without pions in the final state using the T2K off-axis beam, Submitted to PRD; arXiv:1602.03652 [hep-ex]
2015 T2K/ND280 numu CC0pi data relase <http://t2k-experiment.org/publications/nd280data-numu-cc0pi-xs-on-c-2015/>
- [88] K. Abe et al. (The T2K Collaboration), Measurement of the muon-neutrino charged current quasi-elastic cross-section on carbon with the T2K on-axis neutrino beam, *PRD* 91 (2015) 11, 112002; arXiv:1503.07452 [hep-ex]. 2015 T2K/INGRID numu CCQE data relase <http://t2k-experiment.org/results/ingriddata-numu-ccqe-xs-2015/>
- [89] K. Abe et al. (The T2K Collaboration), Measurement of the Inclusive Electron Neutrino Charged Current Cross Section on Carbon with the T2K Near Detector, *PRL* 113 (2014) 24, 241803; arXiv:1407.7389 [hep-ex]. 2014 T2K/ND280 nue CC inclusive data relase <http://t2k-experiment.org/results/t2k-nue-ccinc-2014>
- [90] K. Abe et. al. (The T2K Collaboration), Measurement of the muon-neutrino CCQE cross section on carbon with the ND280 detector at T2K, *PRD* 92 (2015) 112003; arXiv:1411.6264 [hep-ex]. 2014 T2K/ND280 numu CCQE data relase <http://t2k-experiment.org/results/nd280data-energy-dependent-ccqe-xsec-2014/>
- [91] K. Abe et al. (The T2K Collaboration), Measurement of the Inclusive Muon Neutrino Charged Current Cross Section on Carbon in the Near Detector of the T2K Experiment, *PRD* 87 (2013) 9, 092003; arXiv:1302.4908 [hep-ex]. 2013 T2K/ND280 numu CC inclusive data relase <http://t2k-experiment.org/results/nd280data-numu-cc-inc-xs-on-c-2013/>

A 2016a VALOR/GENIE error model: Supporting GENIE / data comparisons

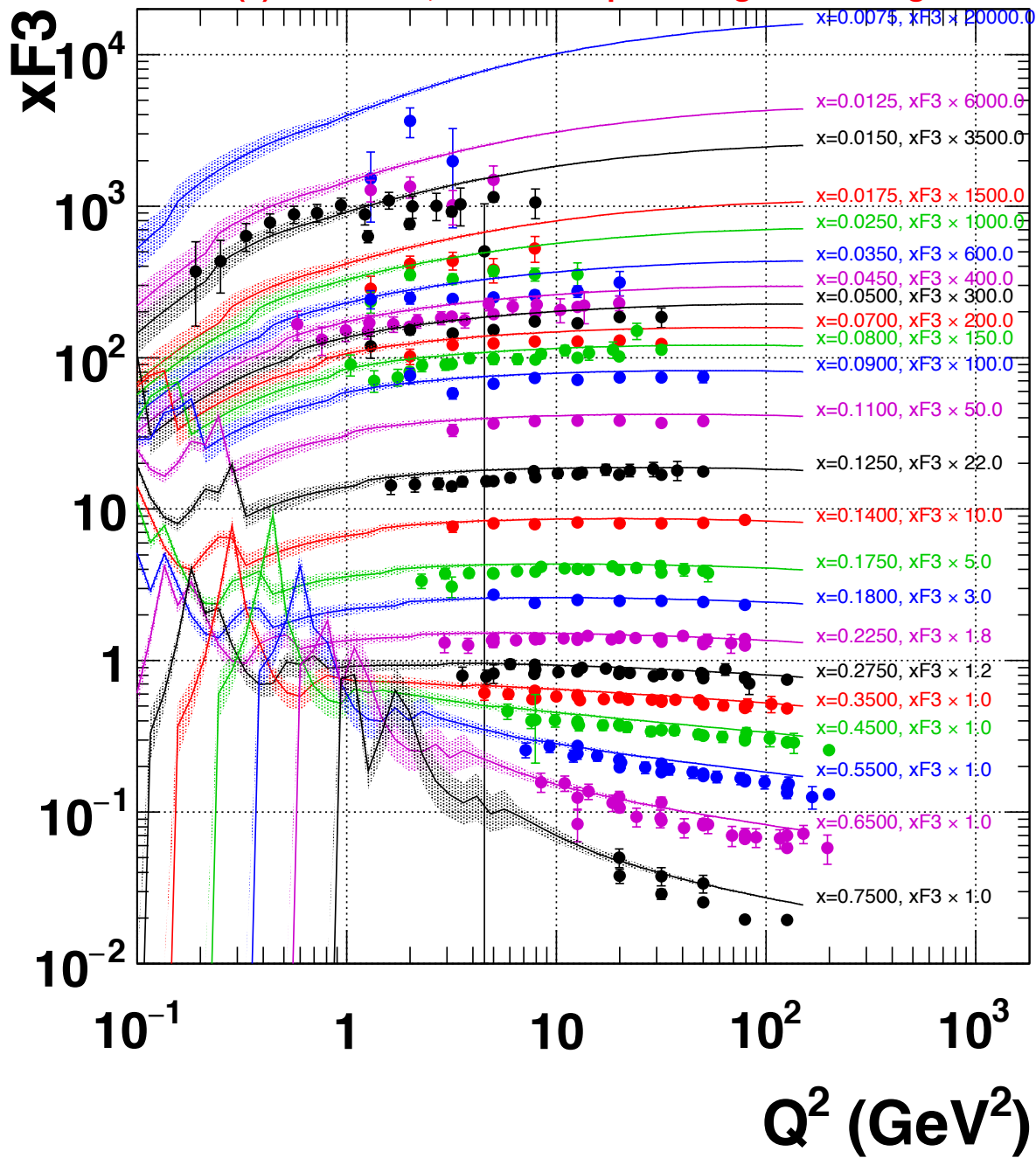
In support of the neutrino interaction error assignments used in the VALOR DUNE analysis, several comparisons between GENIE and external data were performed using GENIE v2.10.6. Error envelopes for the GENIE predictions were computed using a methodology which is similar to the one used for constructing the input neutrino interaction error matrix (see Sec. 3.4.2). Due to the specifics of the GENIE code used for constructing the data/MC comparisons, the error envelopes correspond to somewhat more conservative error assignments than the ones used in the for constructing the error matrix which is input to the VALOR fit. This inconsistency will be addressed in the next revision of data/MC comparisons for the 2016b version of the VALOR fit. In the following pages we present GENIE v2.10.6 predictions and VALOR/GENIE error envelopes. These results are compared against several pieces of data:

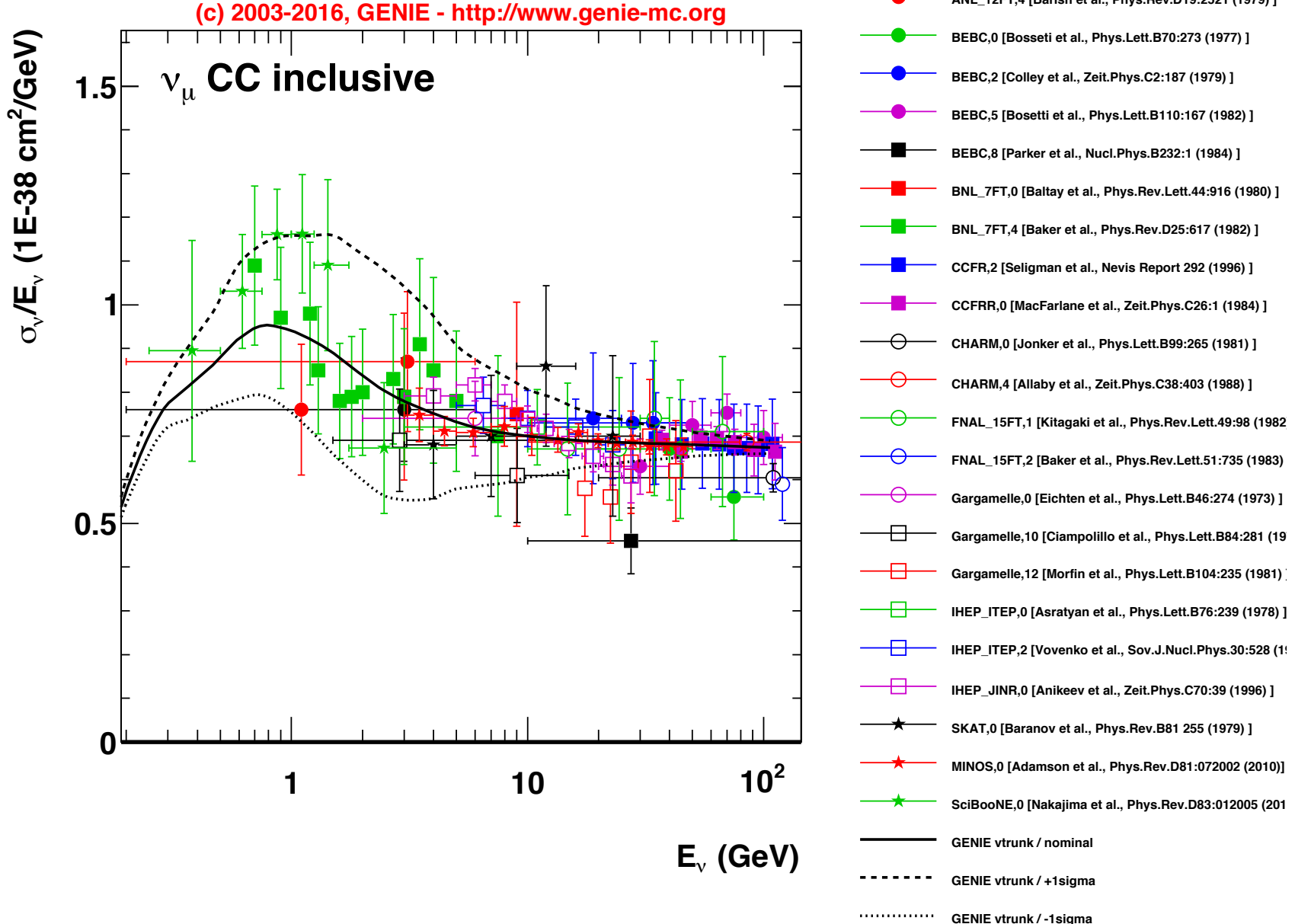
- F_2 and xF_3 structure function data [37].
- Legacy CC inclusive data coming primarily from bubble chamber data [38] [39] [45] [46] [47] [48] [49] [53] [54] [55] [58] [59] [60] [61] [62] [63] [64] [65] [67] [68] [69] [70] [72] [73] [74] [75] [78] [79]
- Legacy CCQE data [40] [41] [50] [56] [55]
- Legacy $CC1\pi$ data [39] [42] [43] [50] [51] [52] [57] [66] [71] [76] [77]
- Legacy $CC2\pi$ data [44] [57]
- Recent MiniBooNE data releases:
 - 2010 Neutrino CCQE data release [80]
 - 2013 Anti-neutrino CCQE data release [81]
 - 2011 Neutrino $CC1\pi^+$ data release [82]
 - 2010 Neutrino $CC1\pi^0$ data release [83]
 - 2010 Neutrino and Anti-neutrino $NC1\pi^0$ data release [84]
 - 2010 Neutrino NCEL data release [85]
 - 2015 Anti-neutrino NCEL data release [86]
- Recent T2K data releases:
 - 2015 T2K/ND280 numu $CC0\pi$ data relase [87]
 - 2015 T2K/INGRID numu CCQE data relase [88]
 - 2014 T2K/ND280 nue CC inclusive data relase [89]
 - 2014 T2K/ND280 numu CCQE data relase [90]
 - 2013 T2K/ND280 numu CC inclusive data relase [91]

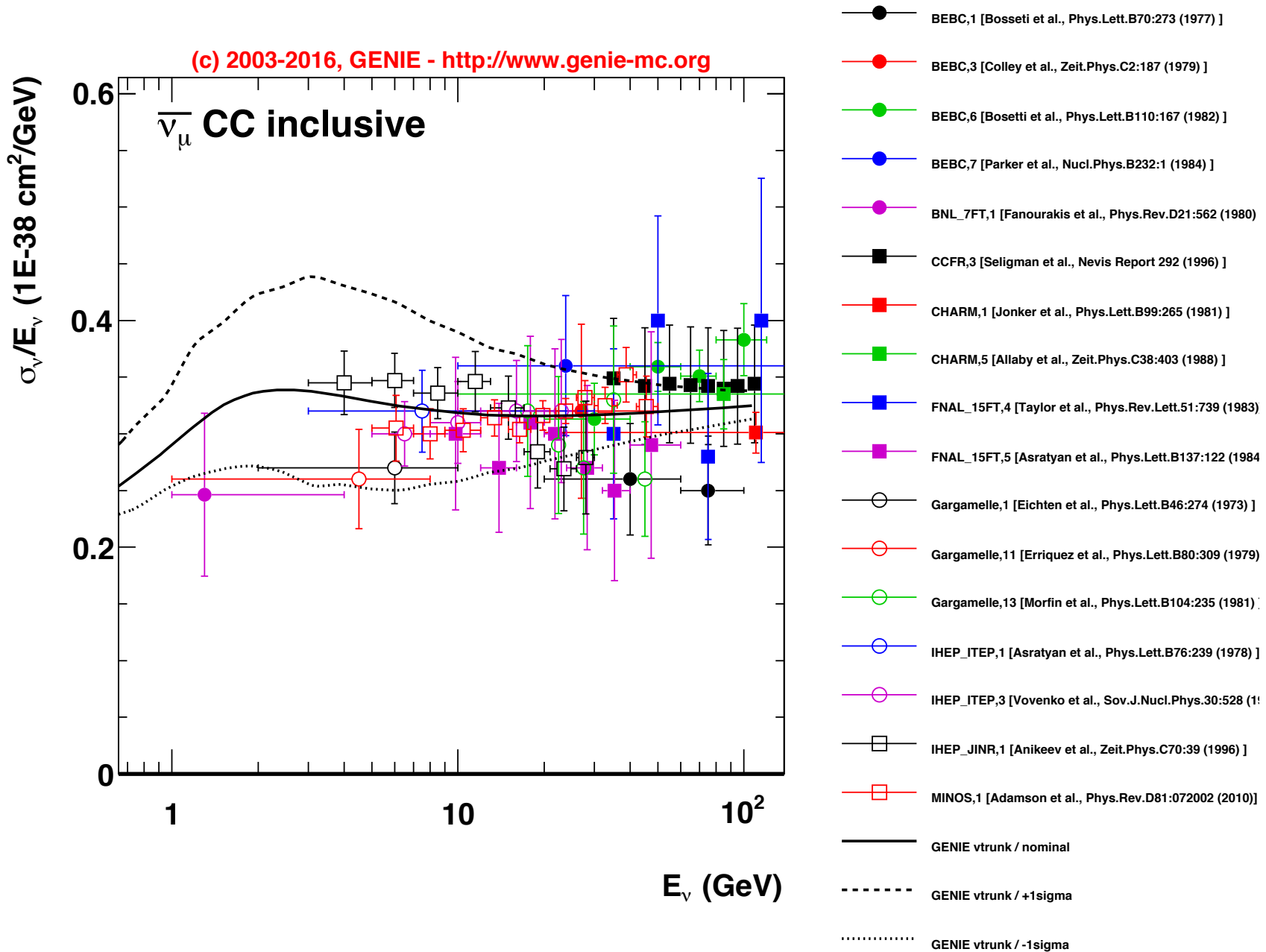
(c) 2003-2016, GENIE - <http://www.genie-mc.org>

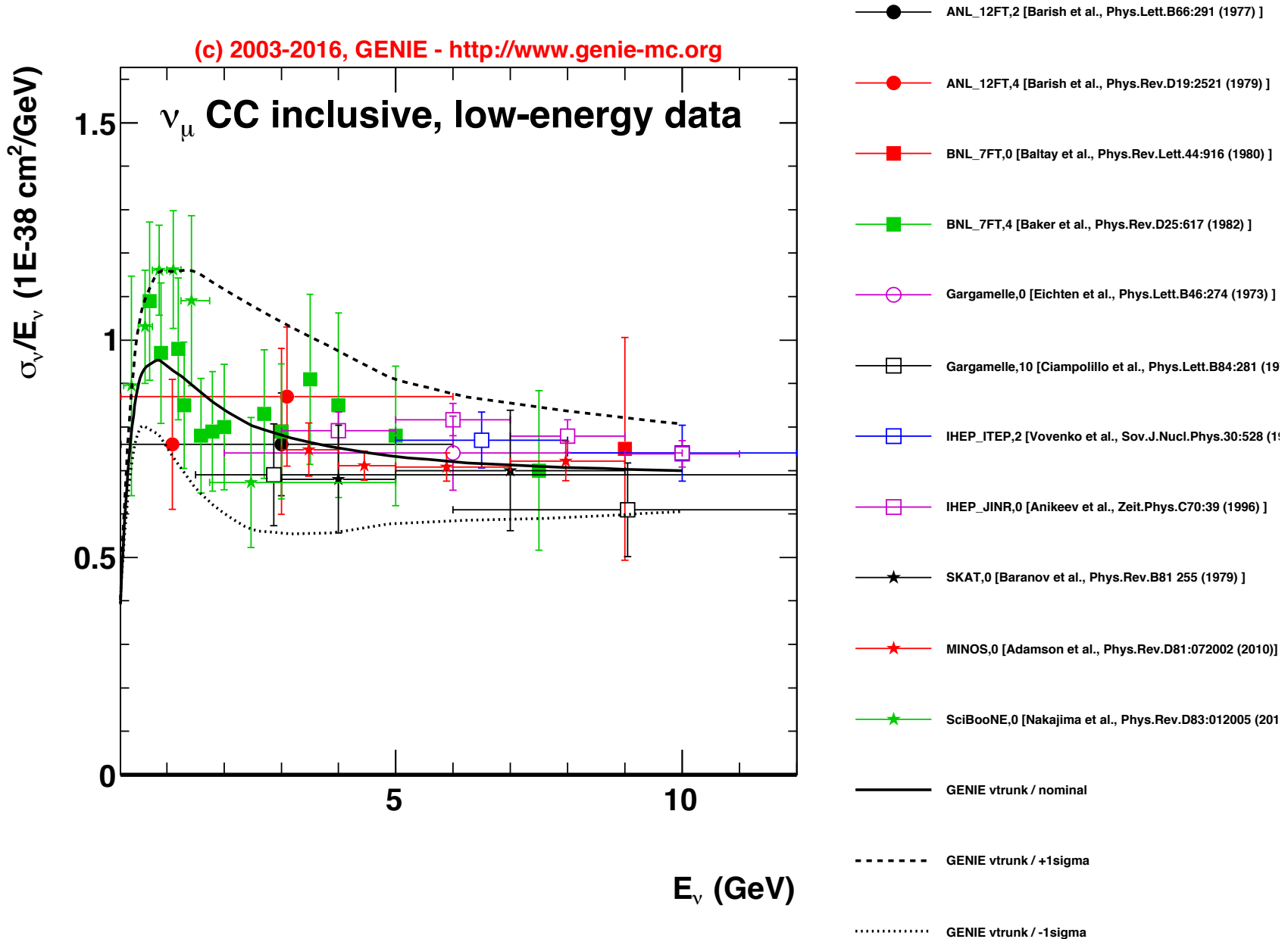


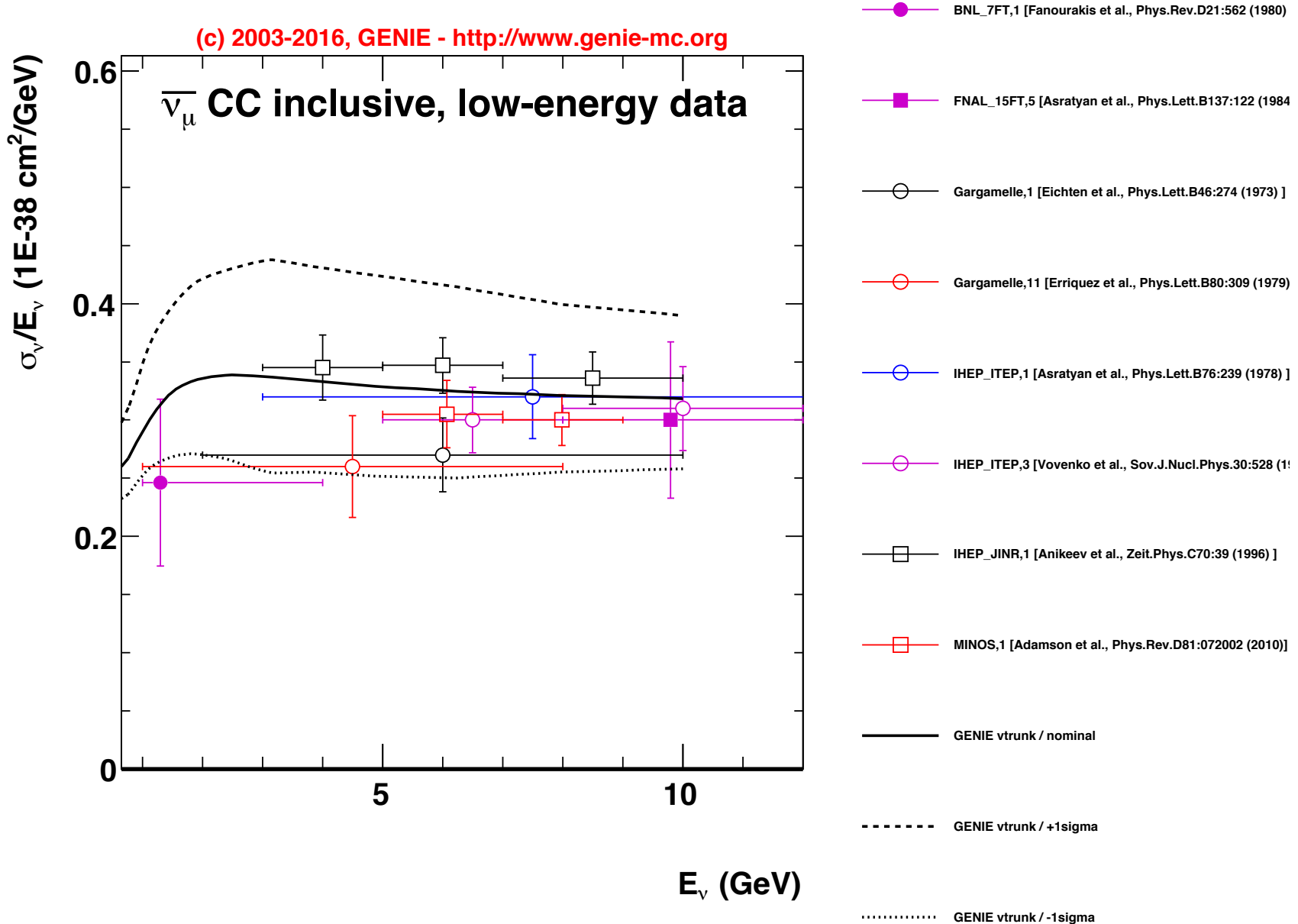
(c) 2003-2016, GENIE - <http://www.genie-mc.org>





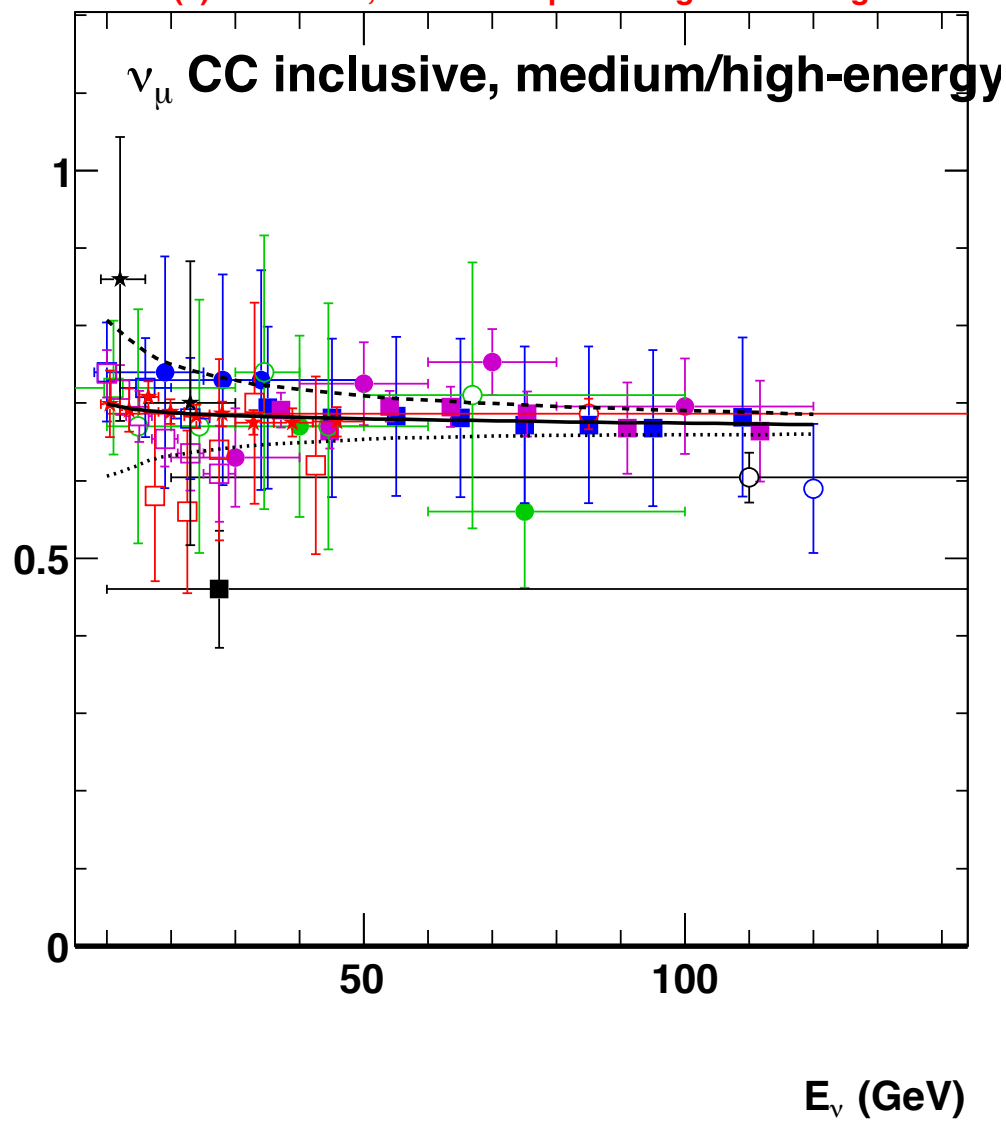




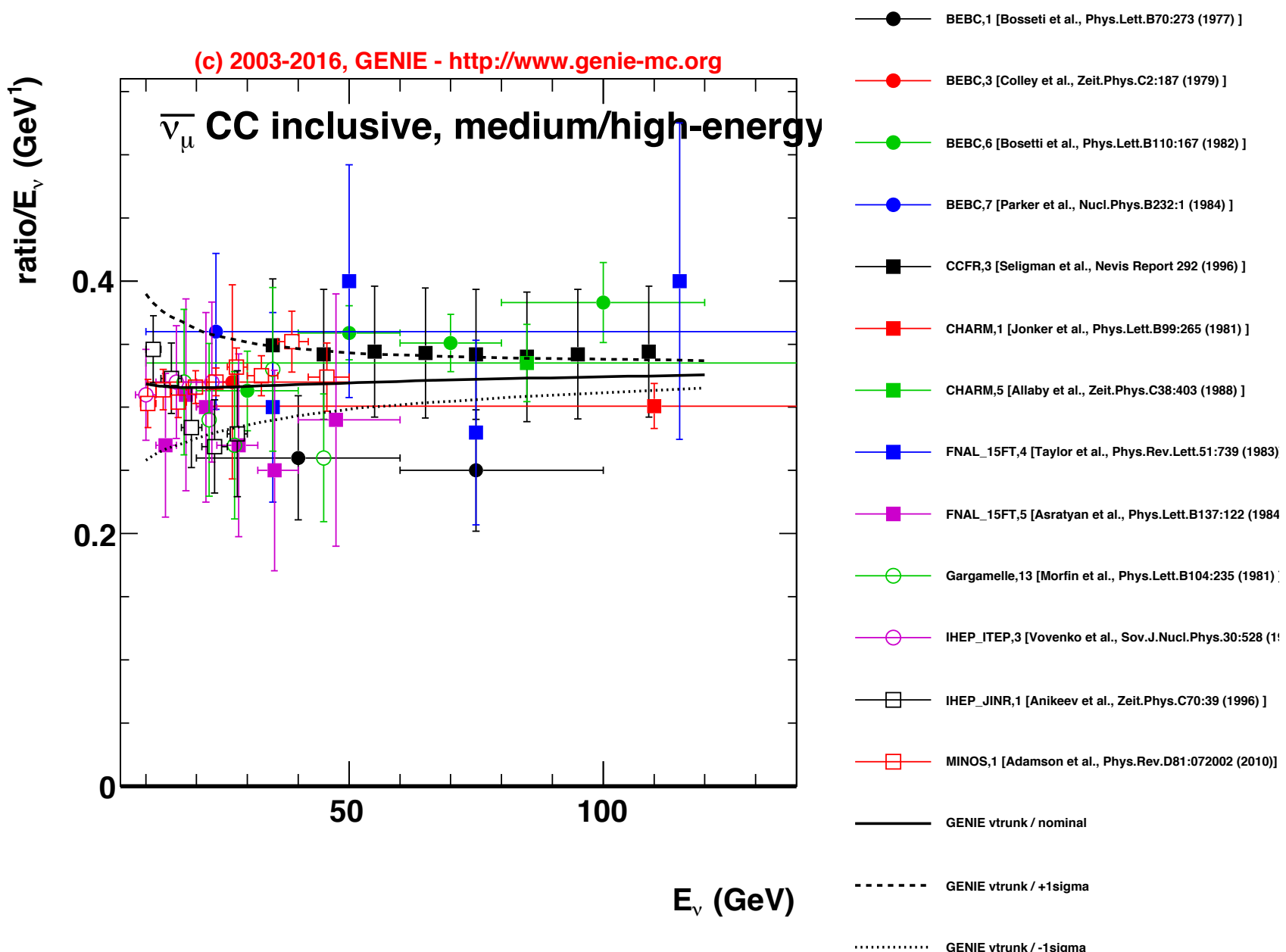


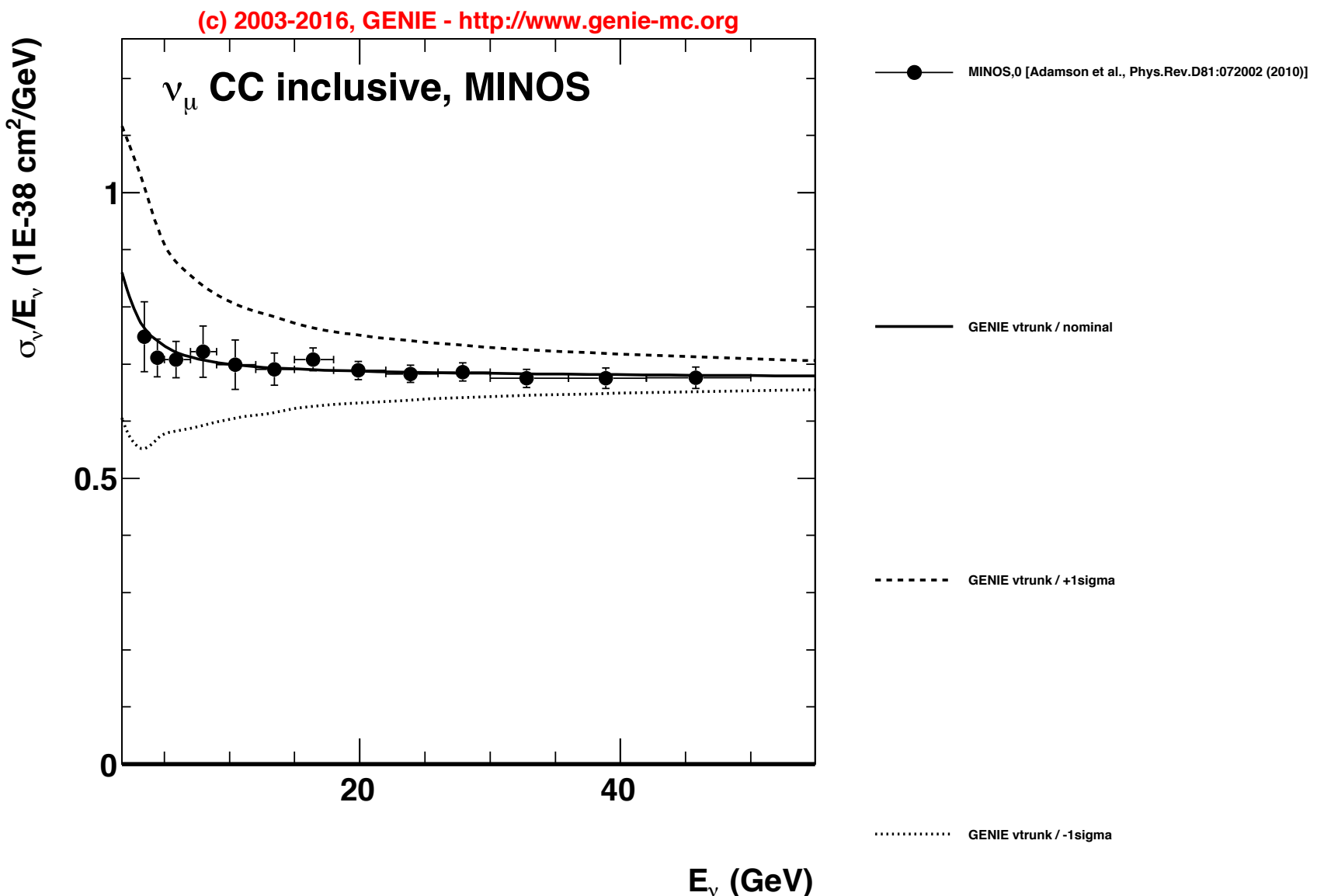
ratio/ E_ν (GeV¹)

(c) 2003-2016, GENIE - <http://www.genie-mc.org>

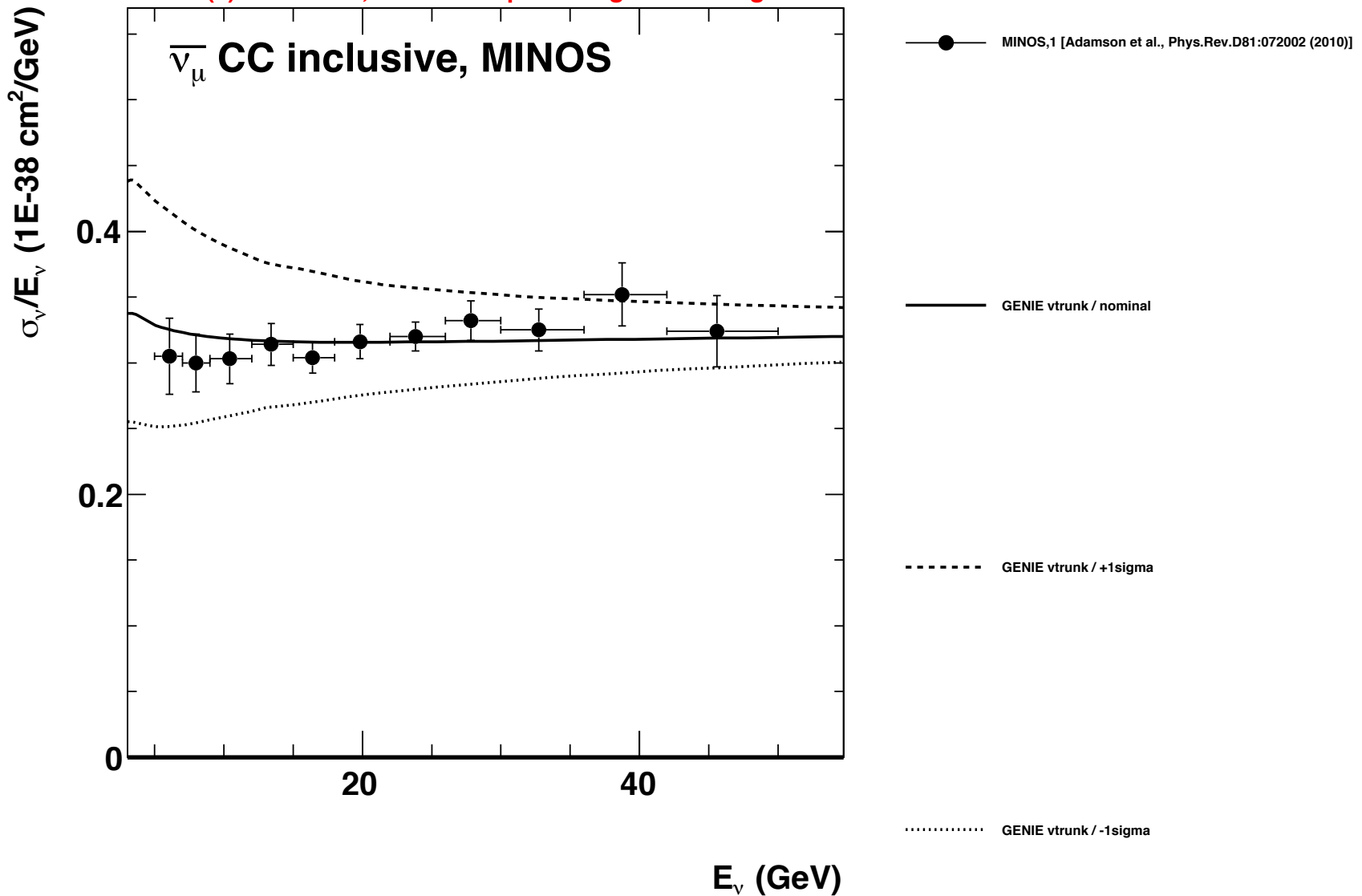


- BEBC,0 [Bossetti et al., Phys.Lett.B70:273 (1977)]
- BEBC,2 [Colley et al., Zeit.Phys.C2:187 (1979)]
- BEBC,5 [Bossetti et al., Phys.Lett.B110:167 (1982)]
- BEBC,8 [Parker et al., Nucl.Phys.B232:1 (1984)]
- CCFR,2 [Seligman et al., Nevis Report 292 (1996)]
- CCFR,0 [MacFarlane et al., Zeit.Phys.C26:1 (1984)]
- CHARM,0 [Jonker et al., Phys.Lett.B99:265 (1981)]
- CHARM,4 [Allaby et al., Zeit.Phys.C38:403 (1988)]
- FNAL_15FT,1 [Kitagaki et al., Phys.Rev.Lett.49:98 (1982)]
- FNAL_15FT,2 [Baker et al., Phys.Rev.Lett.51:735 (1983)]
- Gargamelle,12 [Morfin et al., Phys.Lett.B104:235 (1981)]
- IHEP_ITEP,0 [Asratyan et al., Phys.Lett.B76:239 (1978)]
- IHEP_ITEP,2 [Vovenko et al., Sov.J.Nucl.Phys.30:528 (1979)]
- IHEP_JINR,0 [Anikeev et al., Zeit.Phys.C70:39 (1996)]
- ★ SKAT,0 [Baranov et al., Phys.Rev.B81 255 (1979)]
- ★ MINOS,0 [Adamson et al., Phys.Rev.D81:072002 (2010)]
- GENIE vtrunk / nominal
- - - GENIE vtrunk / +1sigma
- GENIE vtrunk / -1sigma

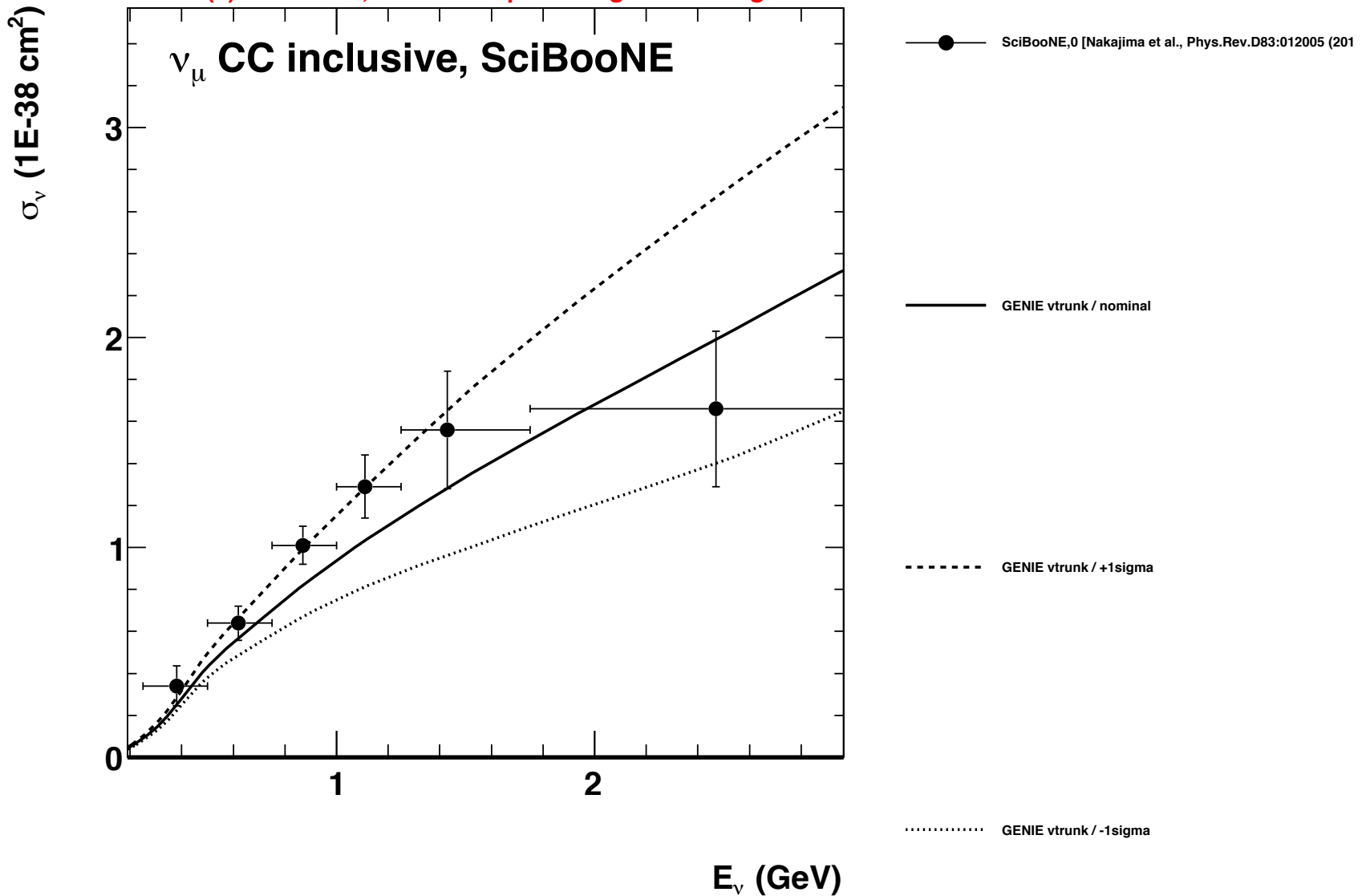


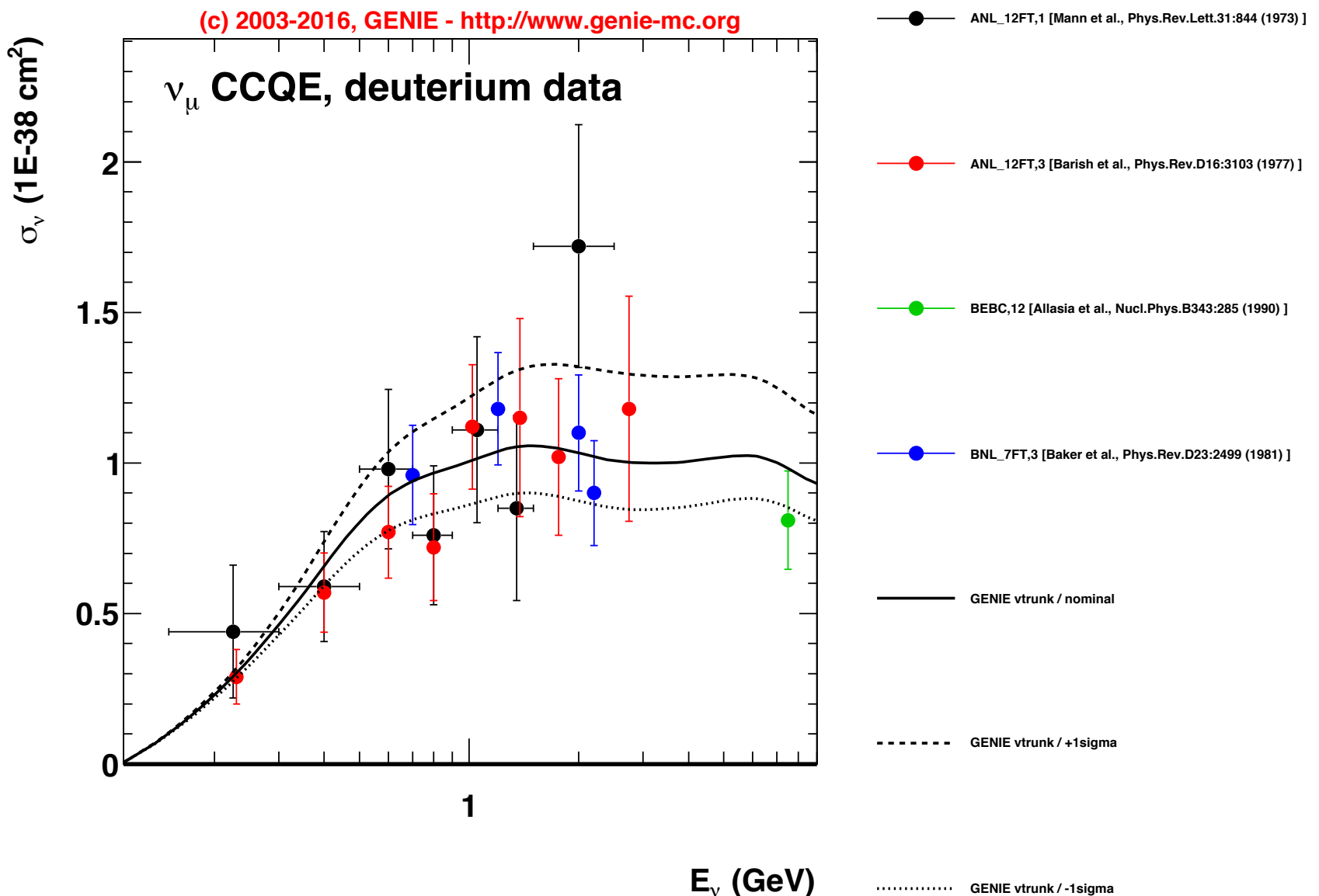


(c) 2003-2016, GENIE - <http://www.genie-mc.org>

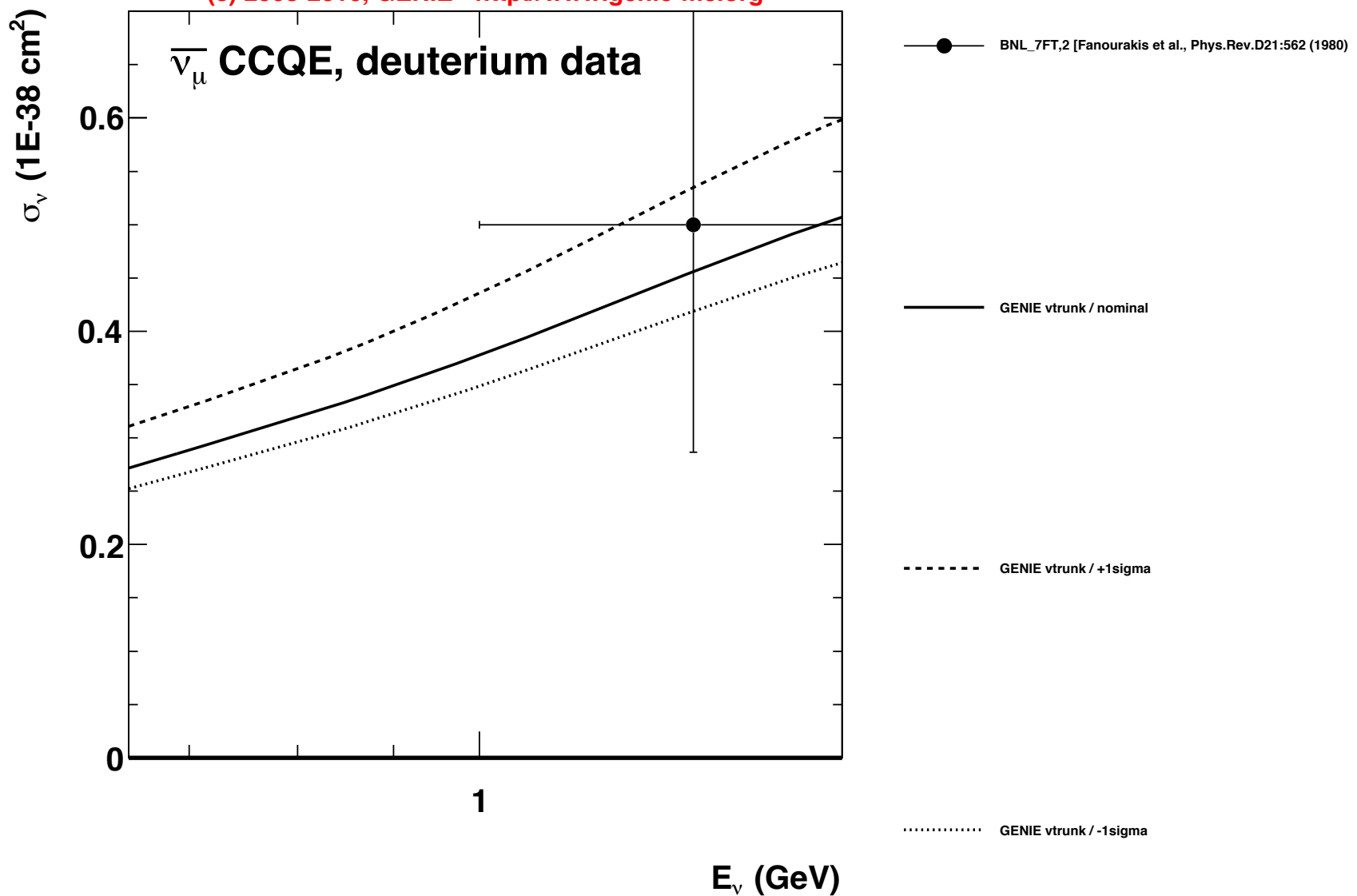


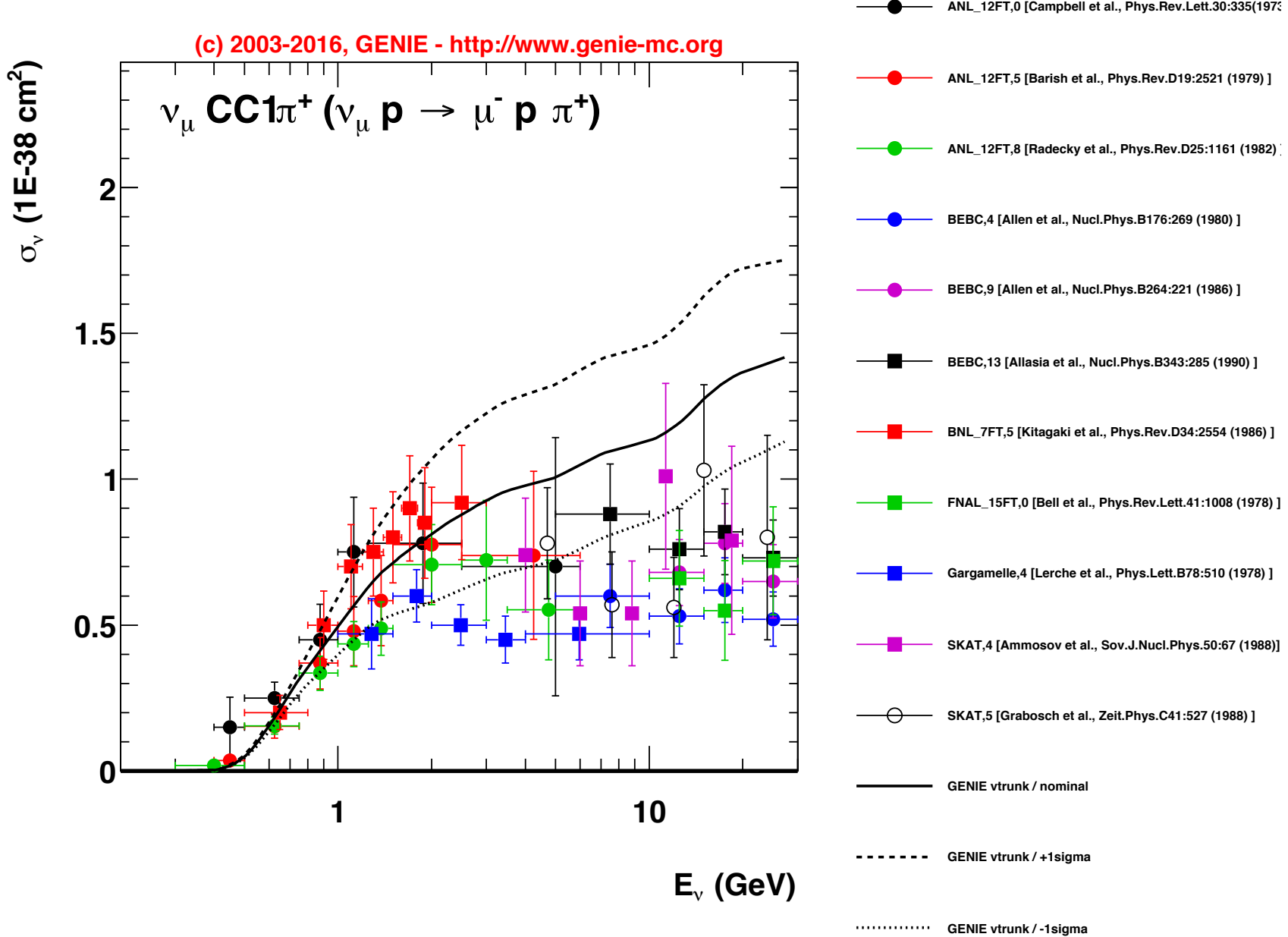
(c) 2003-2016, GENIE - <http://www.genie-mc.org>

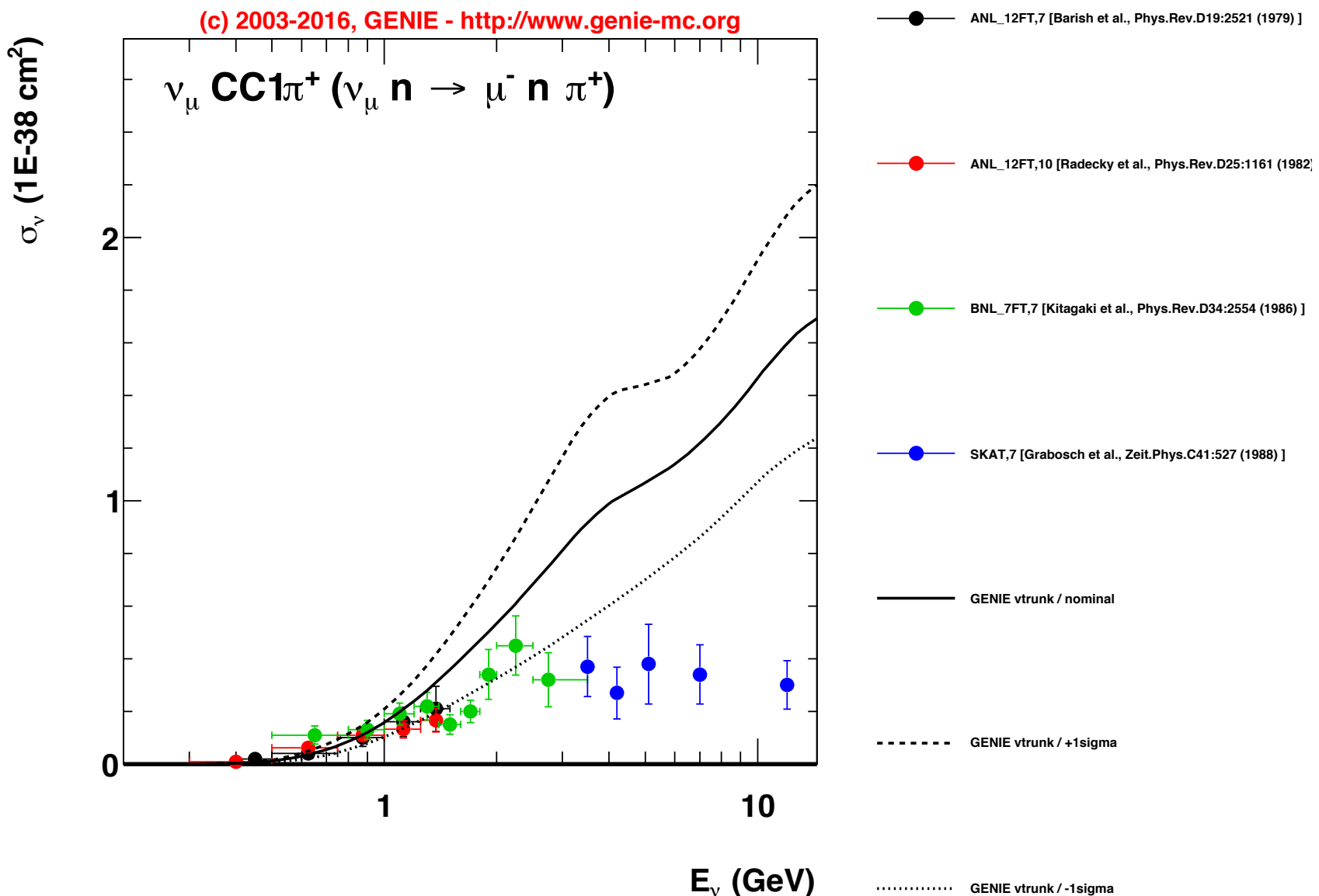


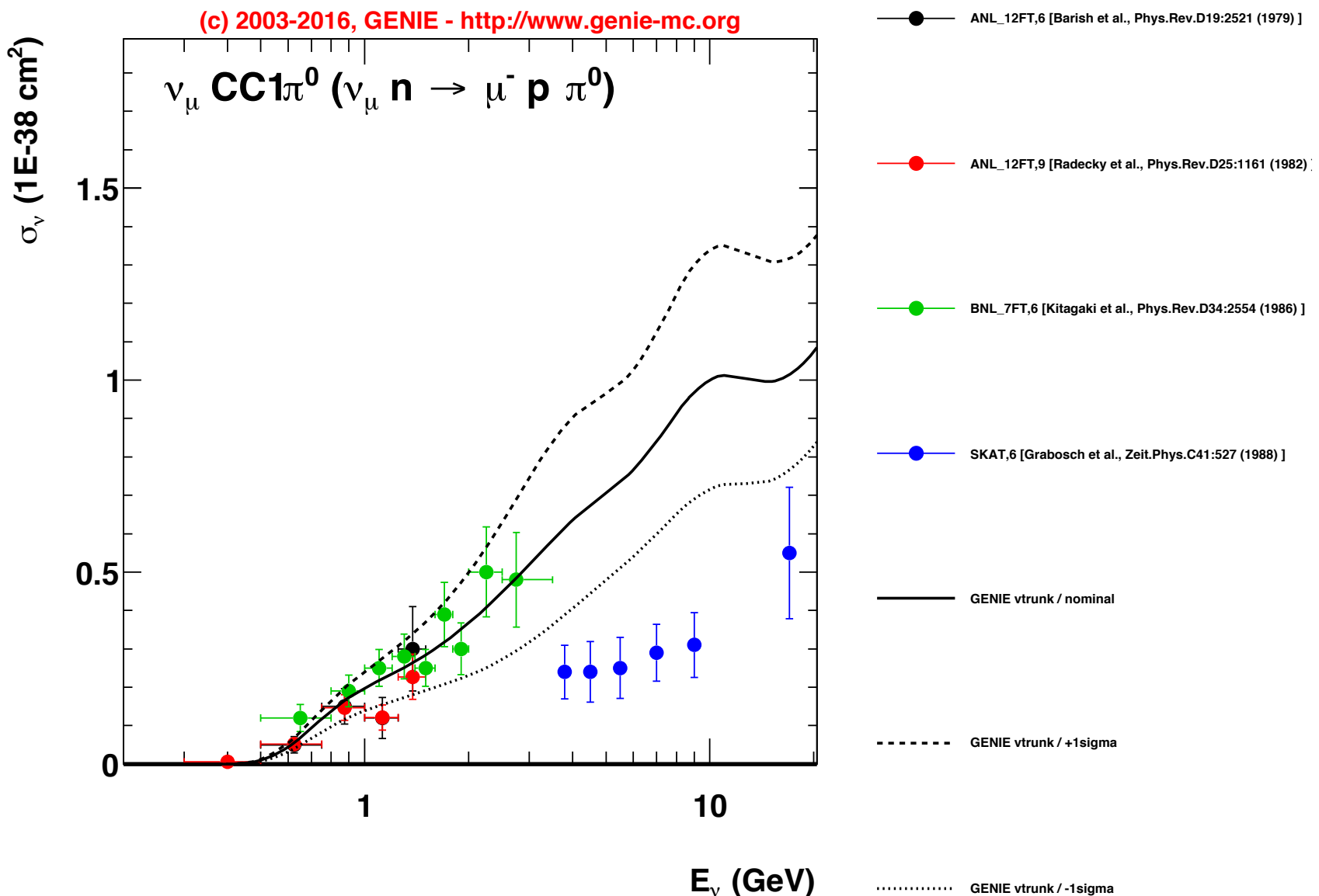


(c) 2003-2016, GENIE - <http://www.genie-mc.org>

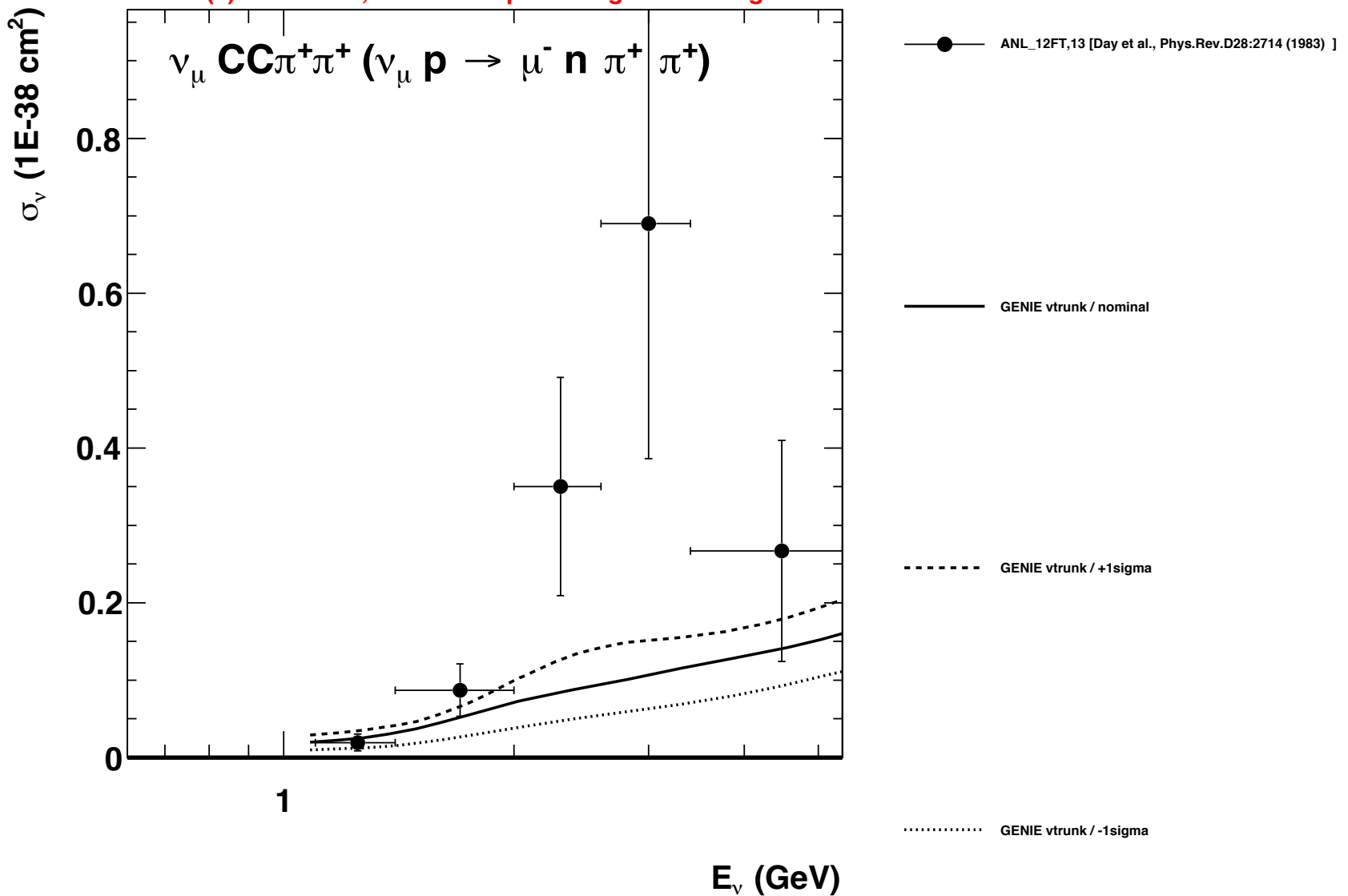


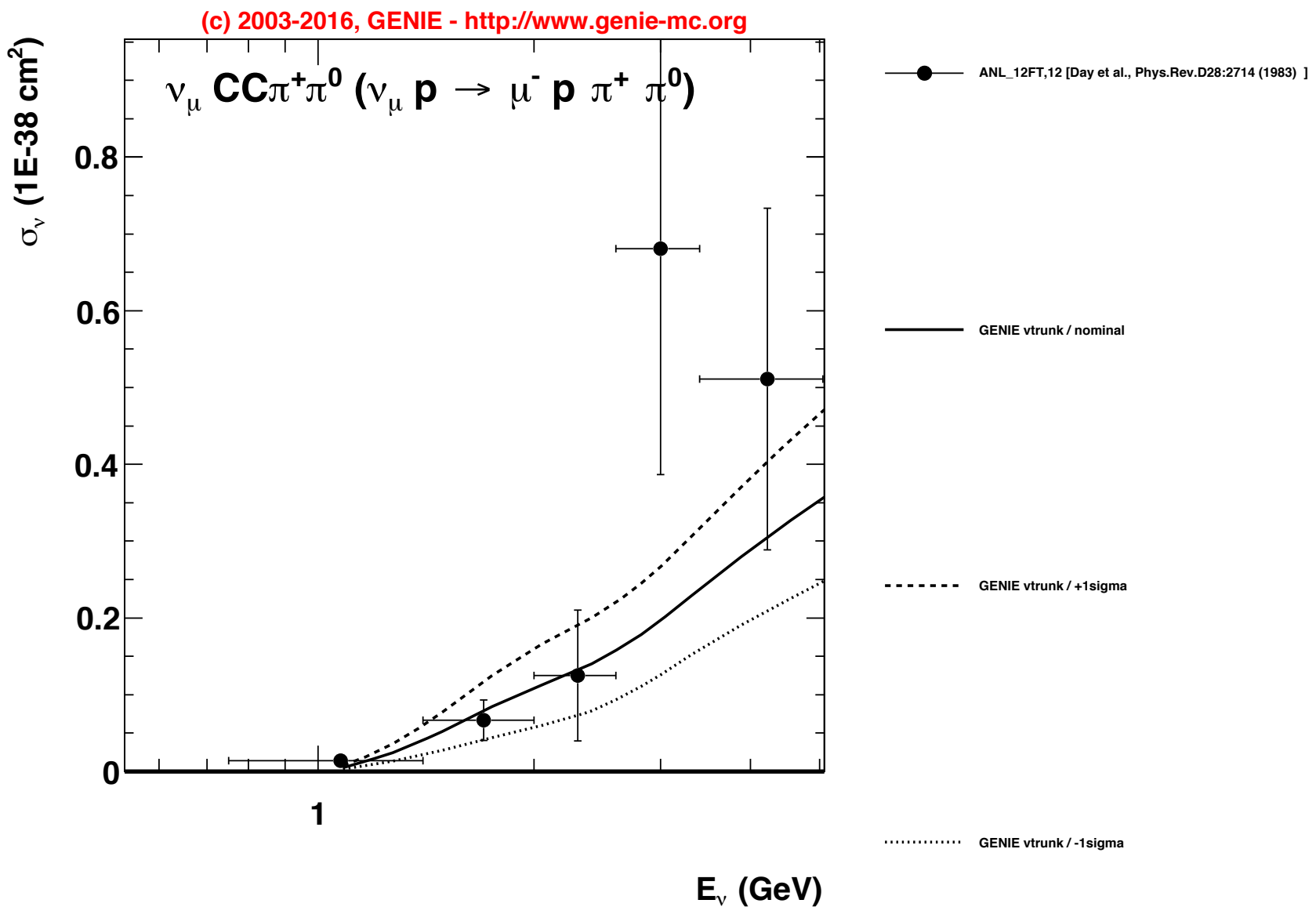


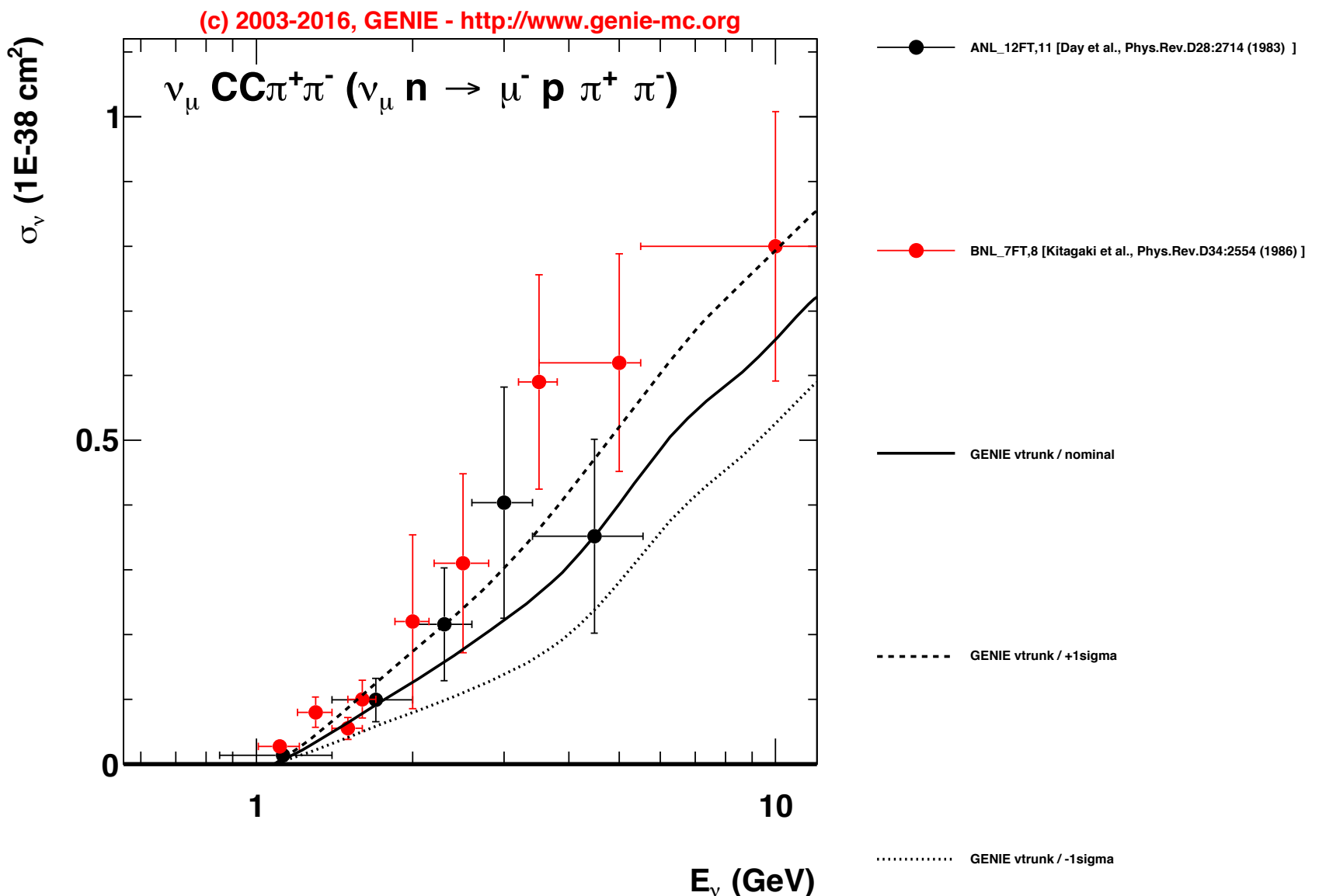


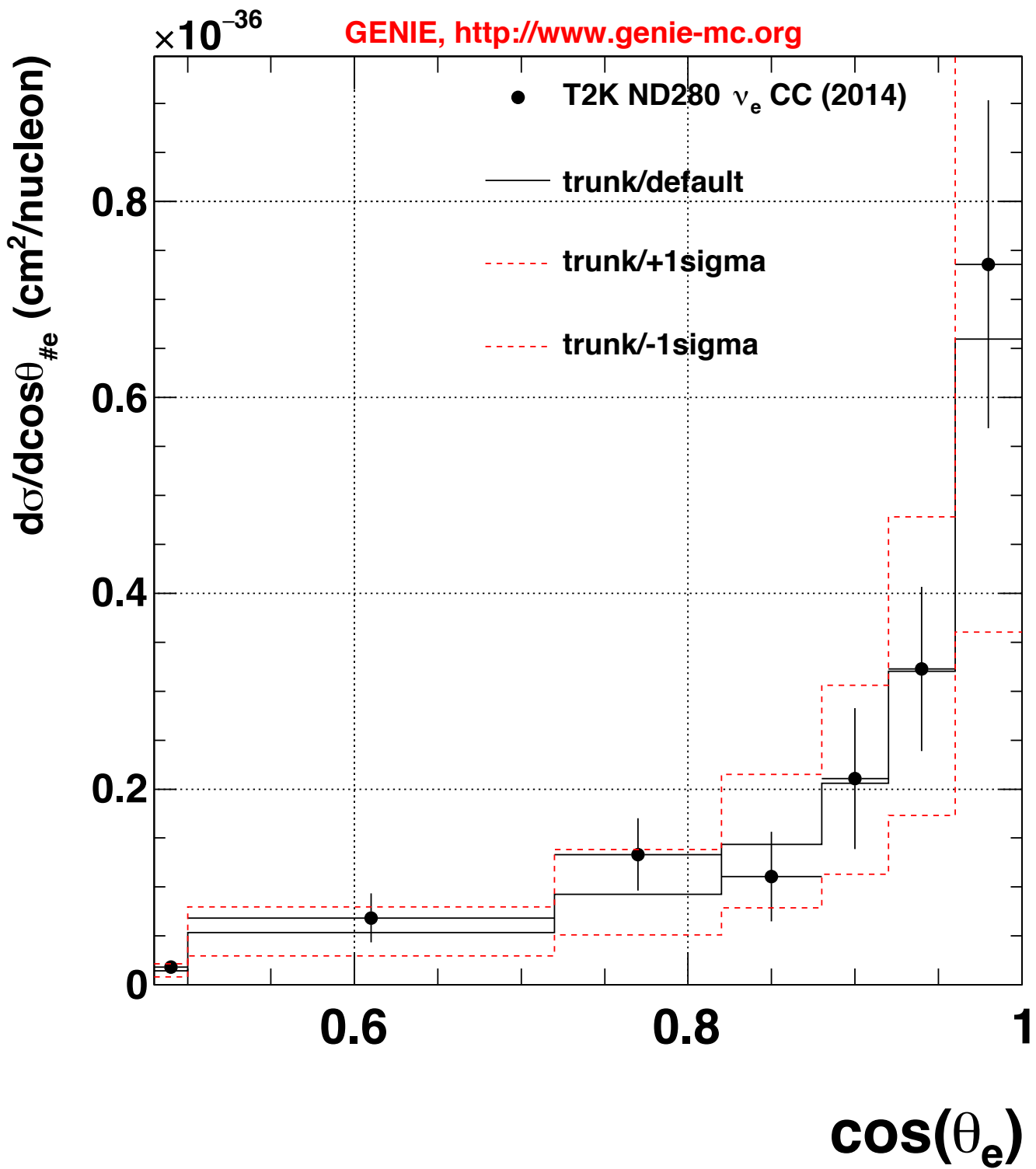


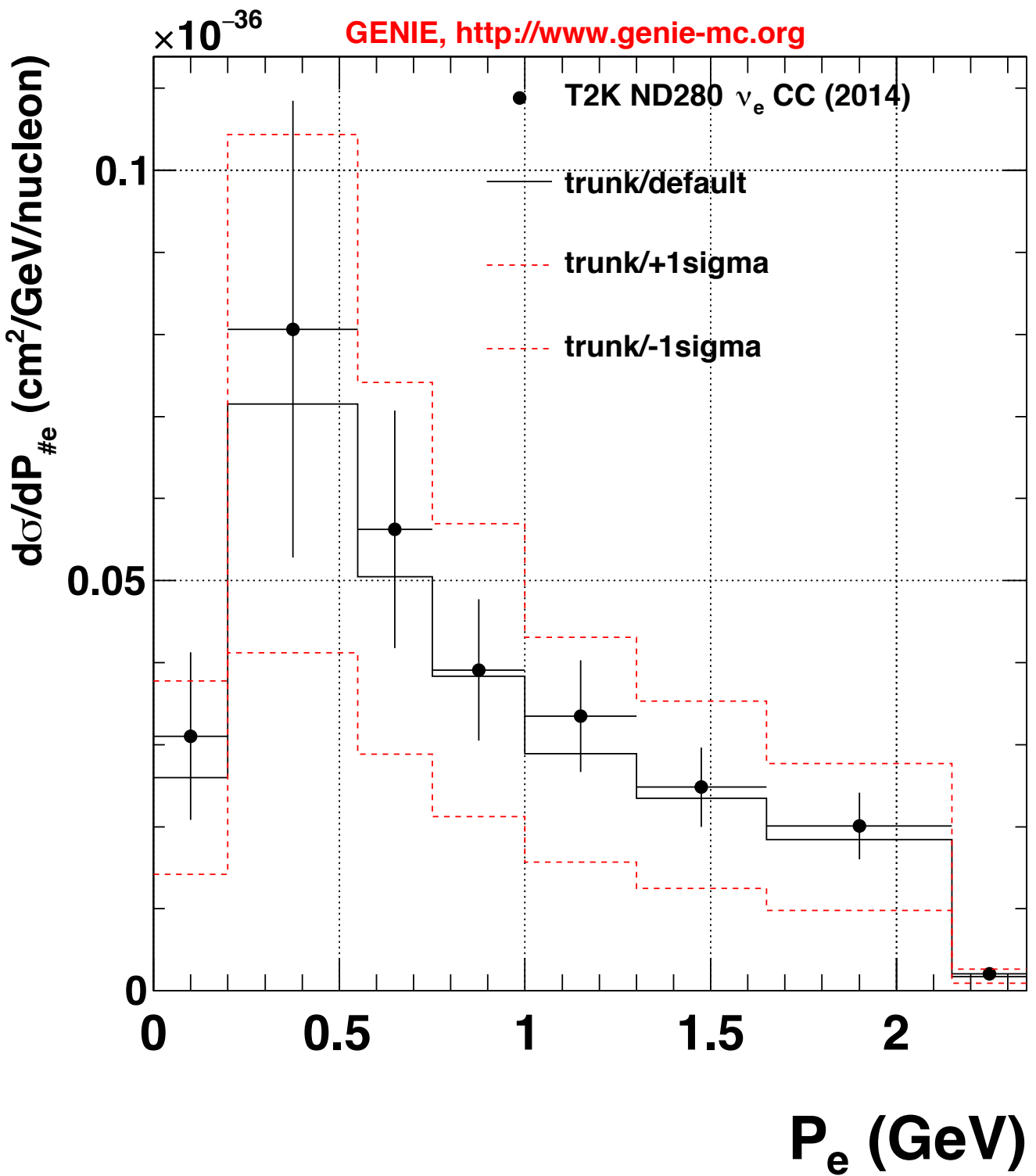
(c) 2003-2016, GENIE - <http://www.genie-mc.org>

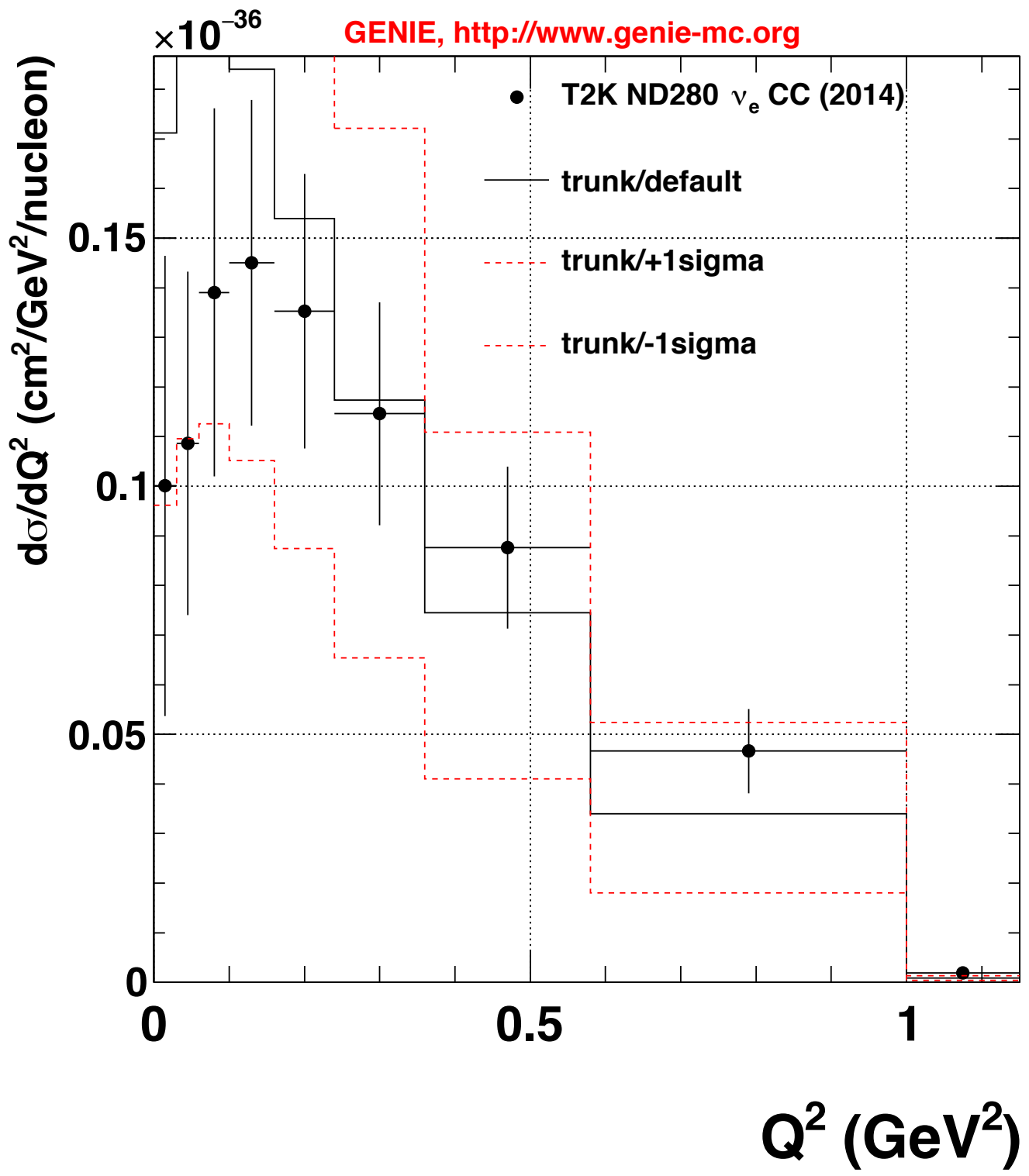


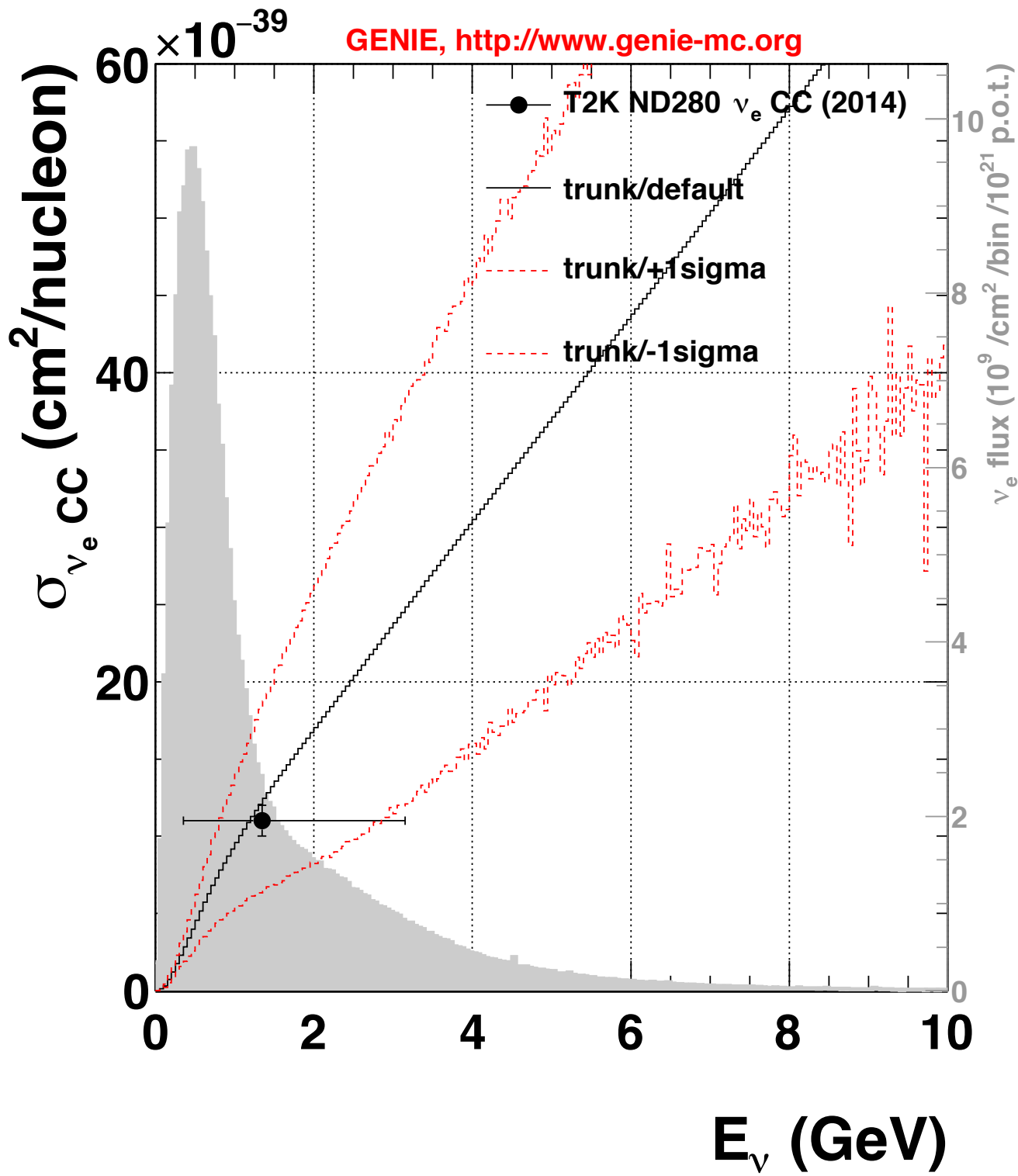


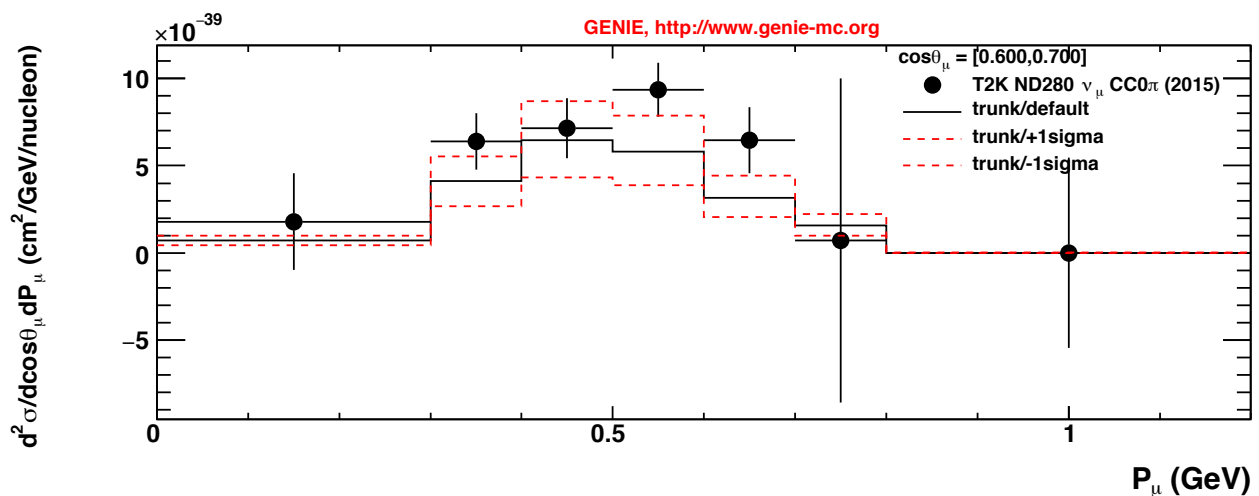
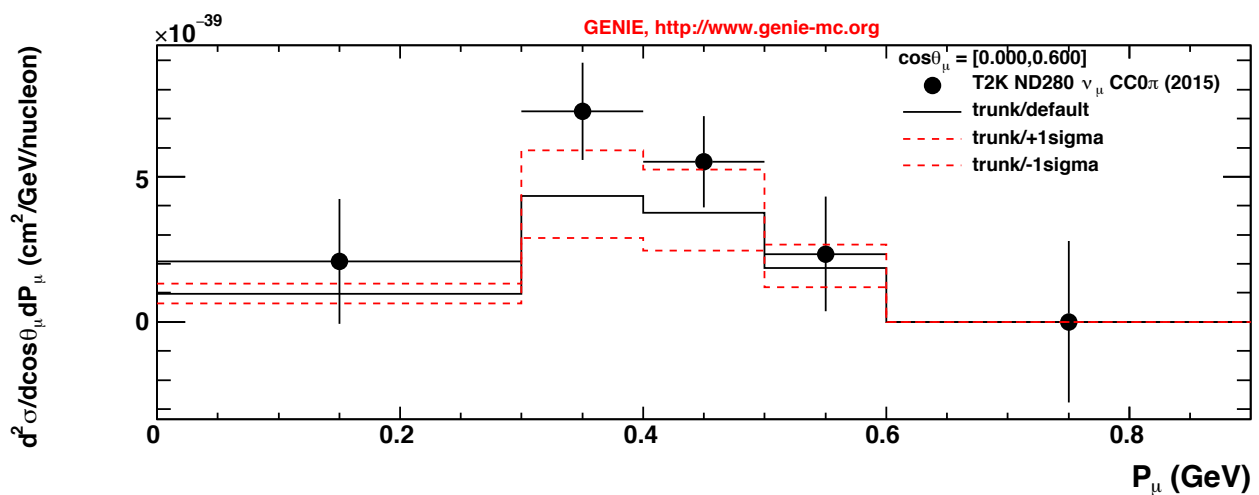
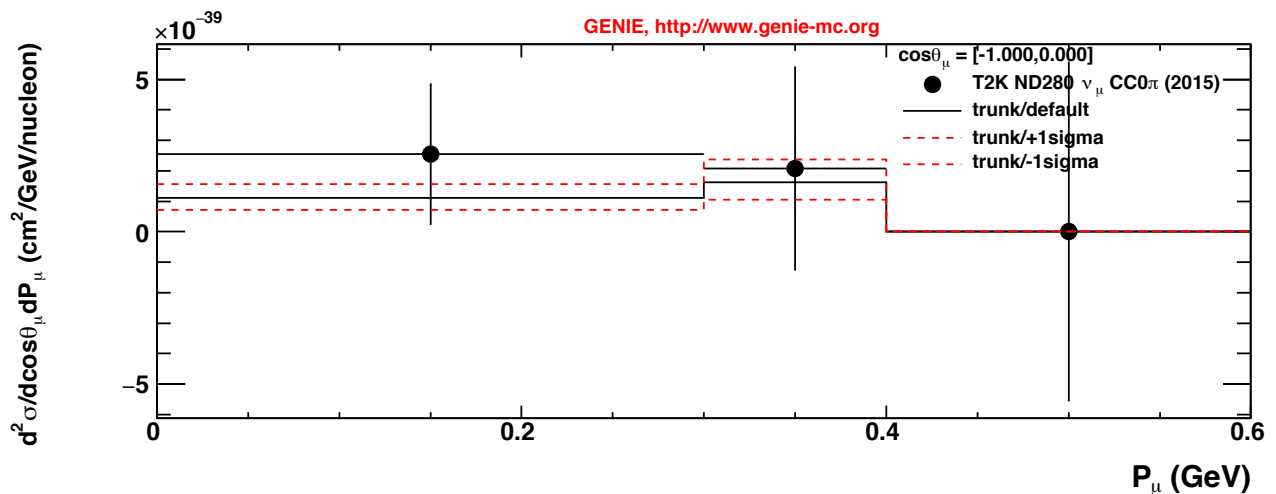


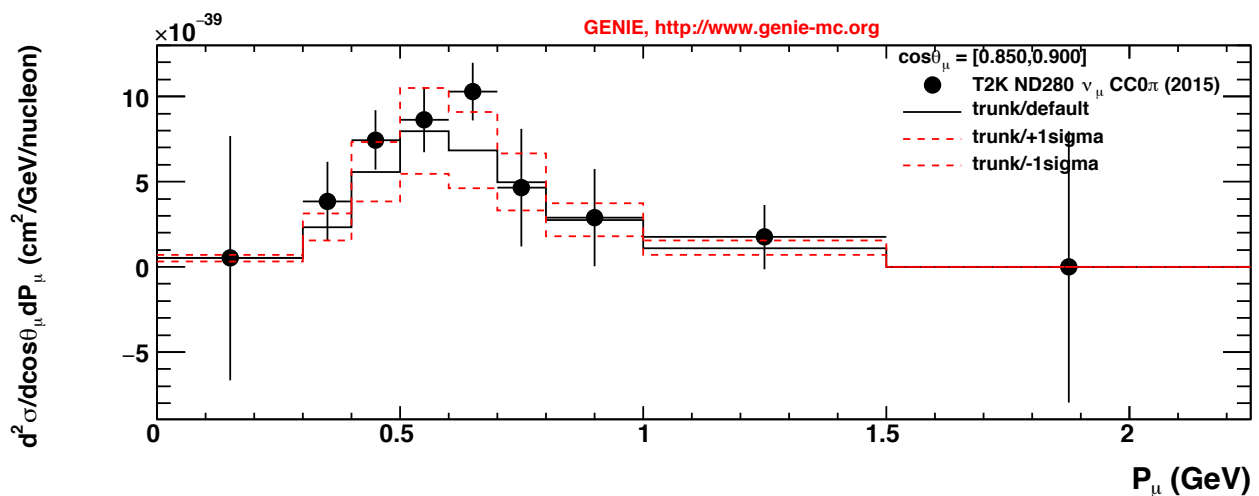
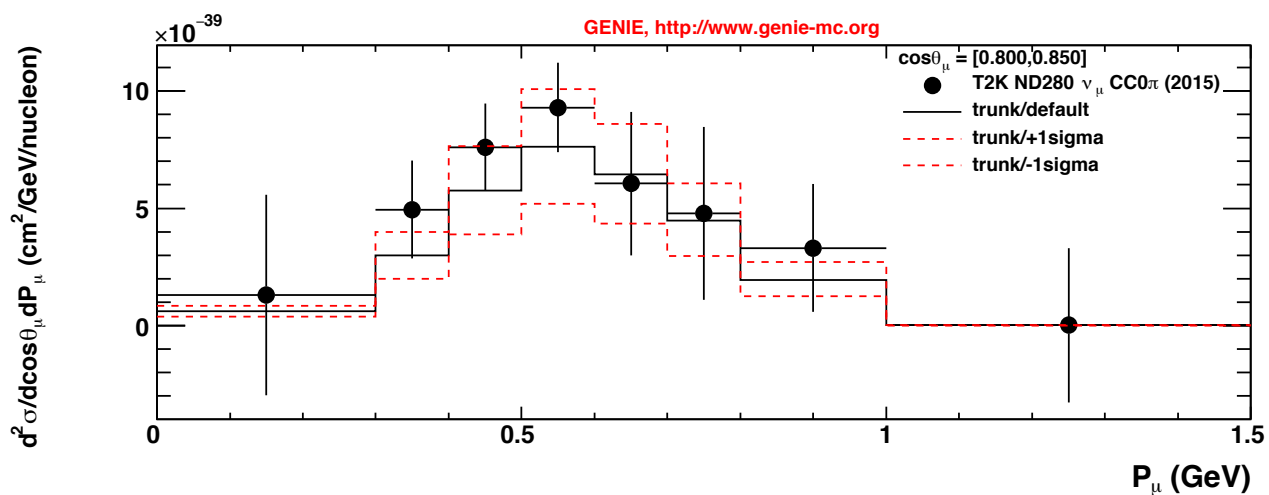
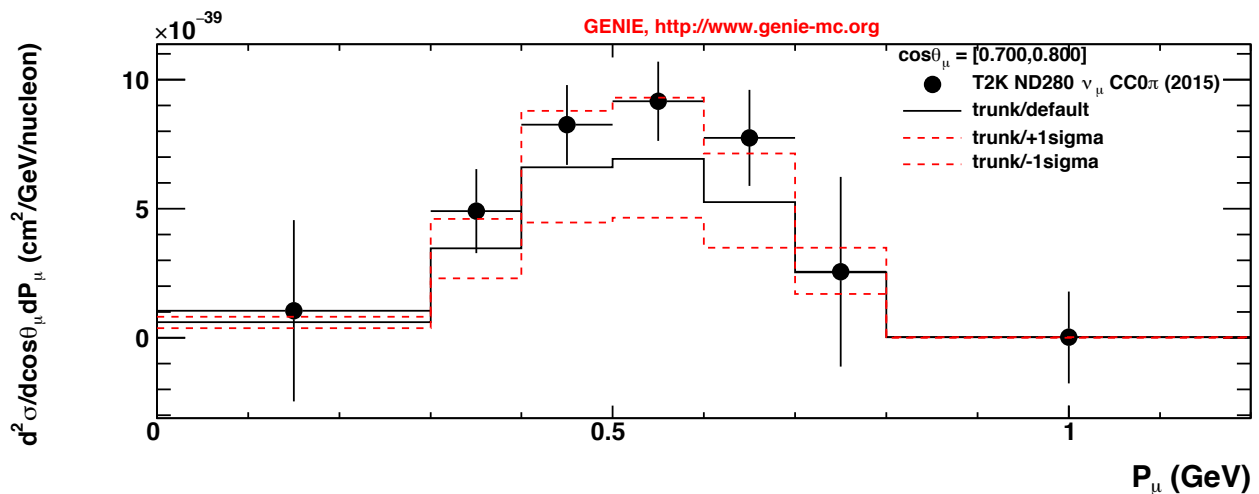


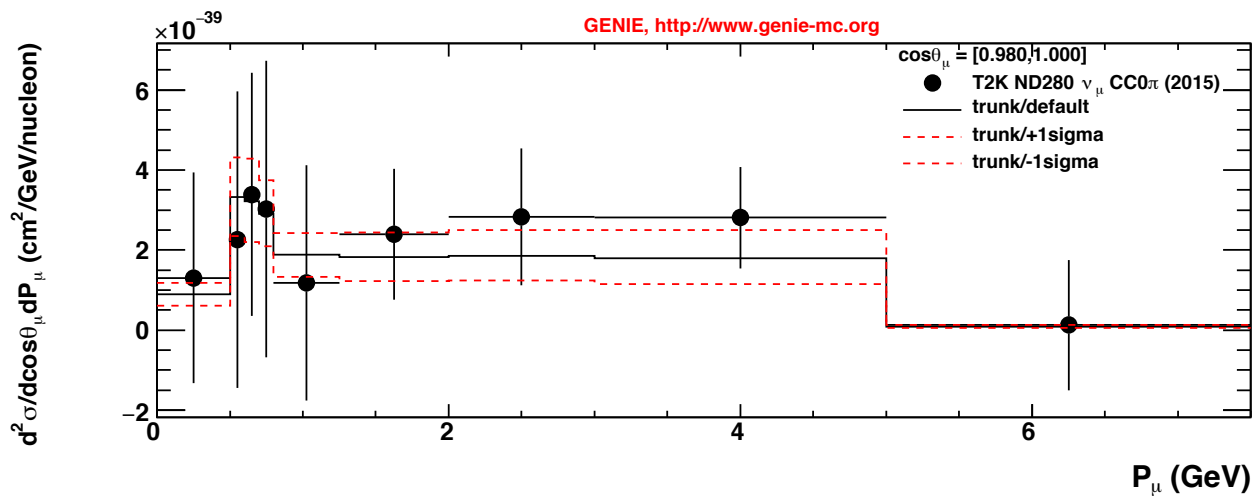
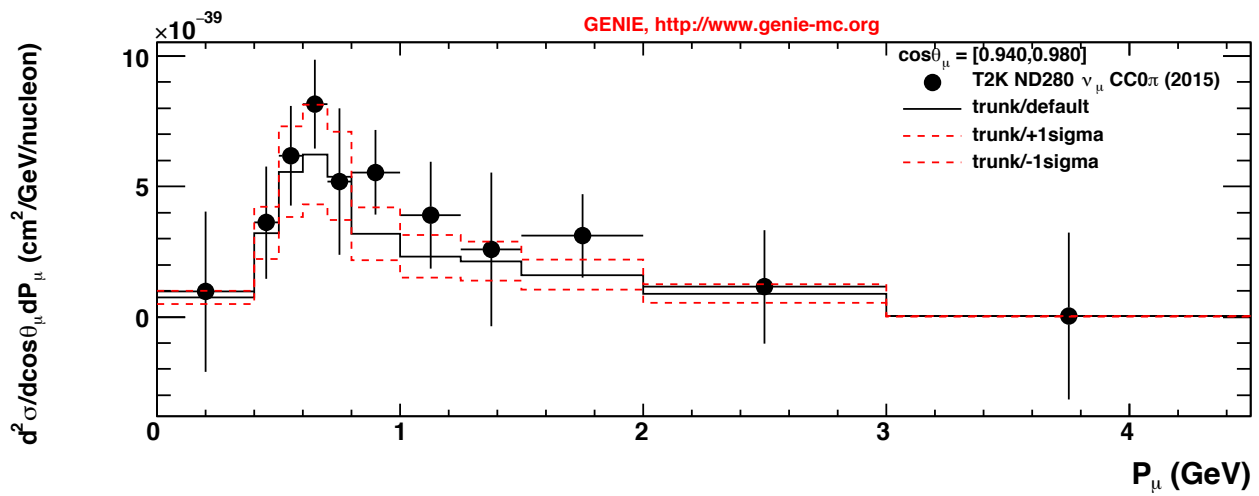
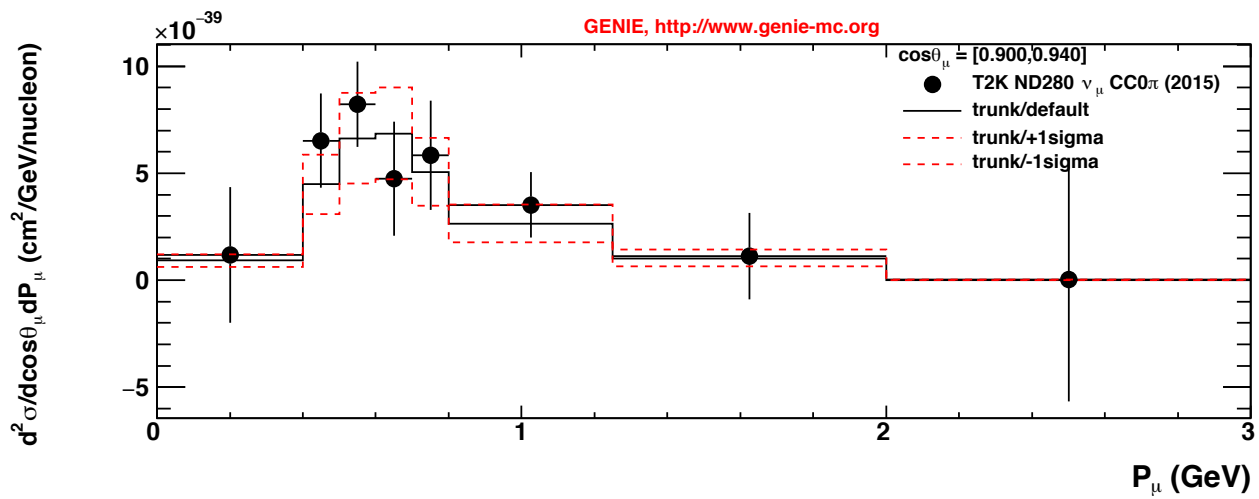


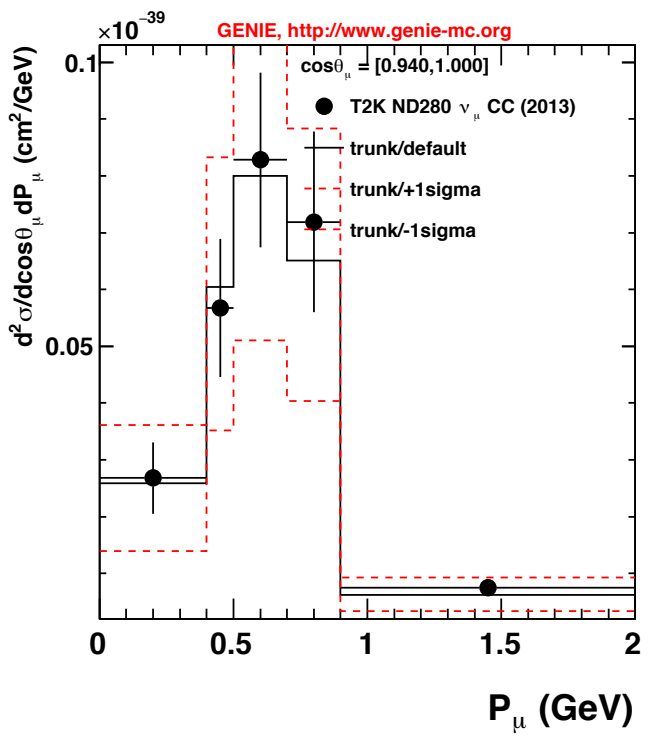
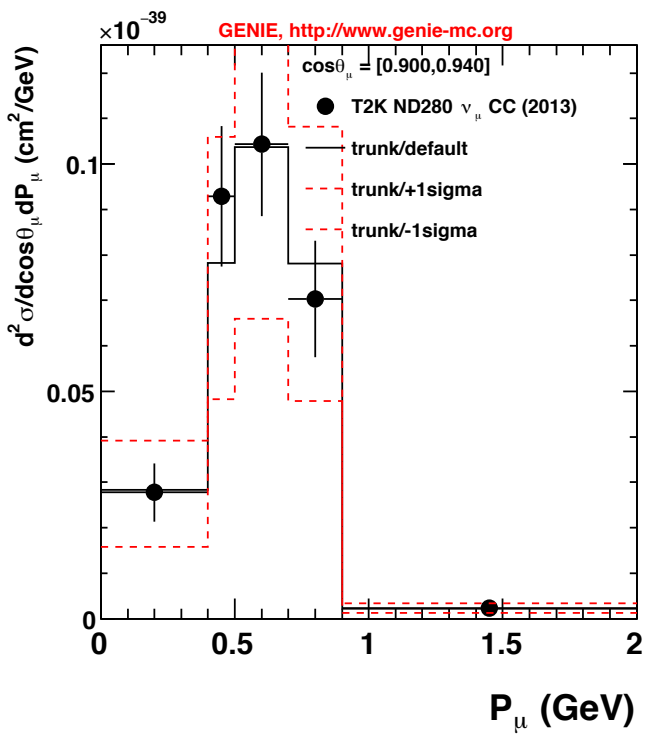
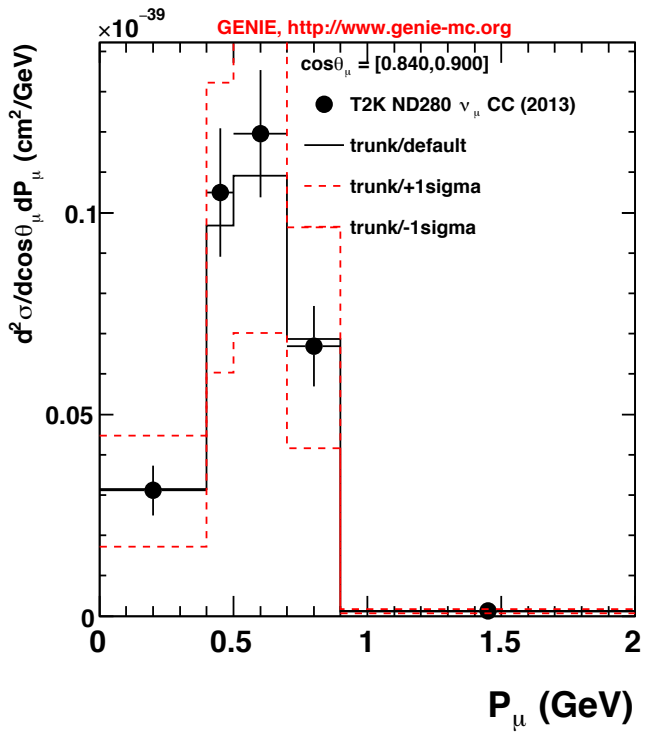
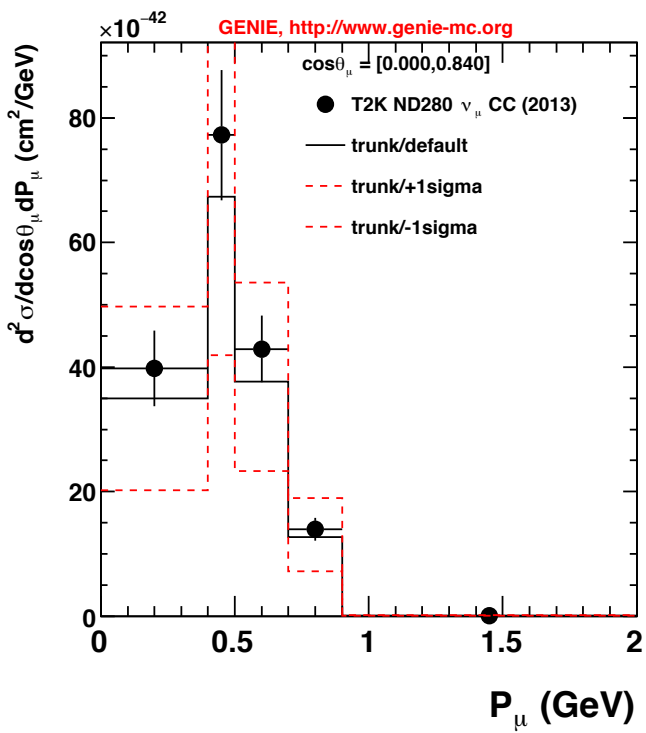


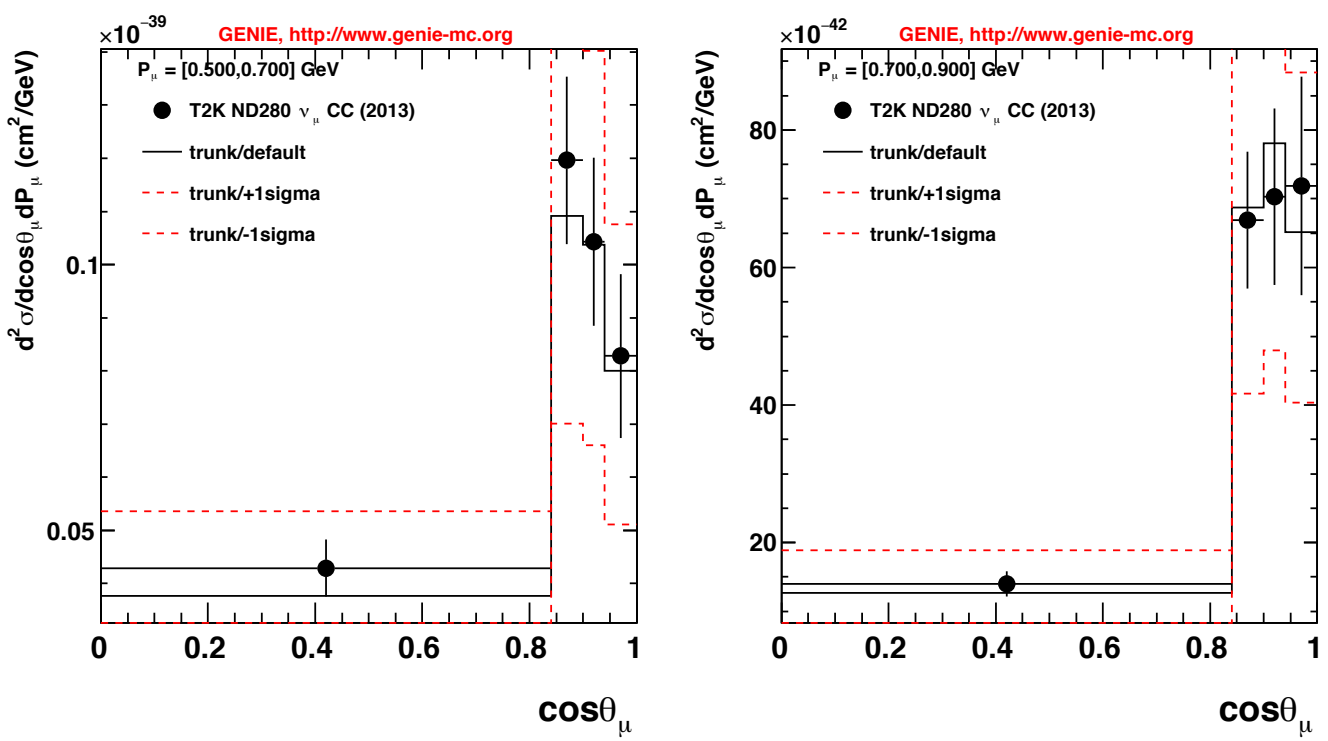
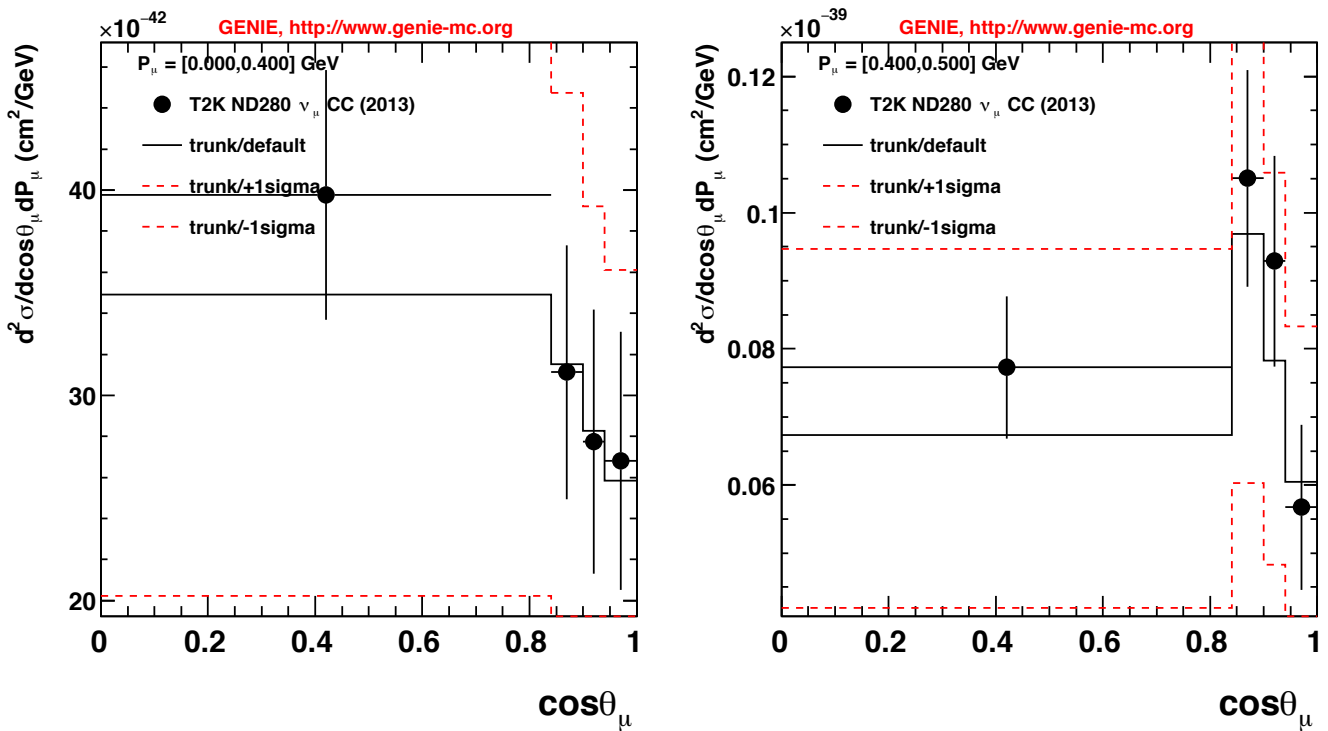


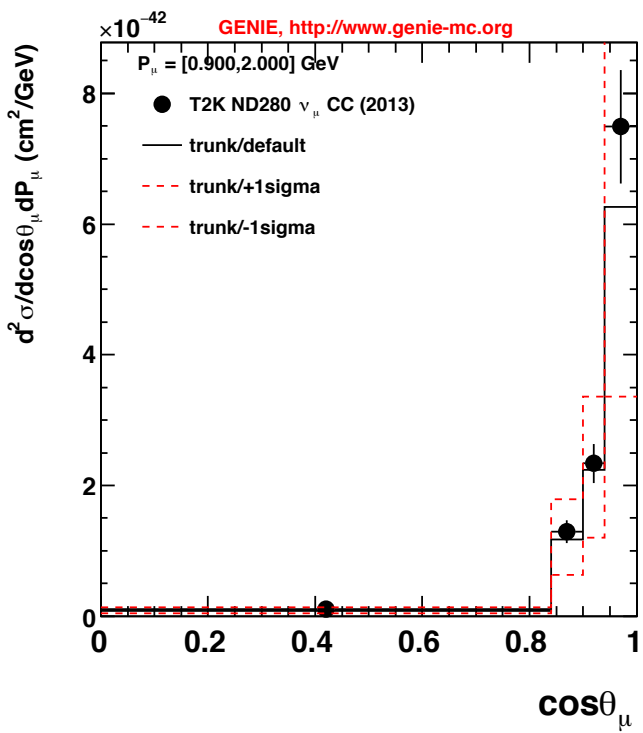




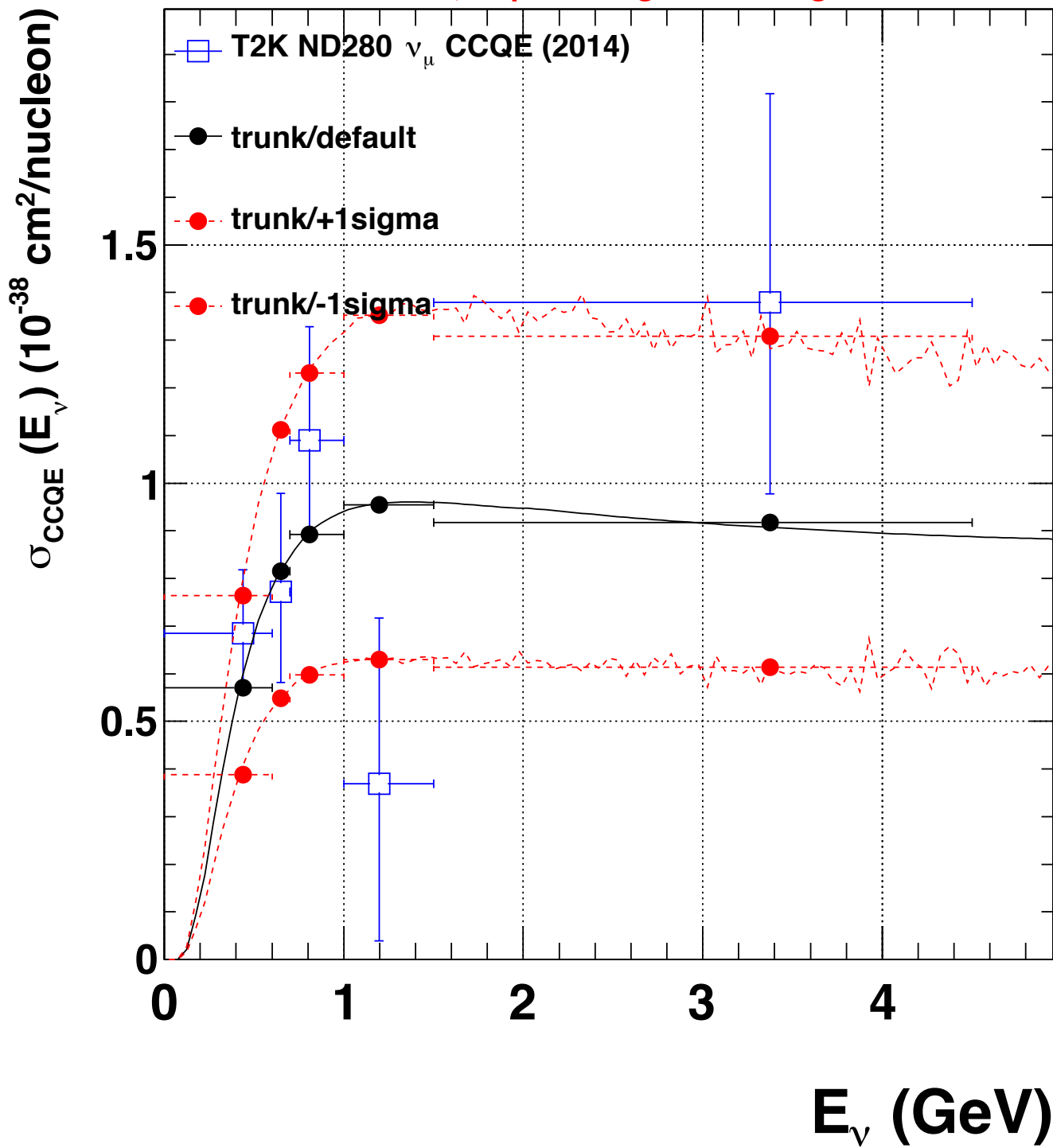


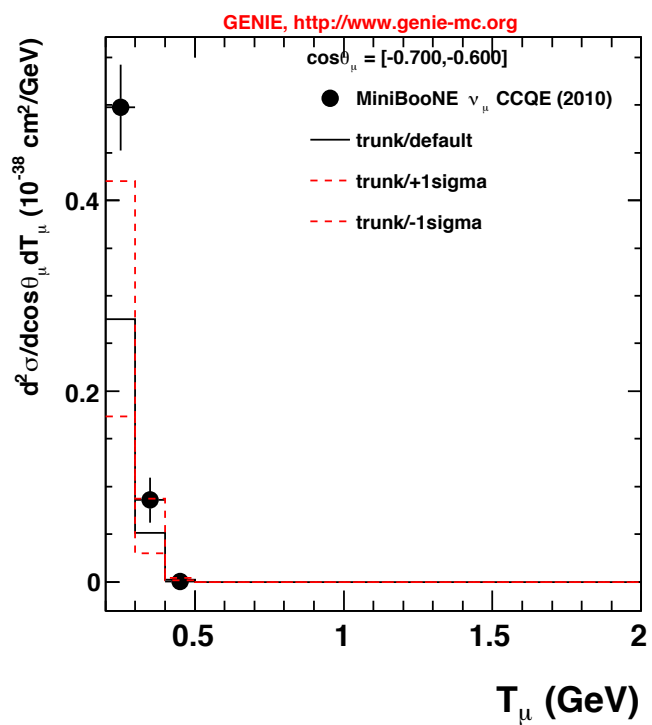
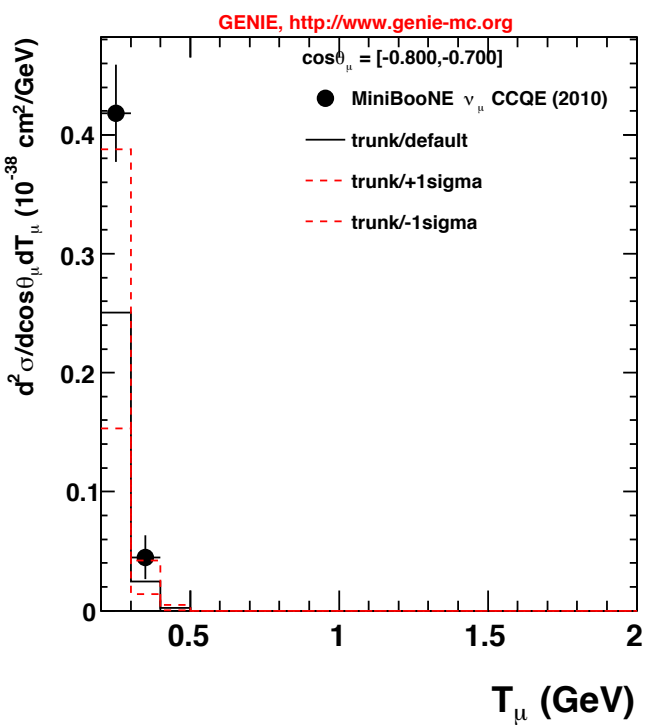
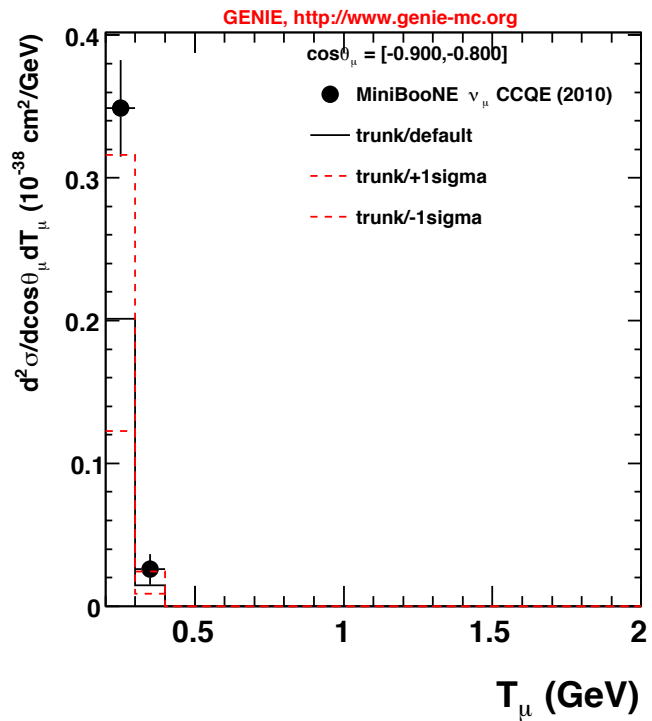
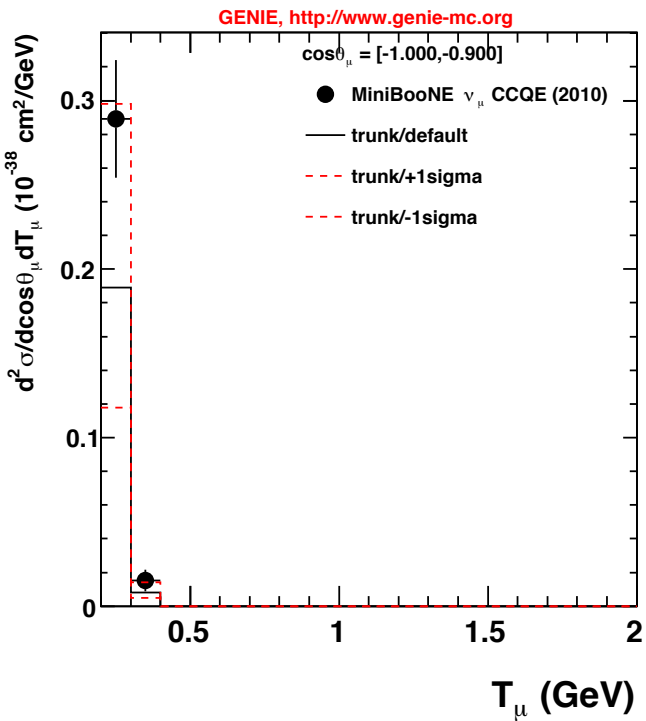


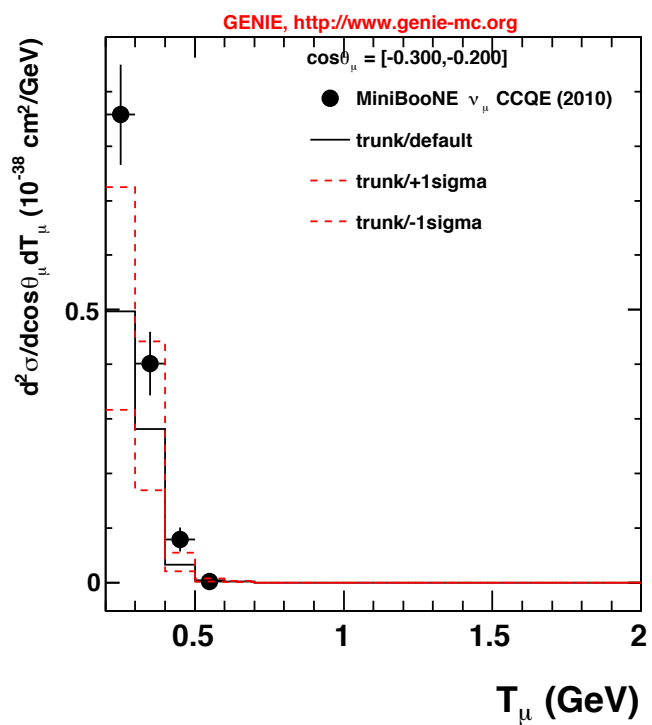
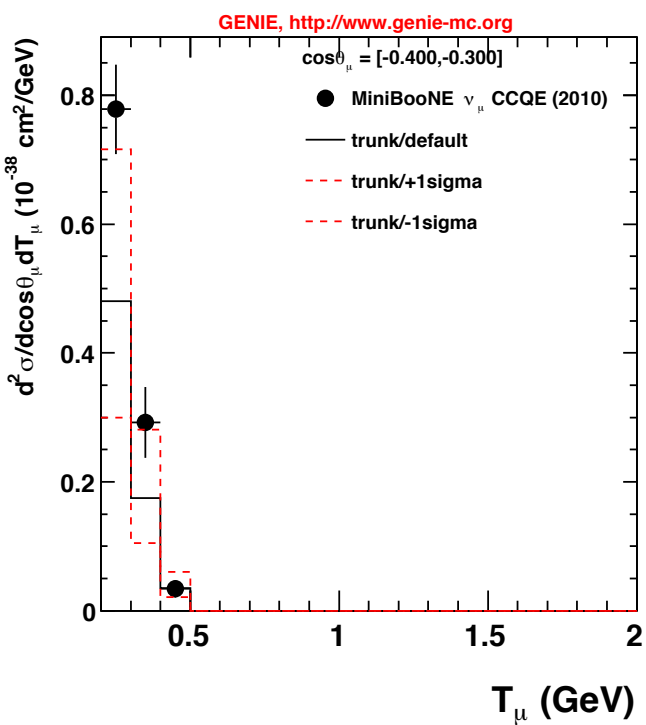
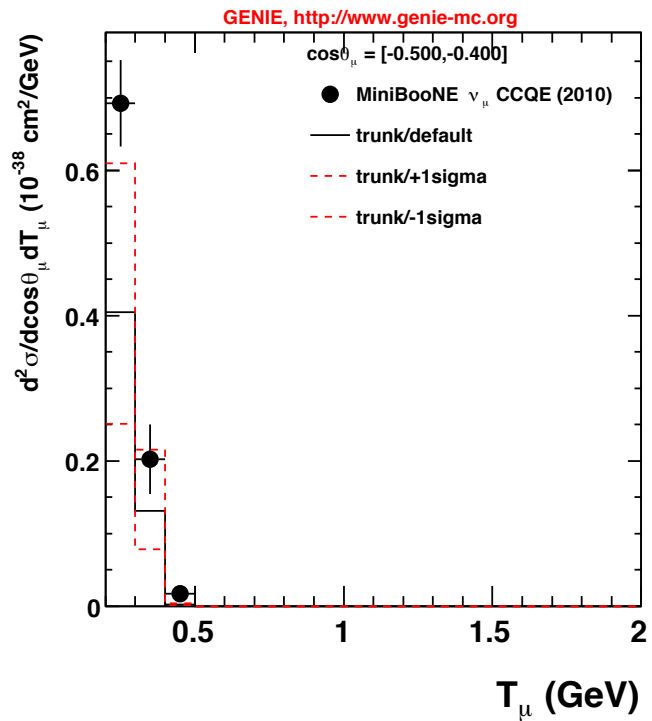
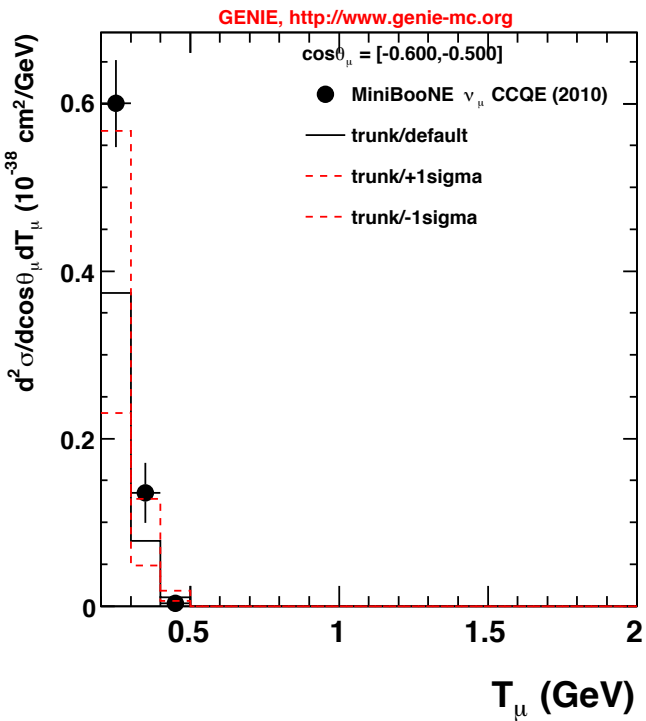


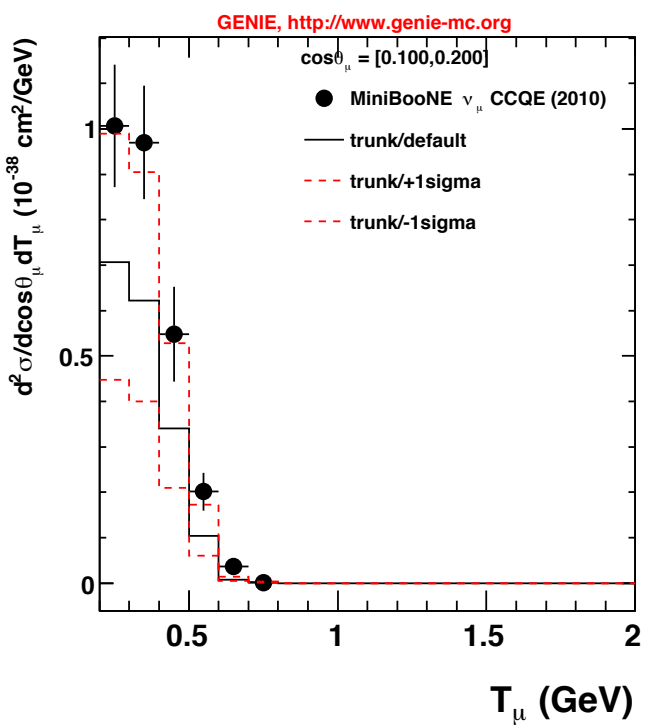
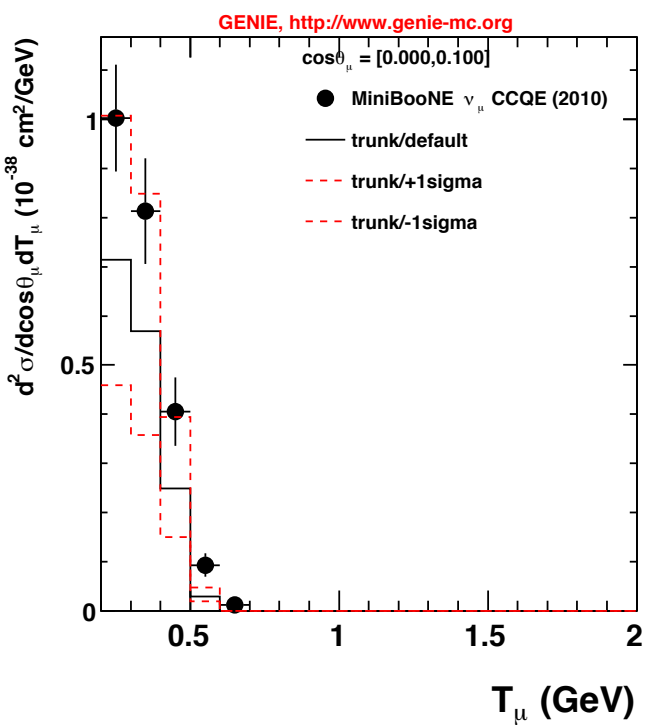
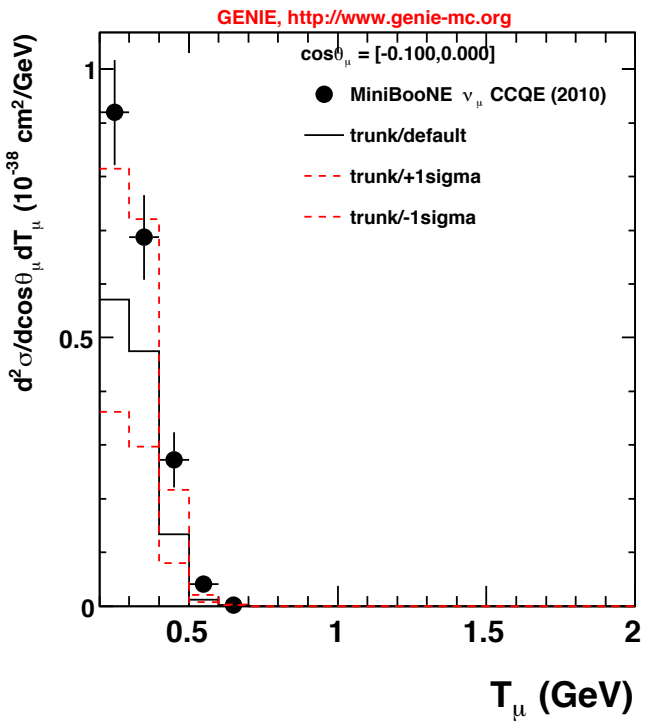
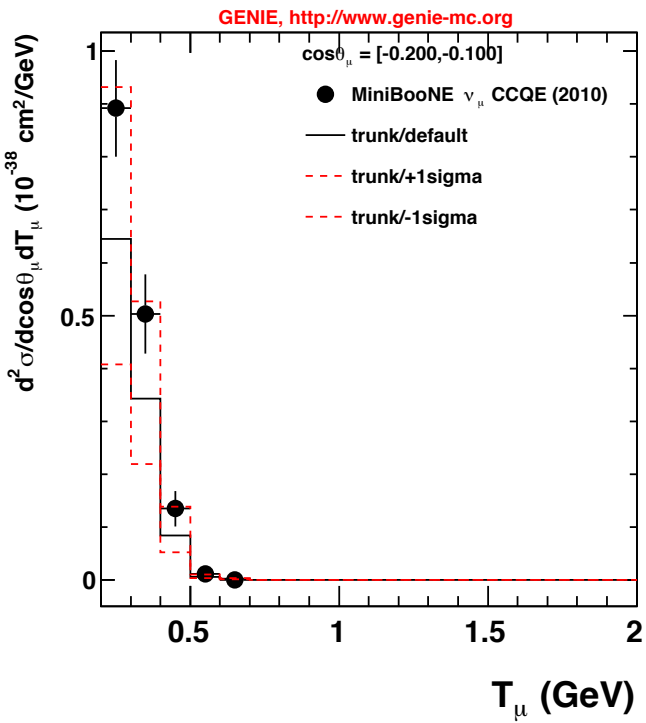


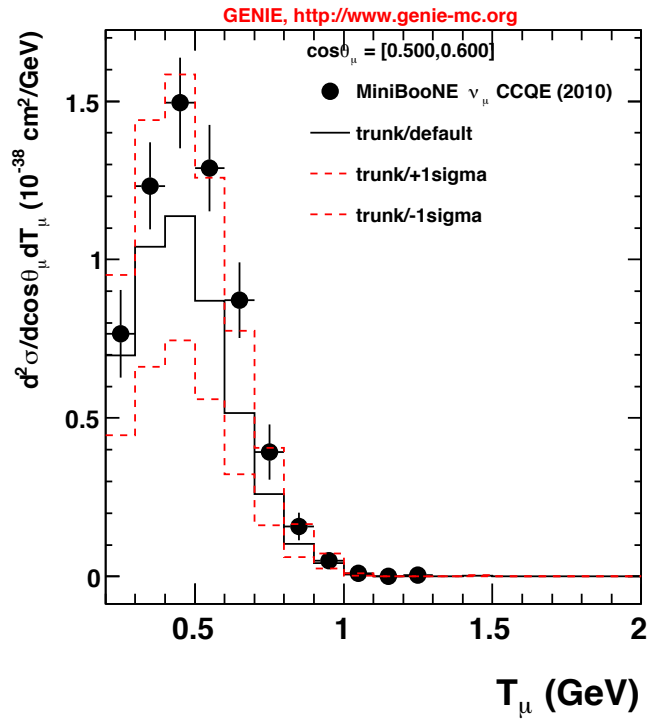
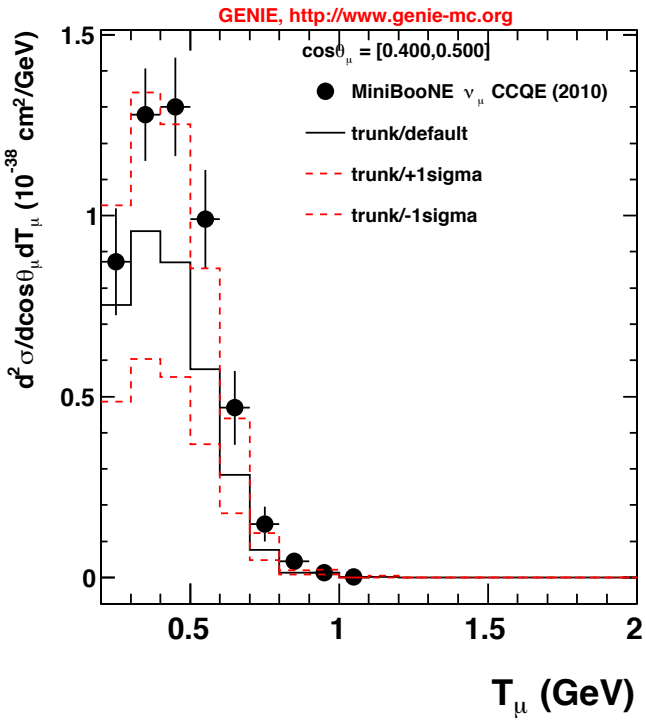
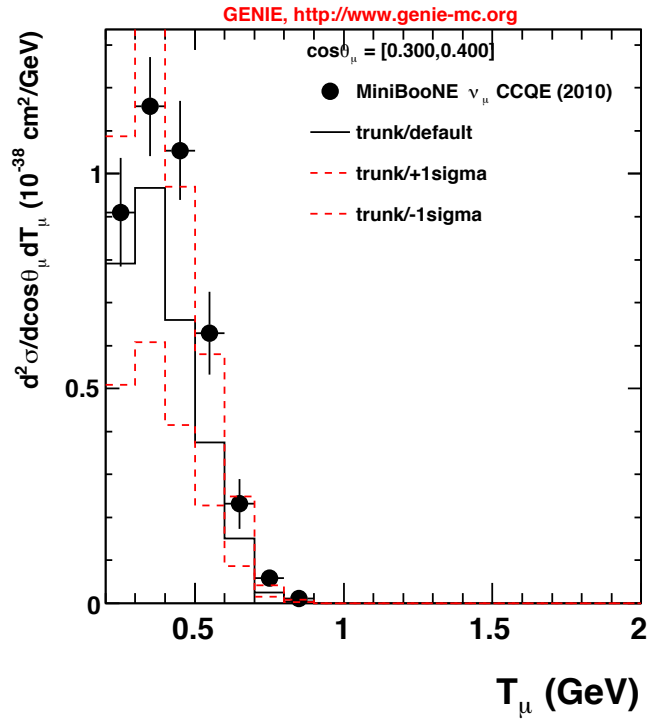
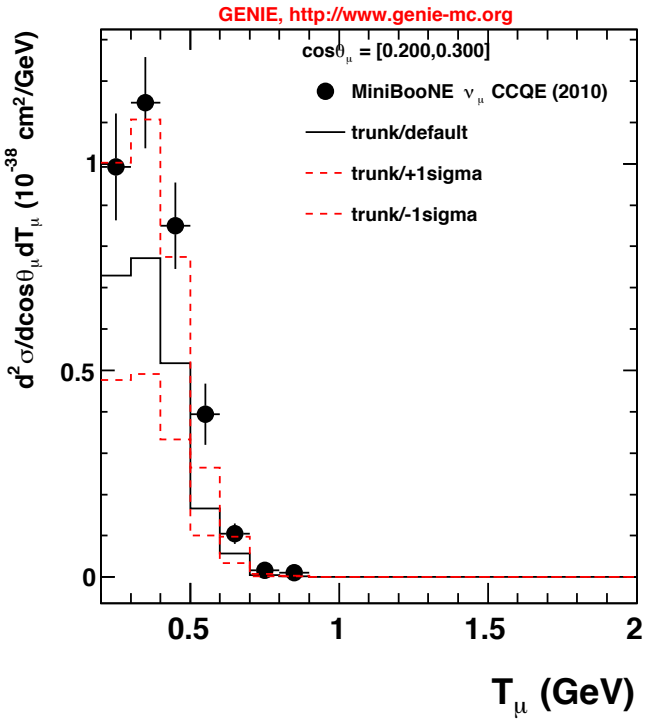
GENIE, <http://www.genie-mc.org>

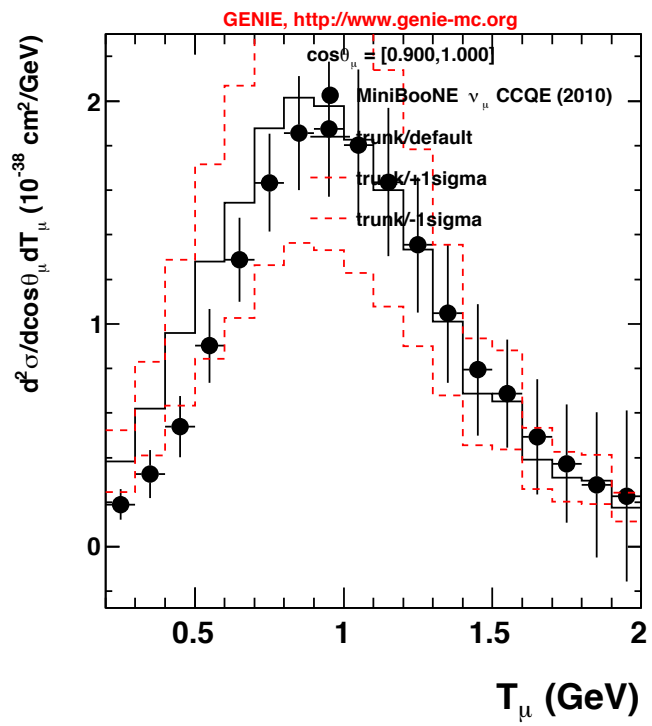
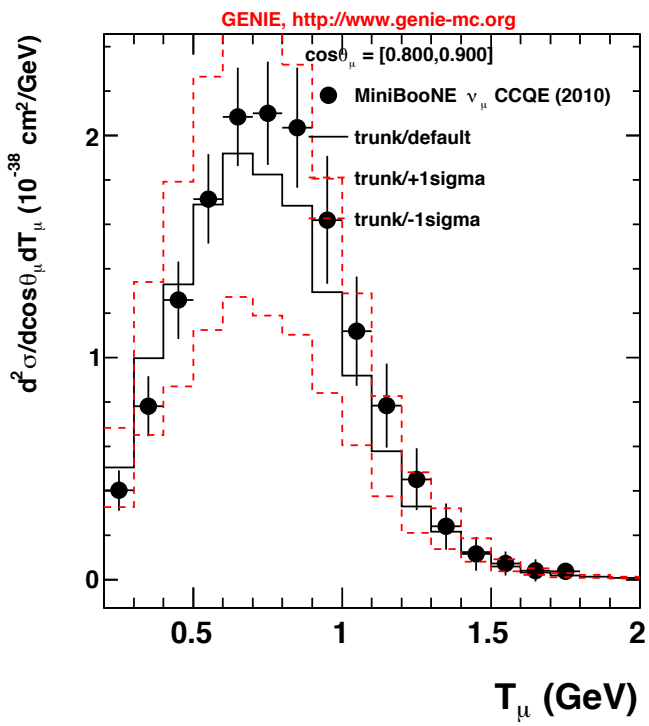
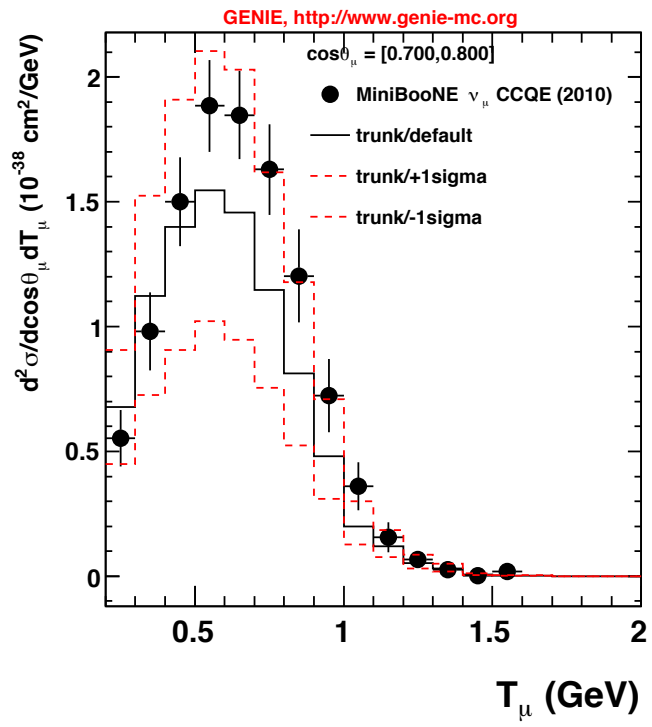
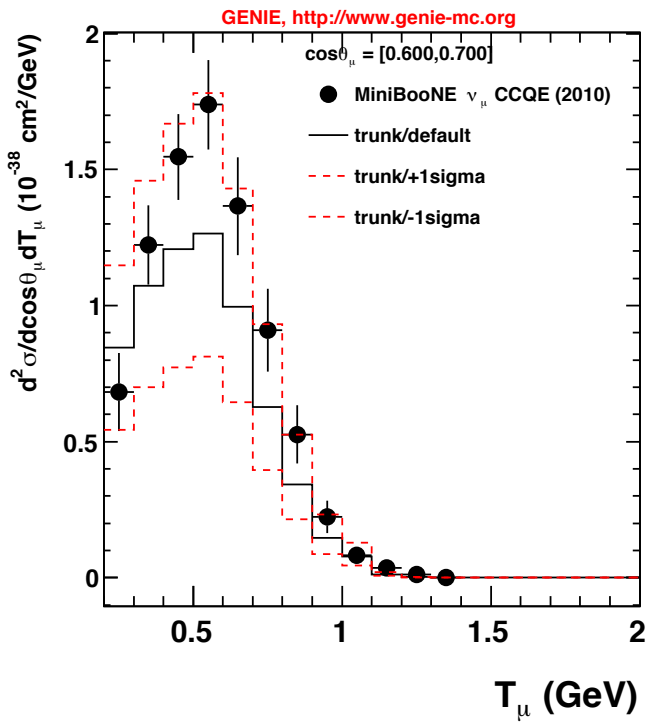


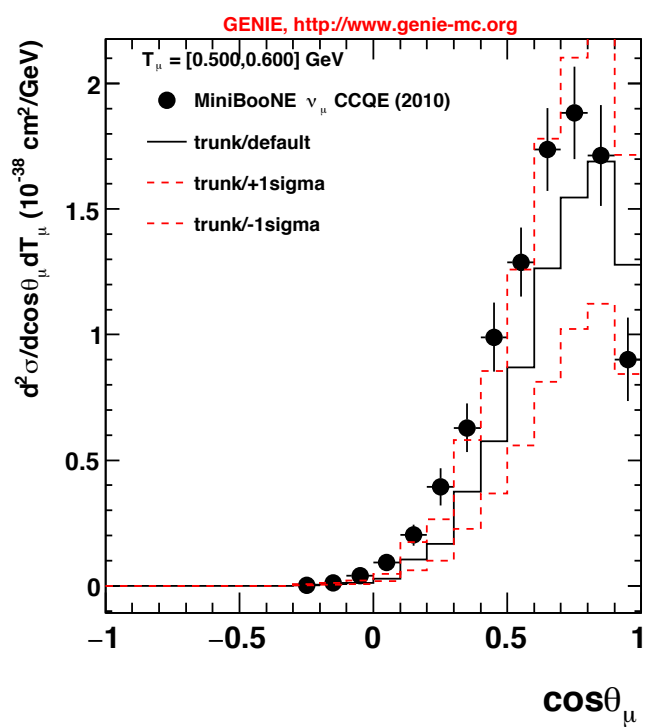
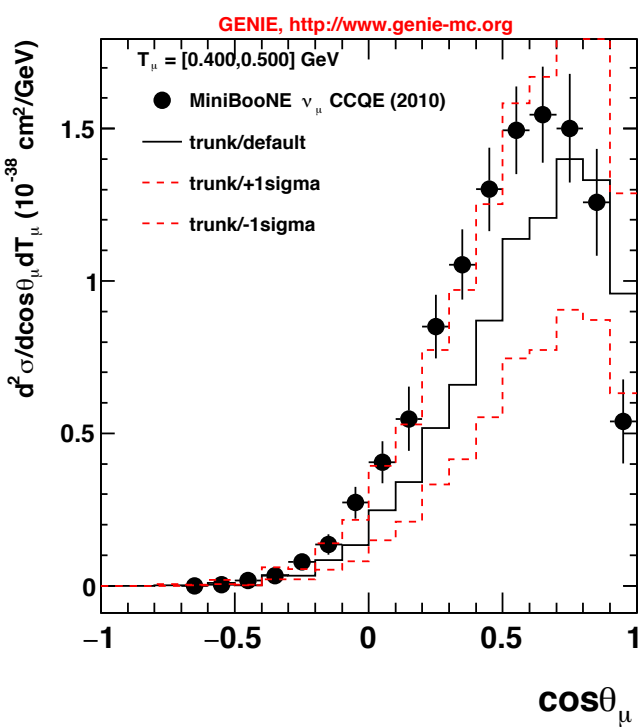
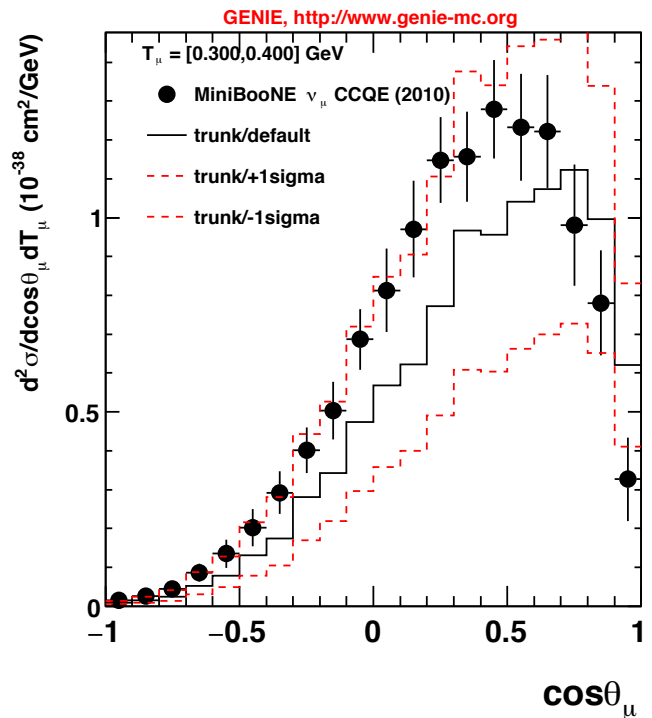
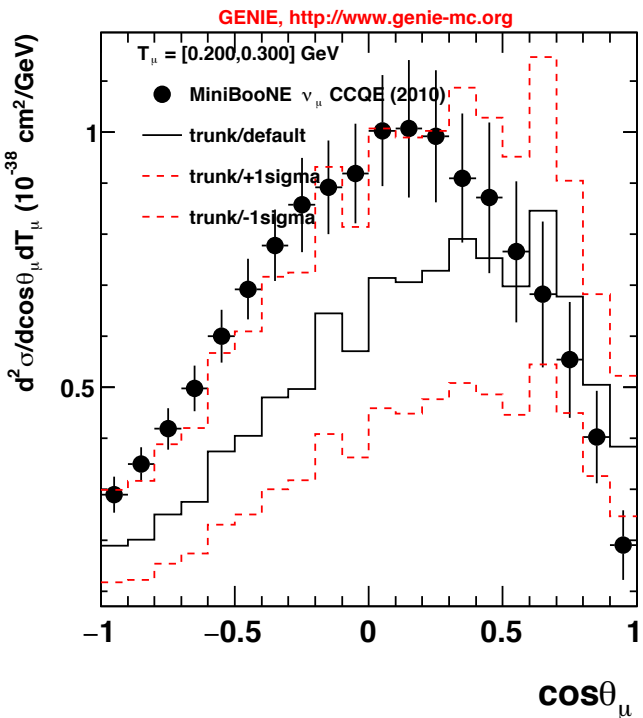


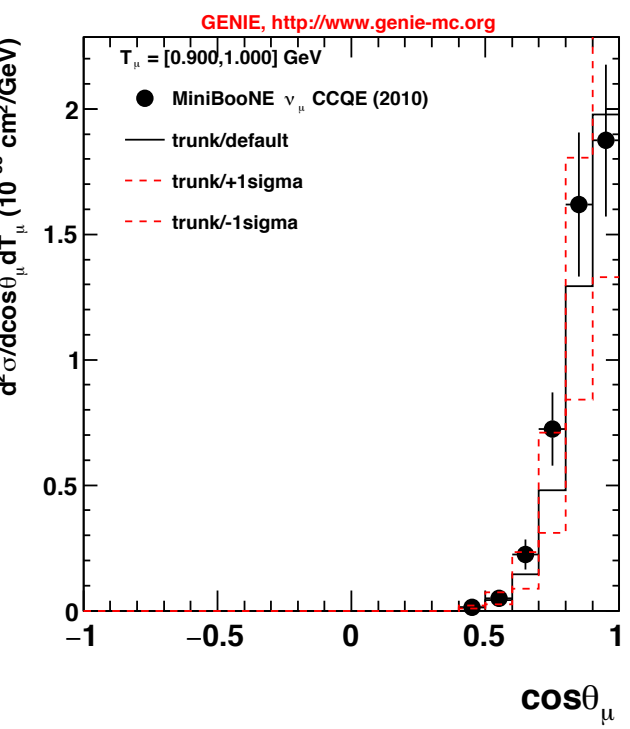
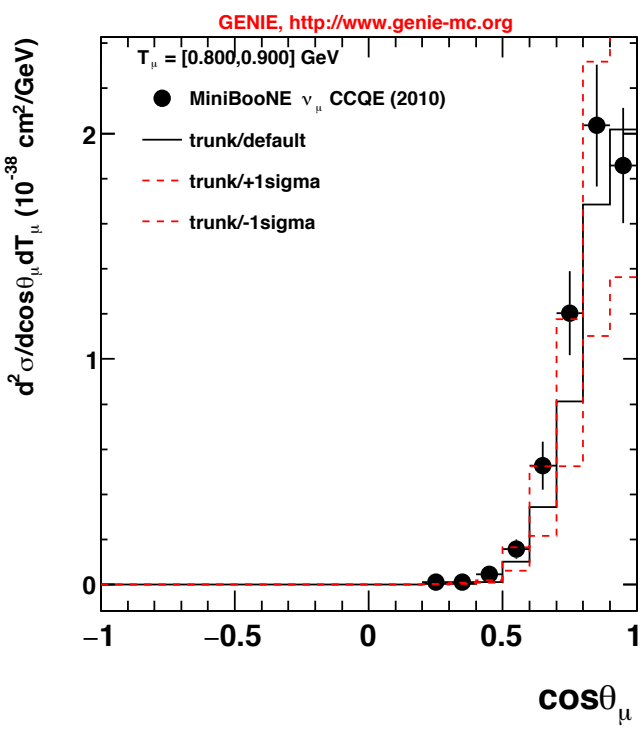
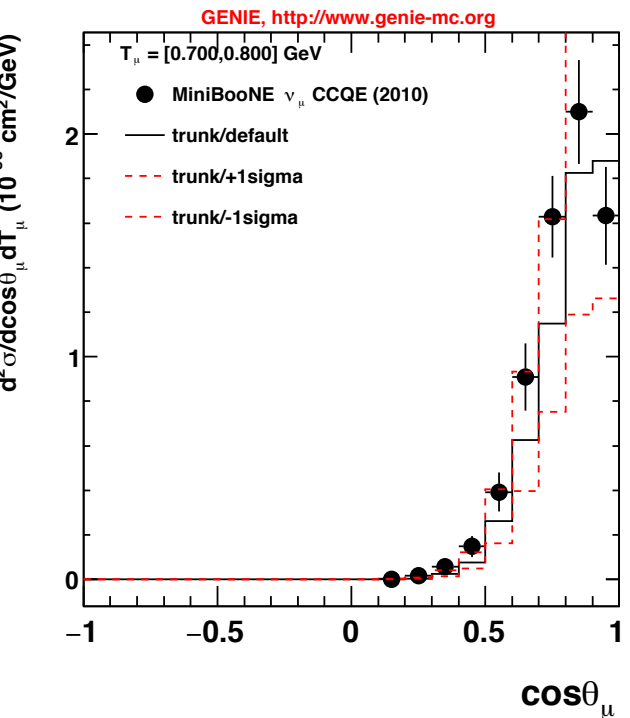
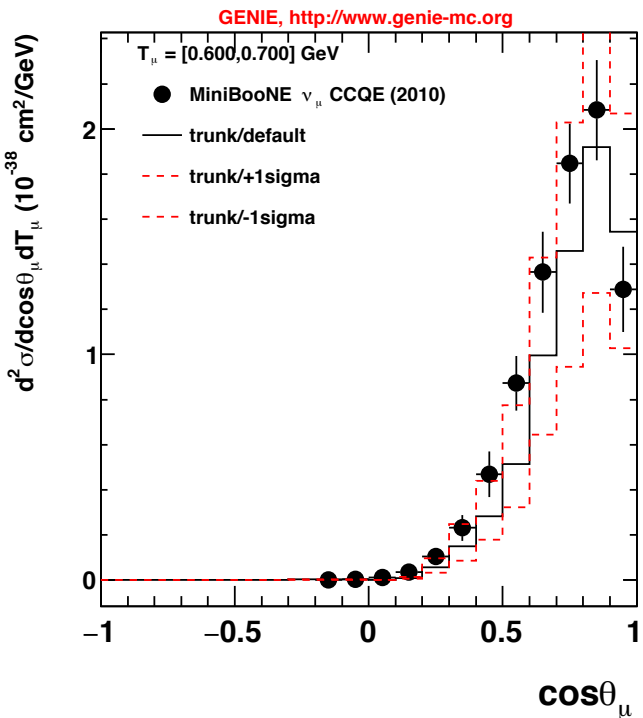


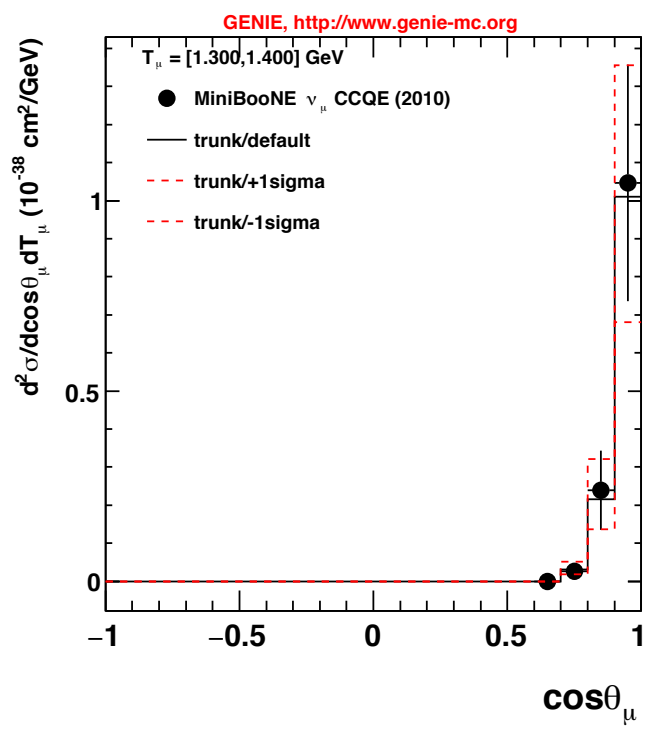
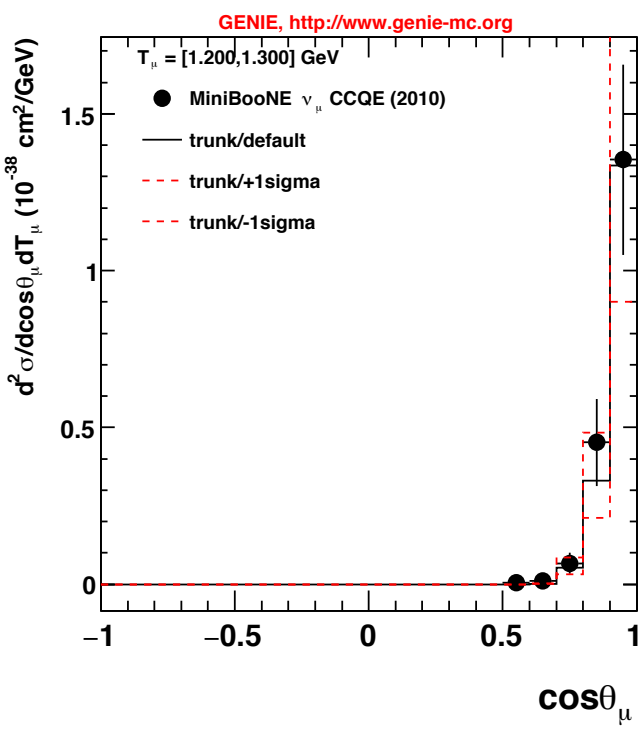
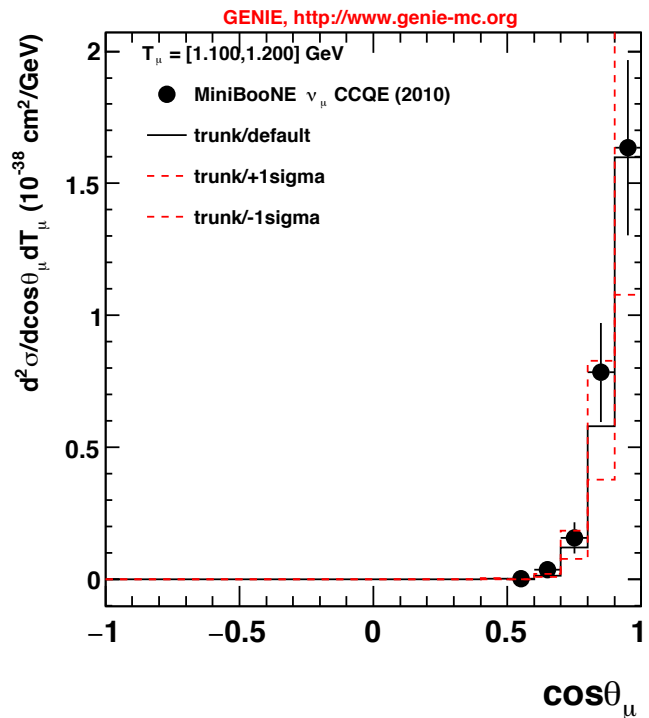
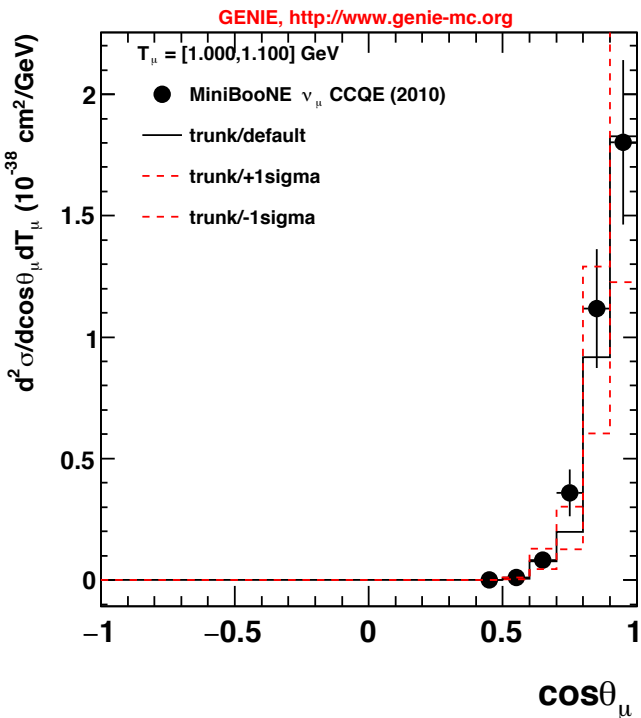


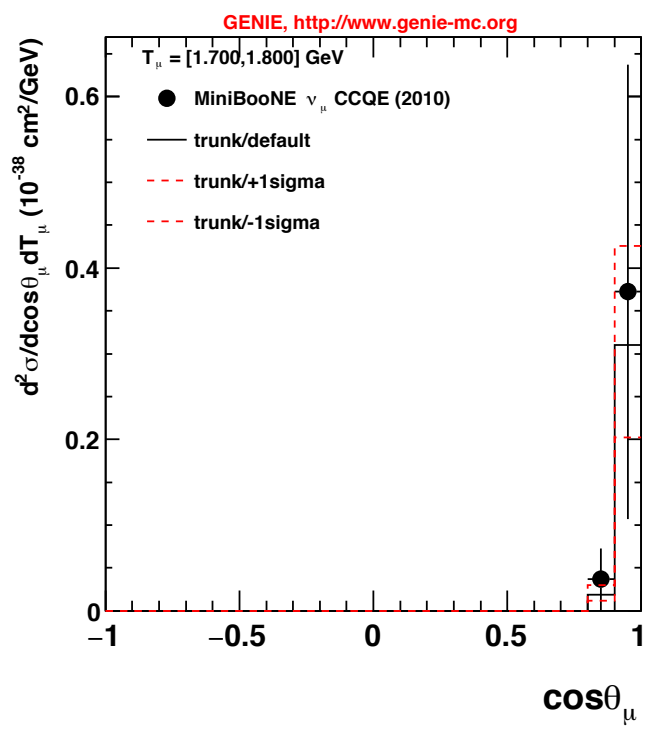
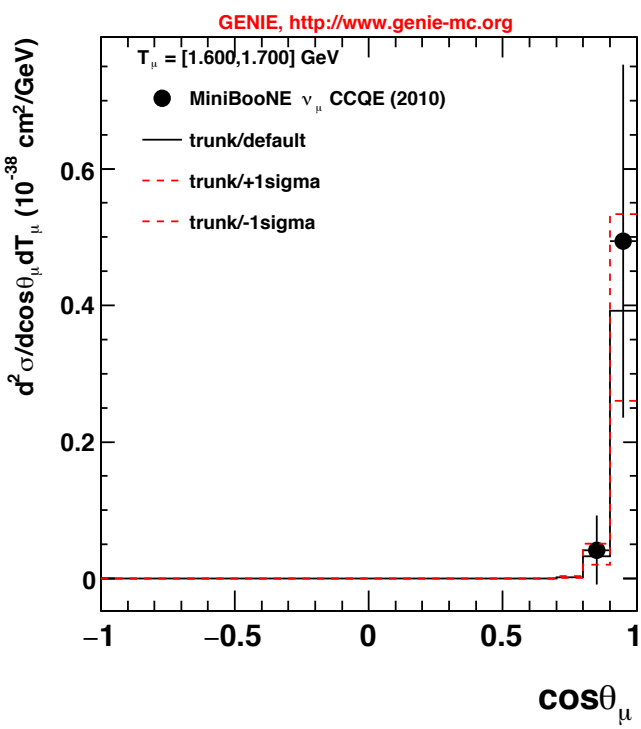
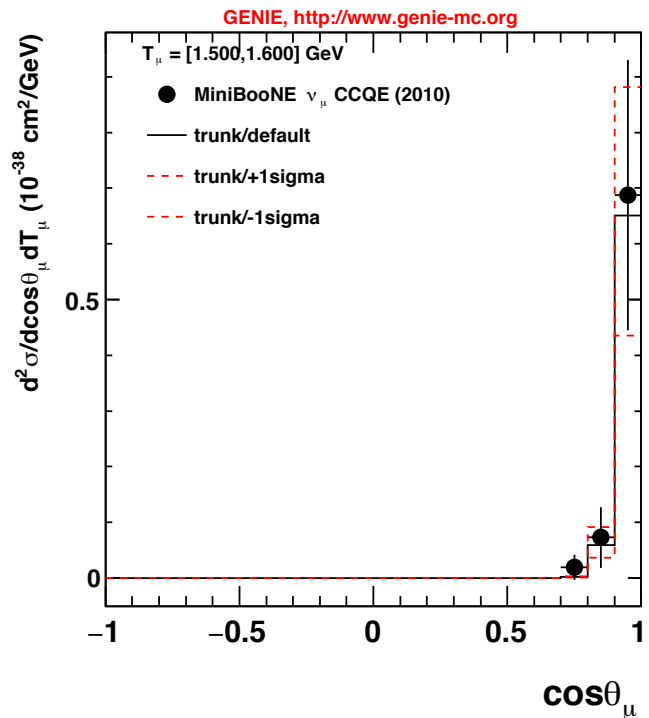
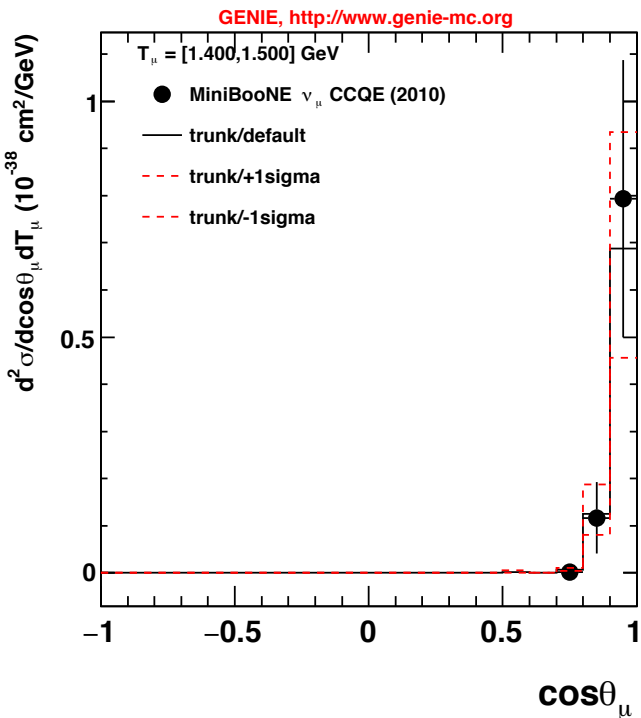


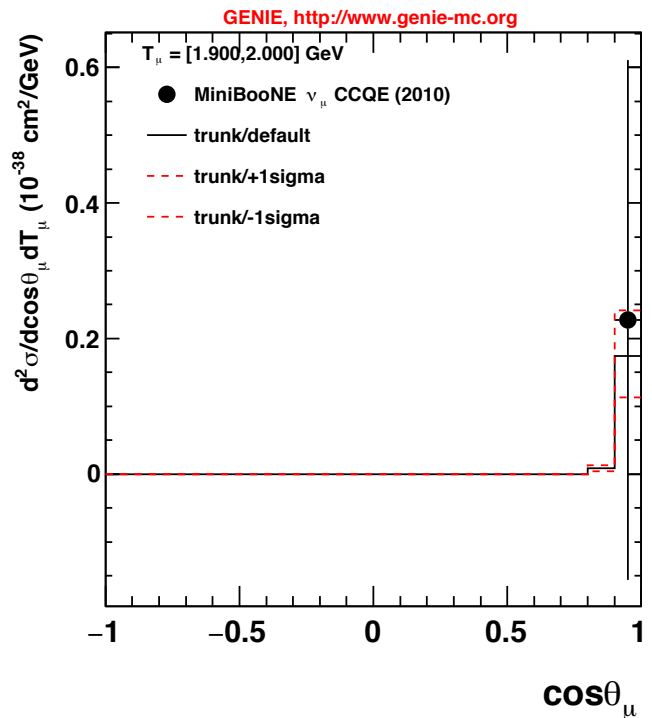
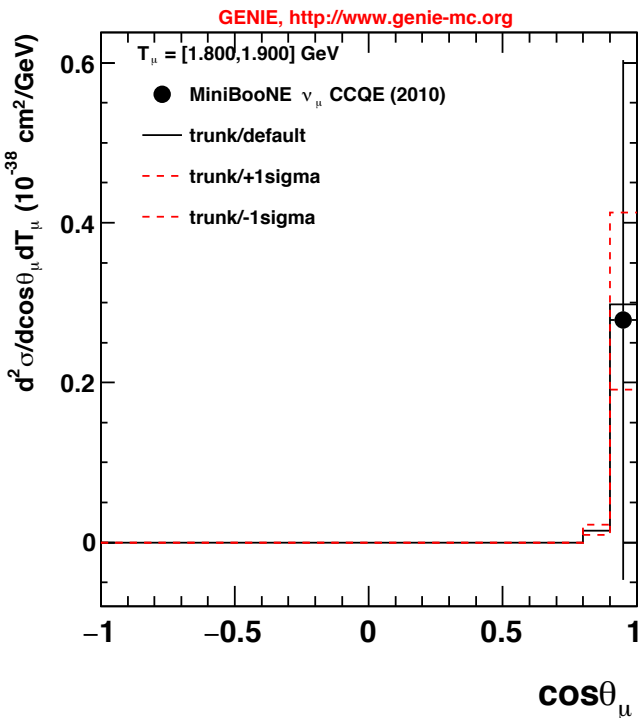


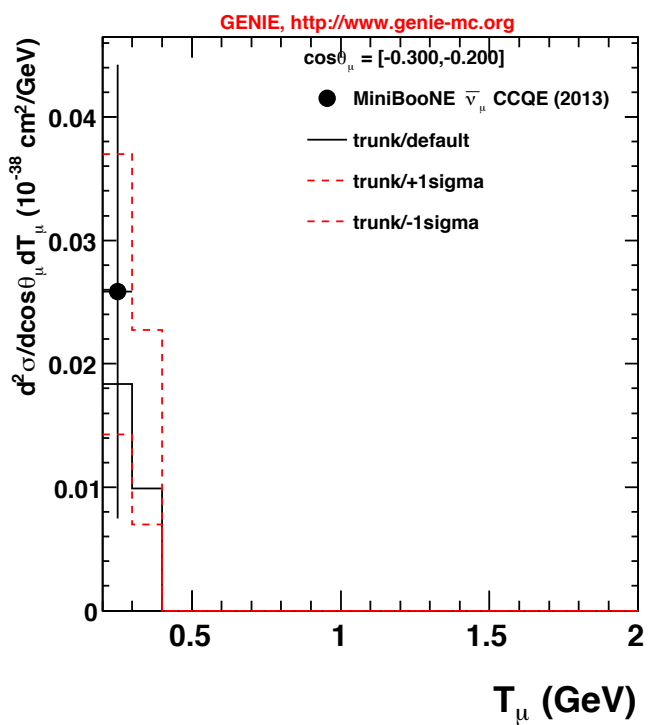
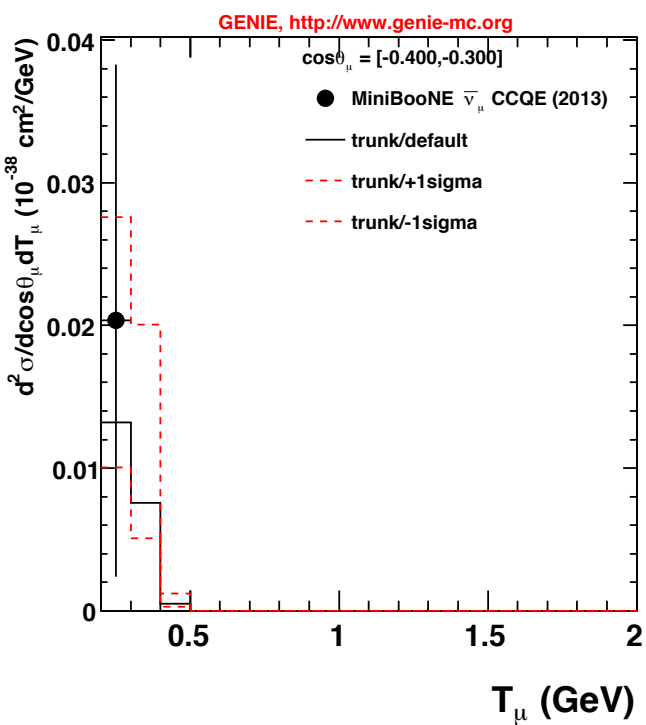
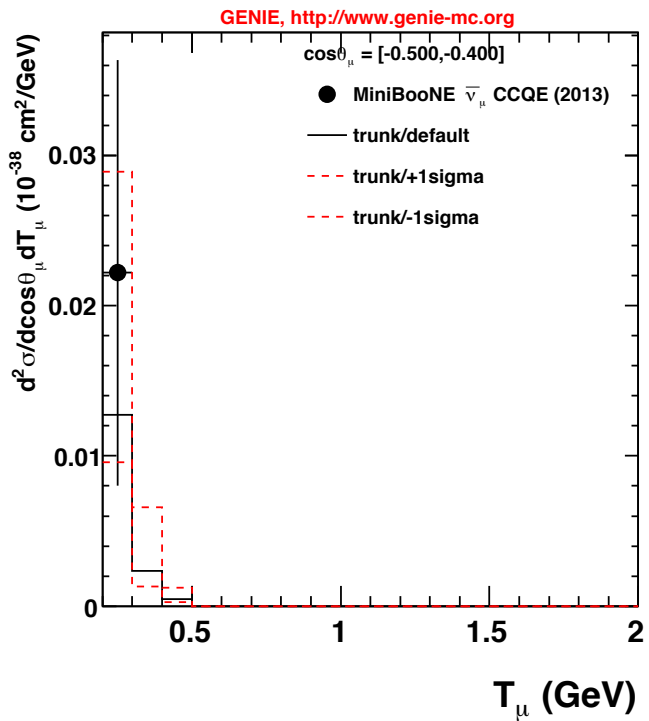
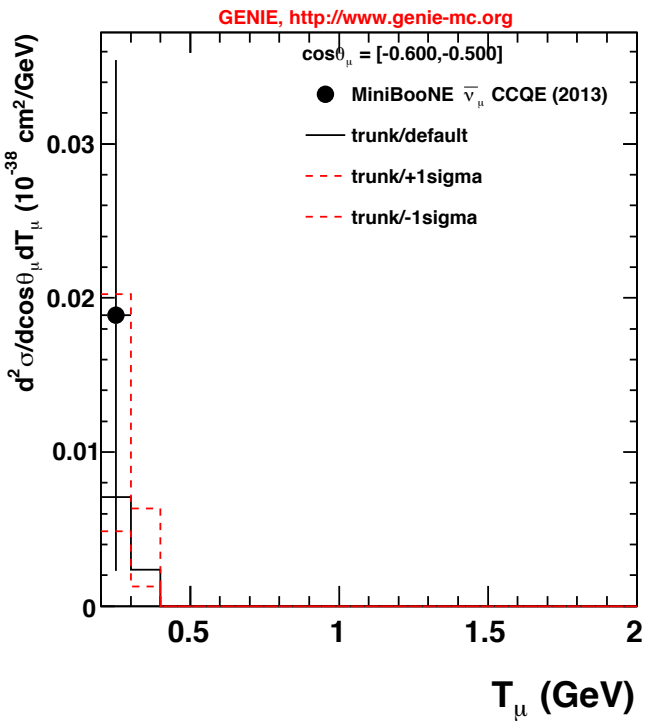


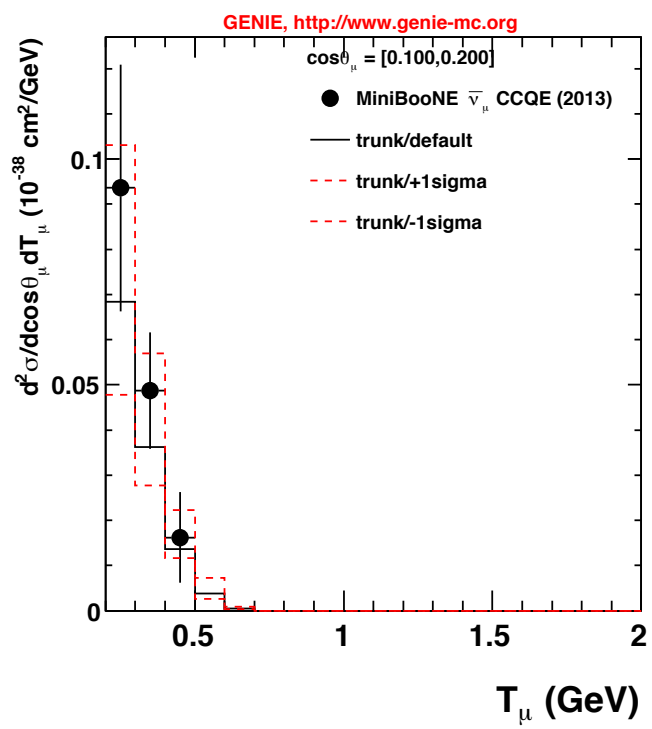
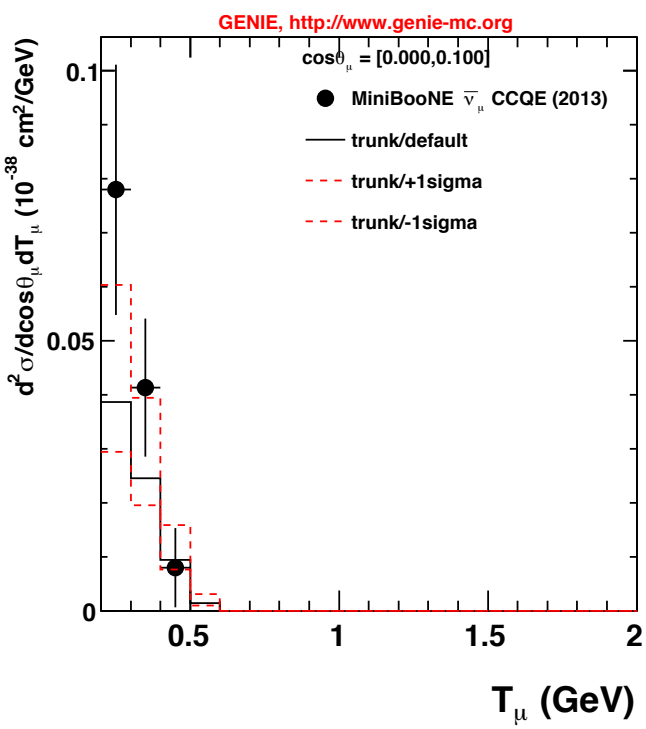
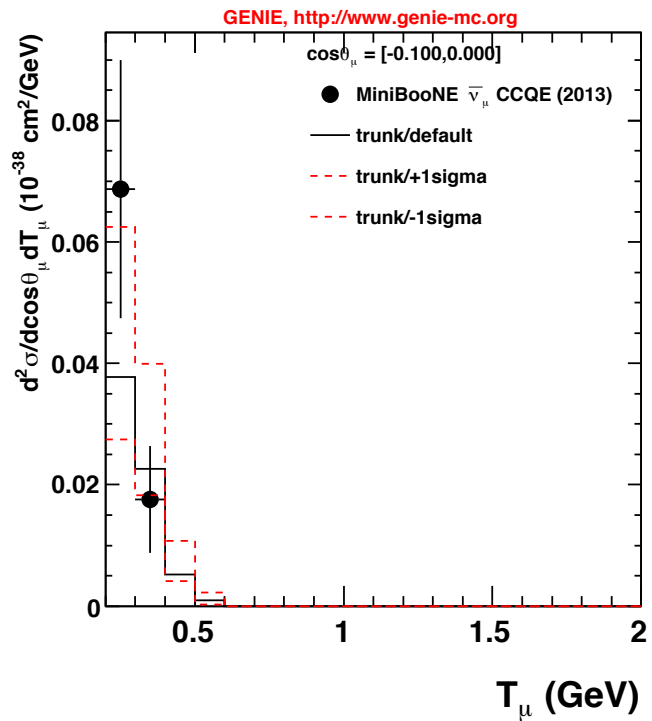
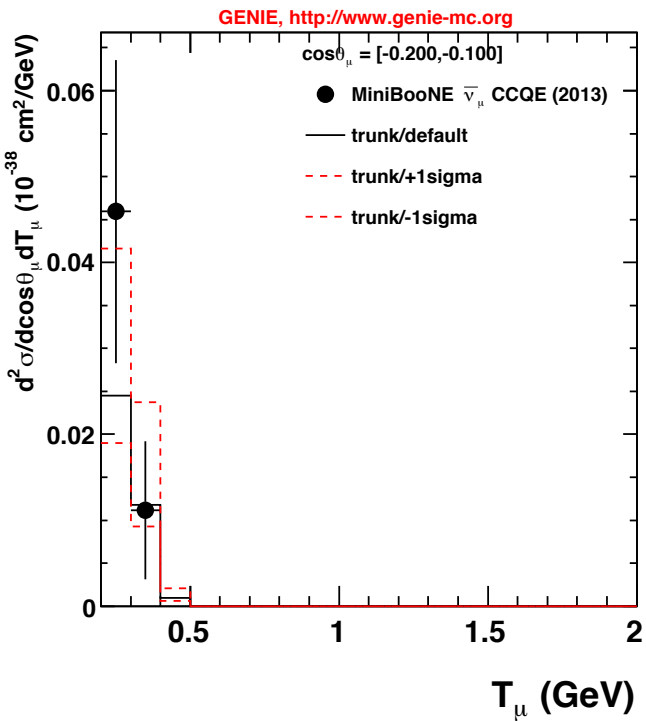


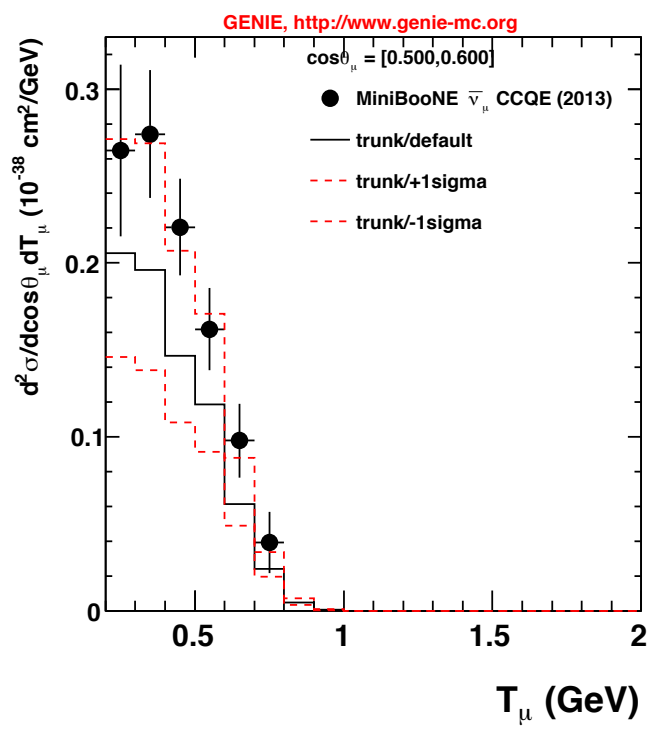
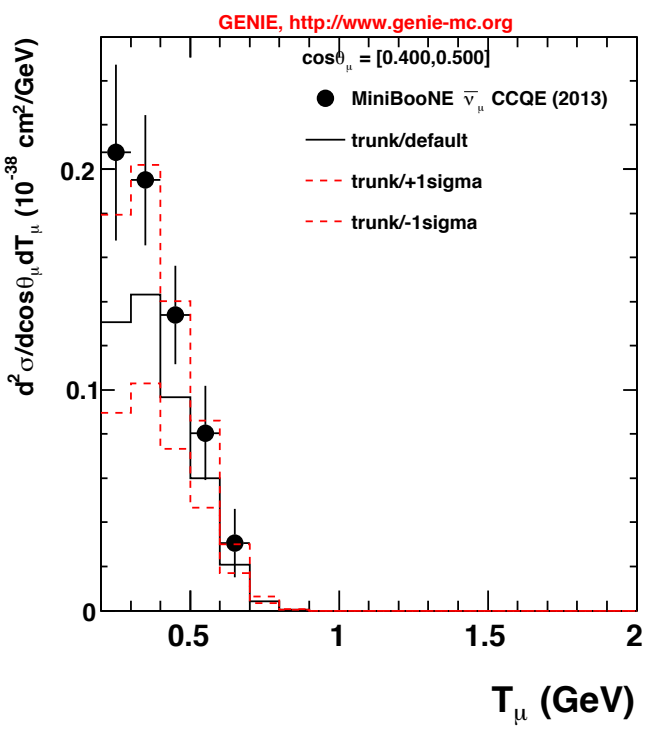
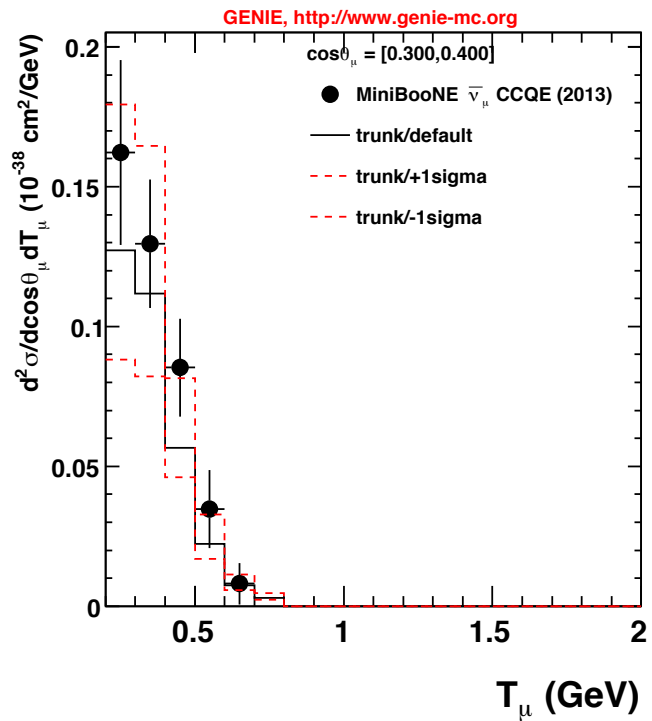
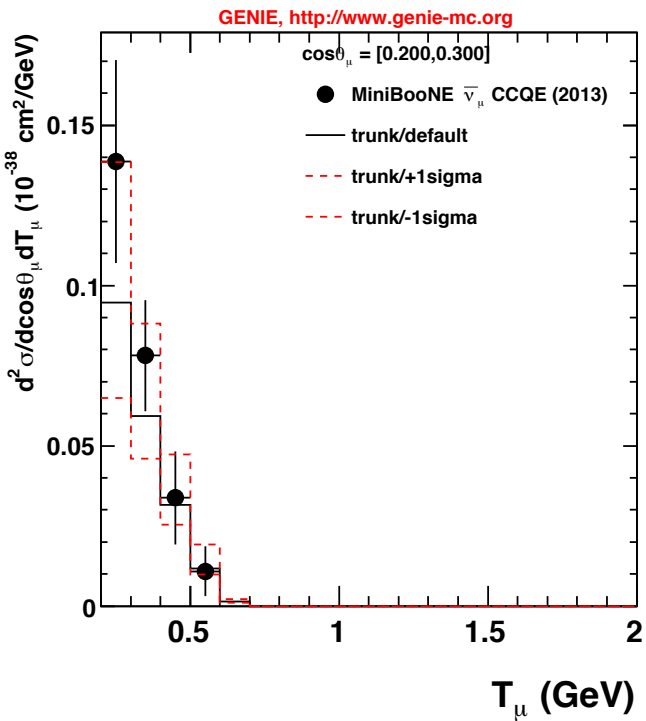


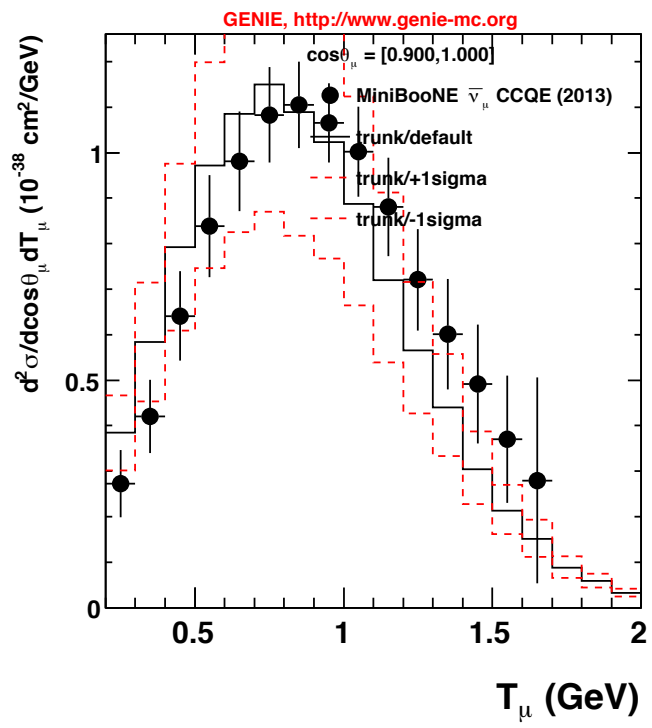
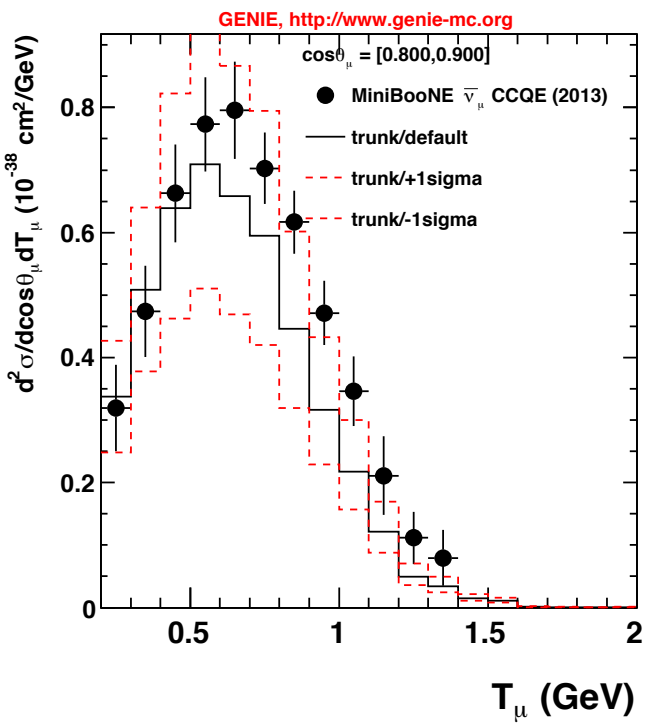
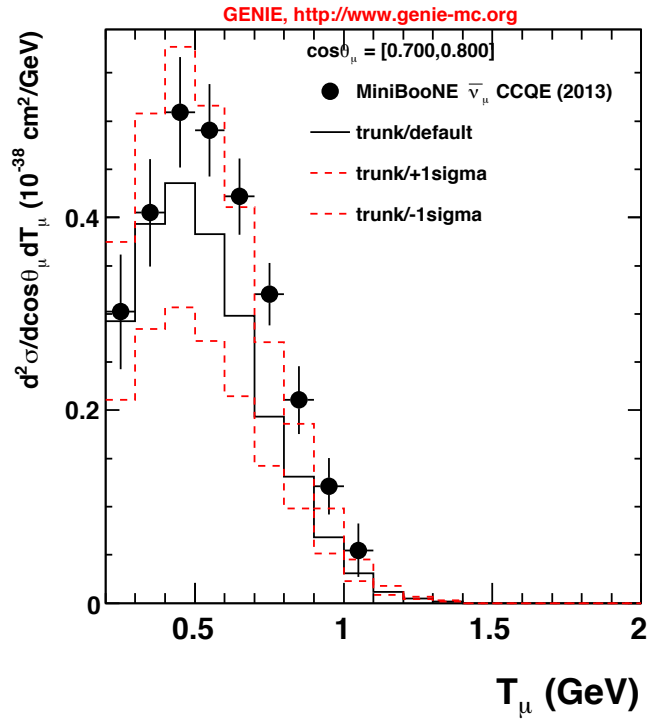
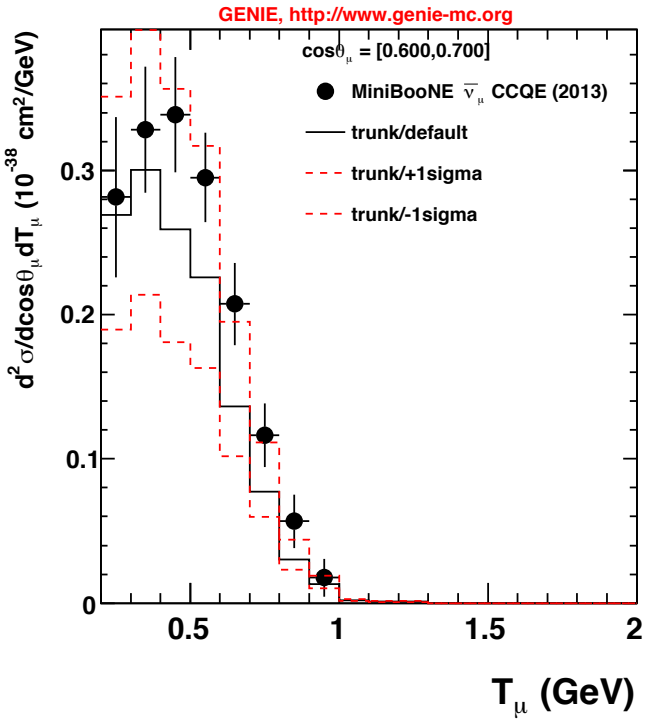


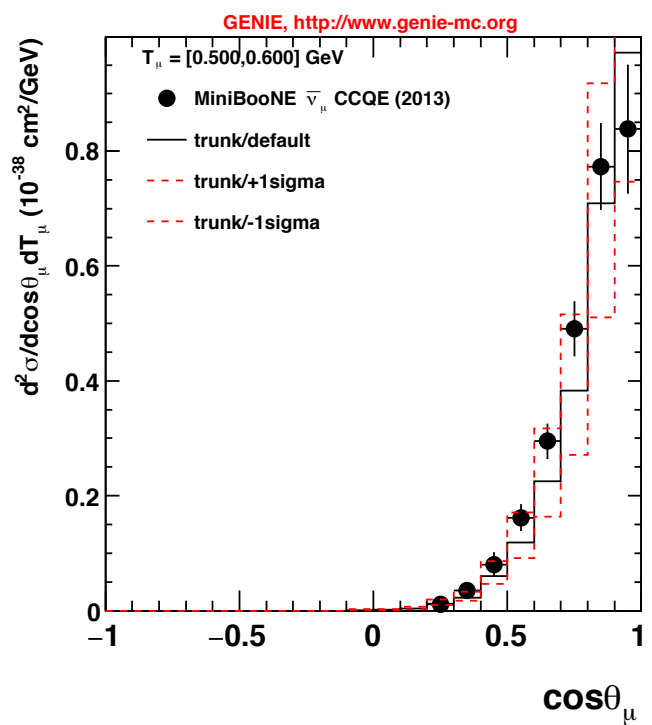
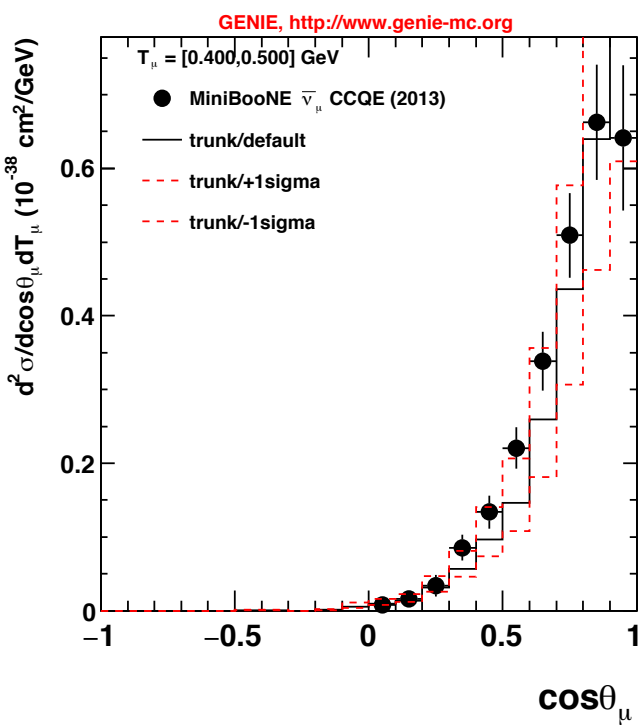
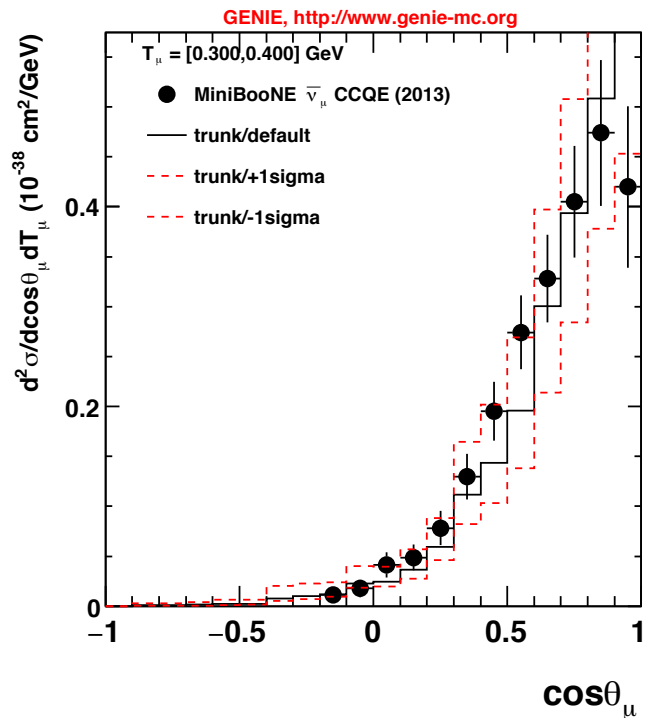
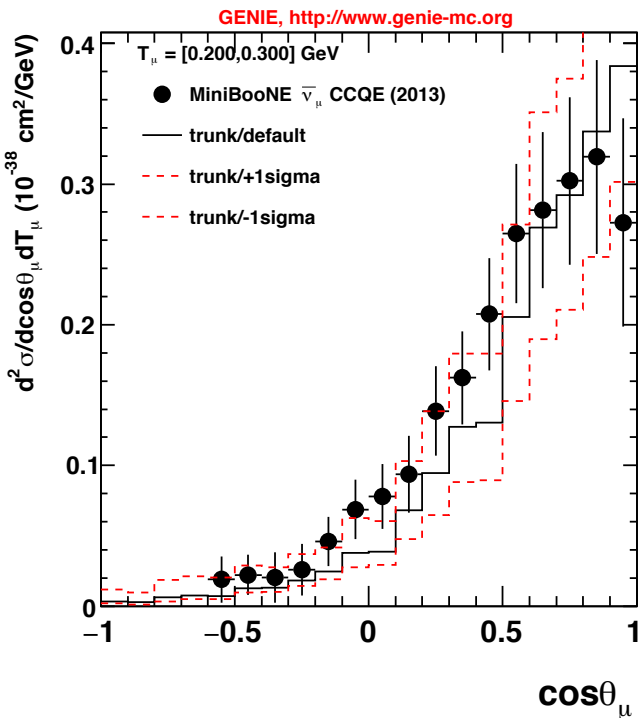


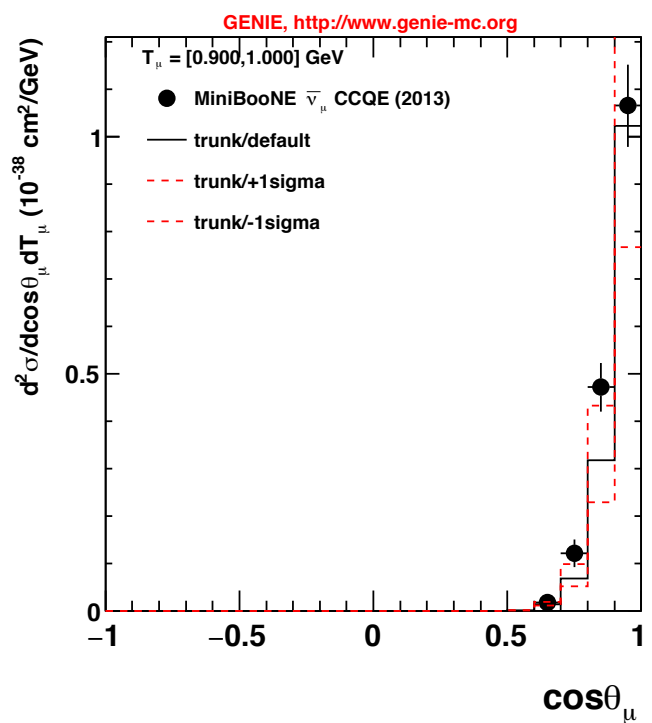
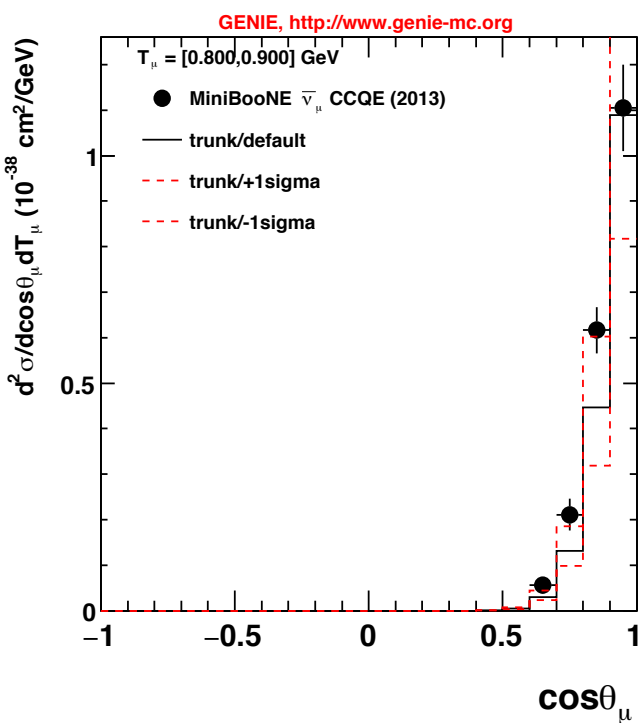
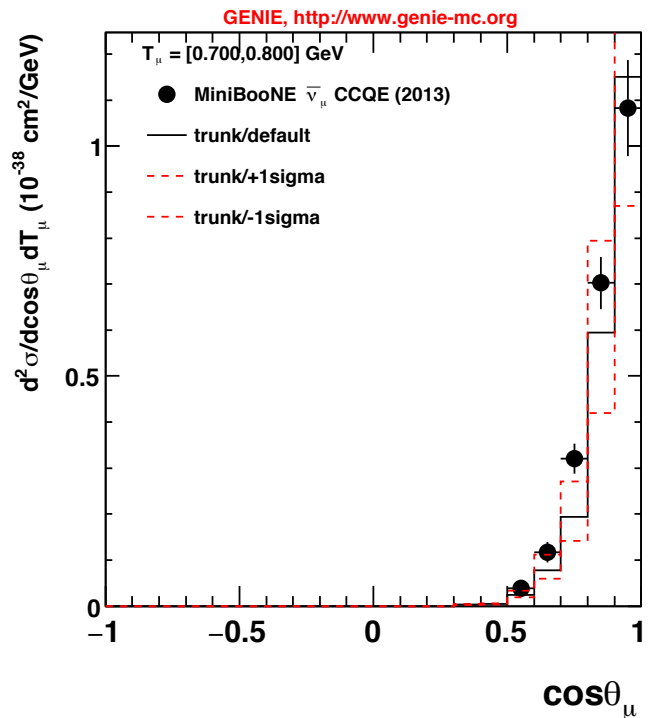
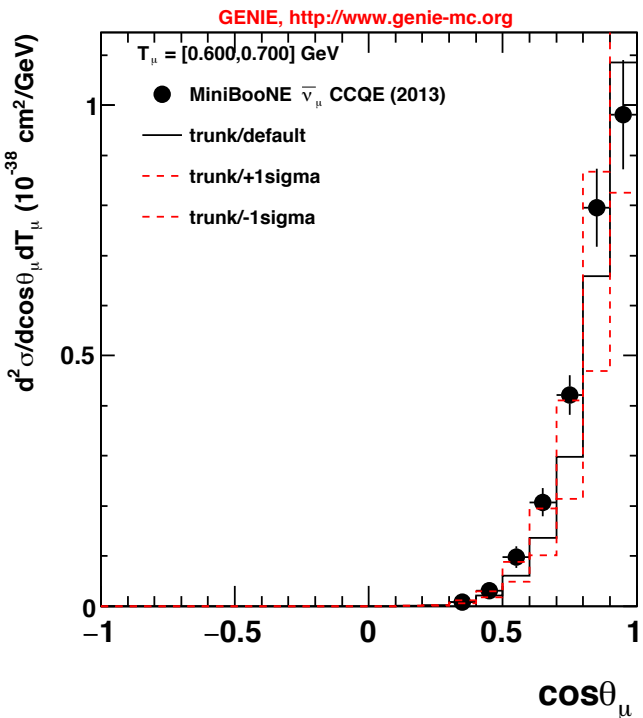


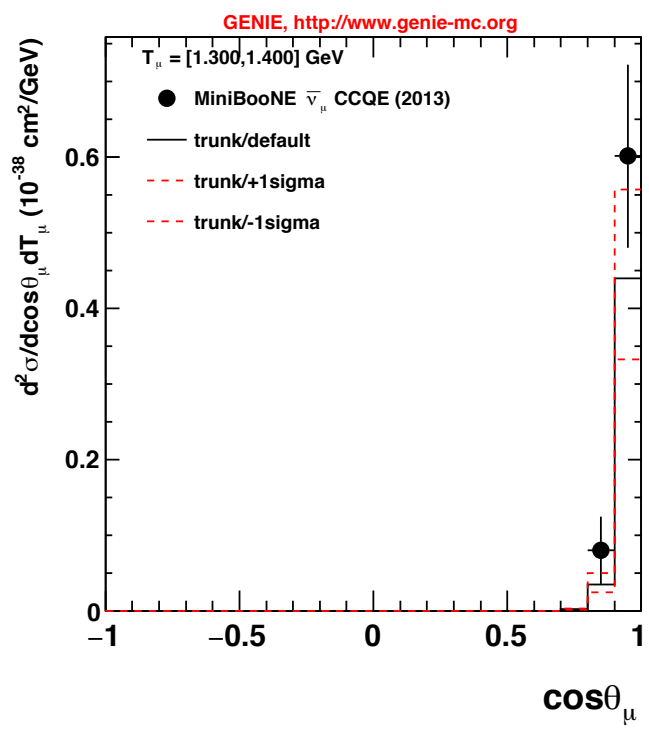
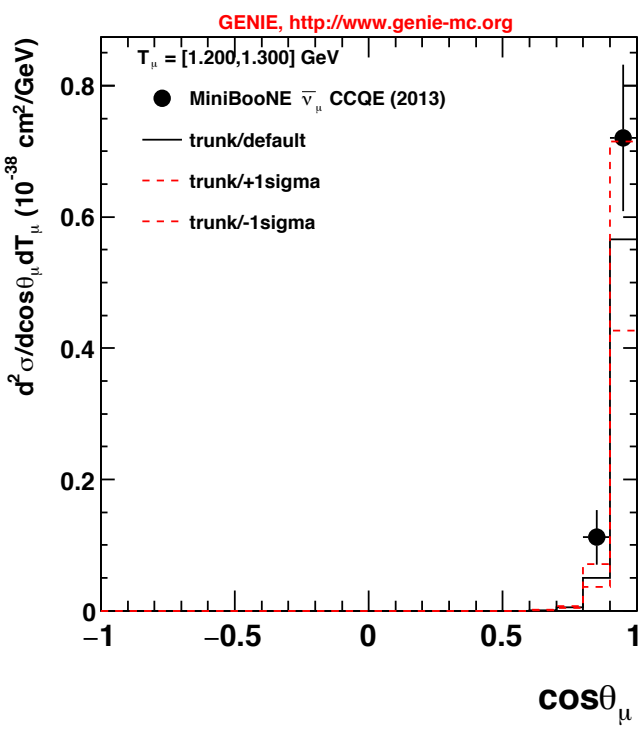
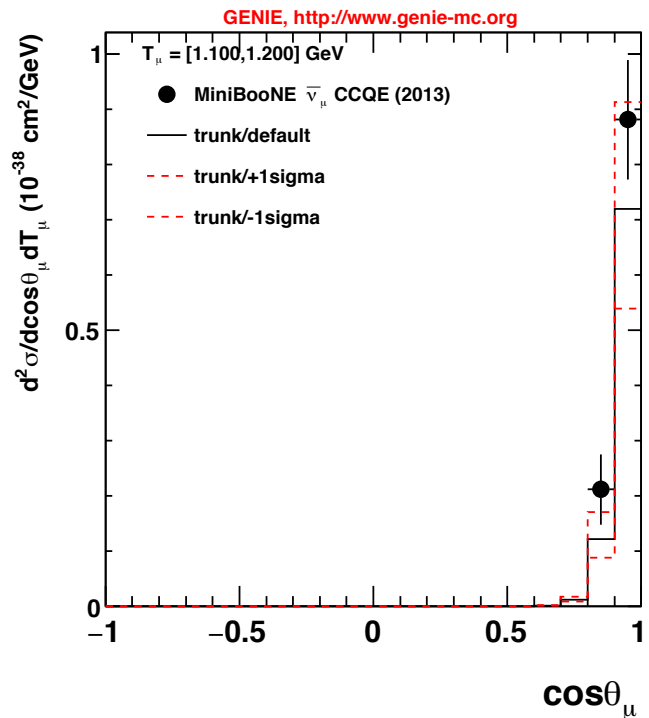
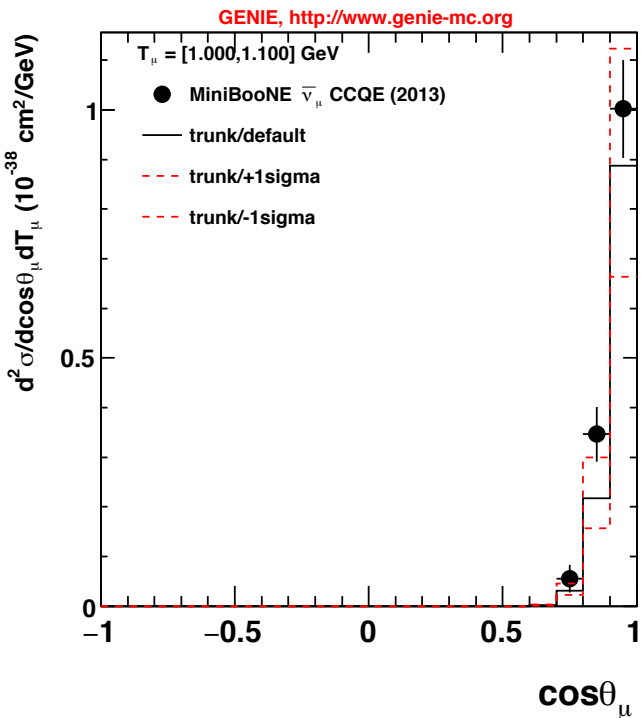


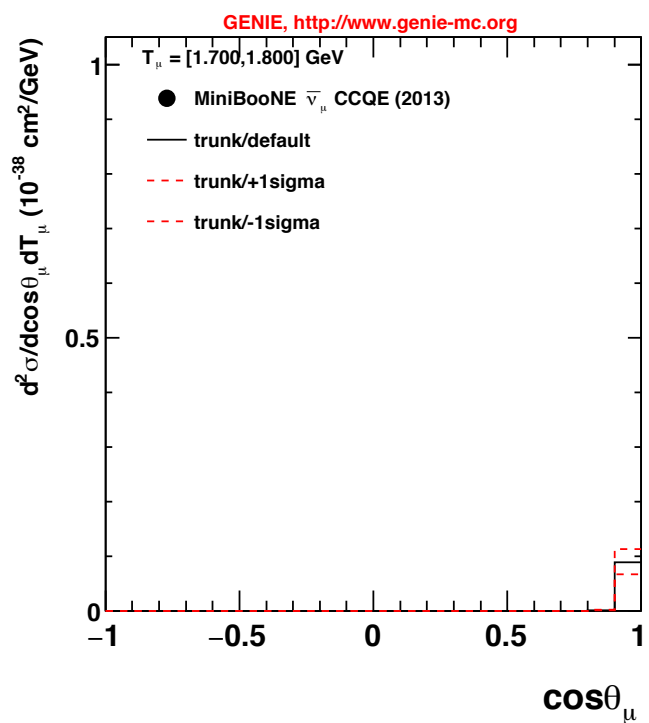
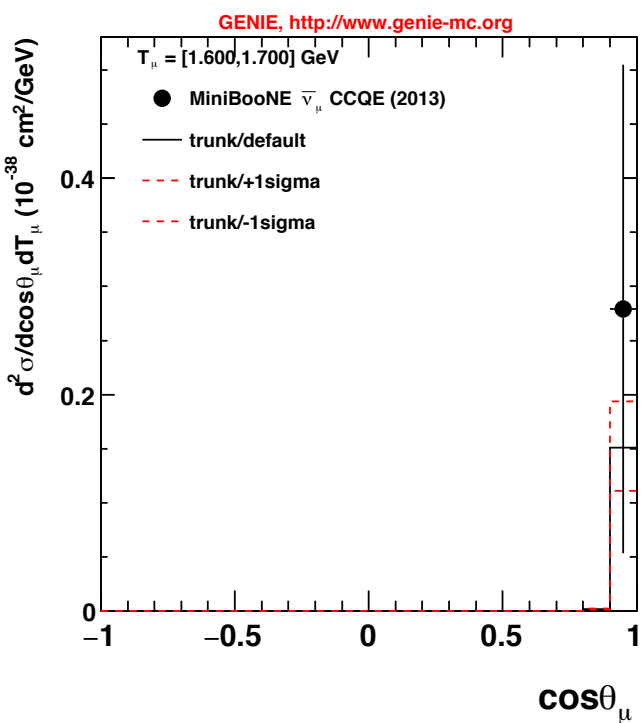
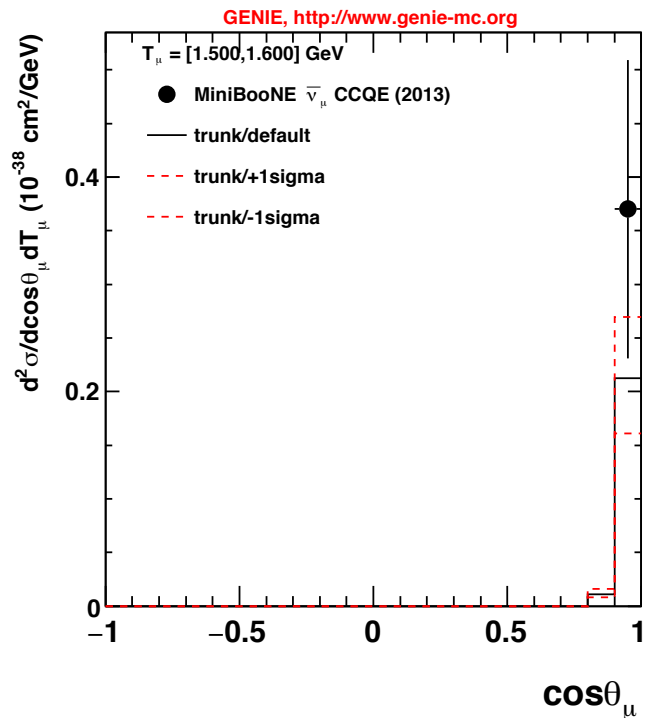
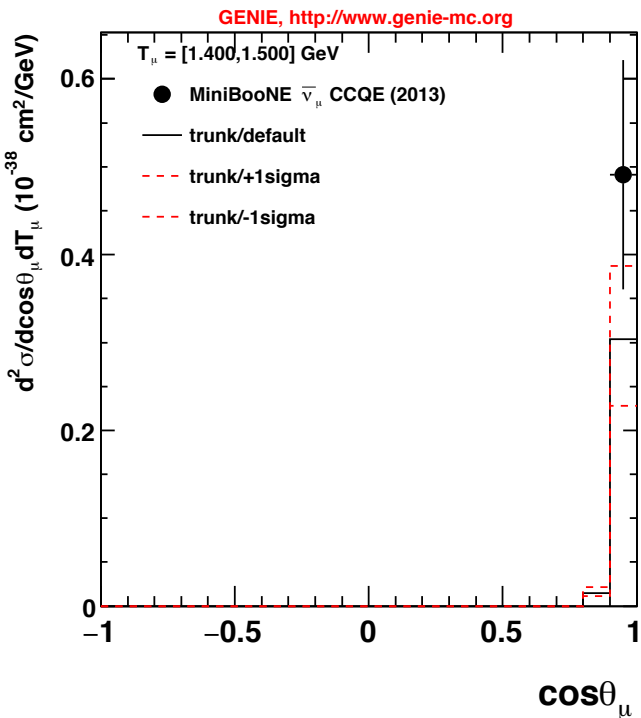


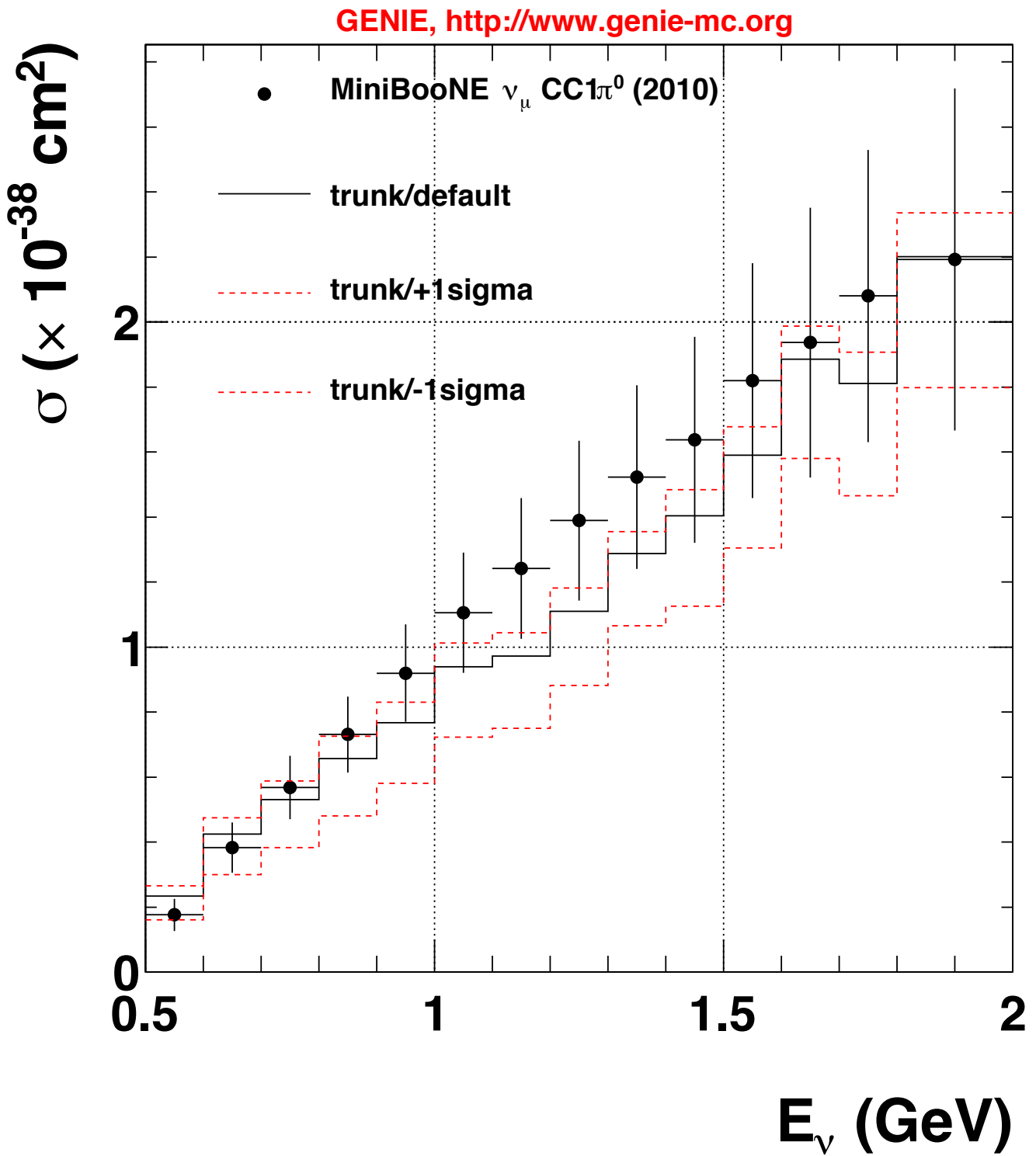


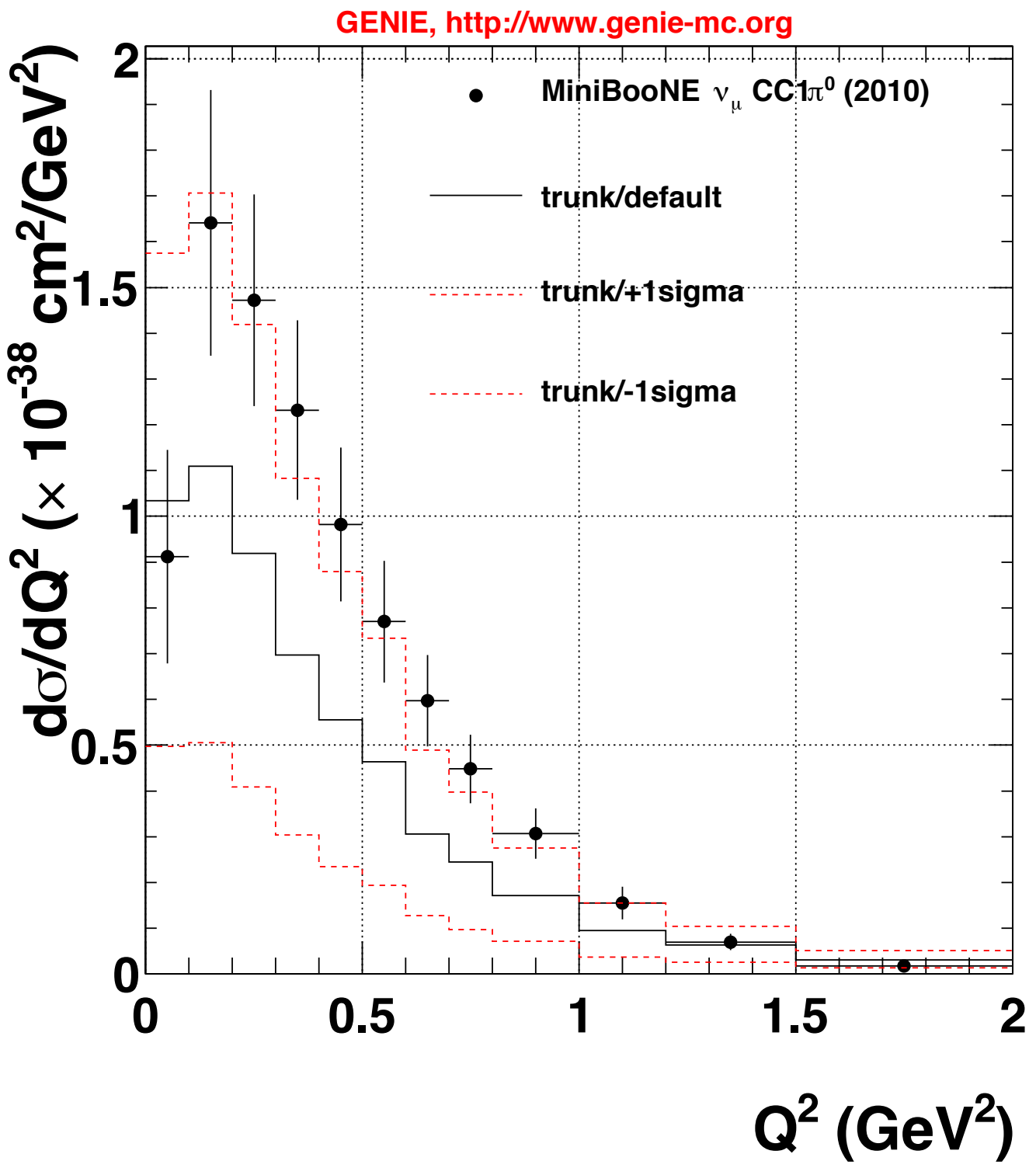


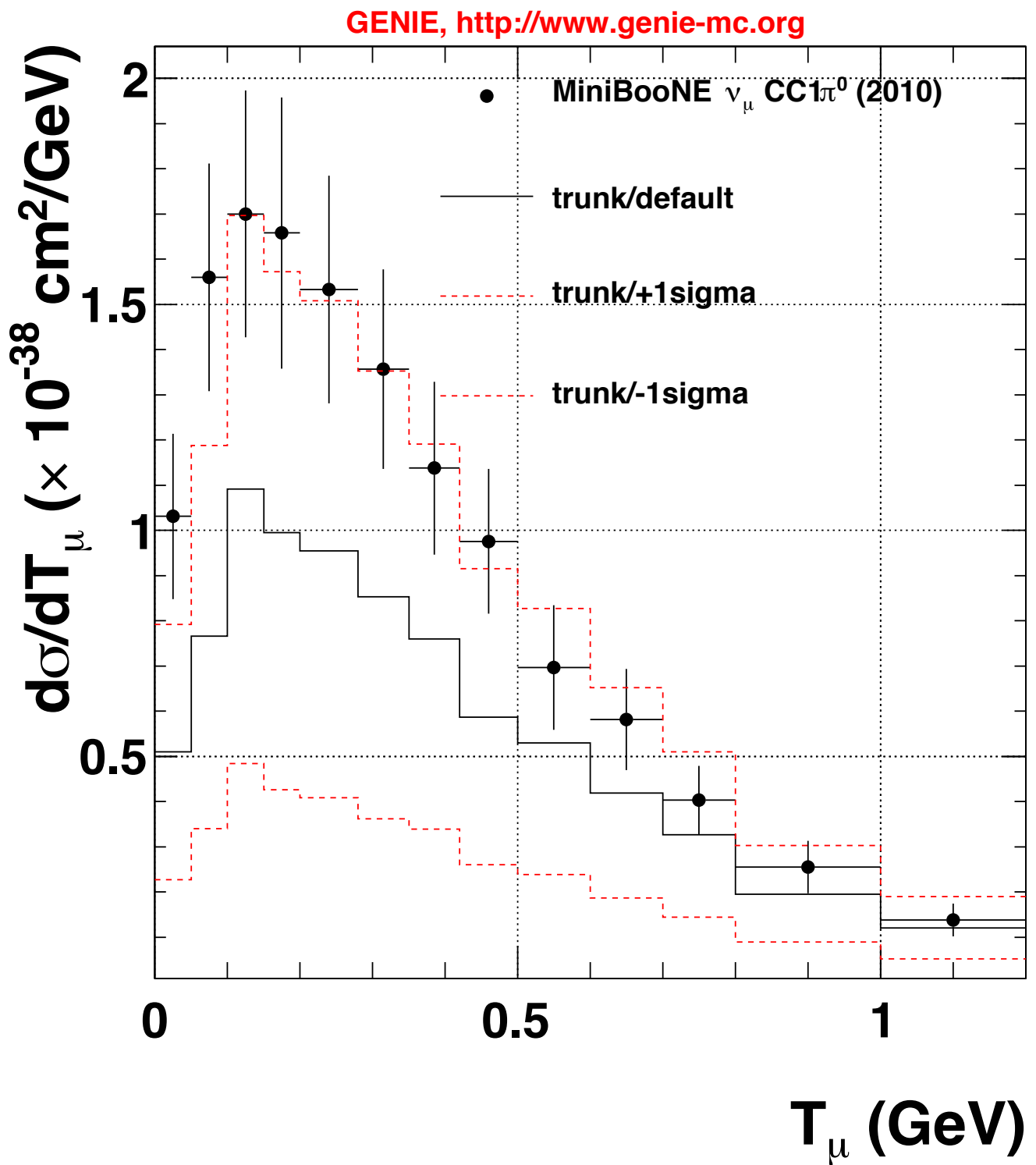


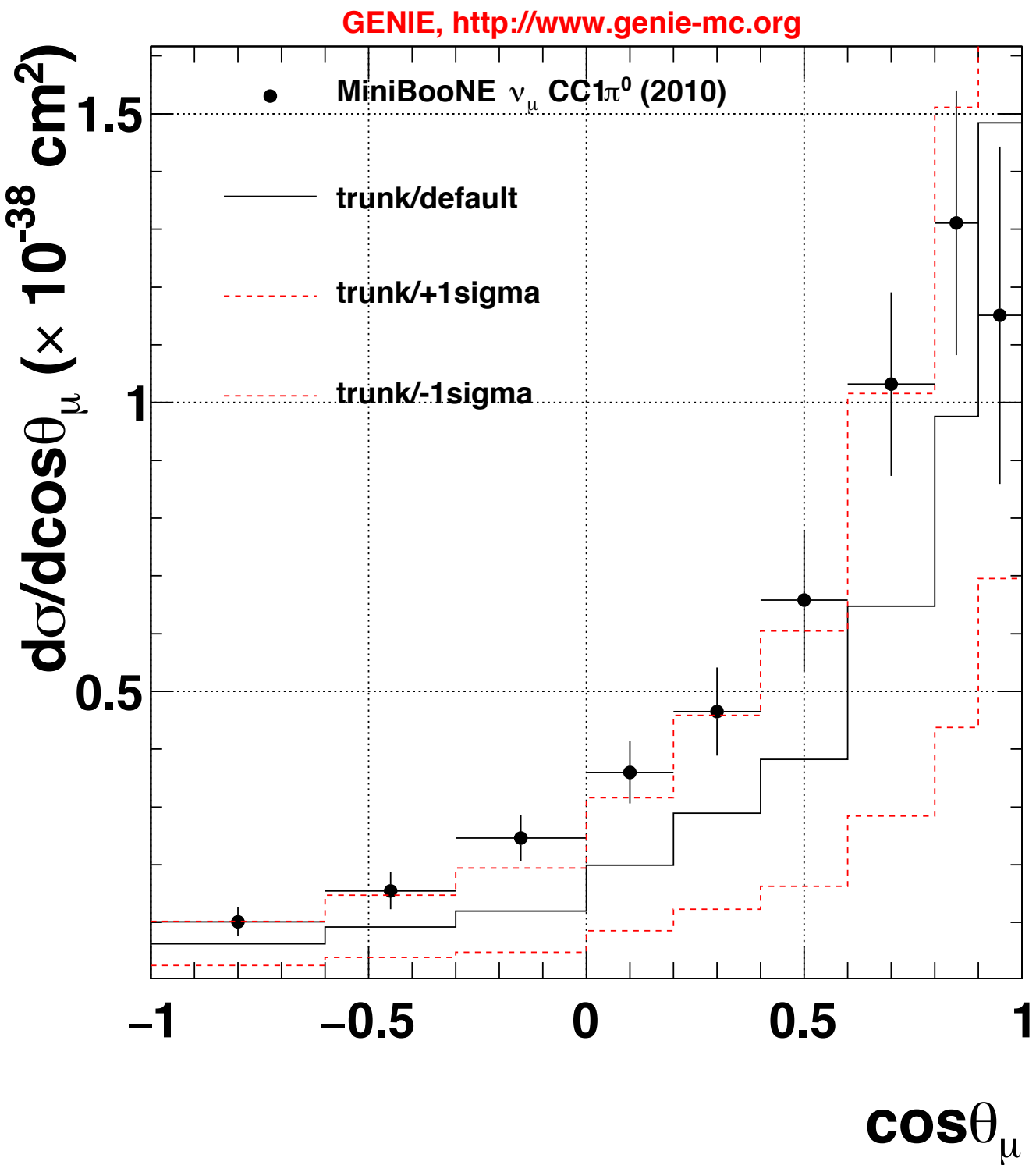


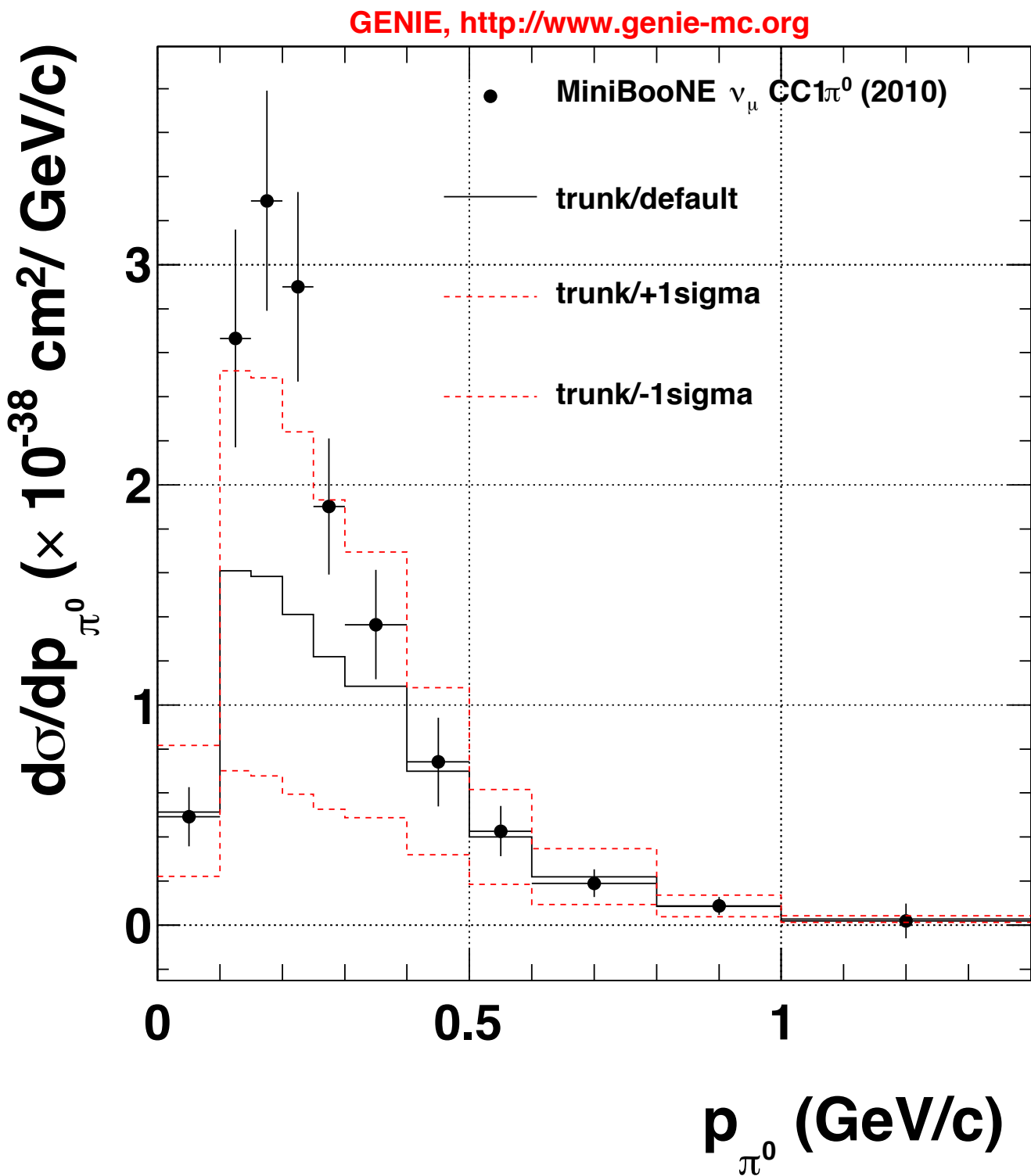


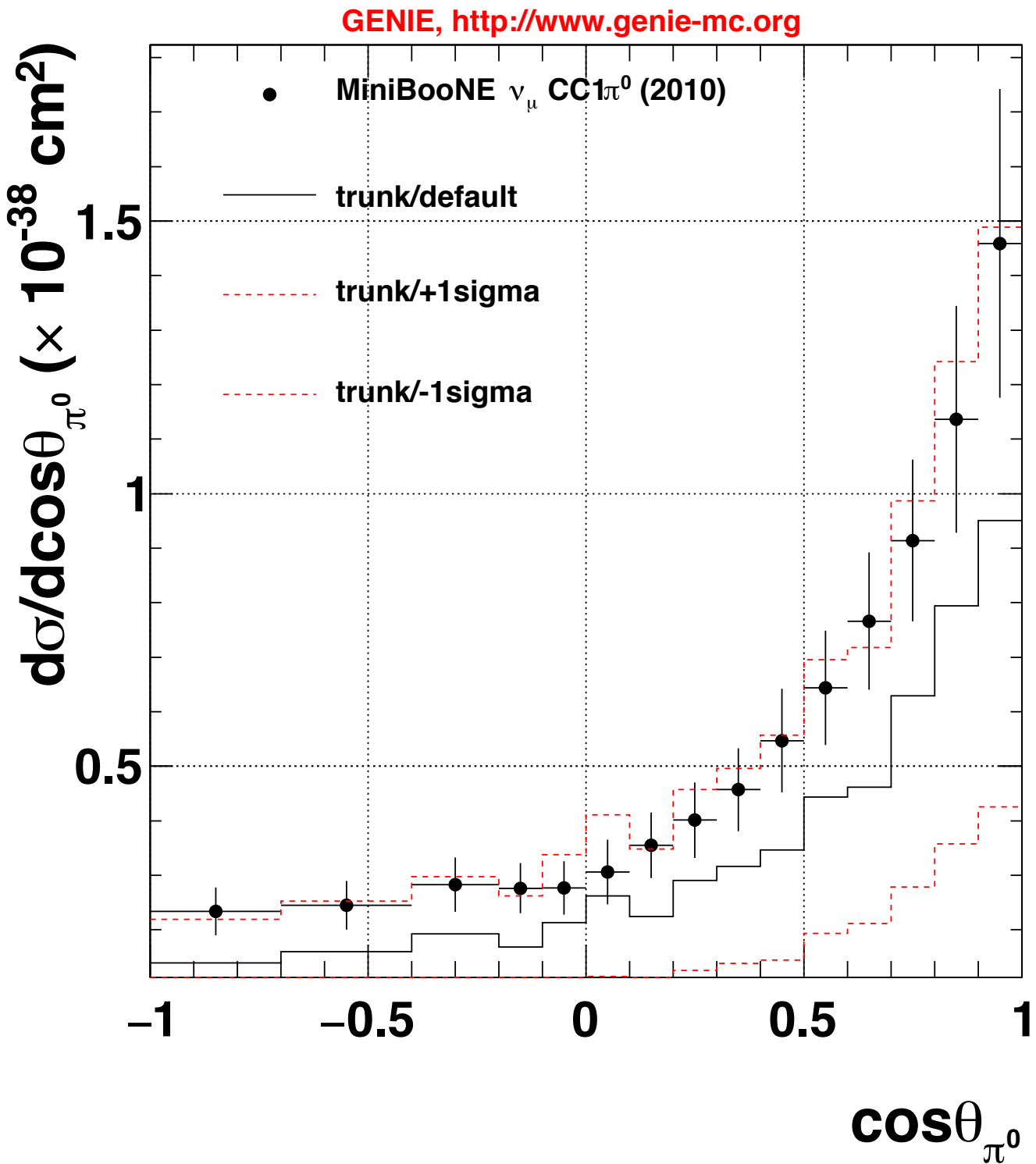


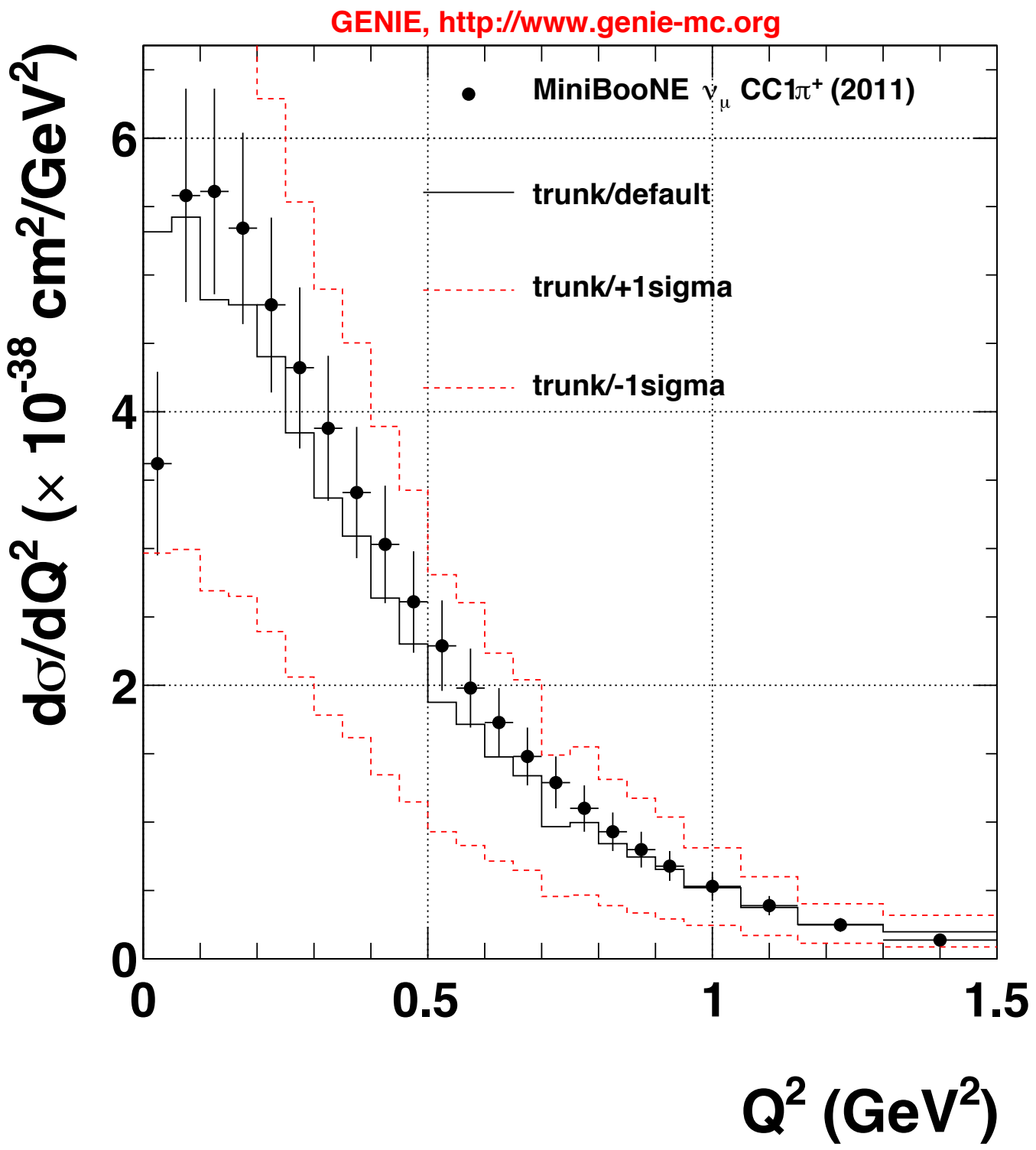


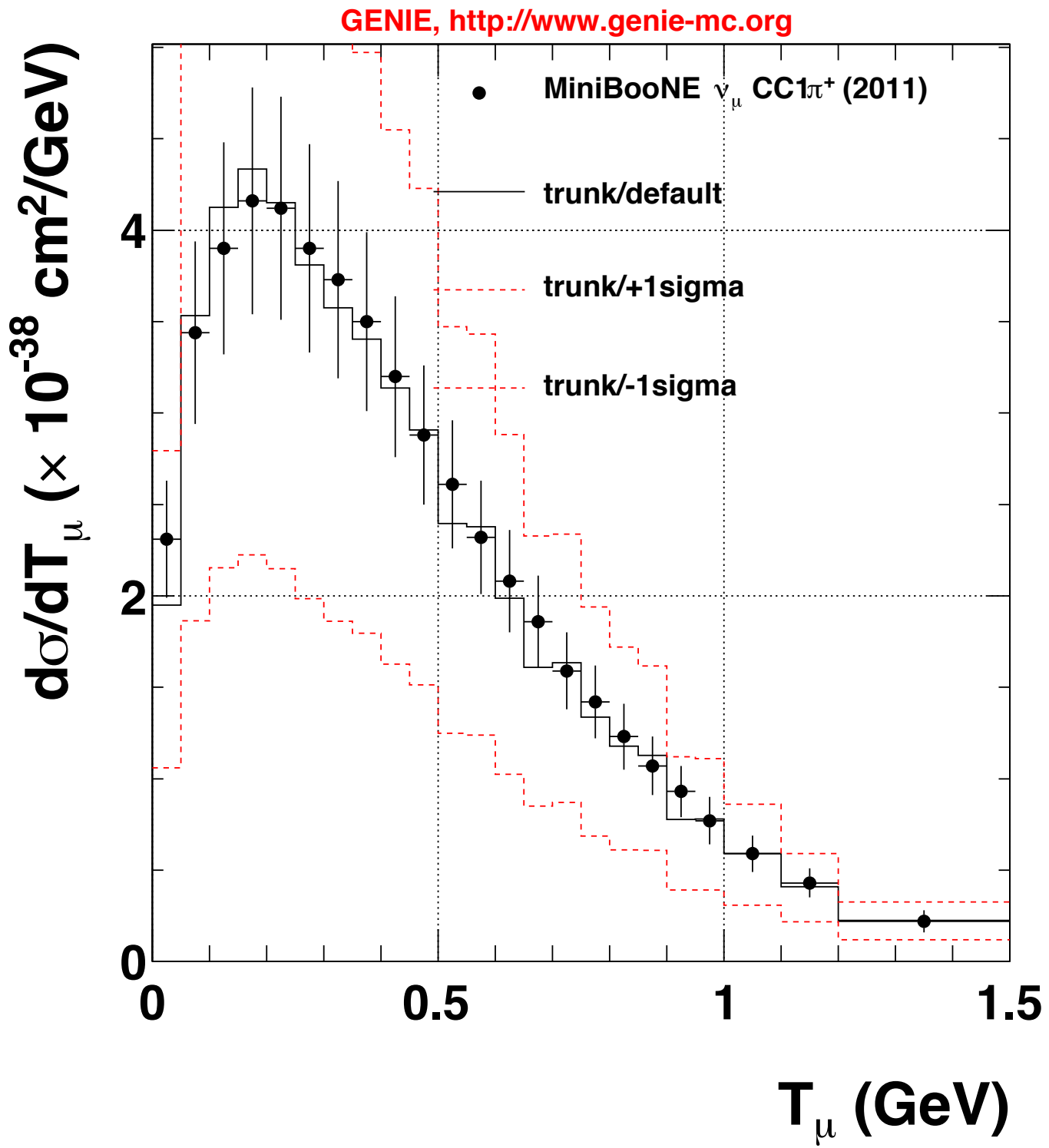


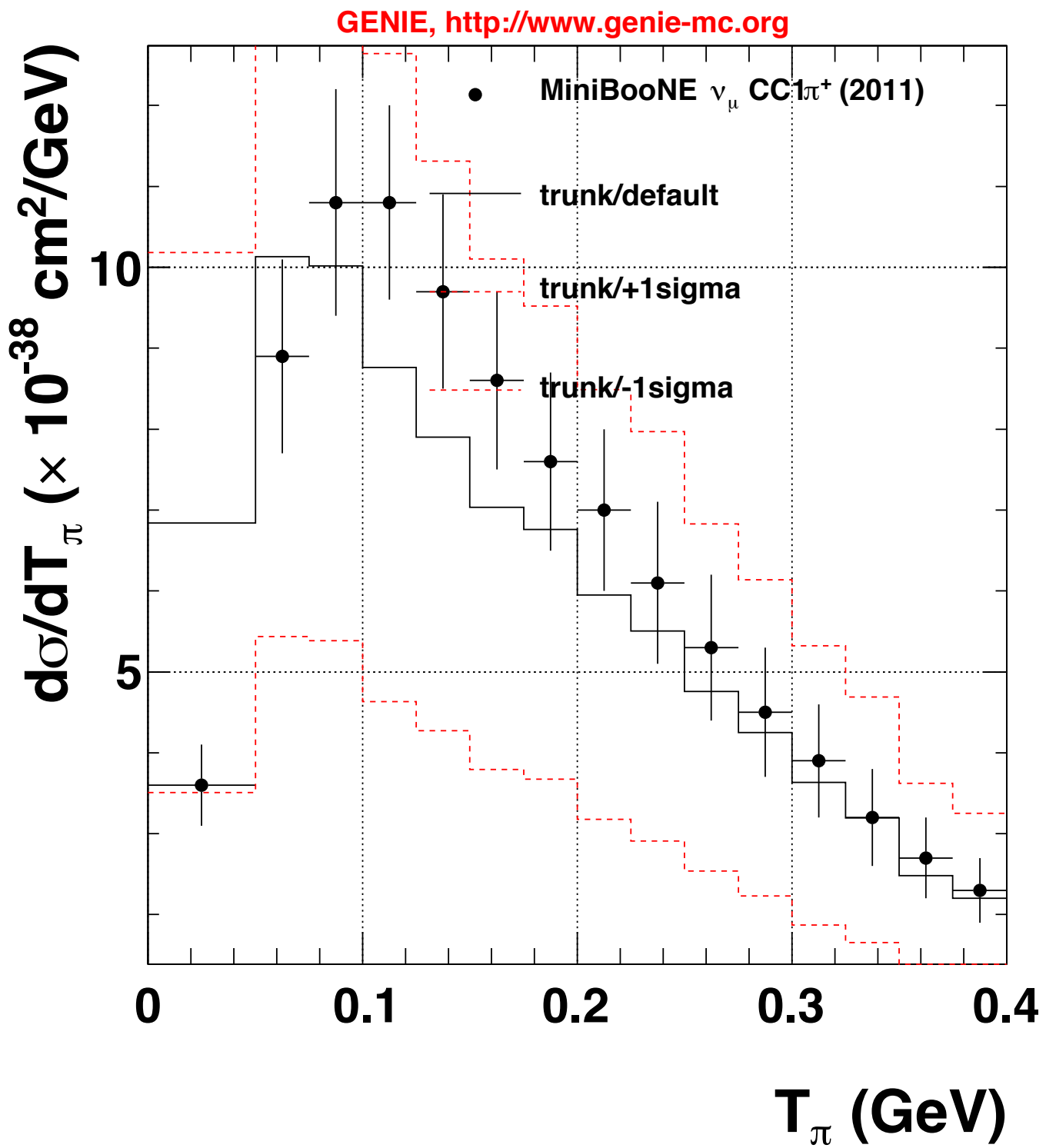


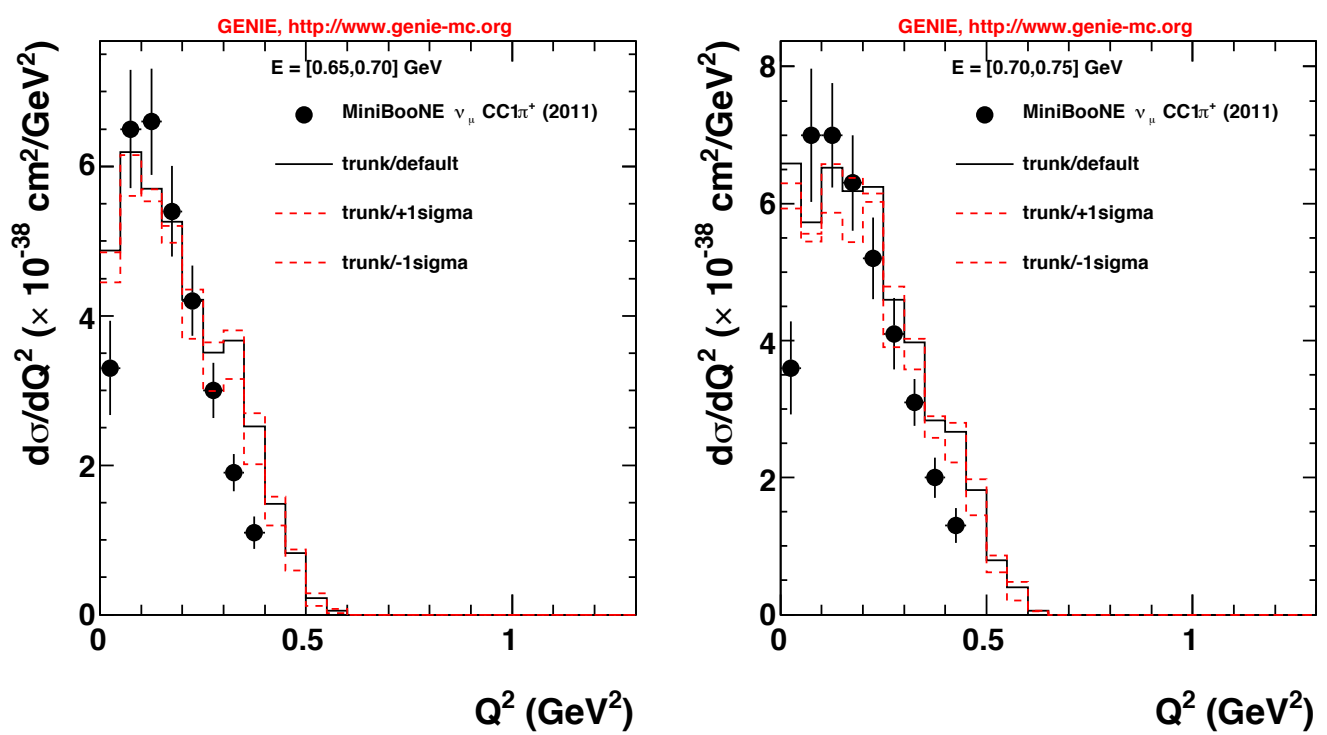
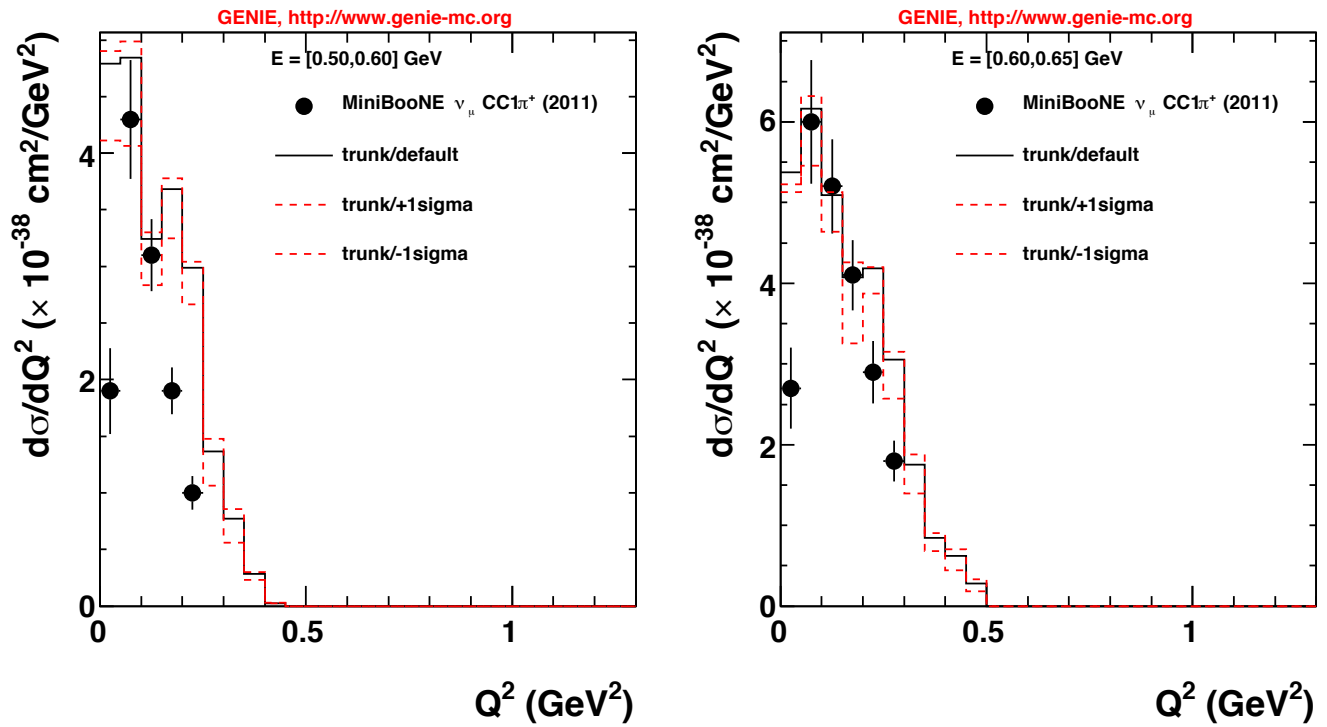


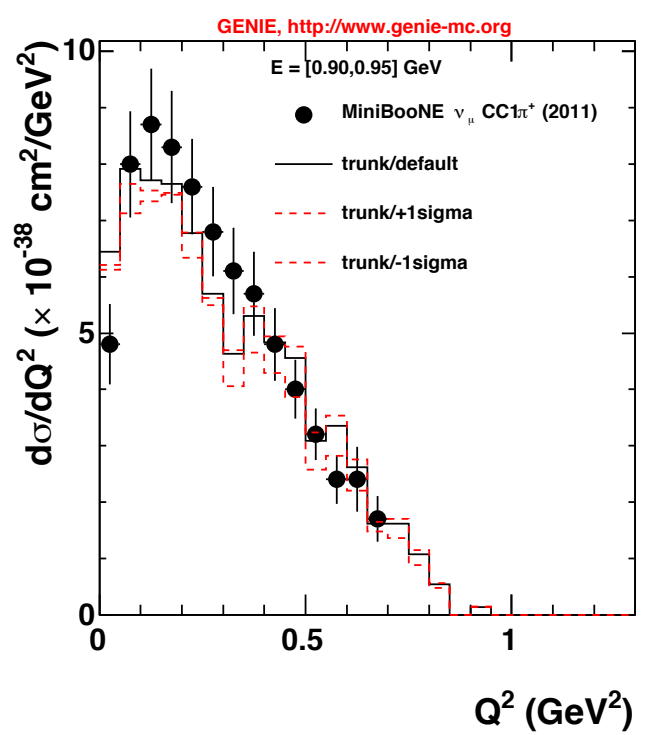
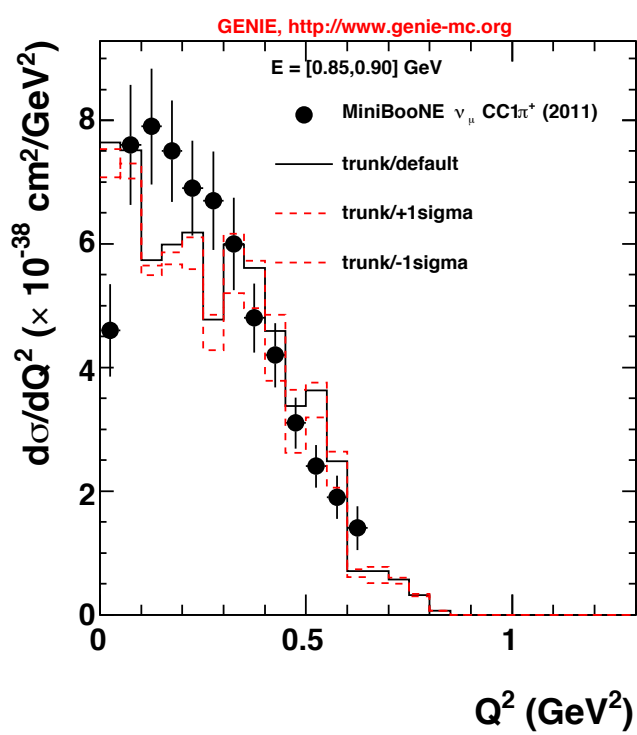
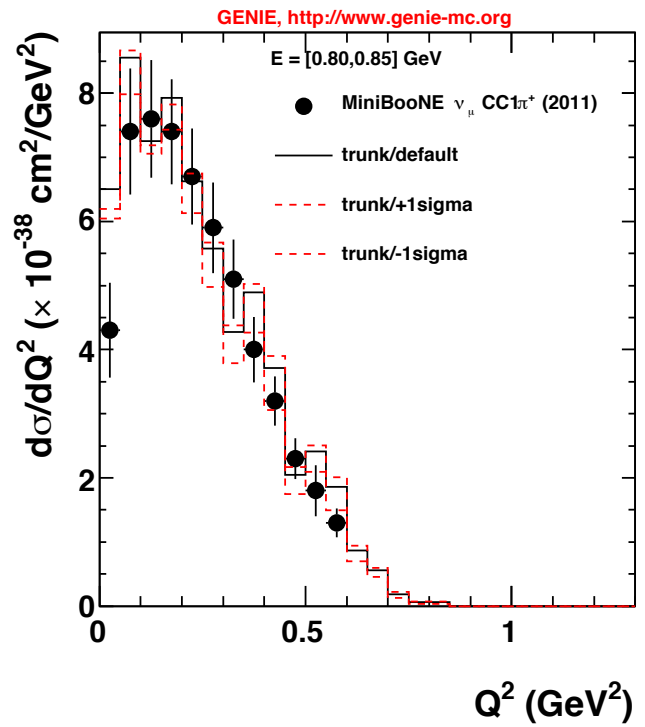
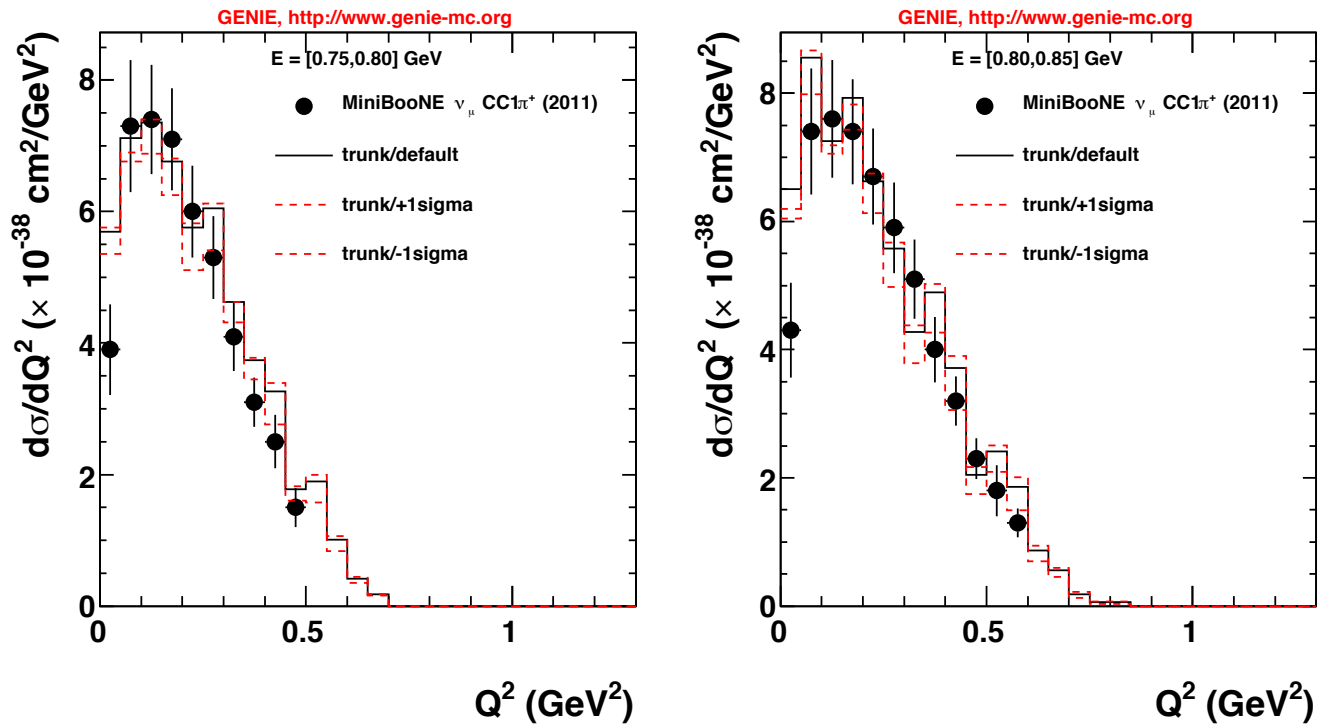


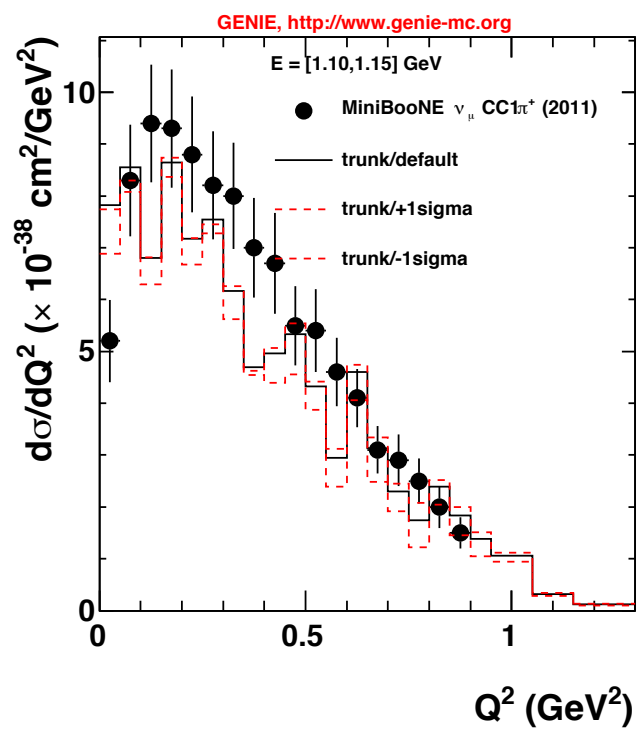
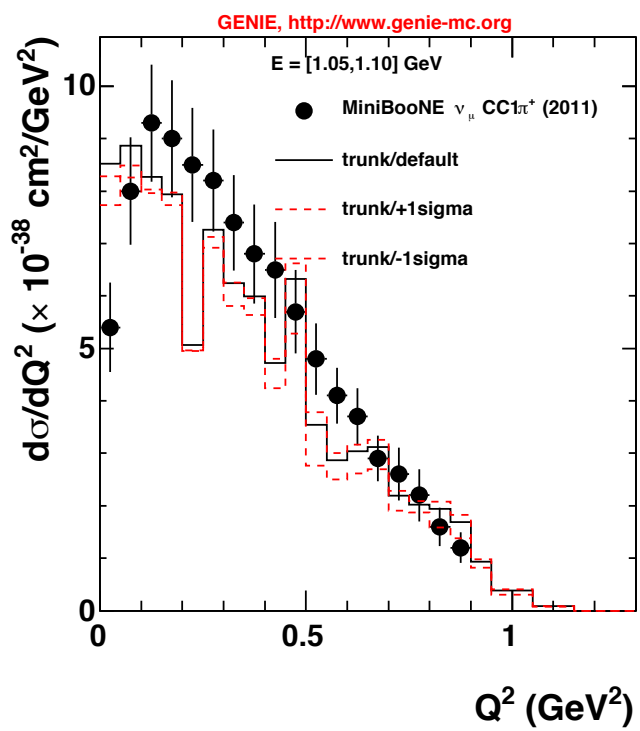
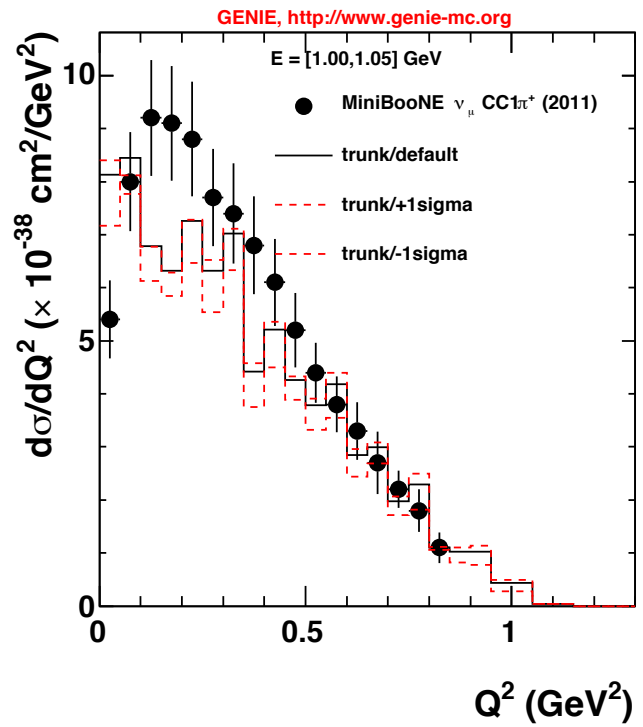
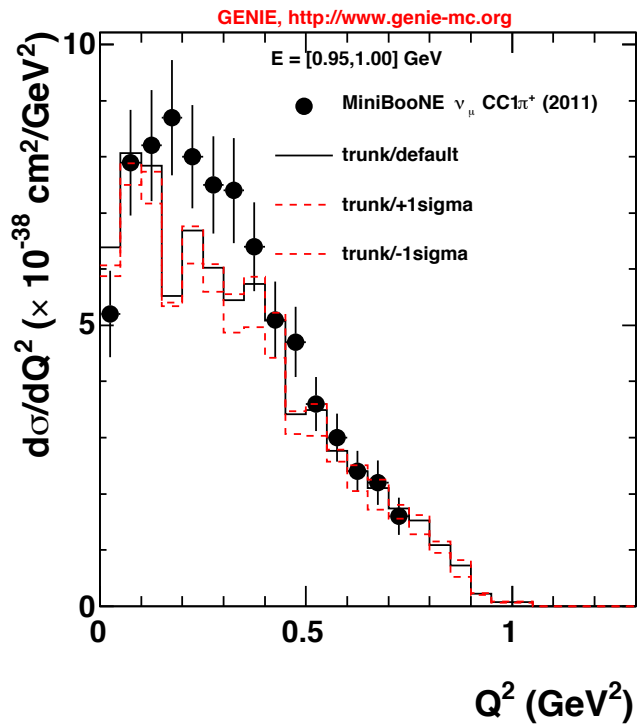


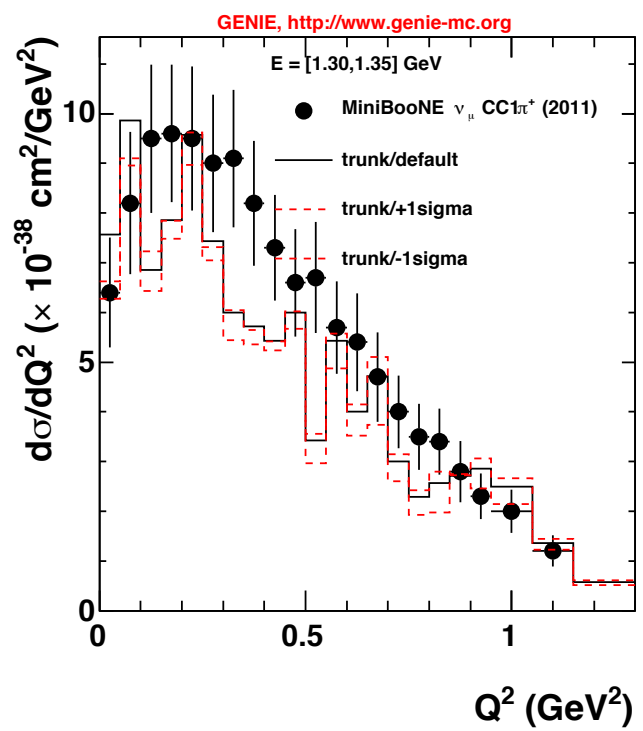
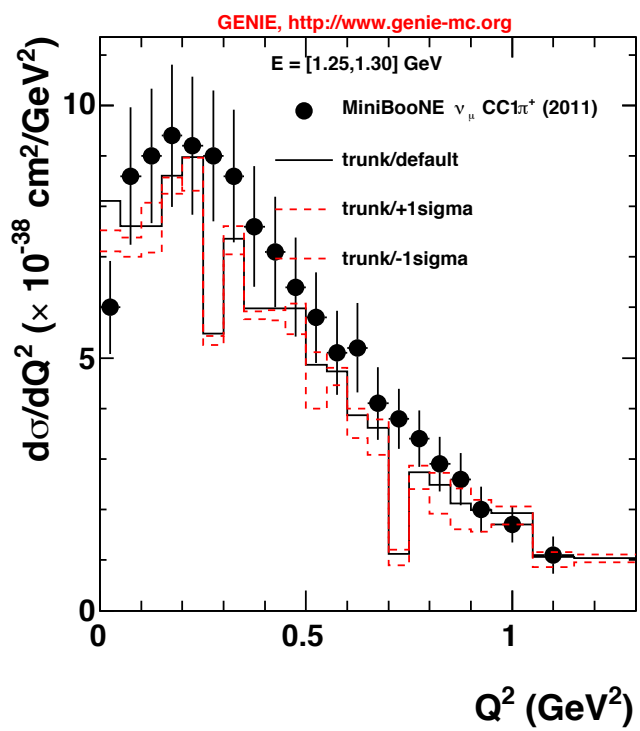
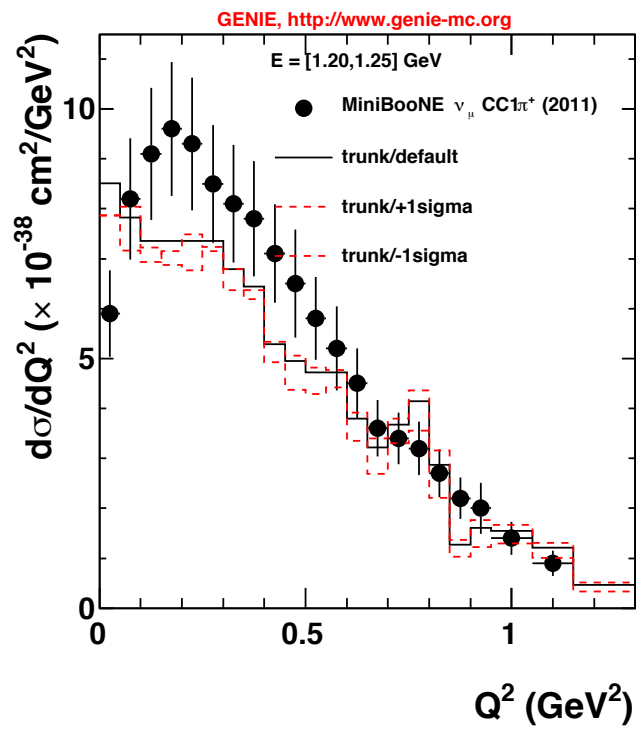
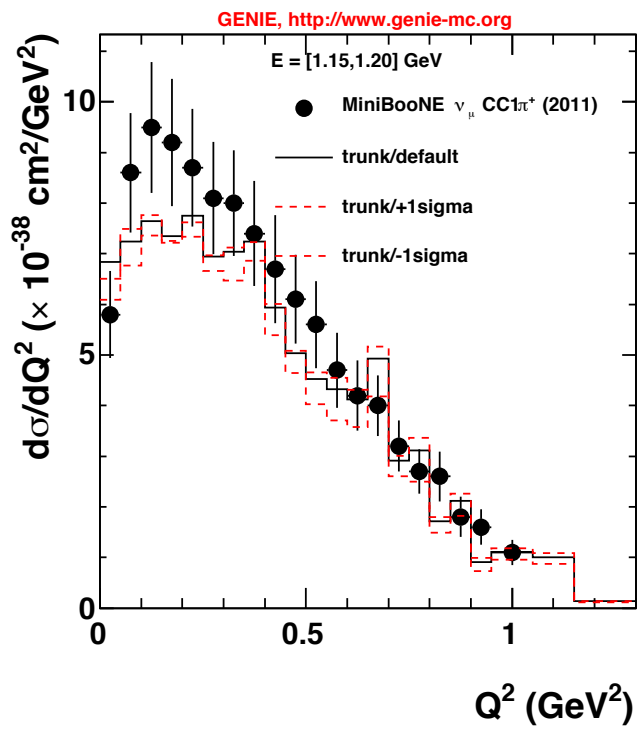


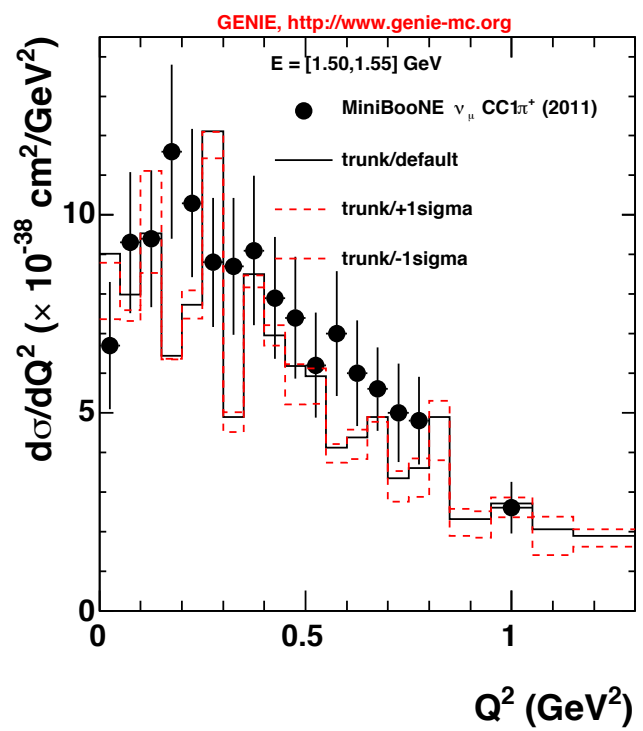
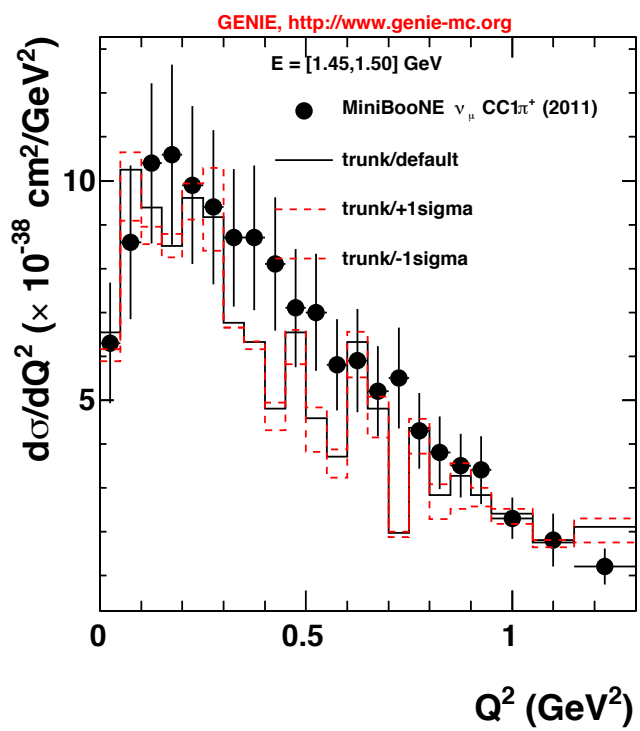
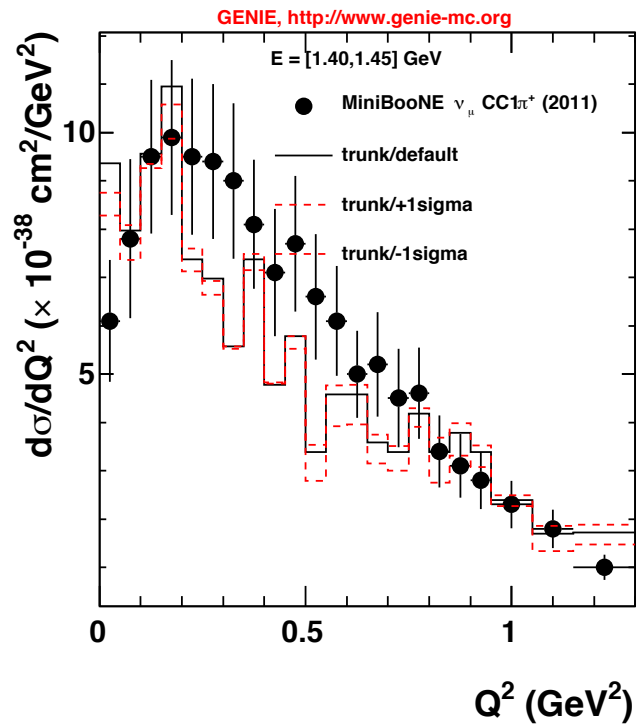
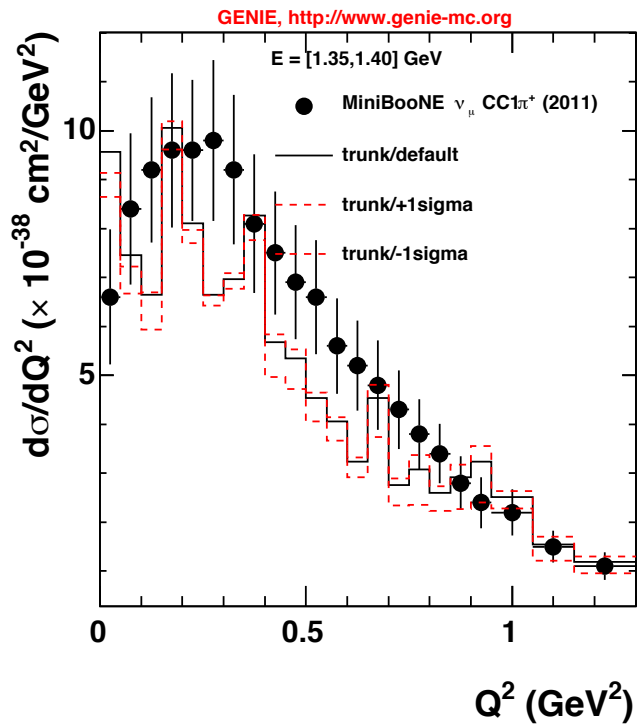


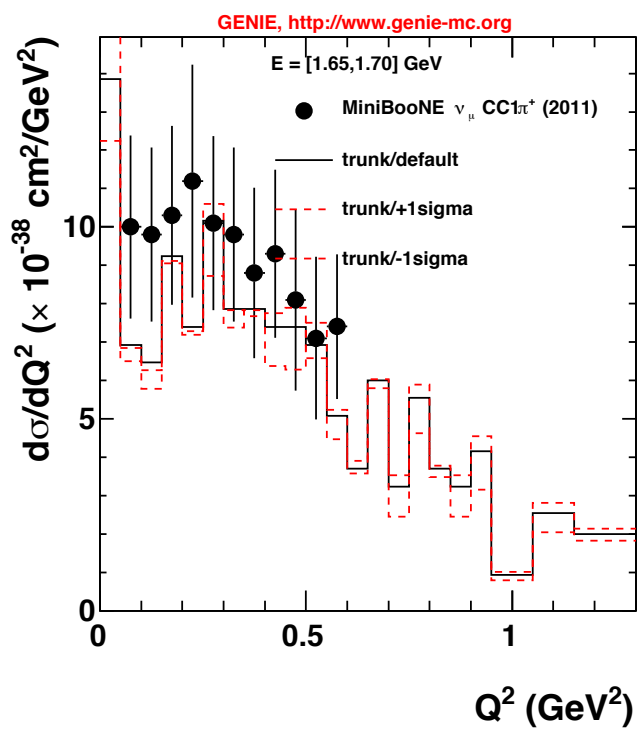
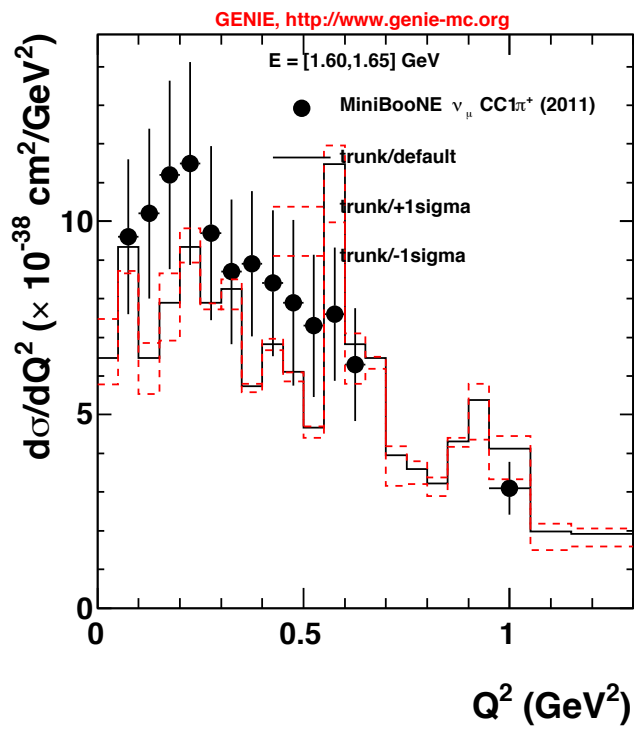
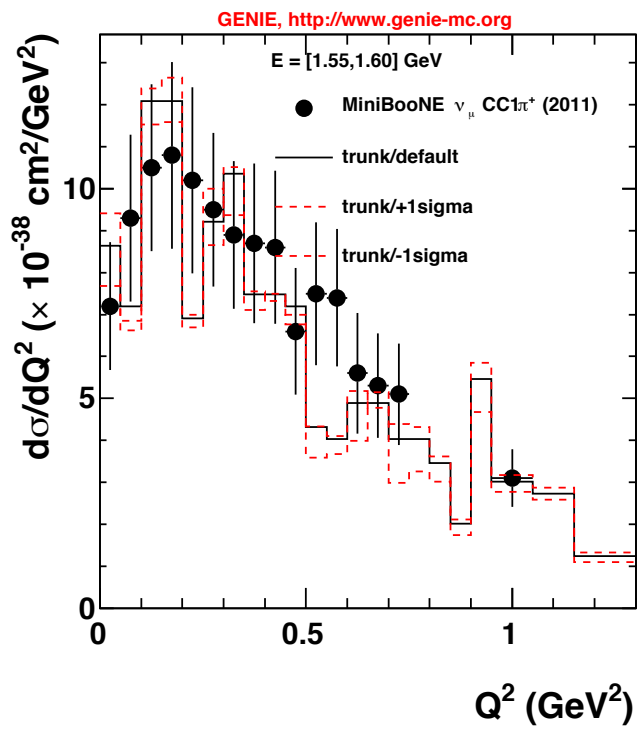


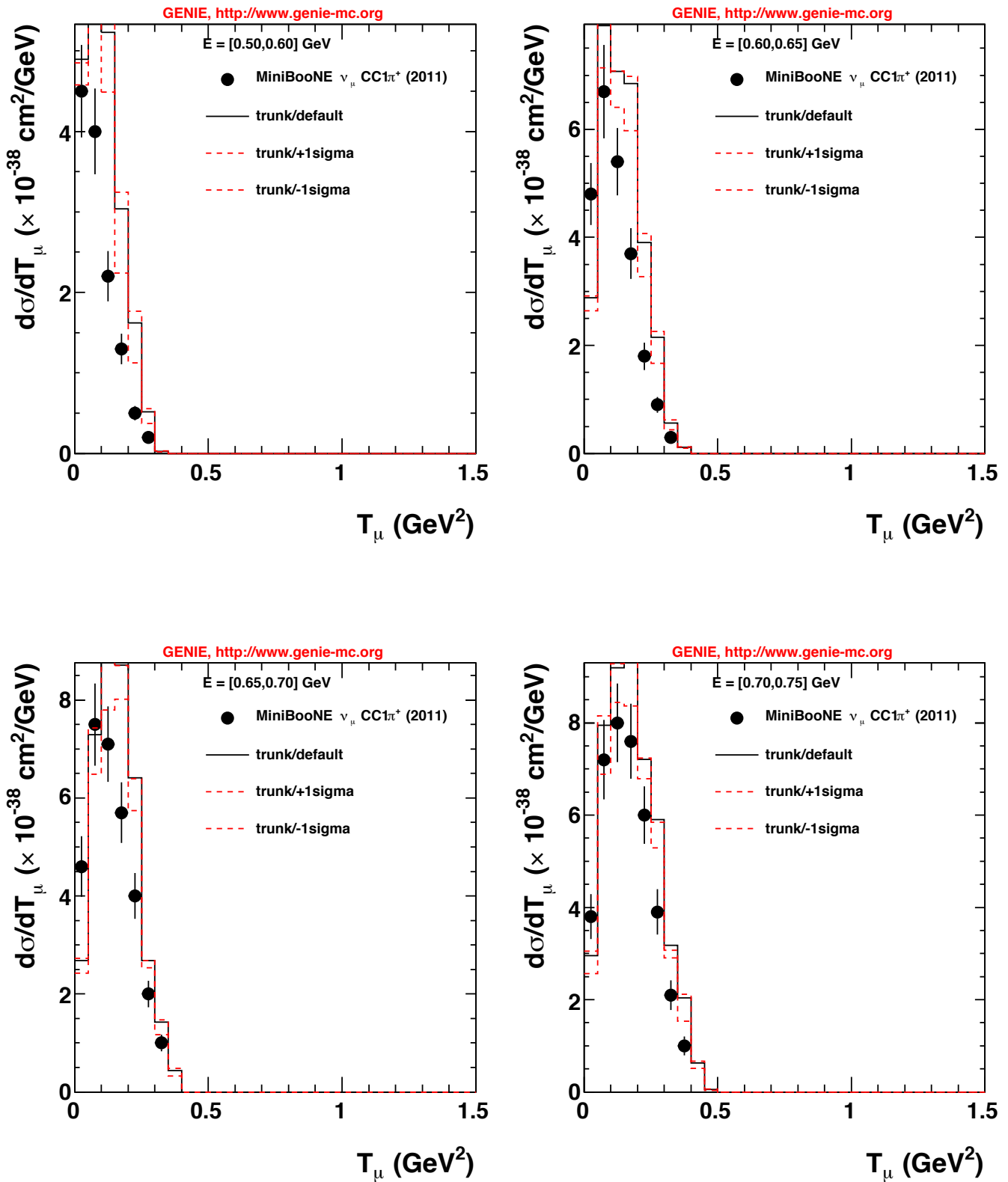


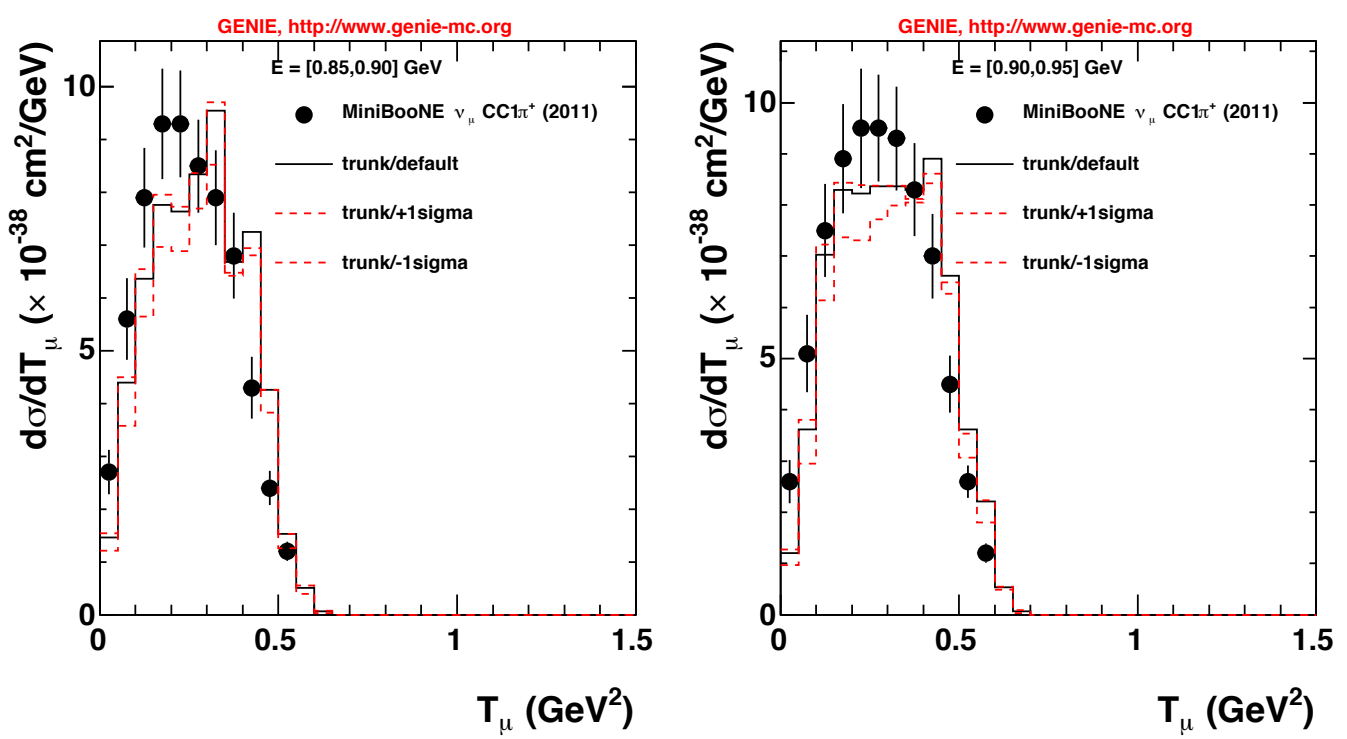
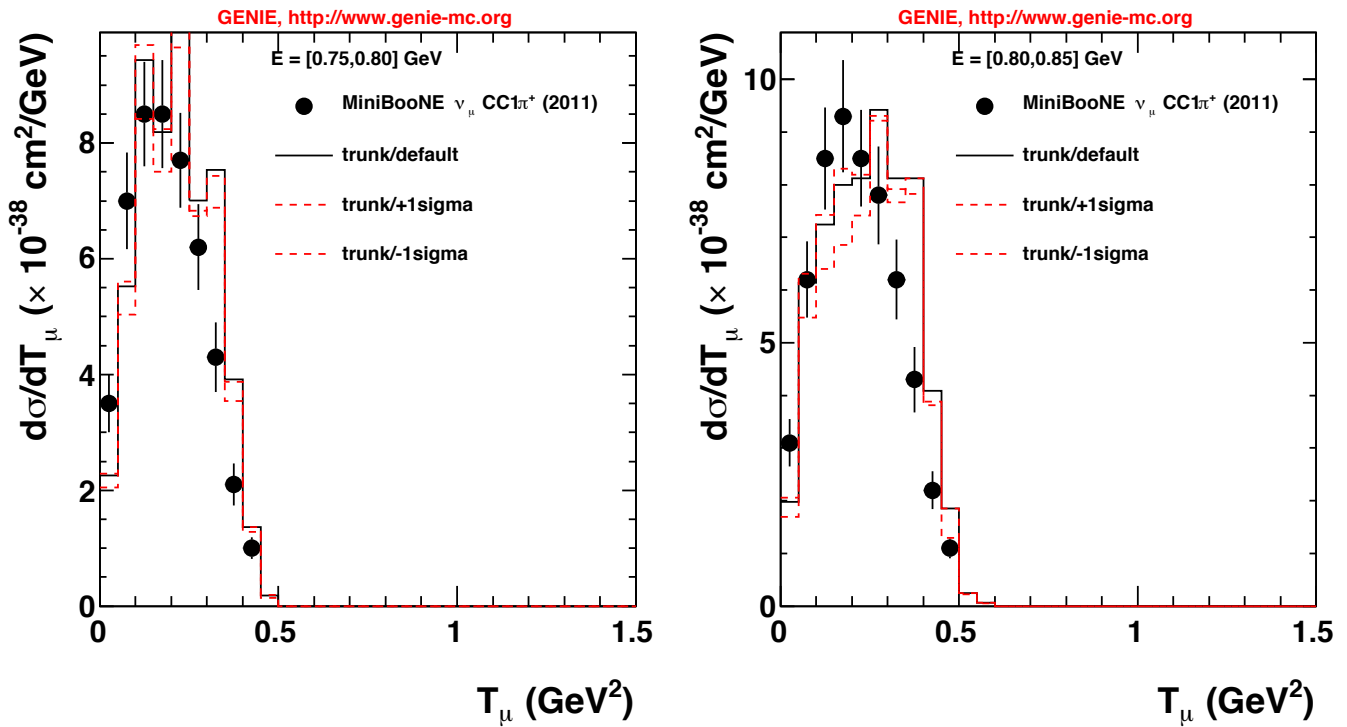


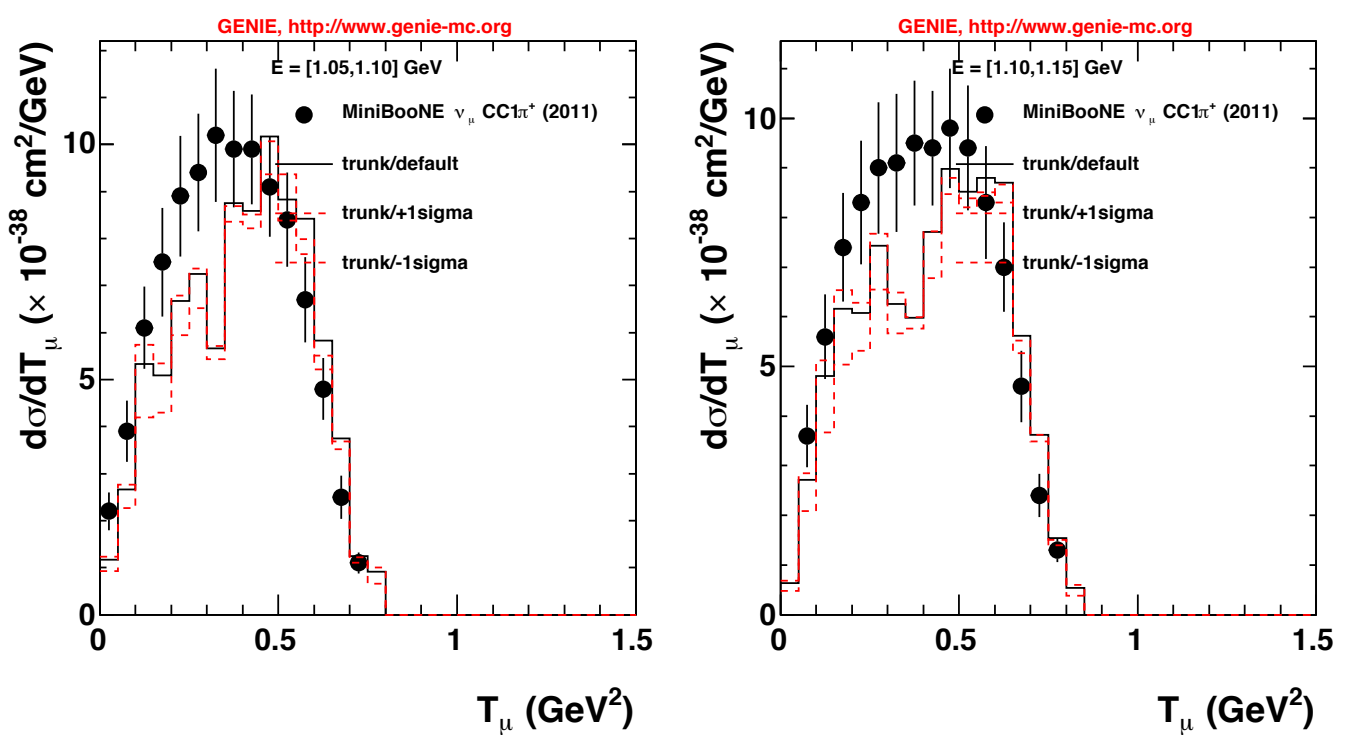
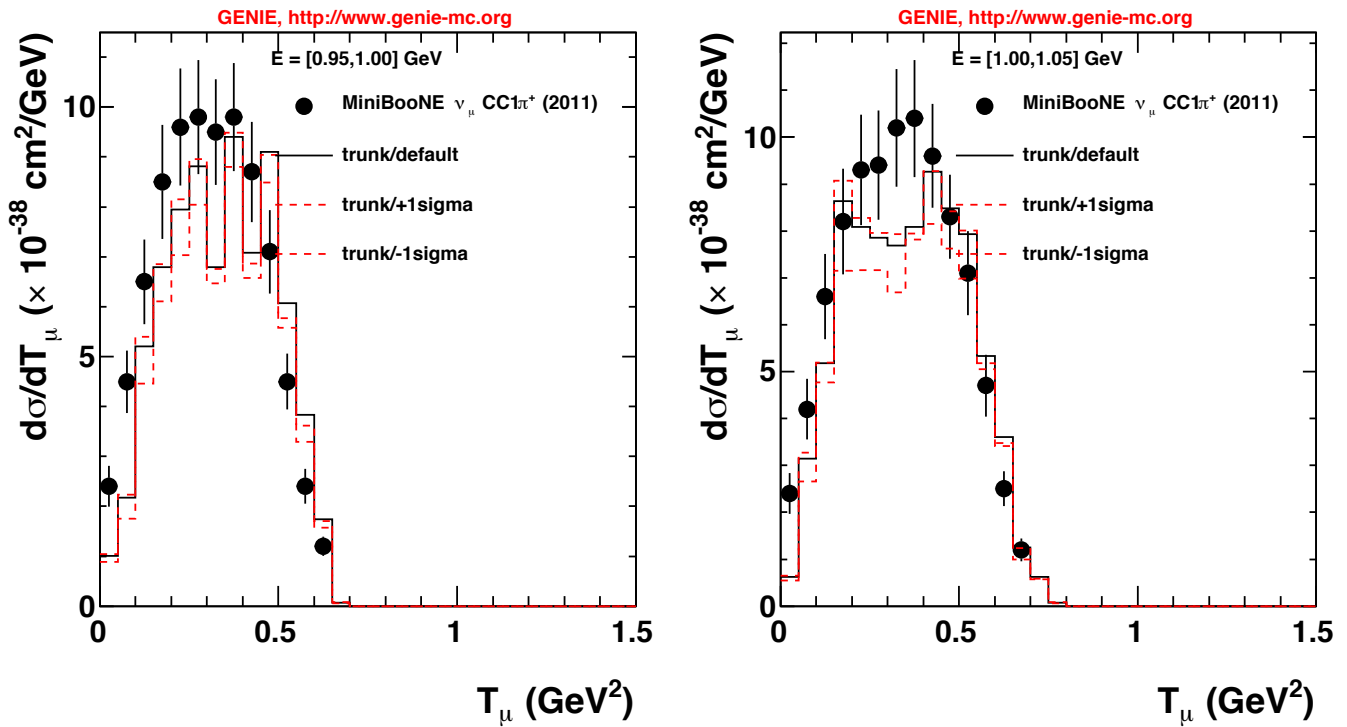


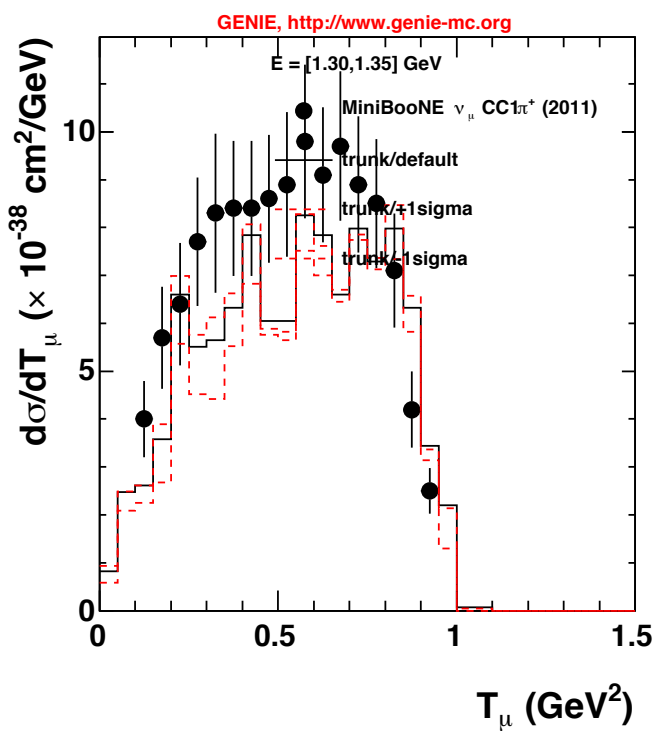
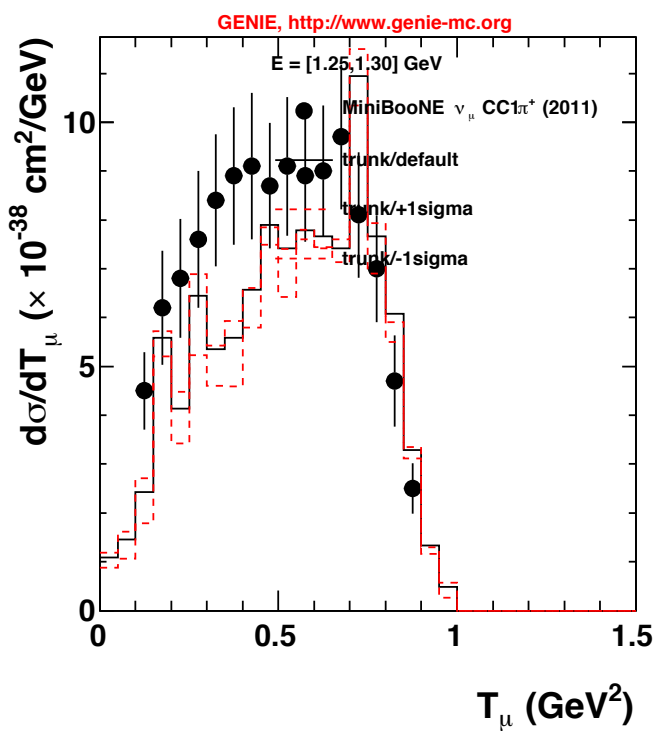
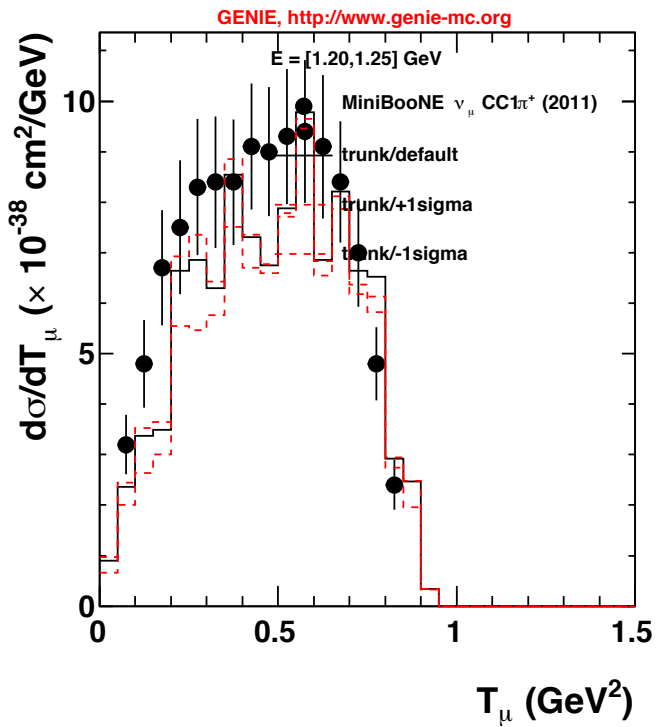
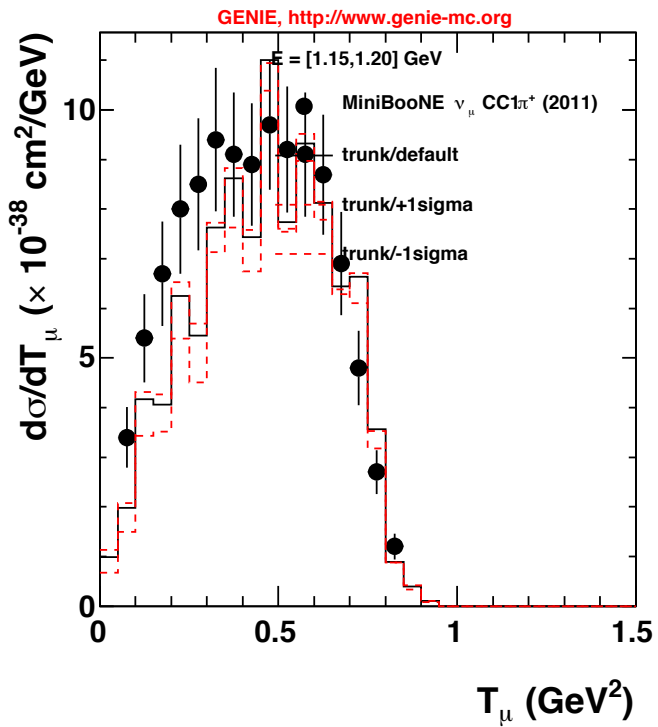


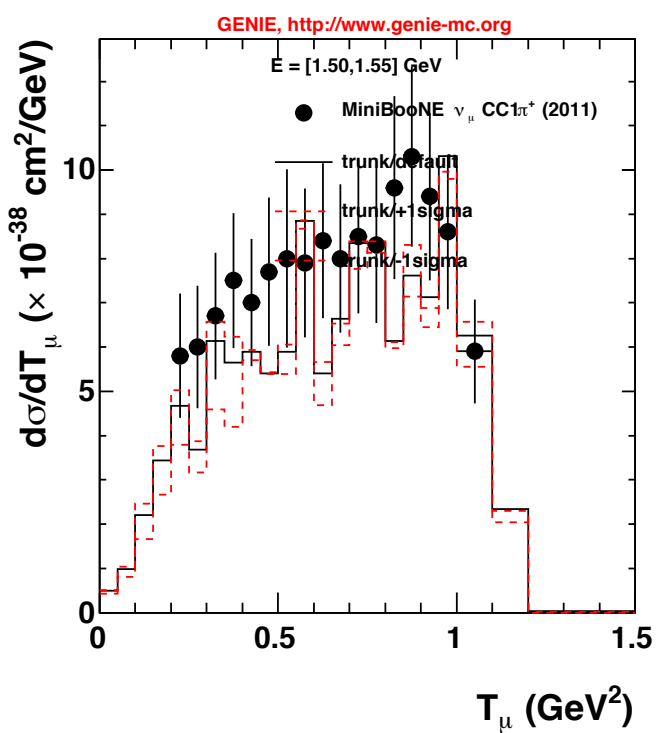
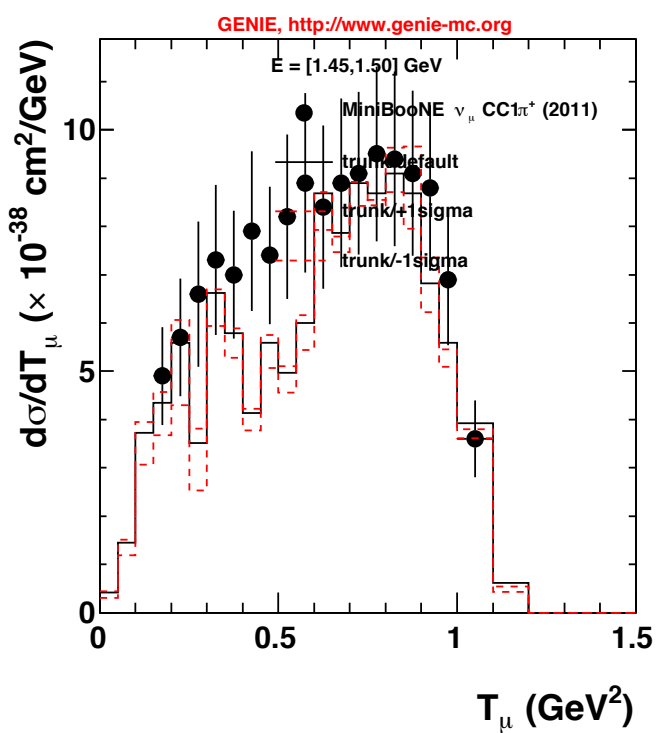
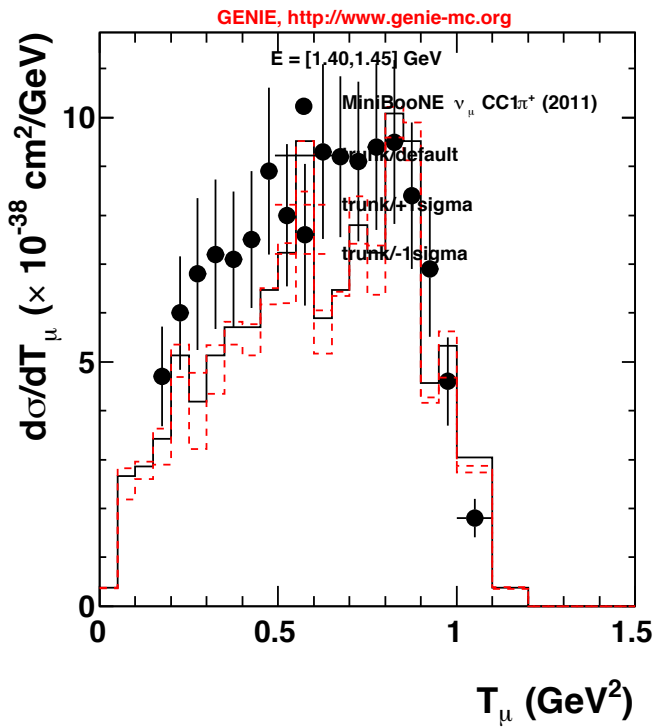
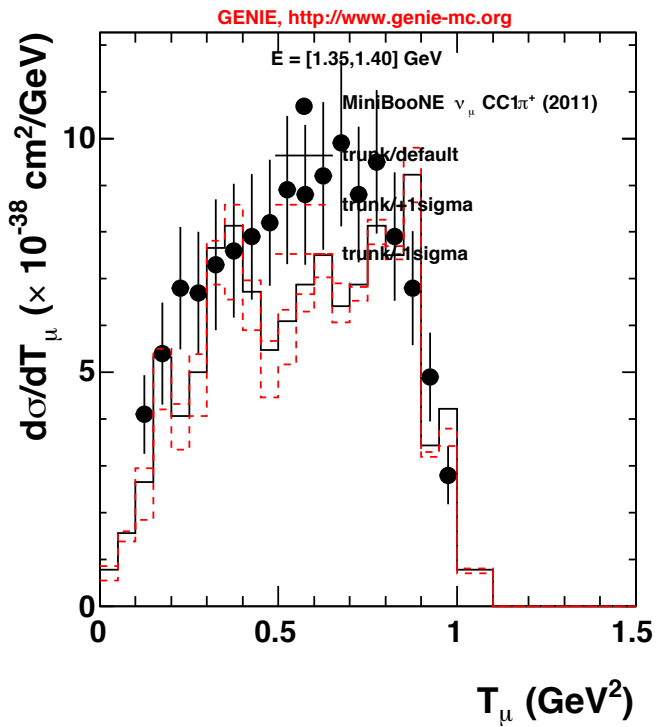


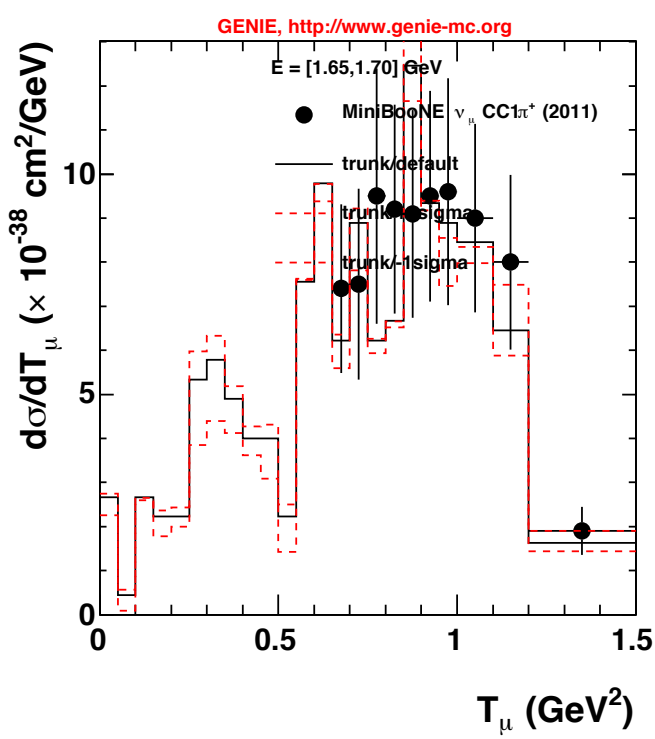
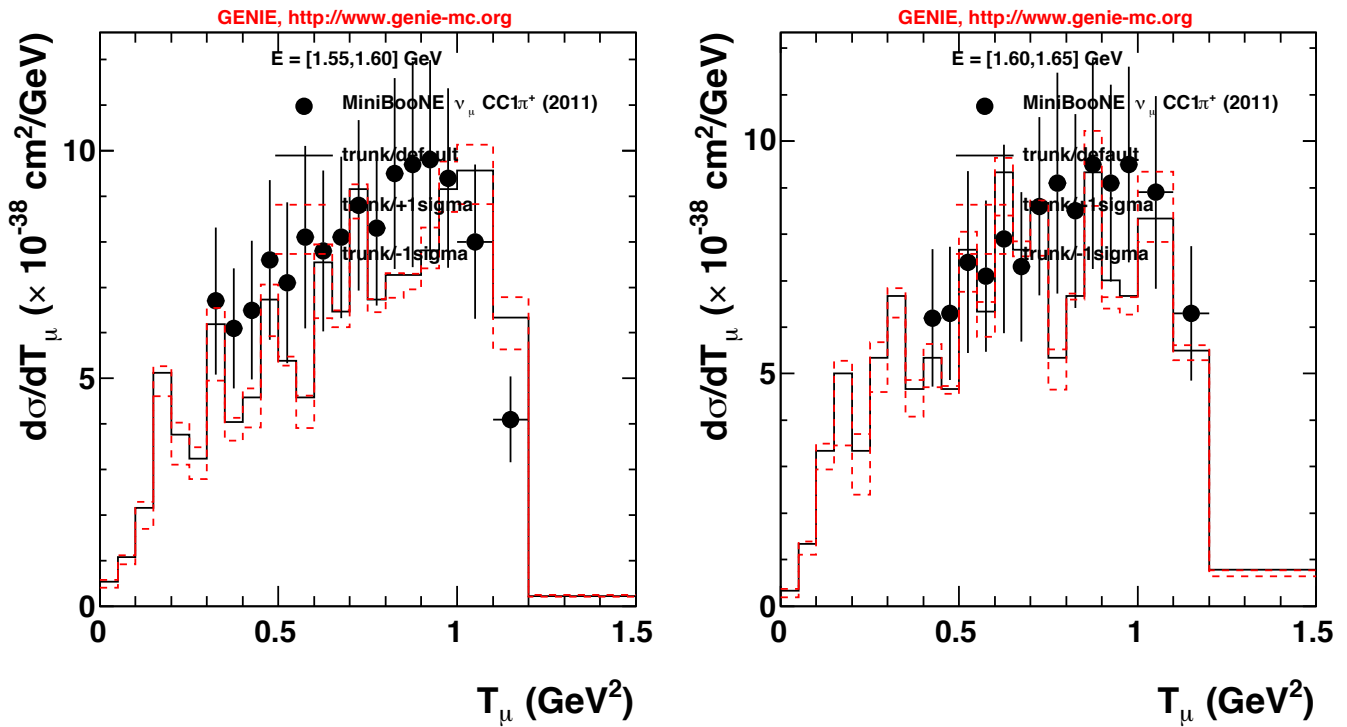


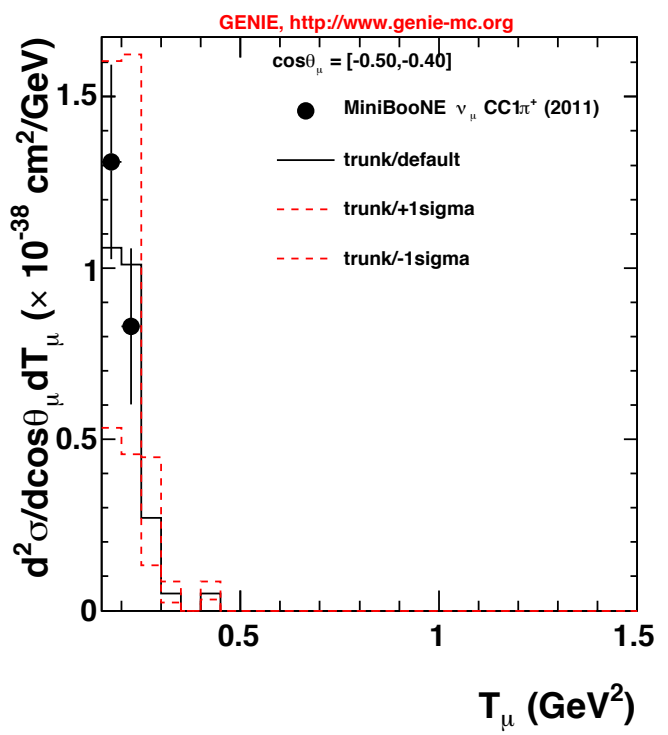
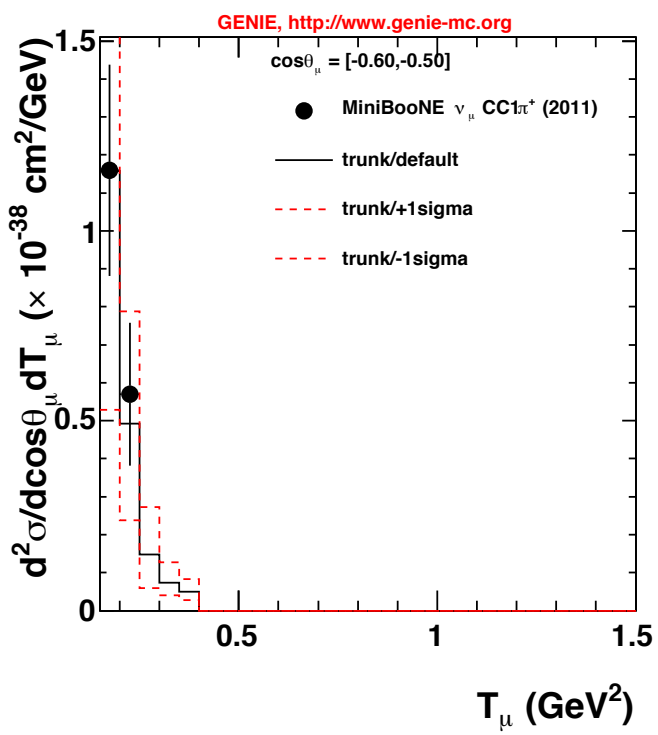
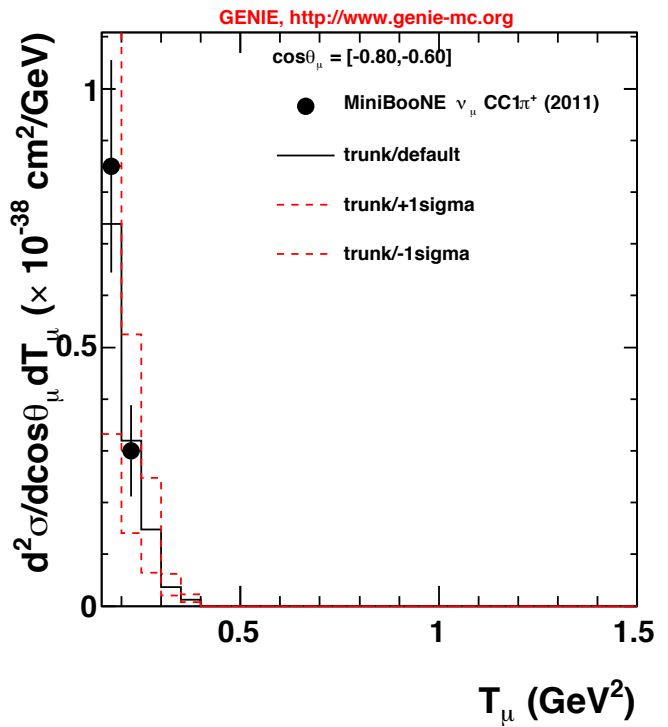
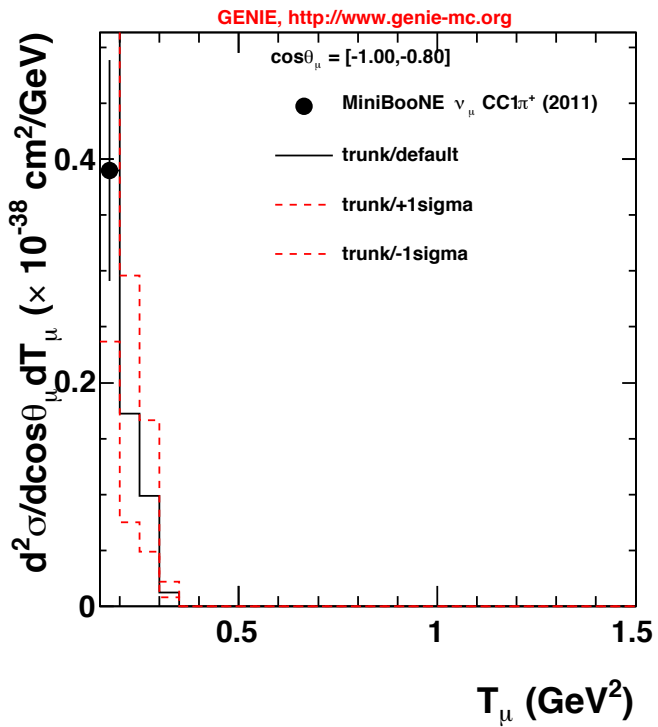


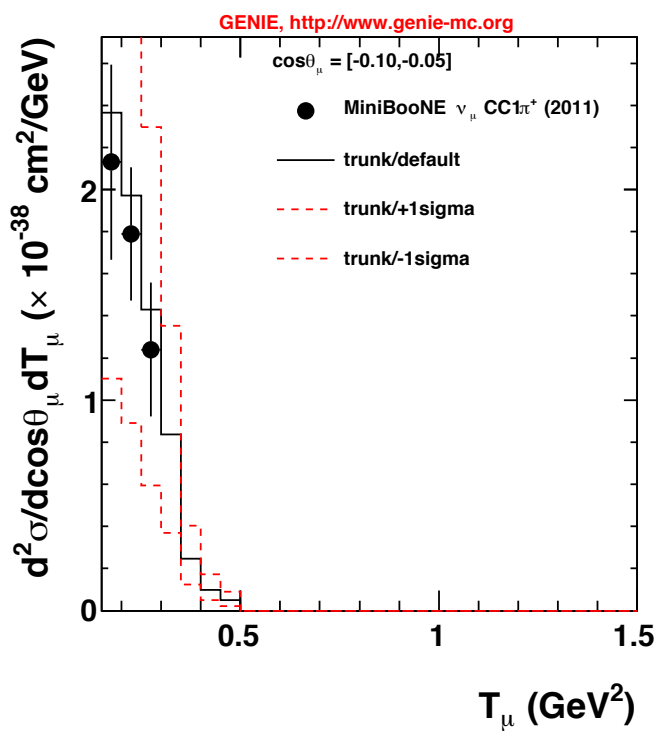
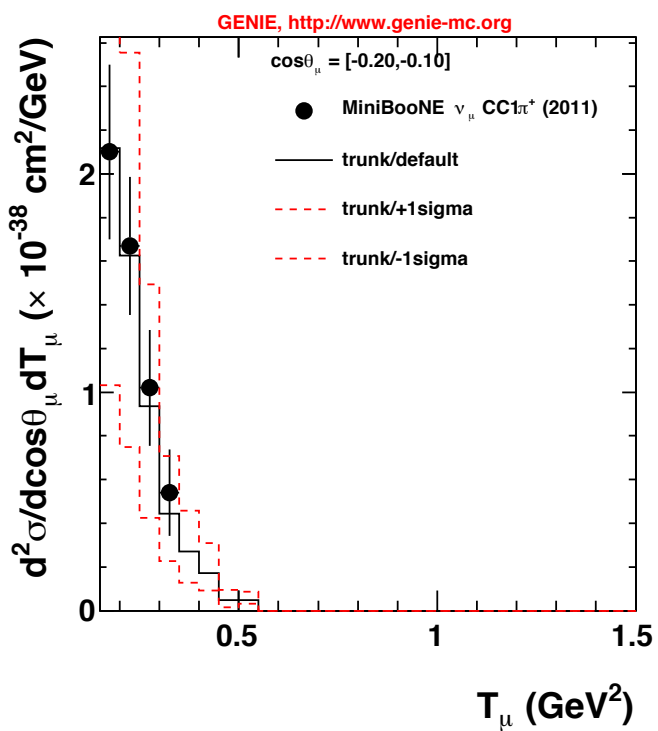
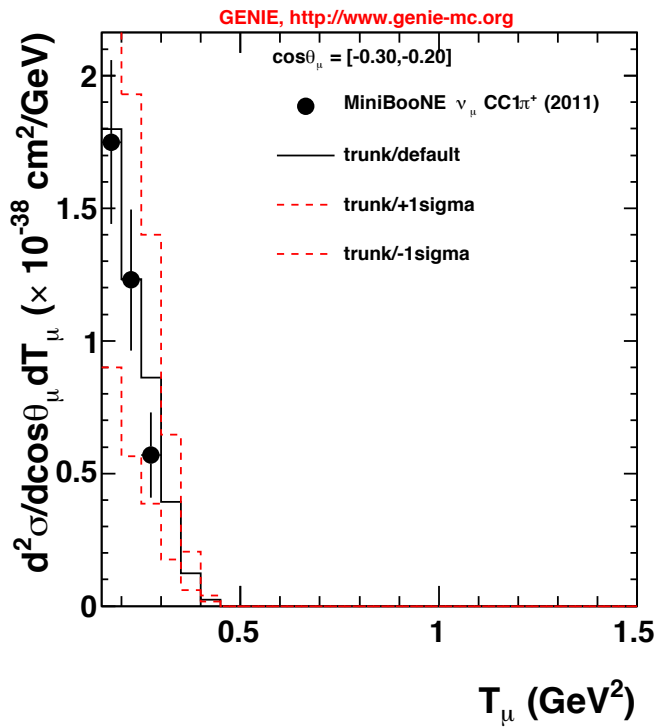
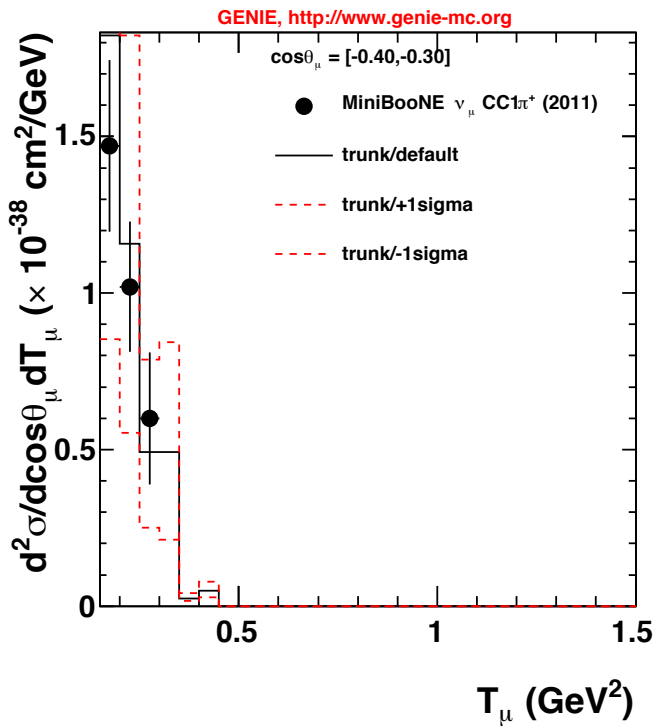


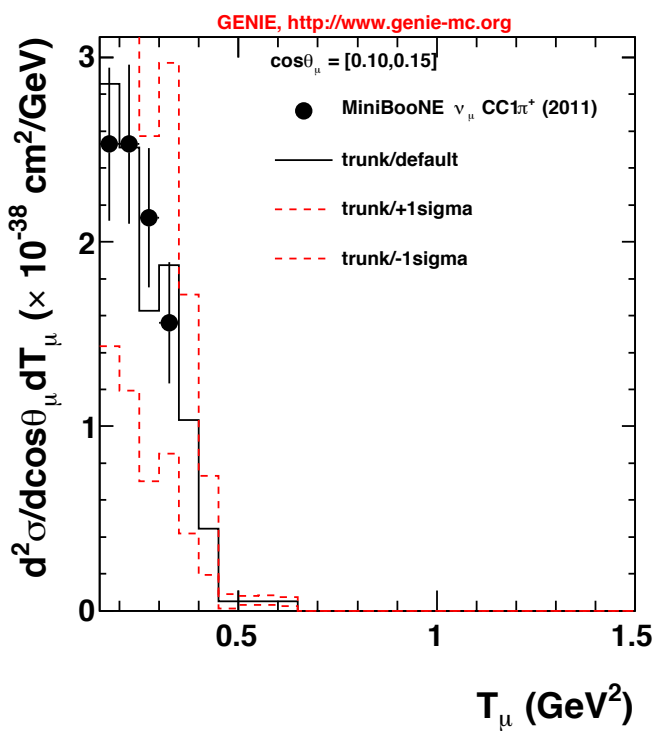
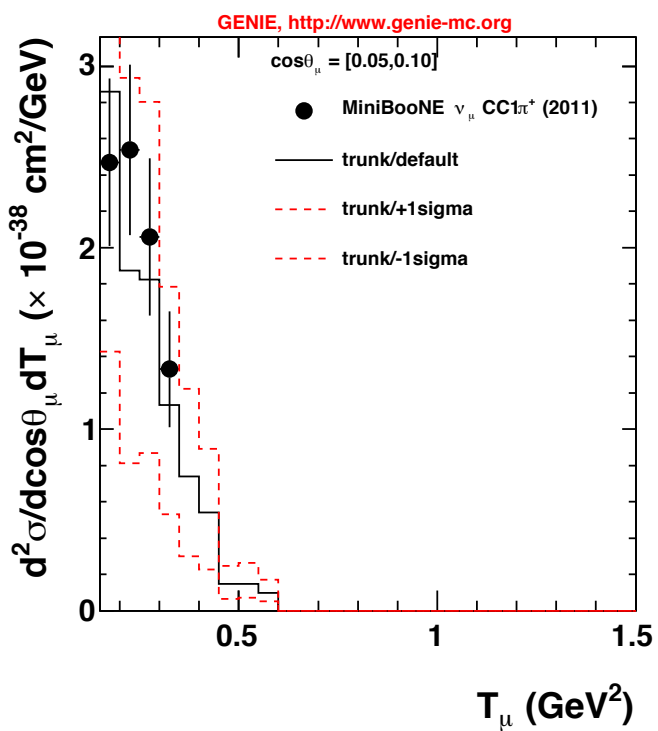
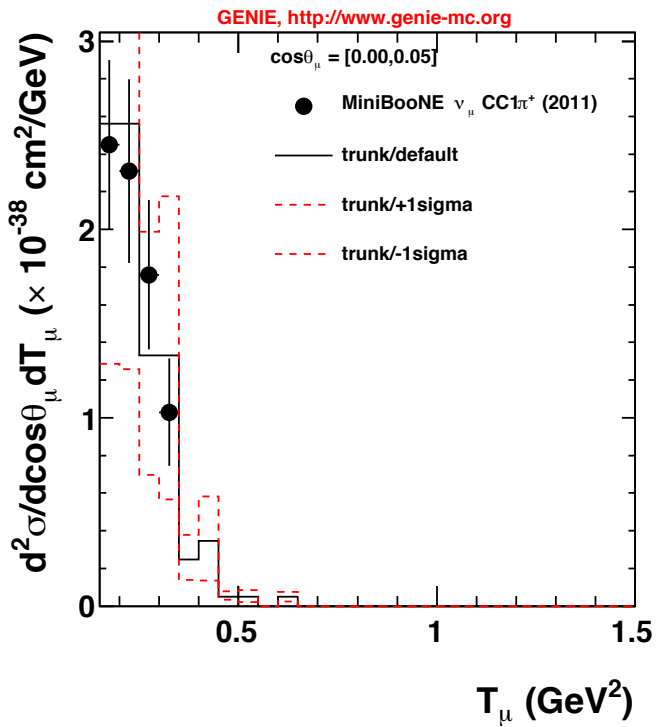
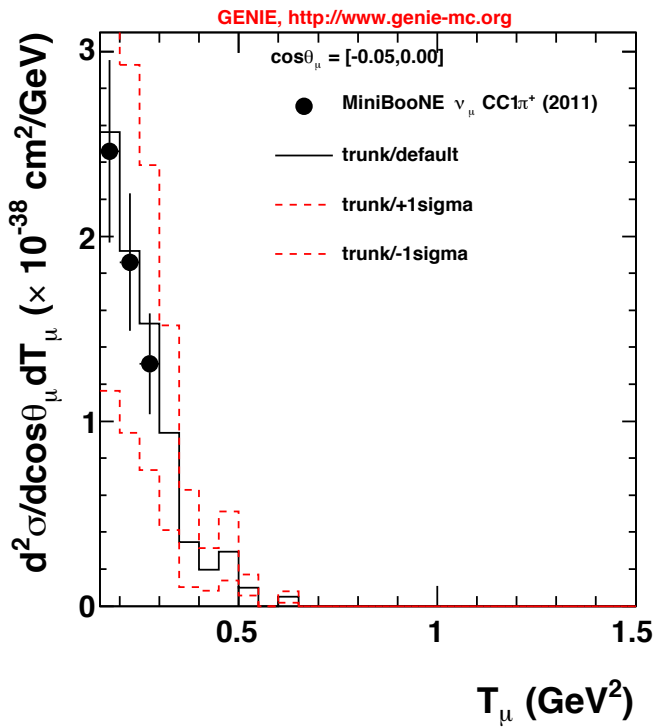


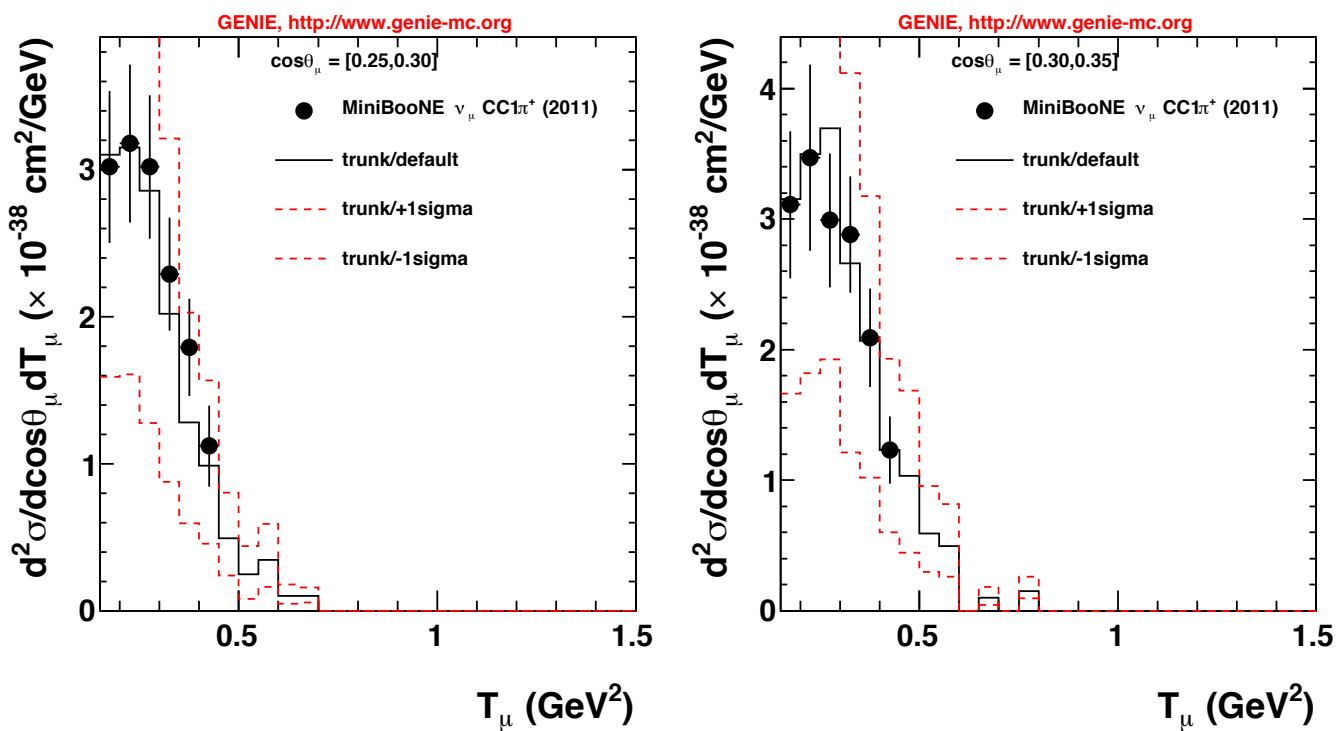
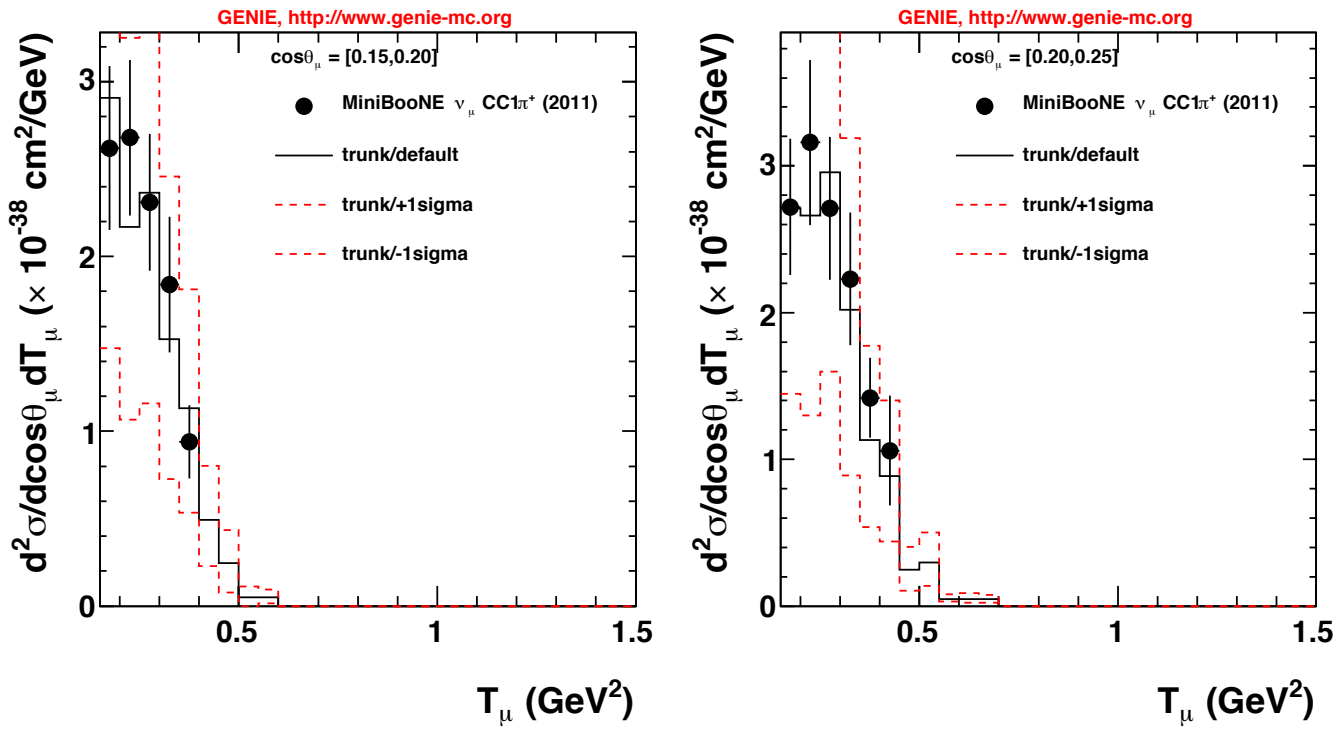


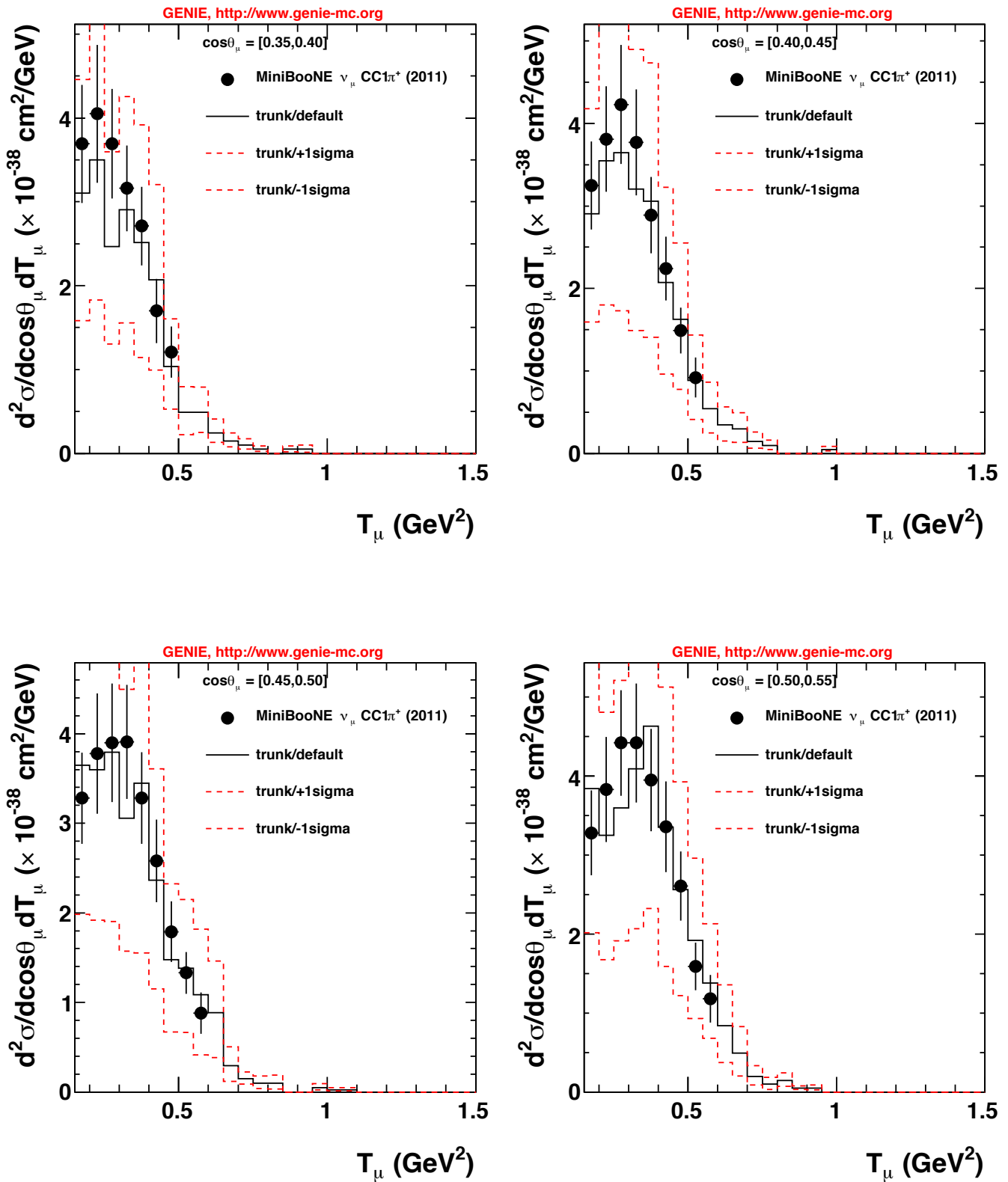


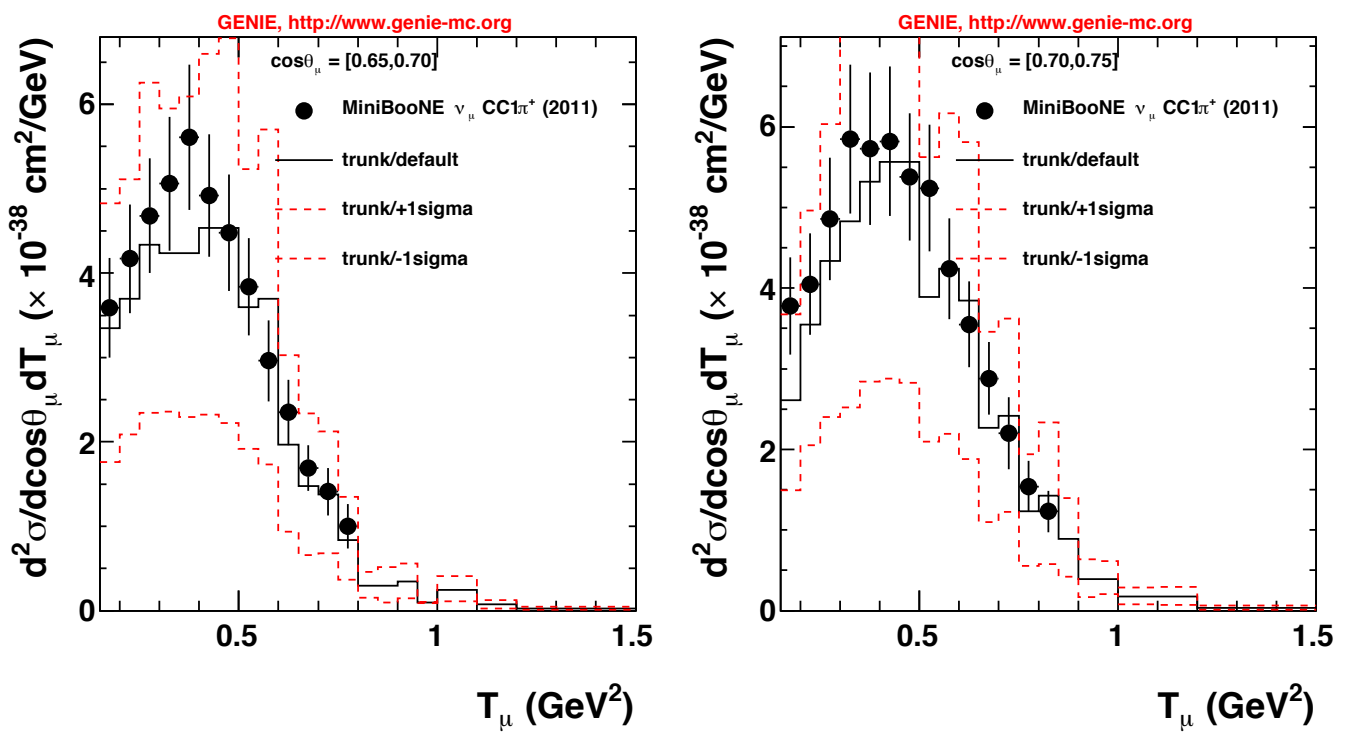
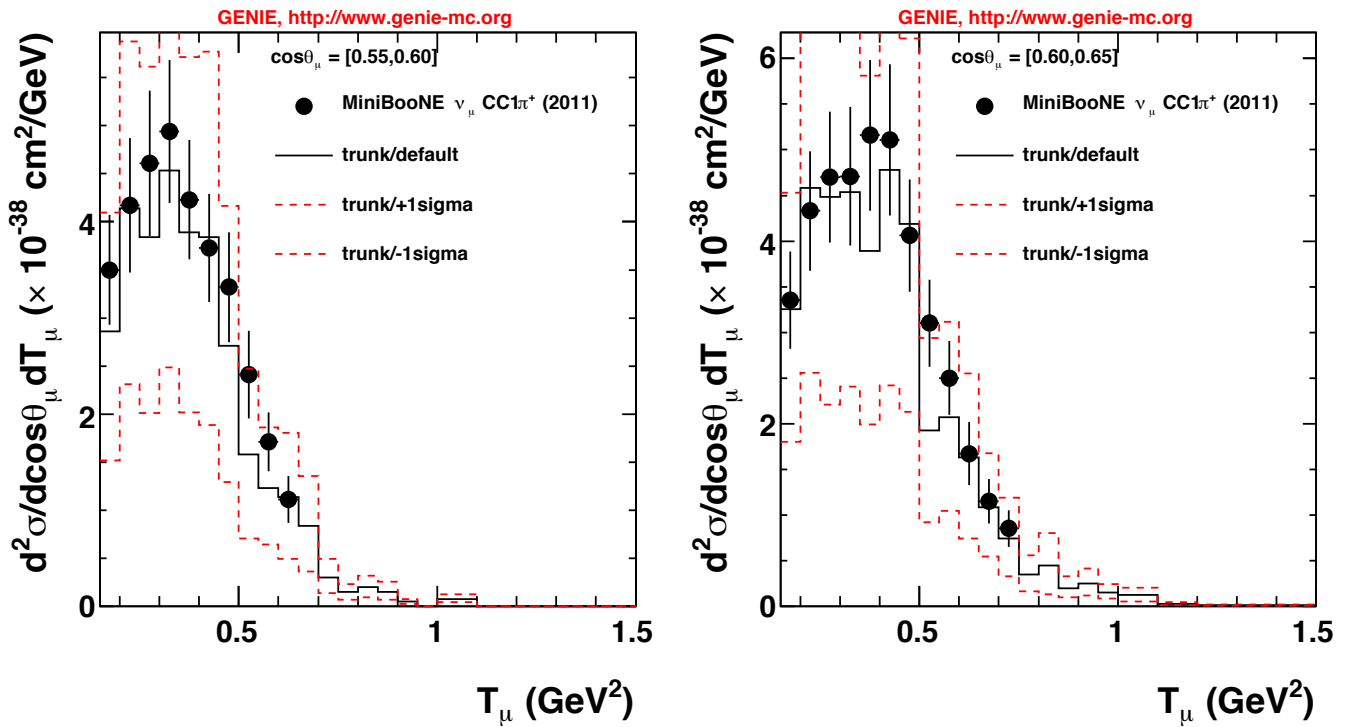


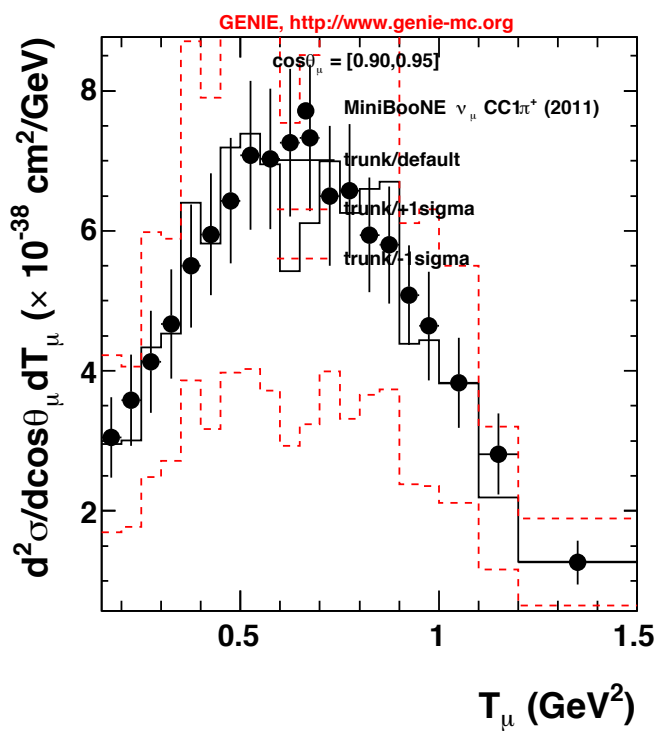
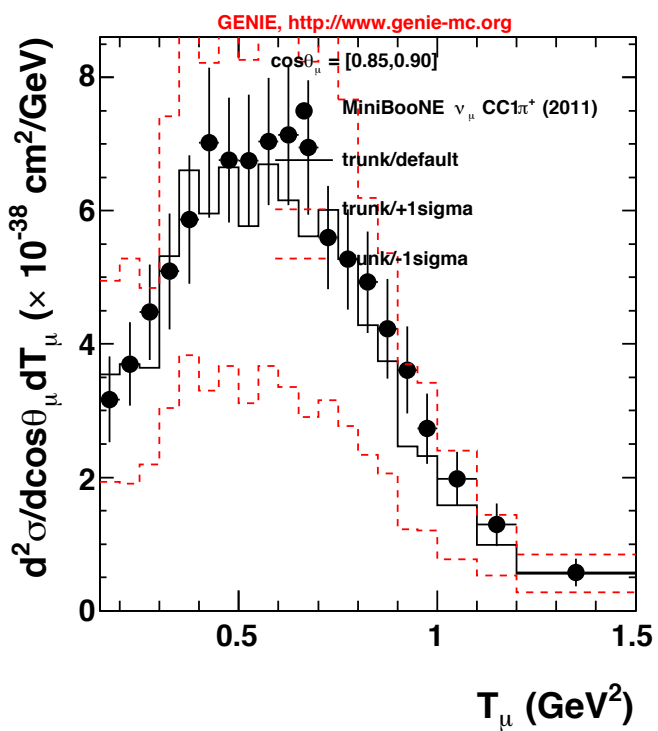
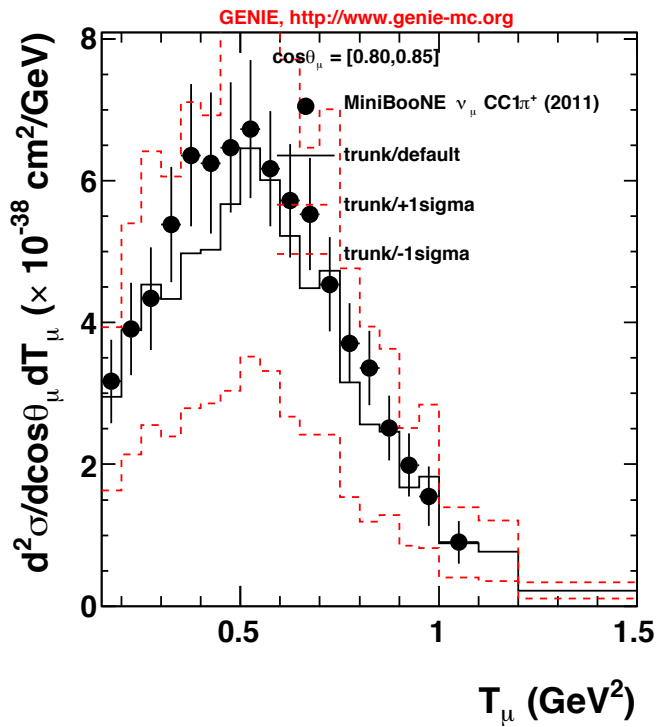
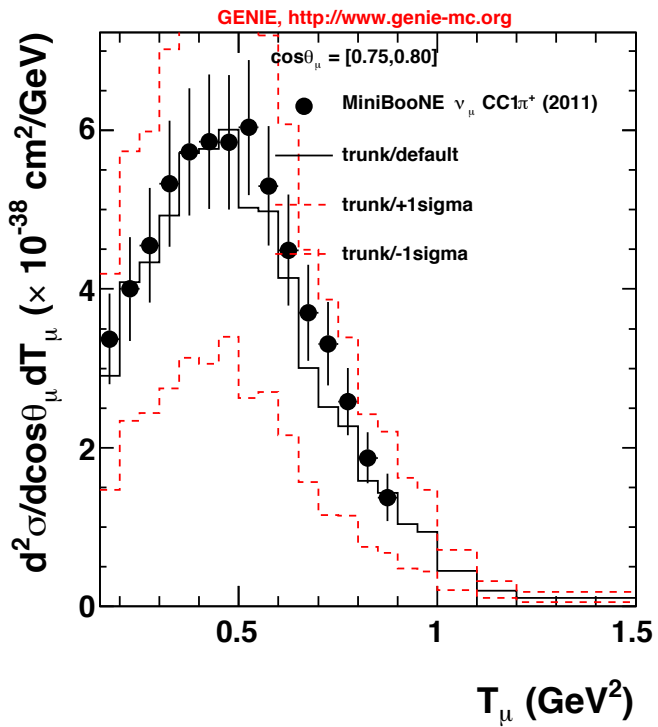


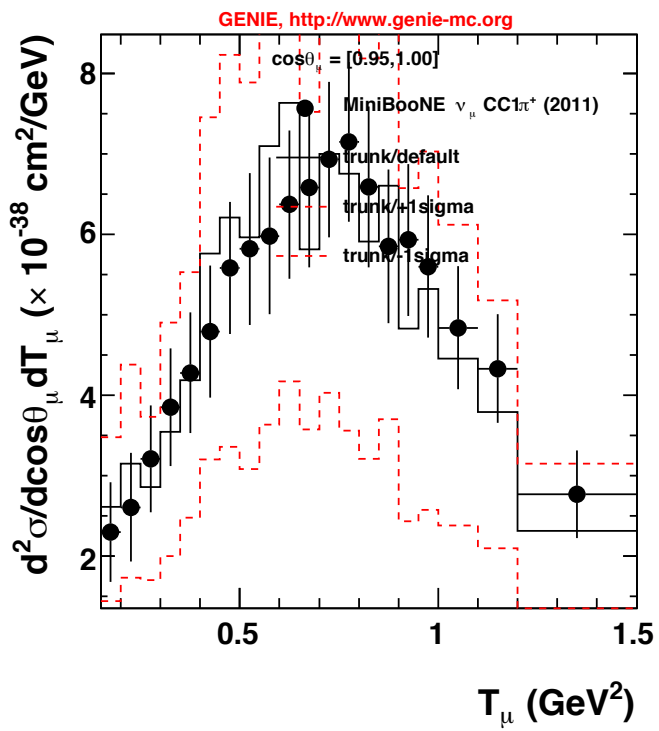


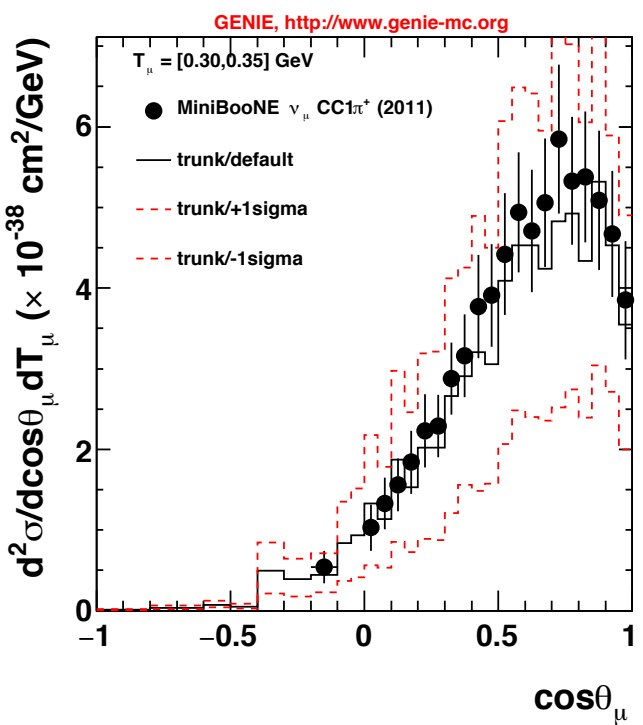
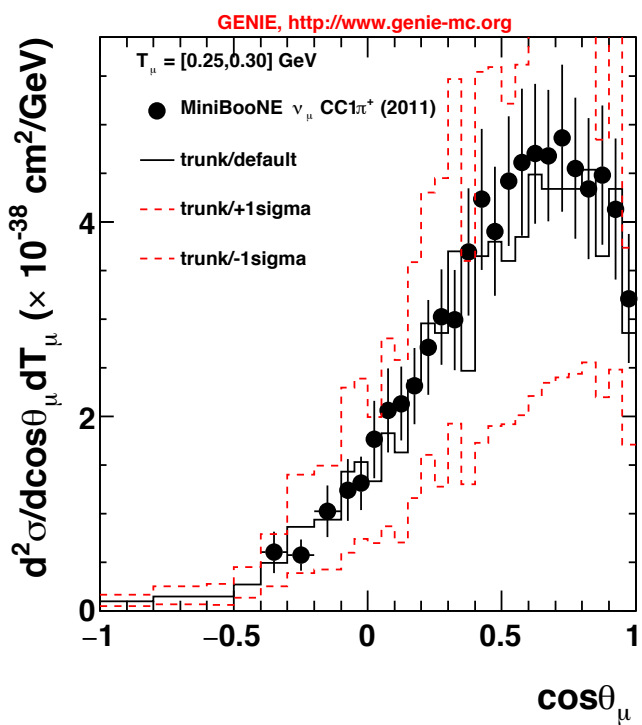
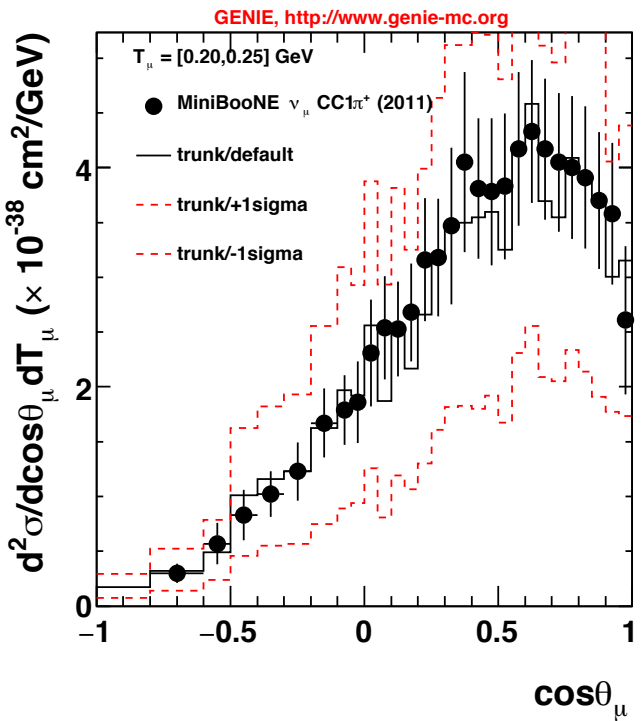
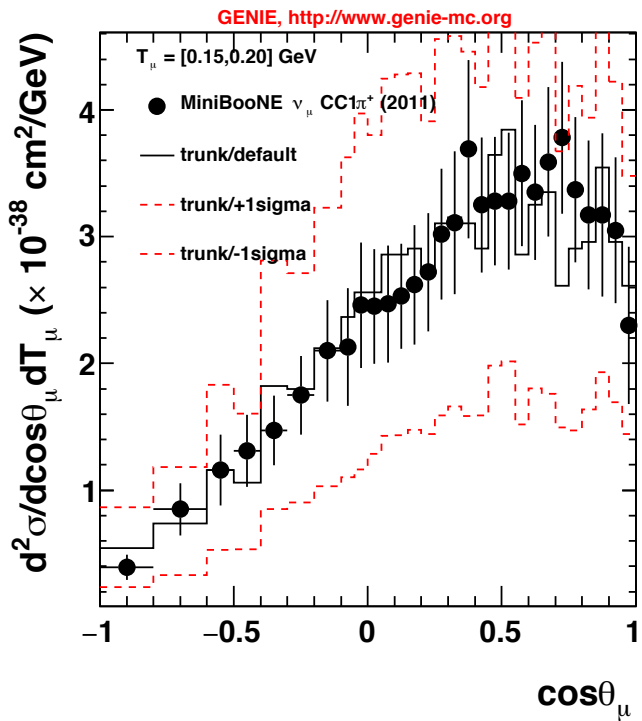


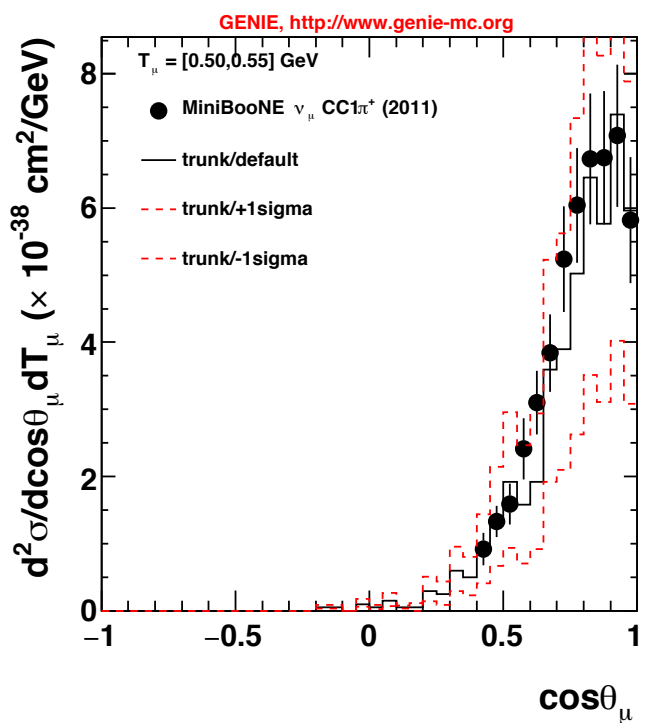
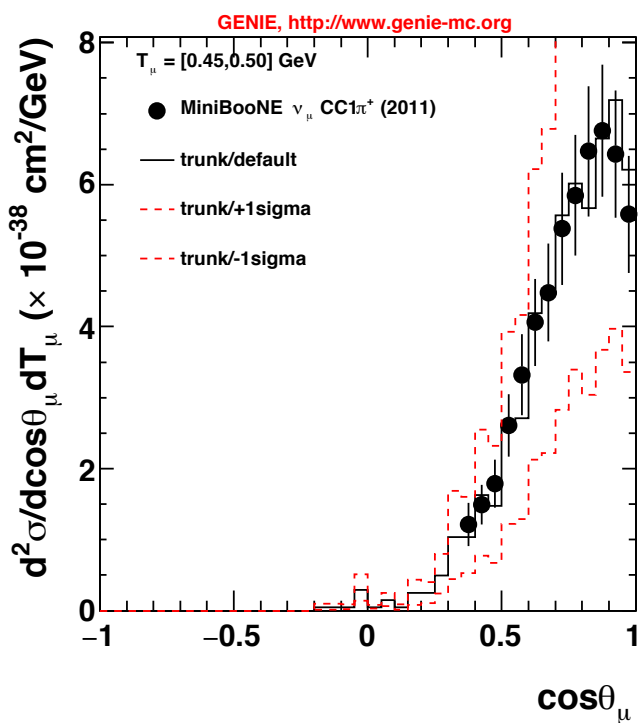
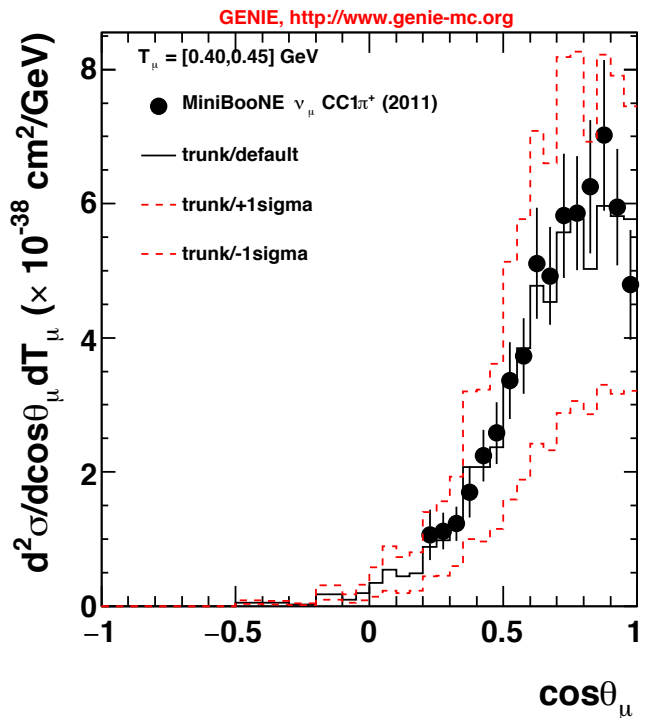
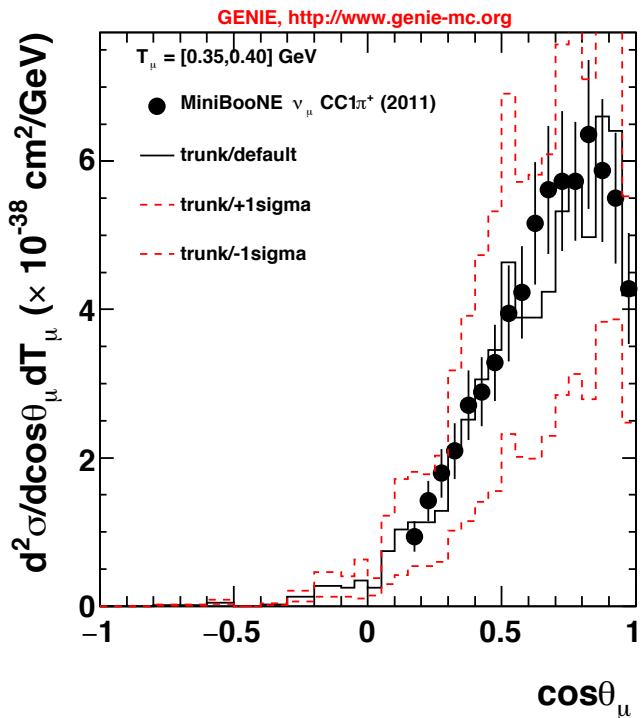


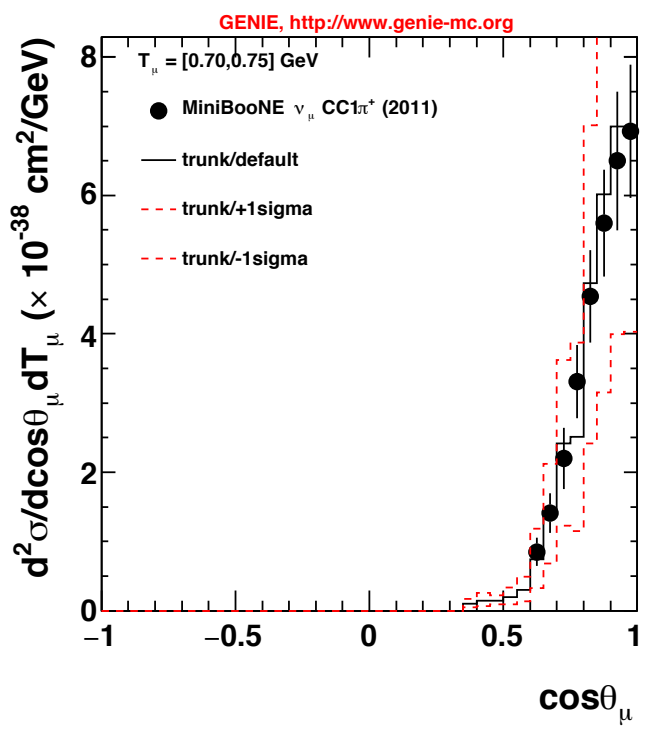
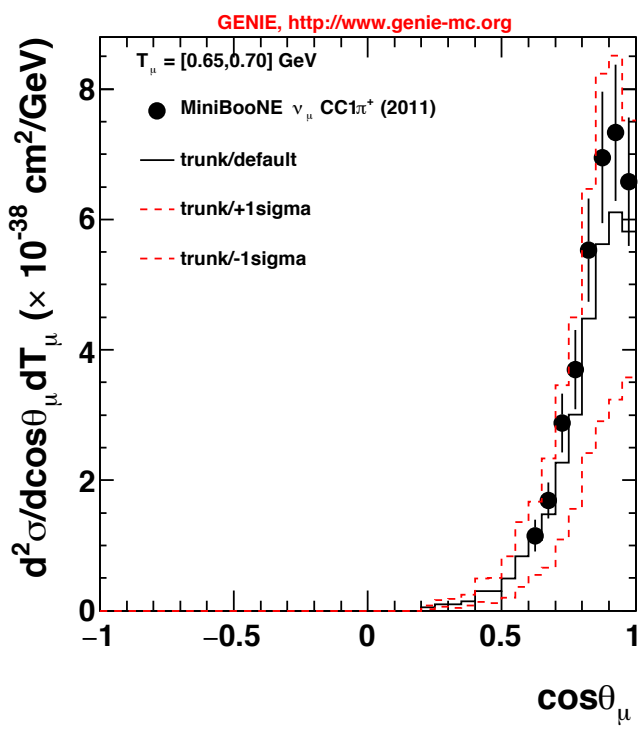
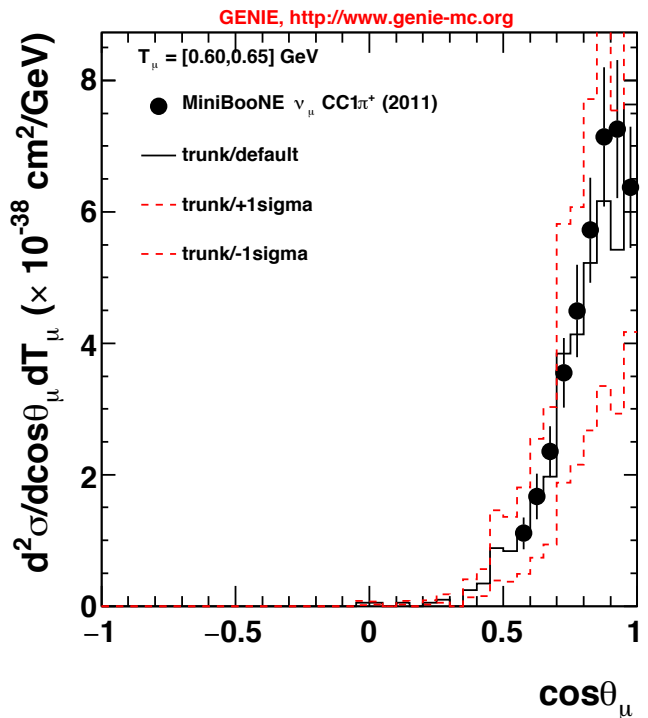
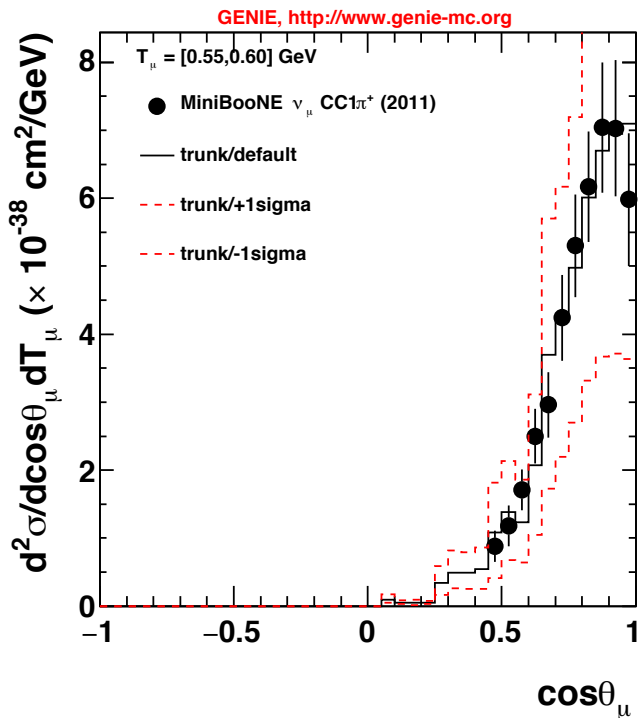


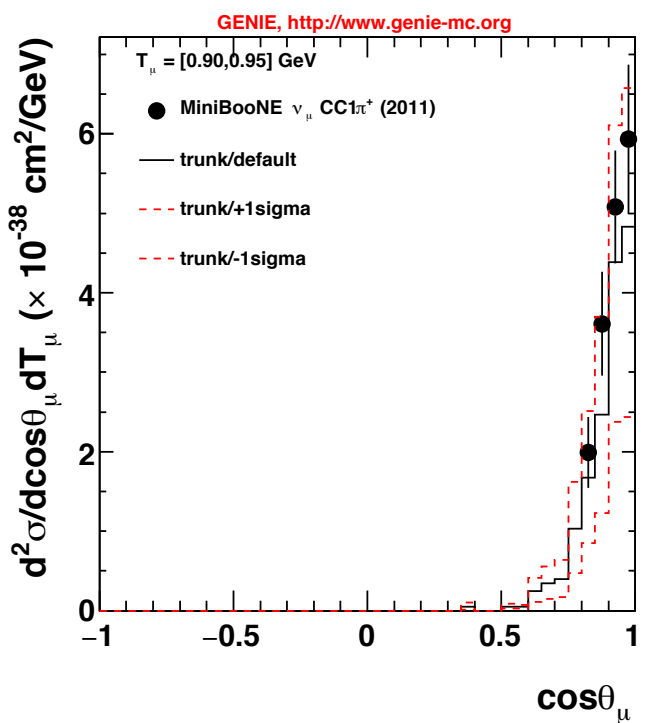
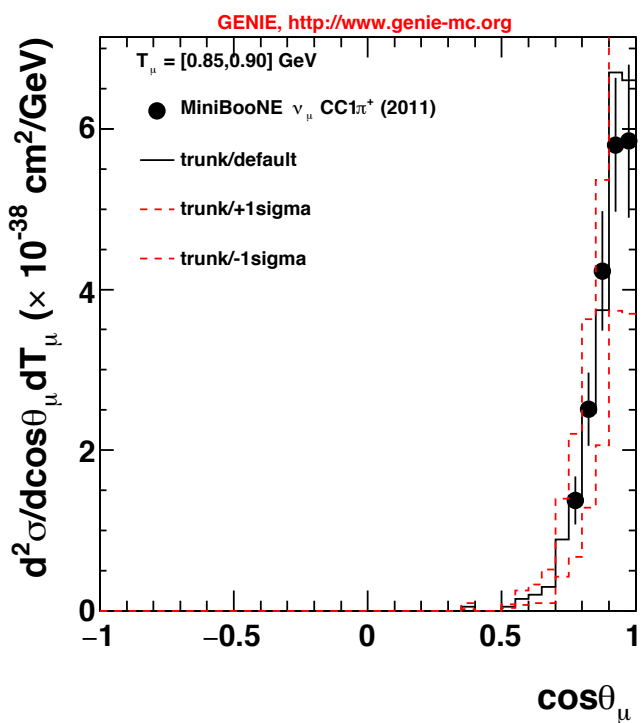
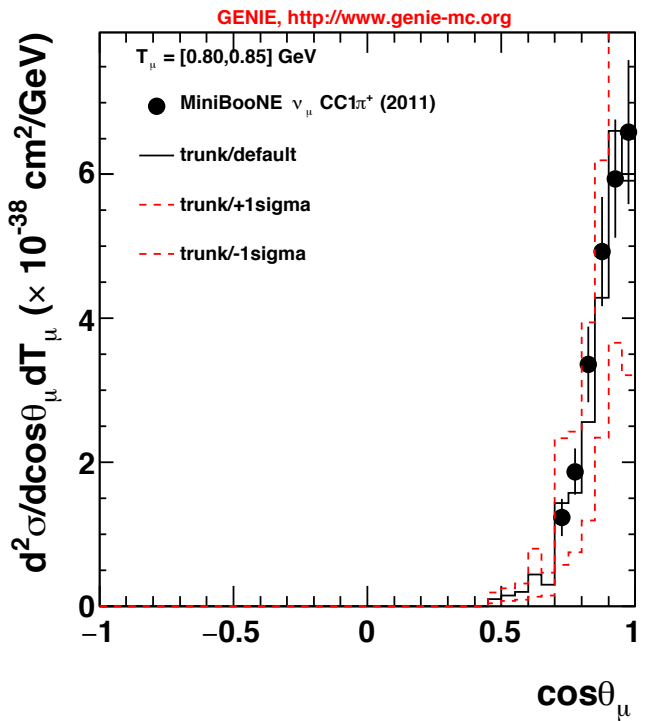
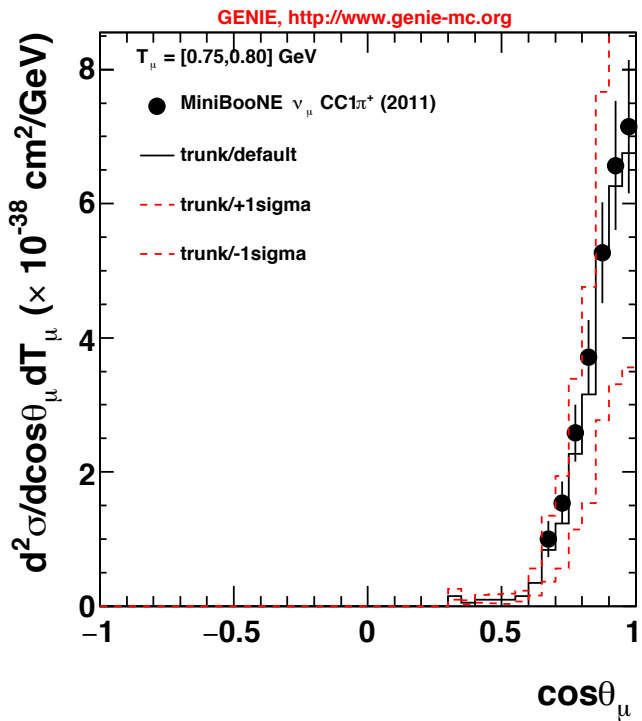


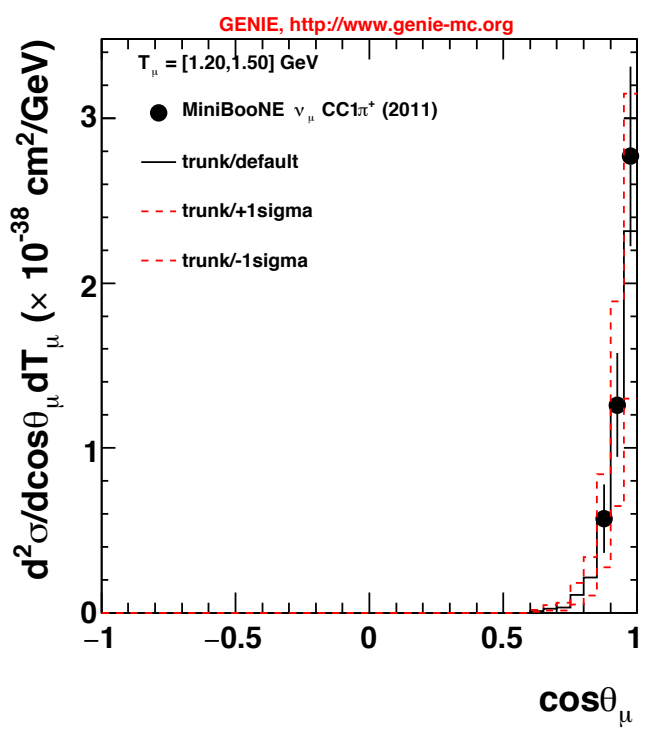
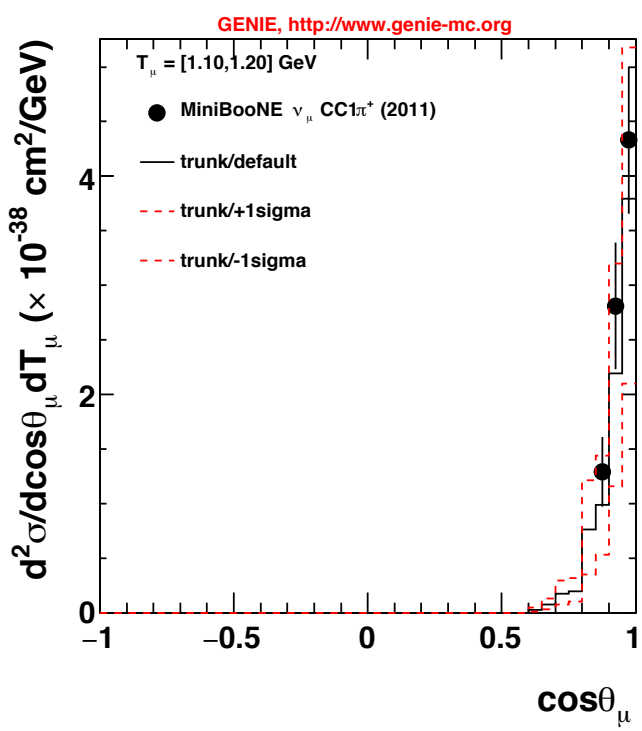
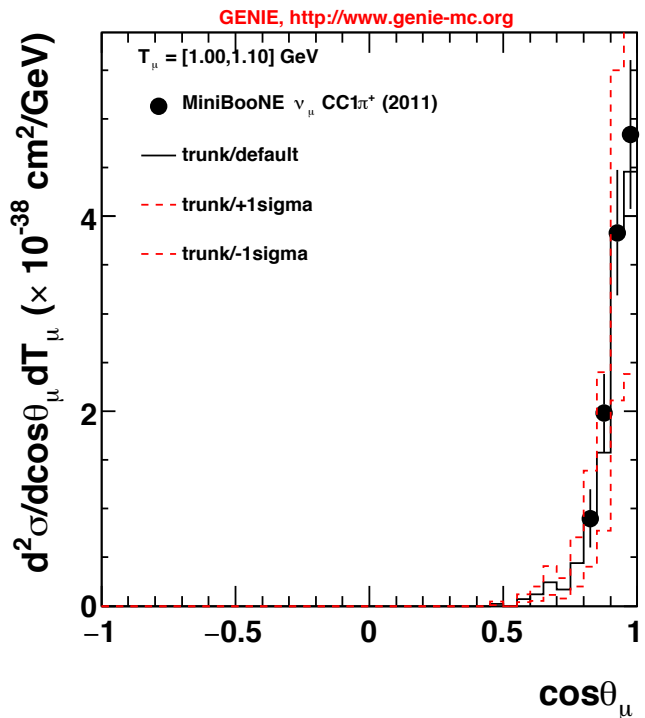
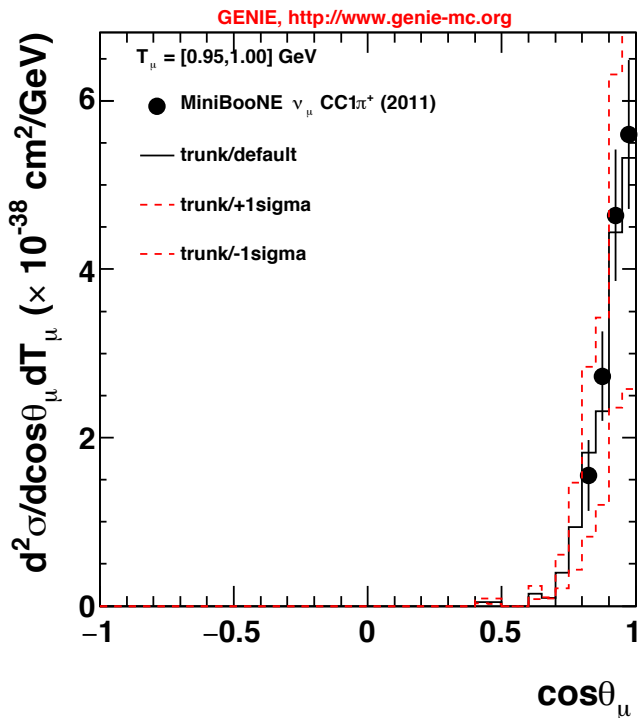


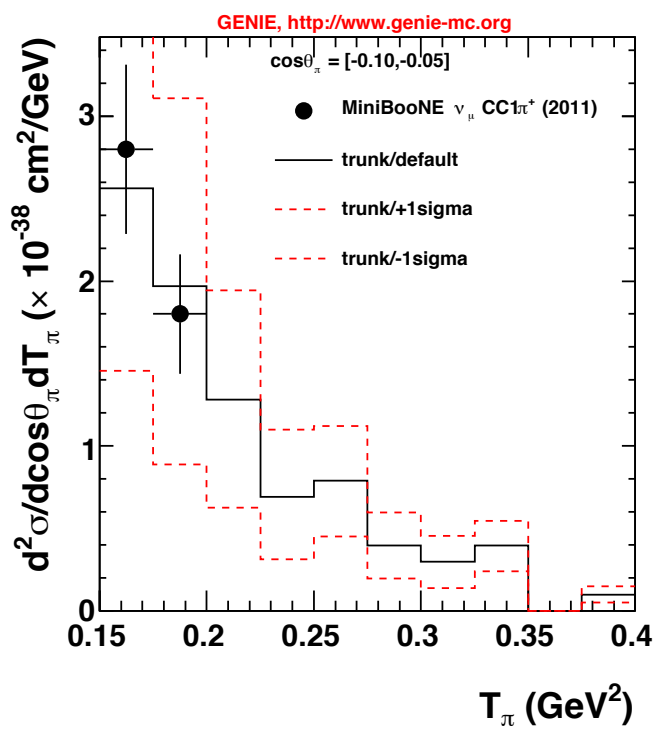
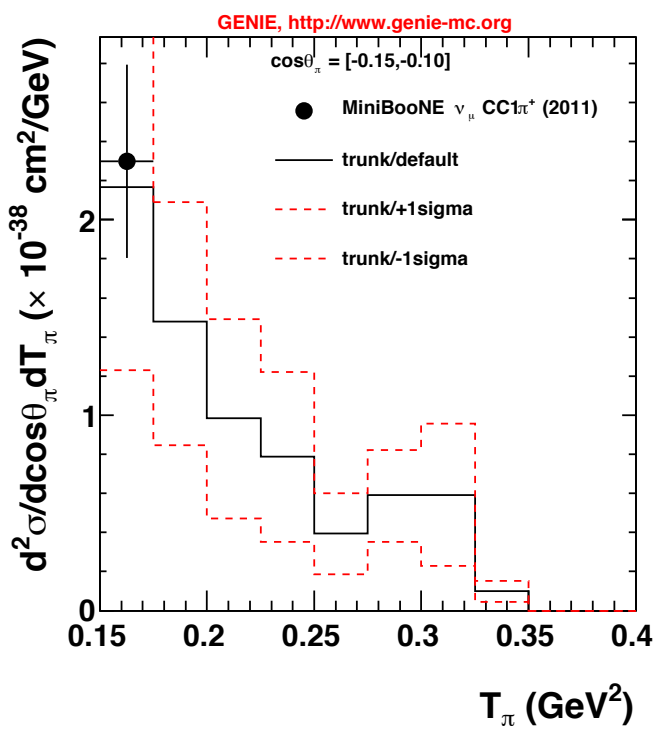
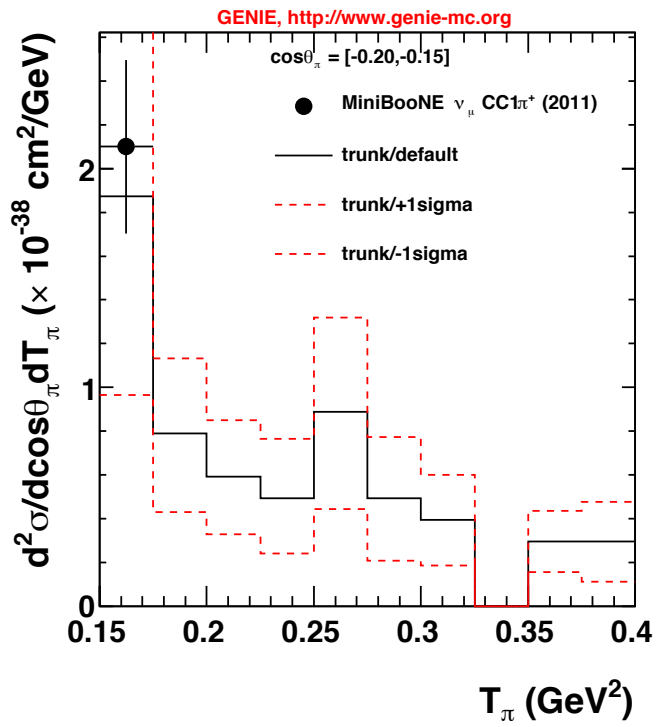
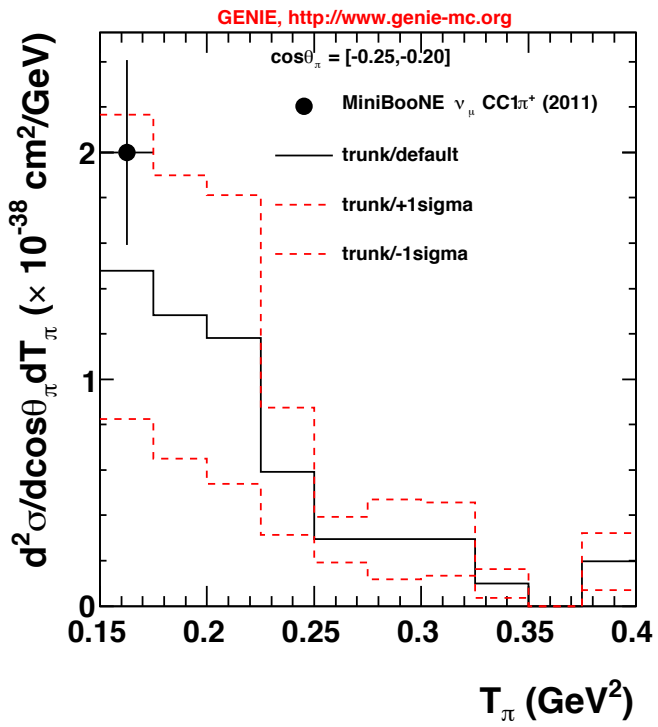


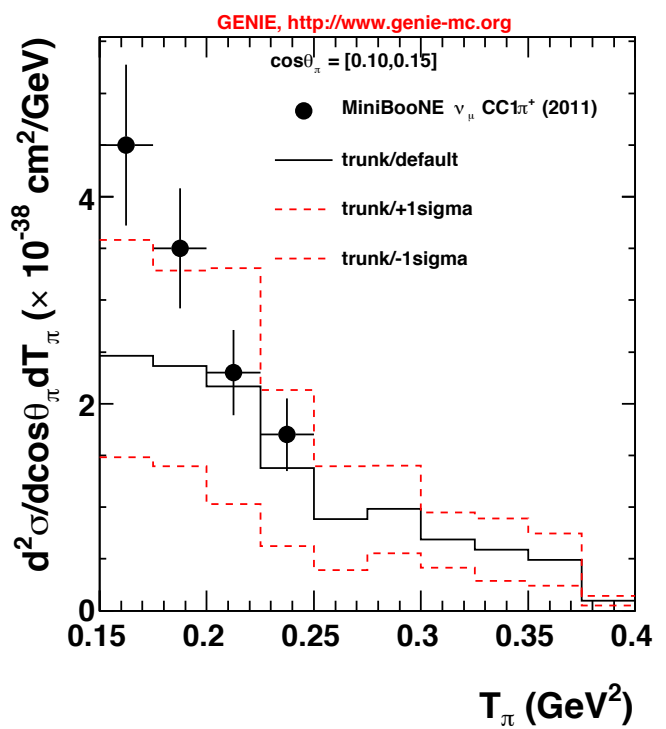
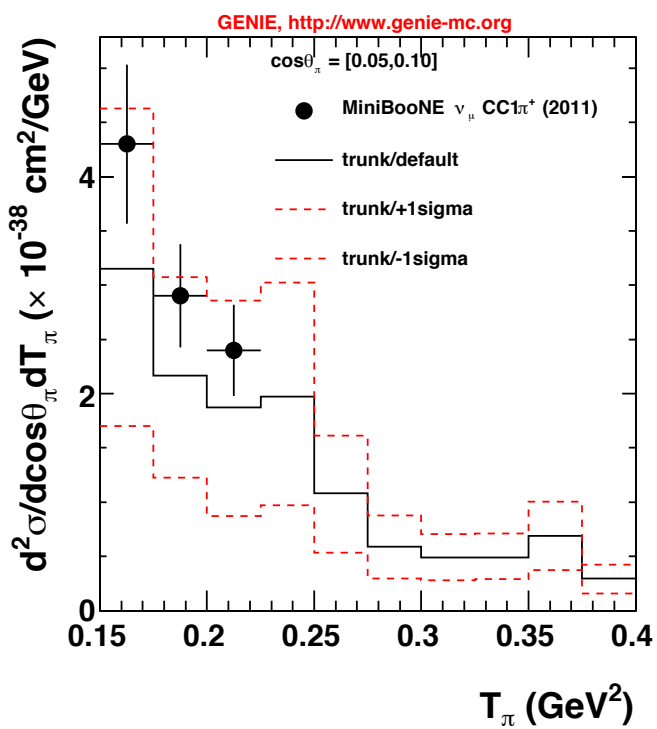
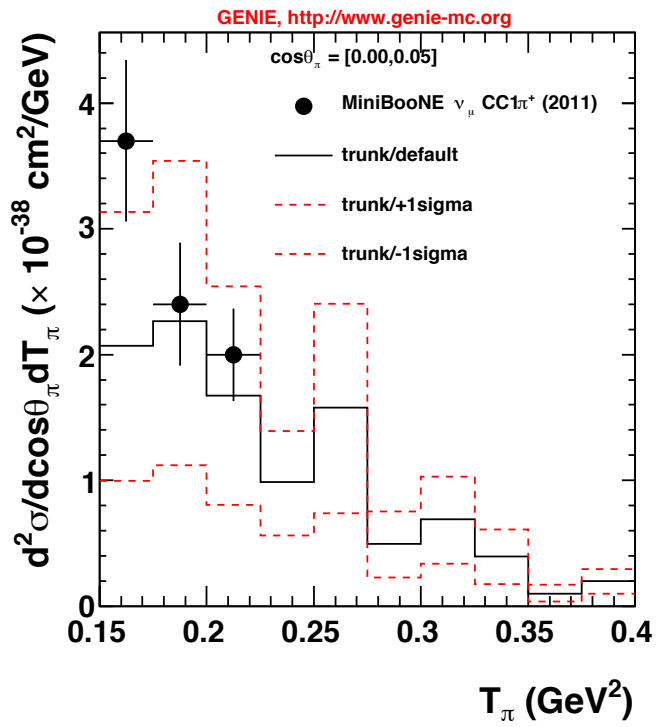
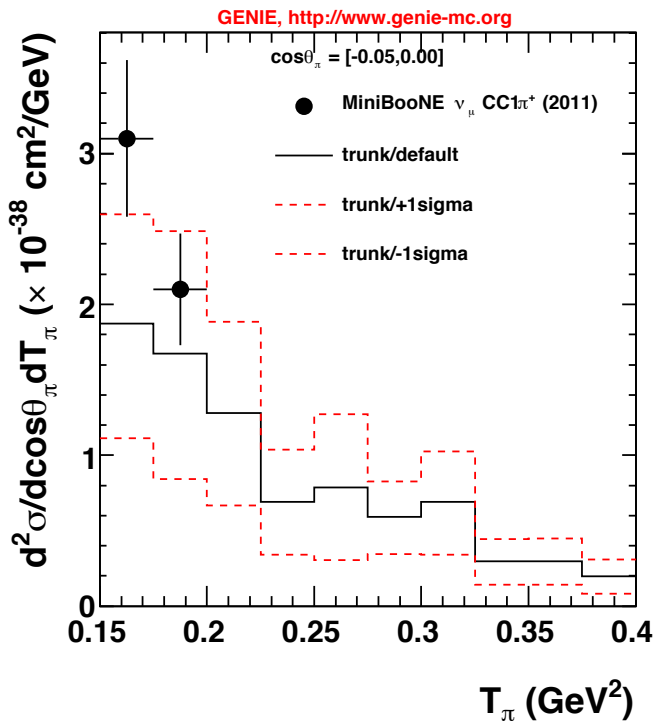


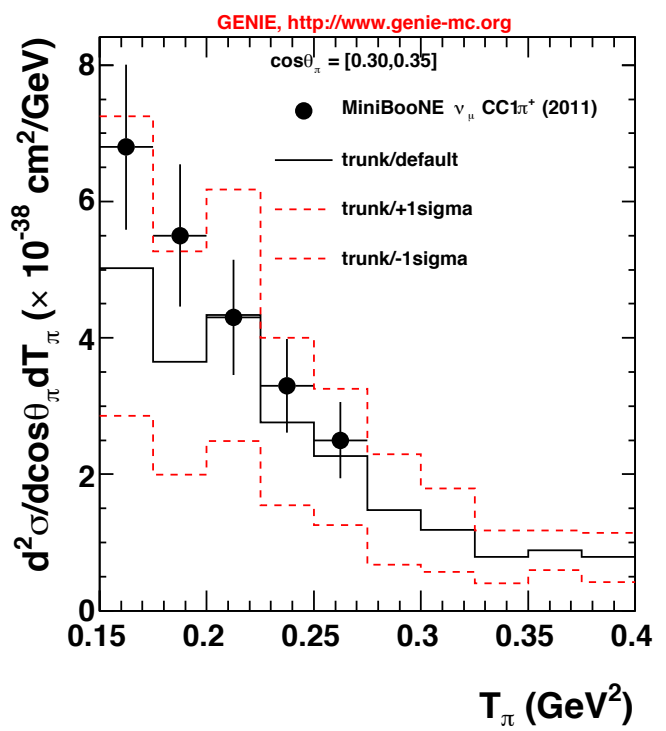
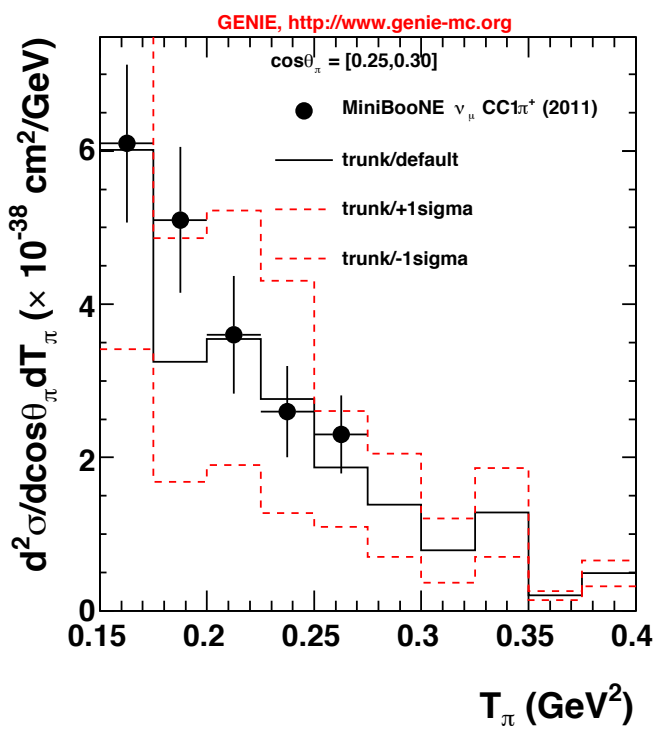
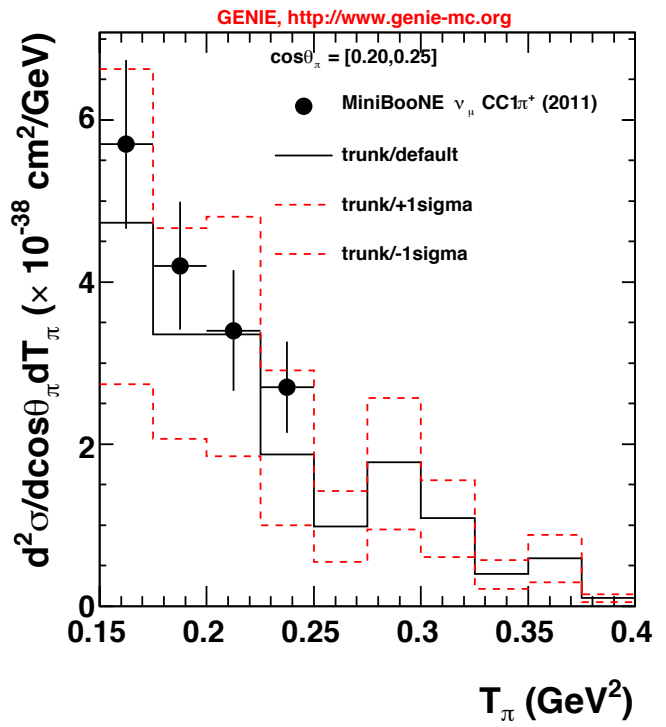
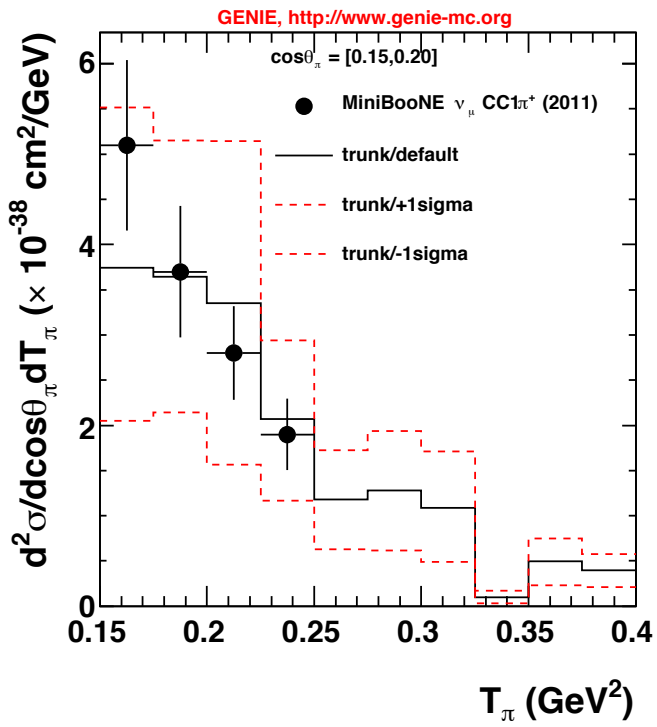


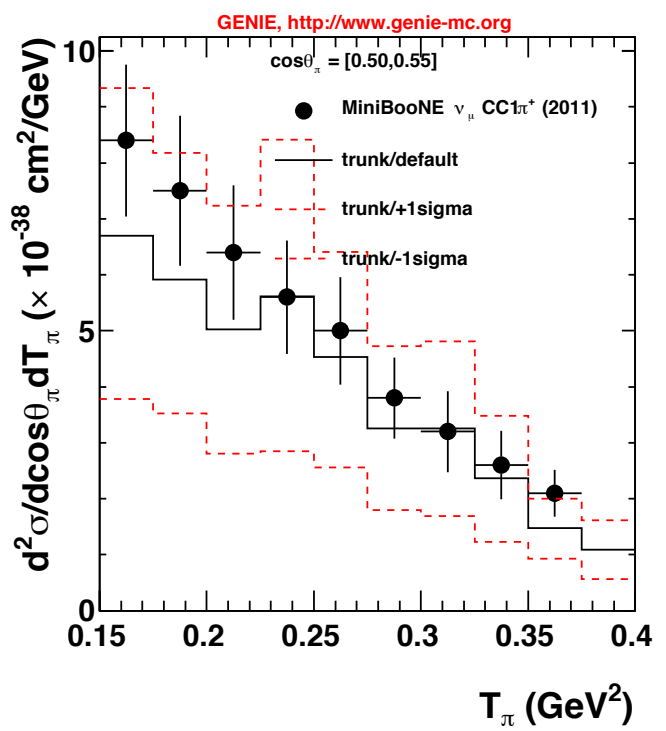
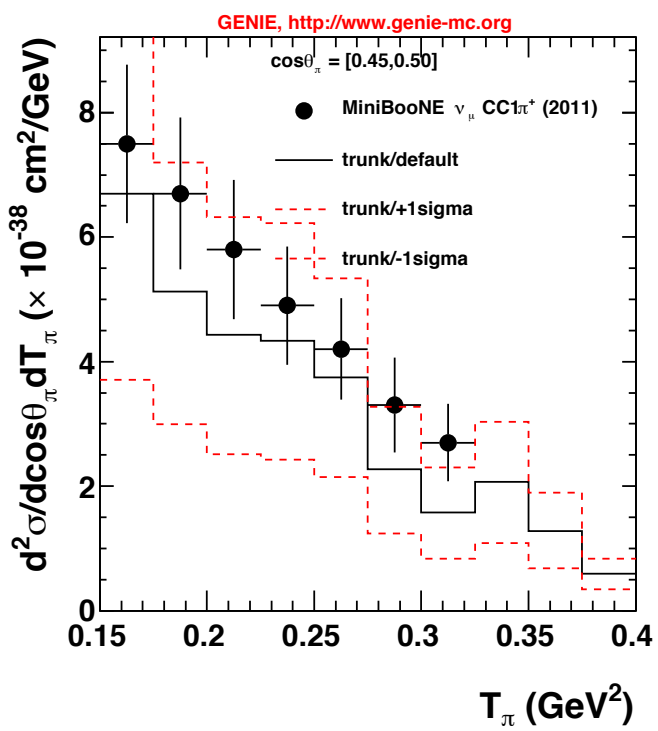
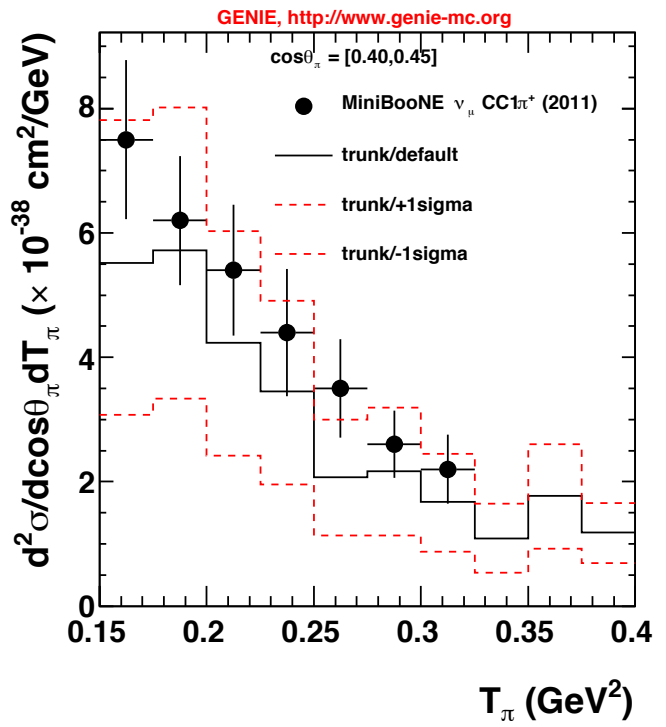
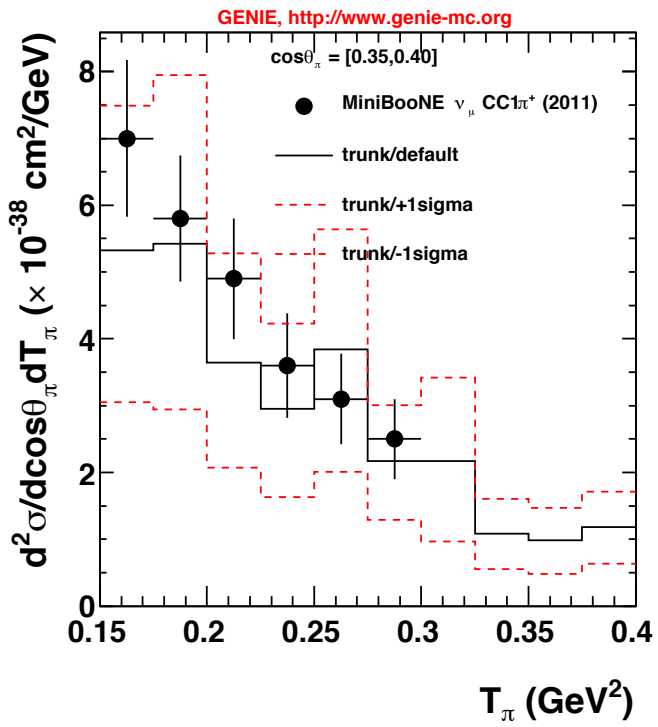


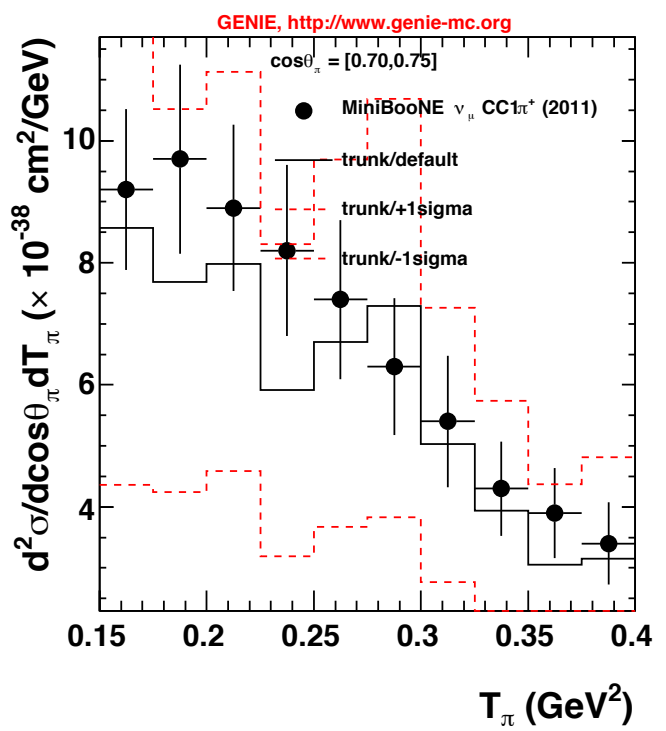
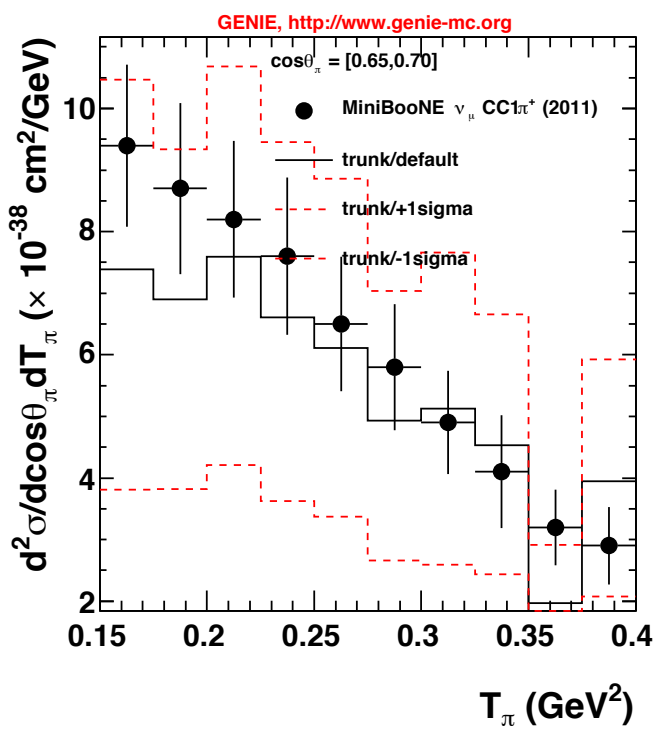
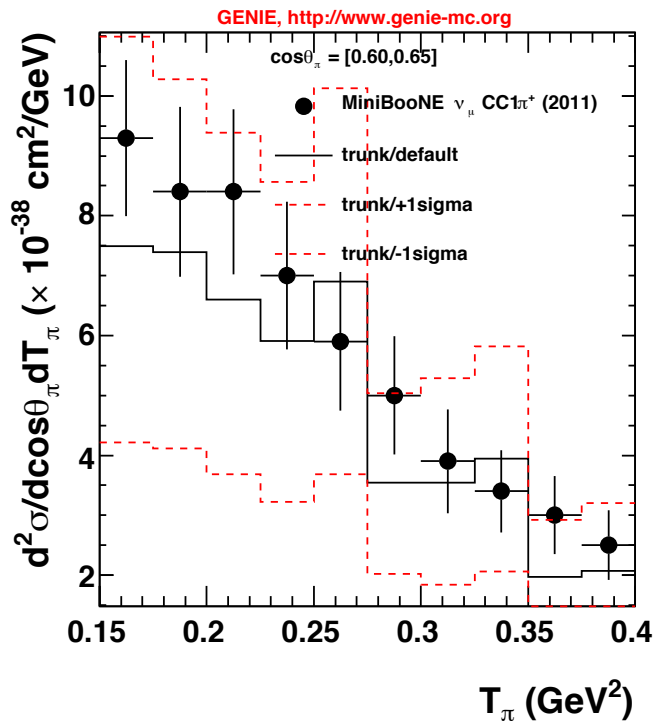
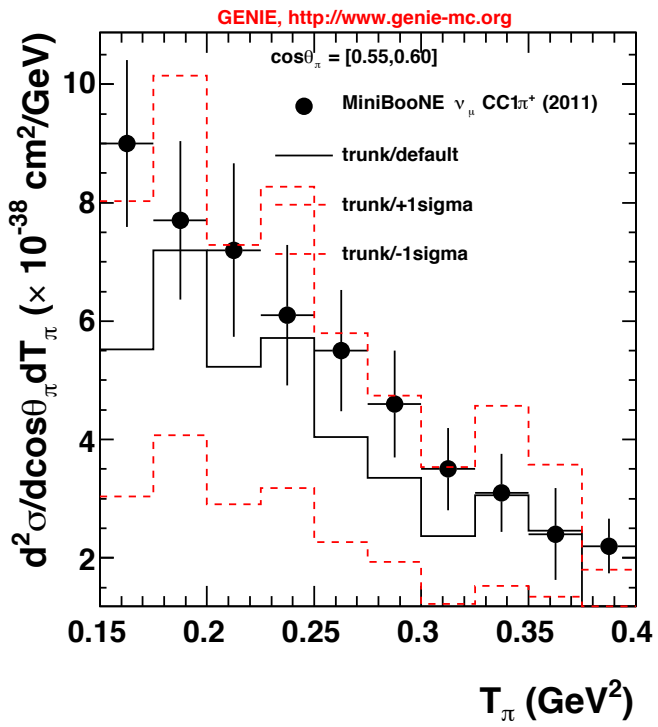


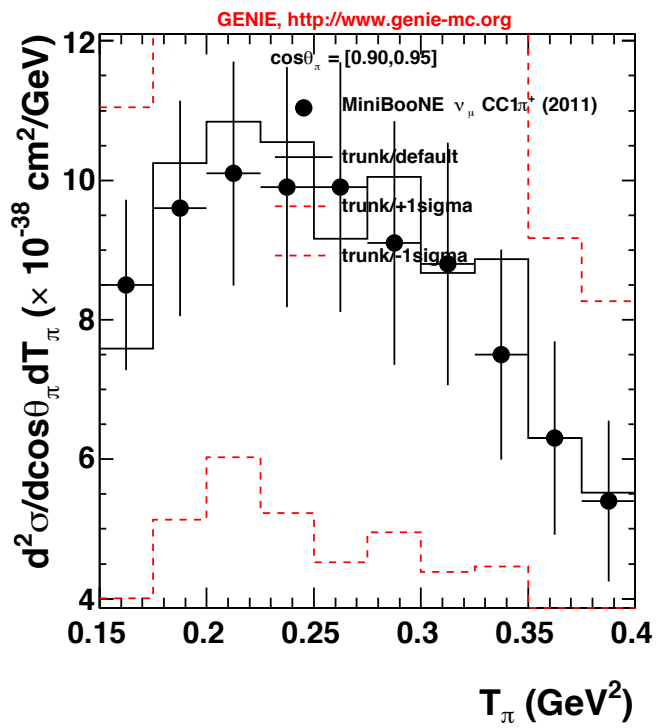
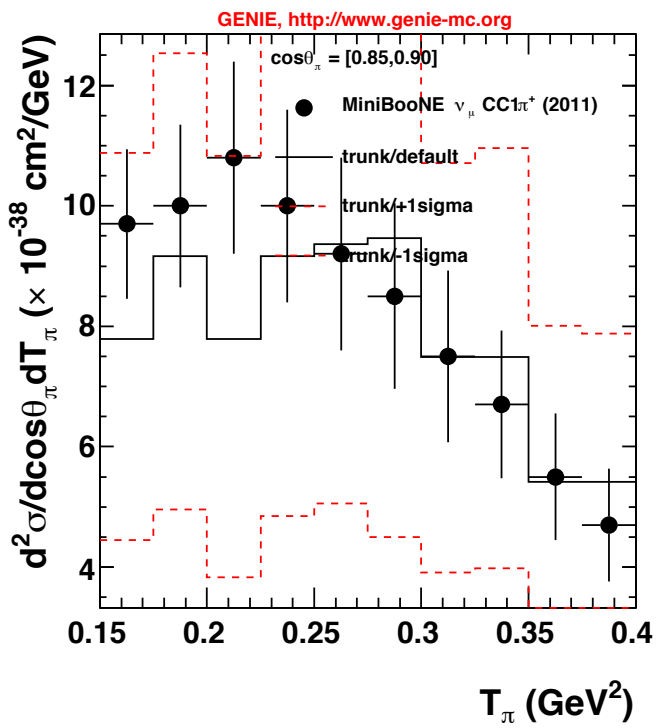
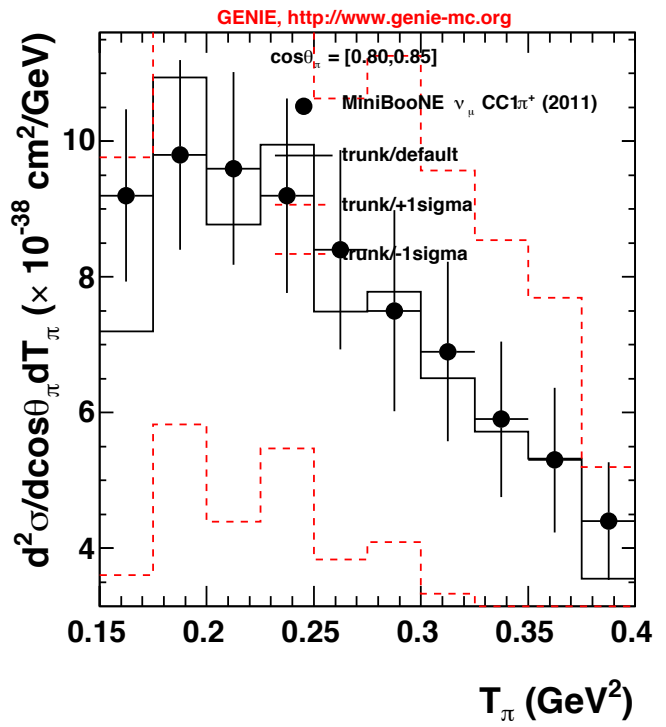
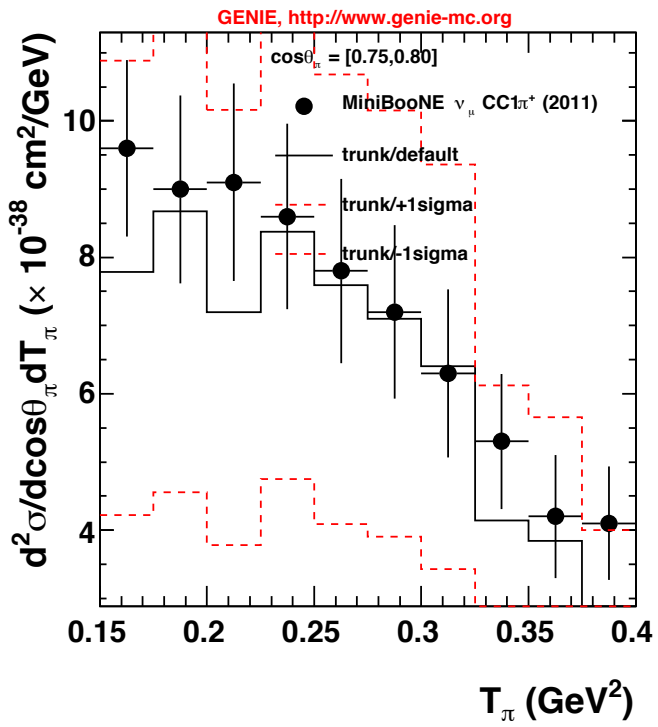


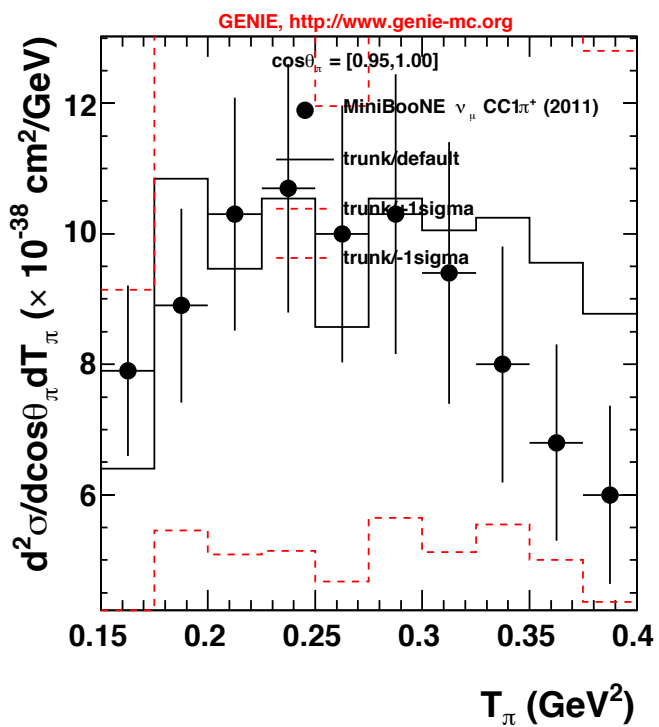


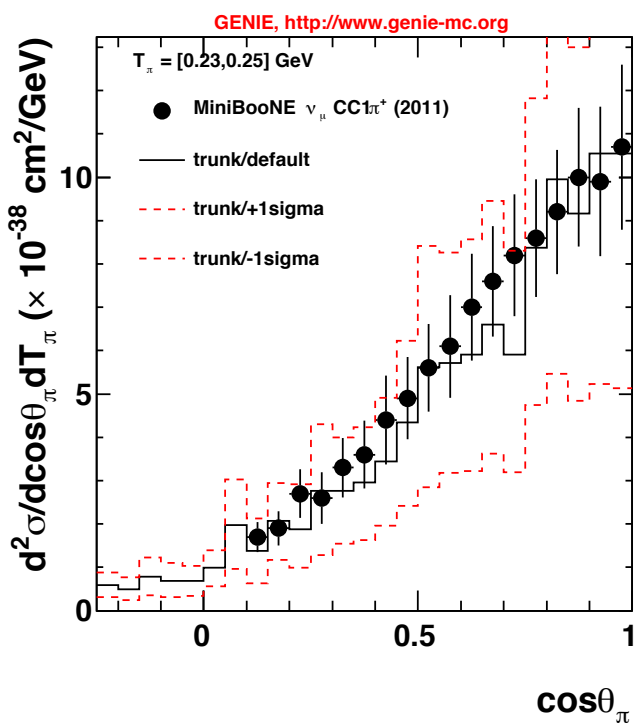
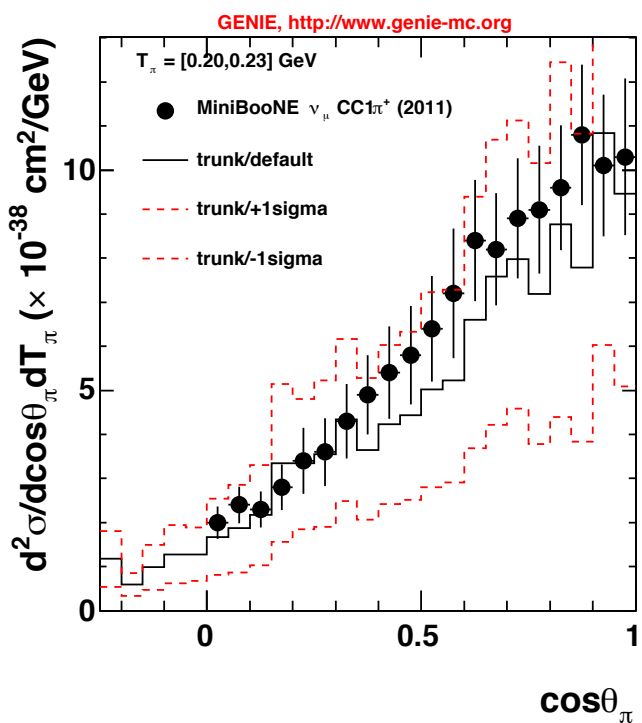
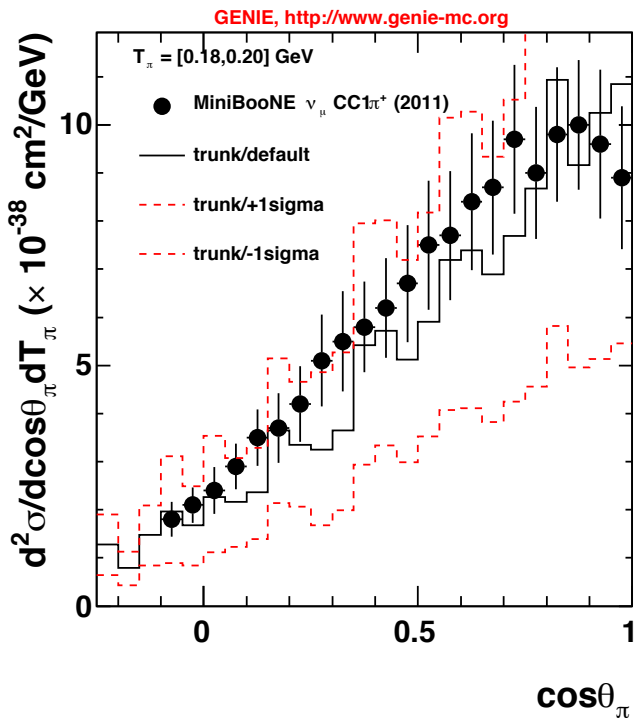
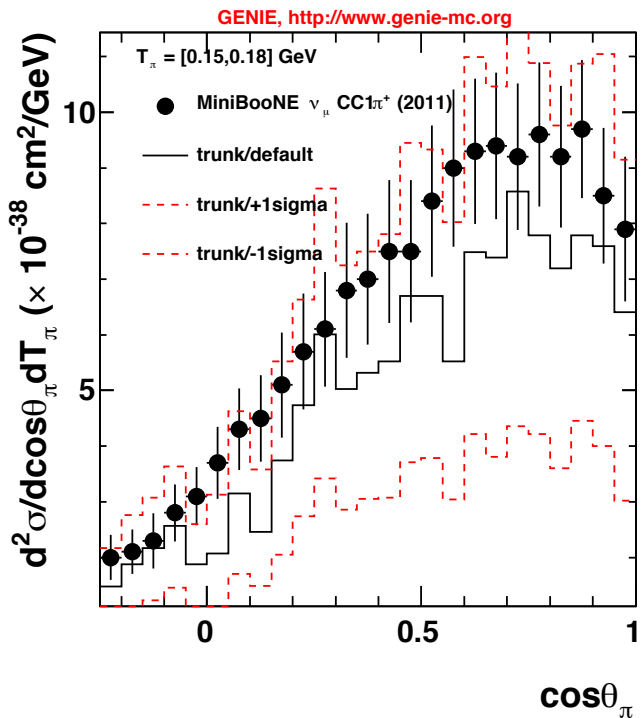


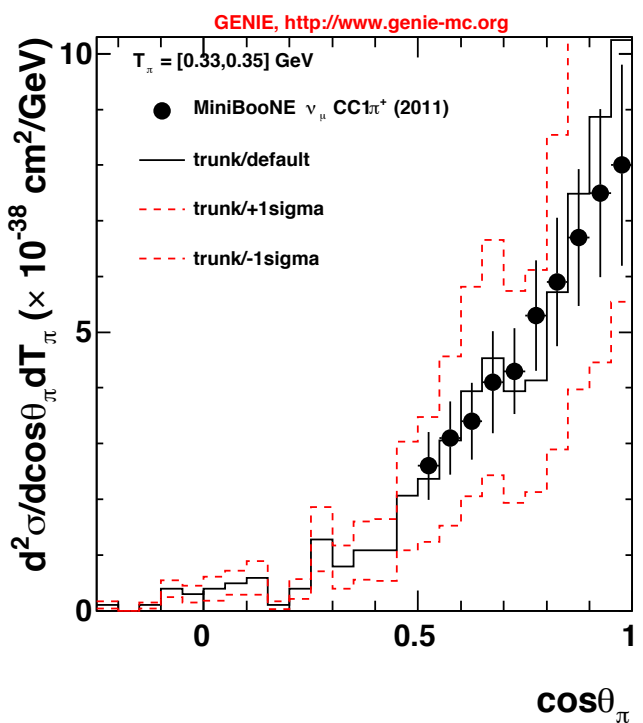
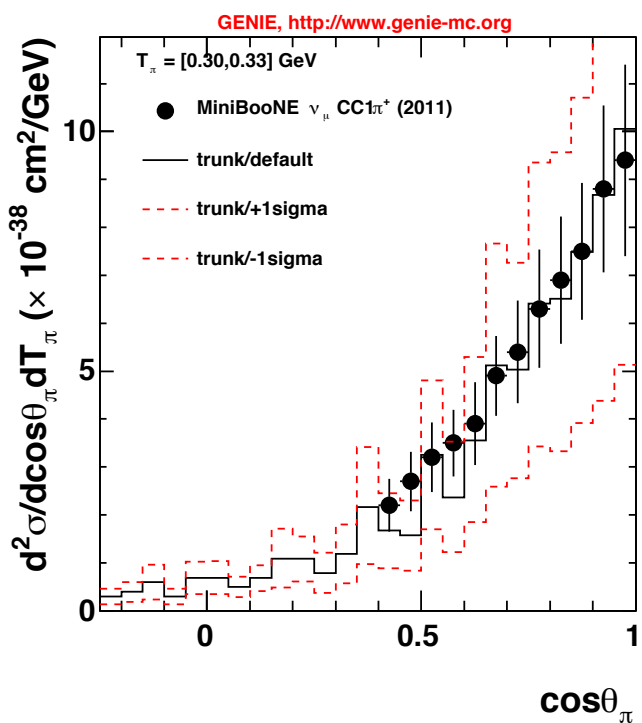
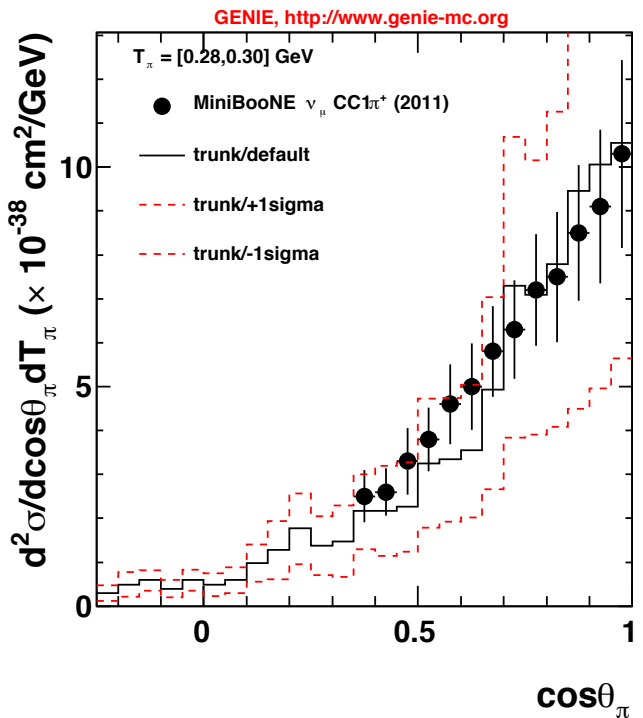
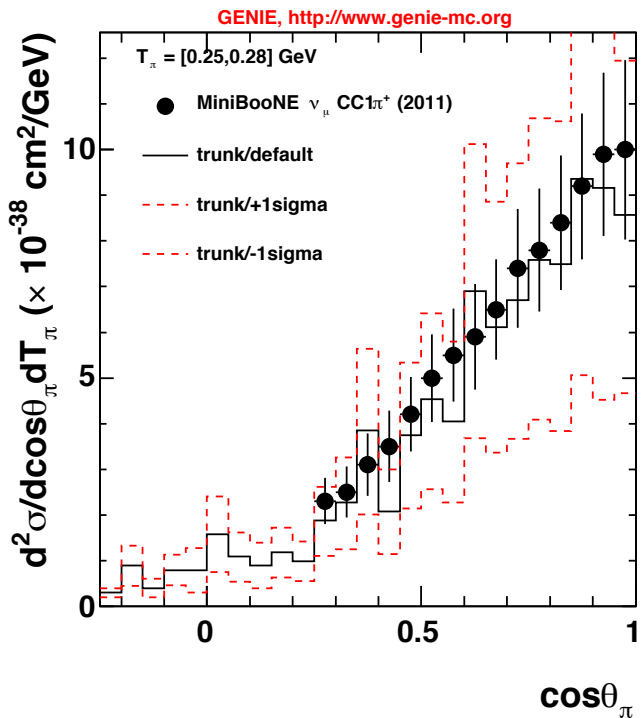


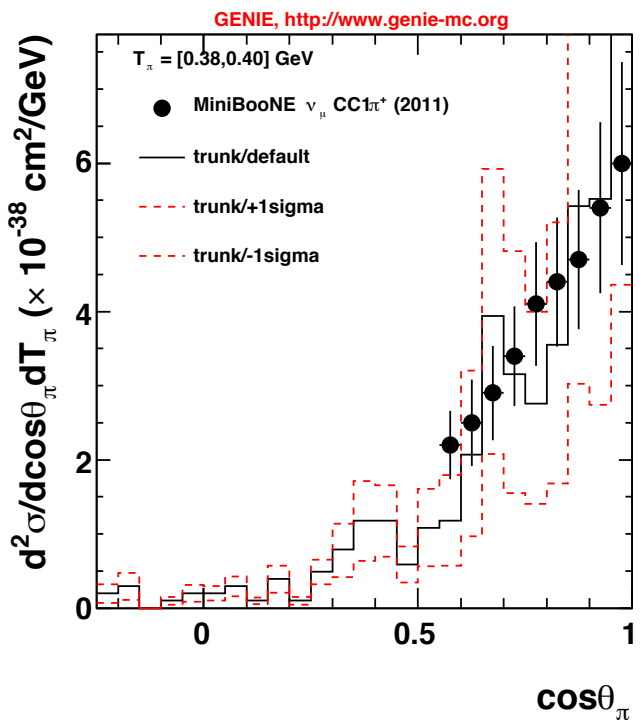
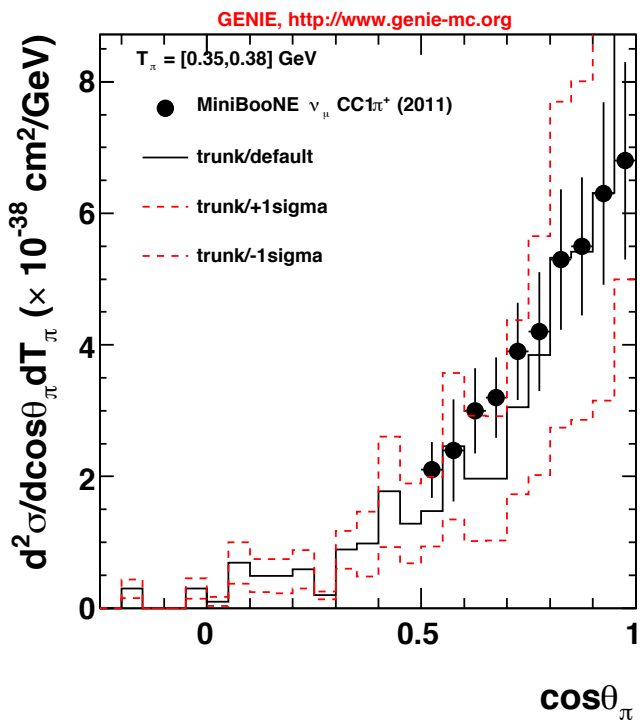




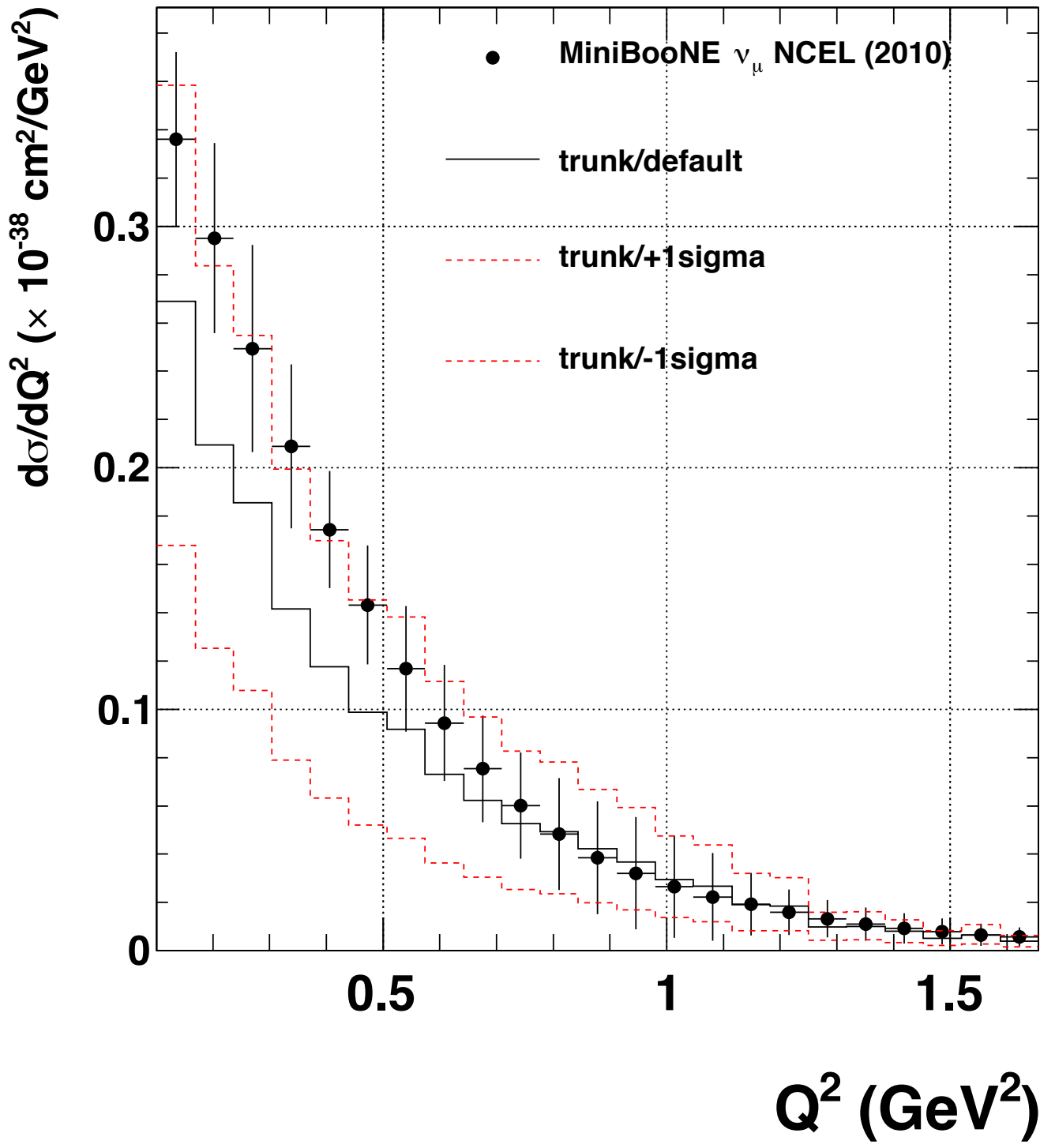


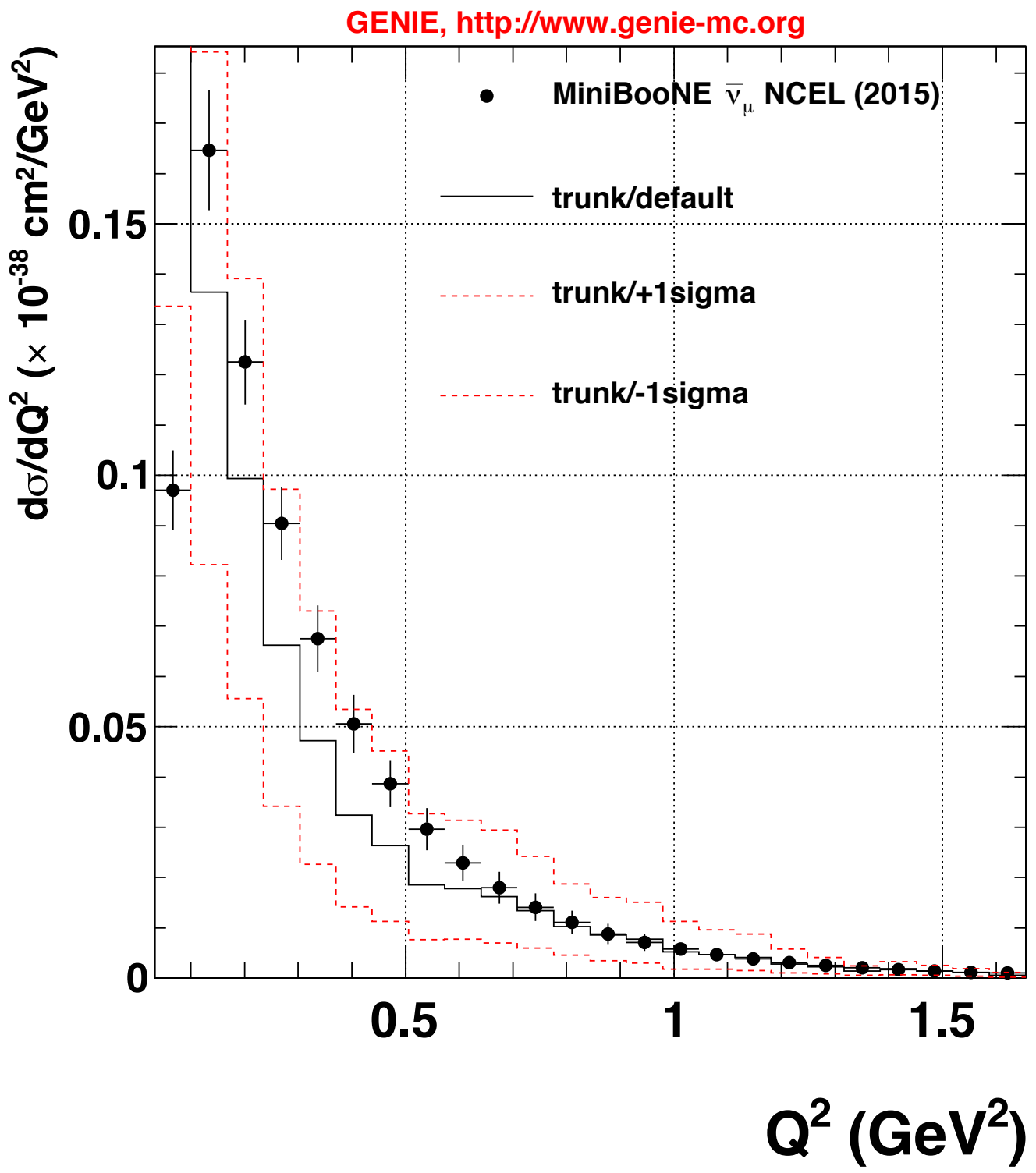


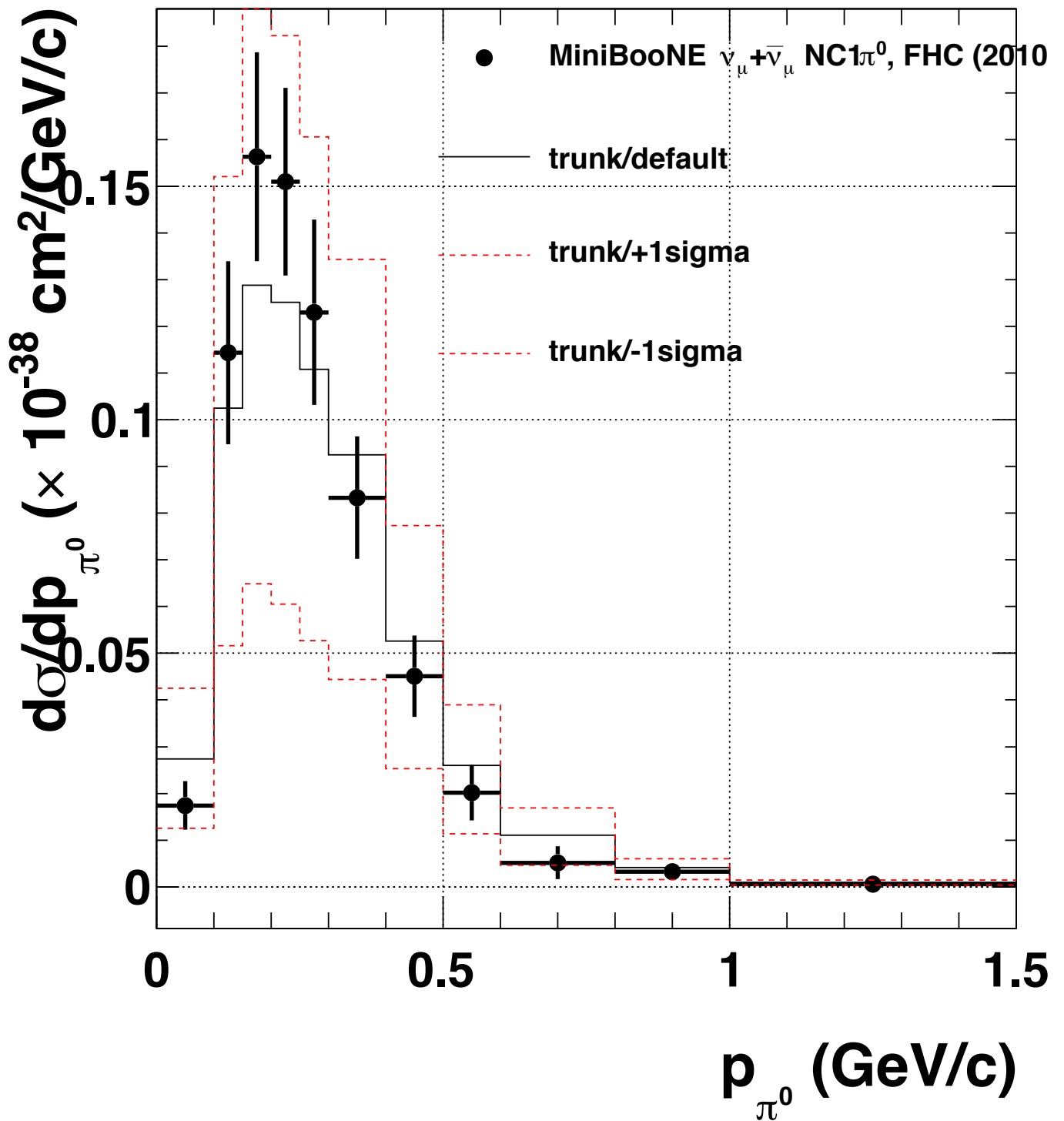


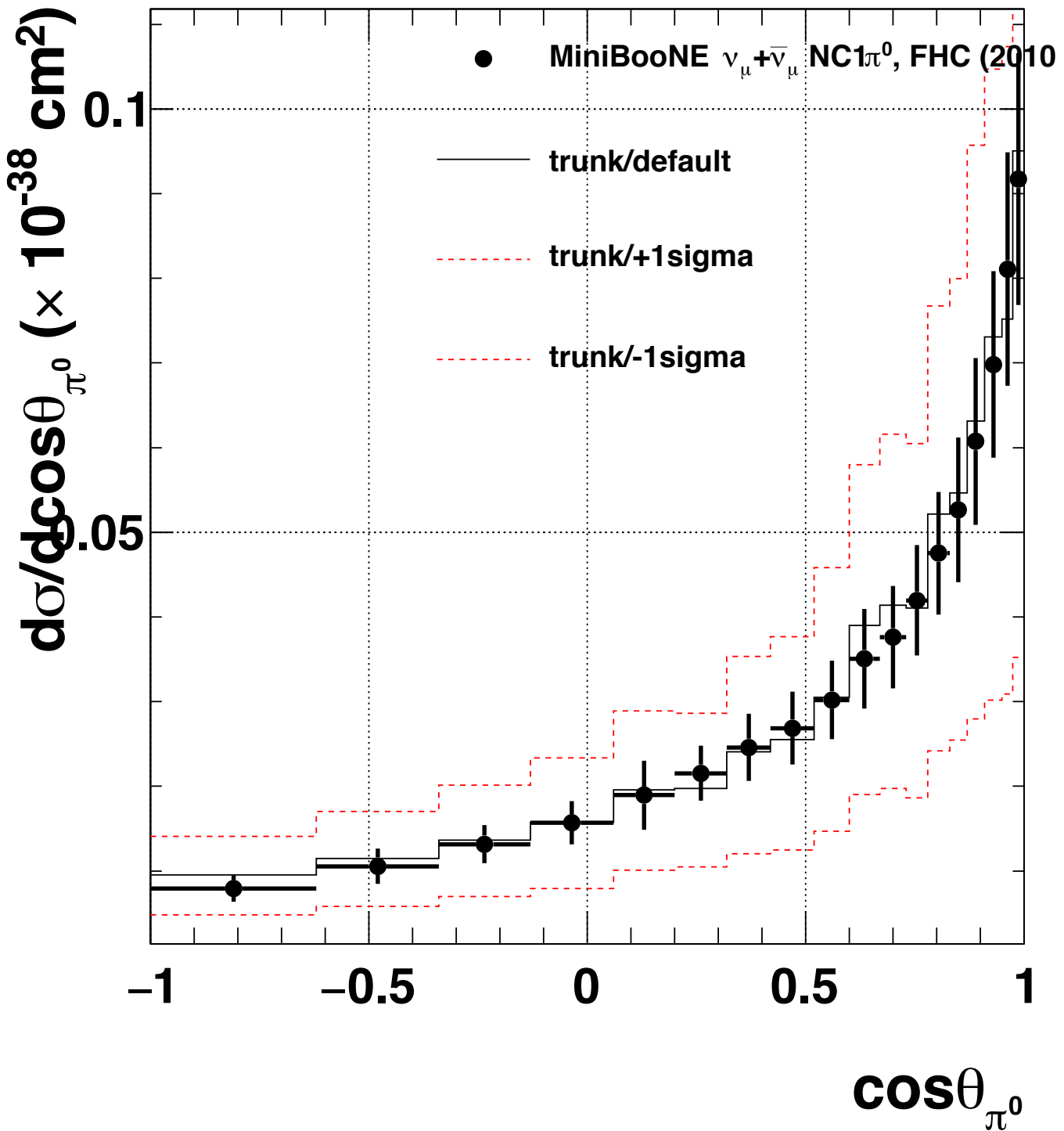


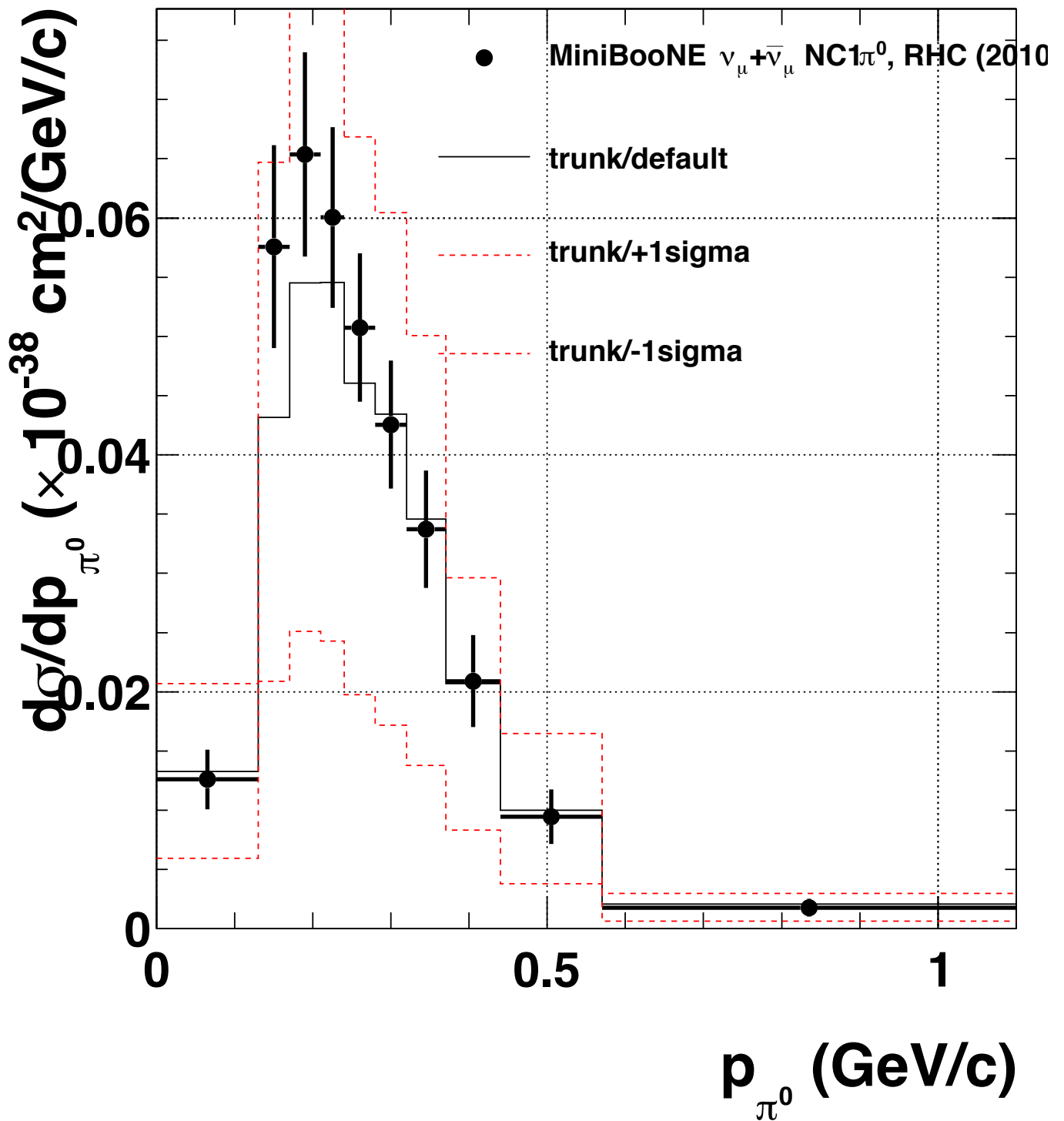
GENIE, <http://www.genie-mc.org>

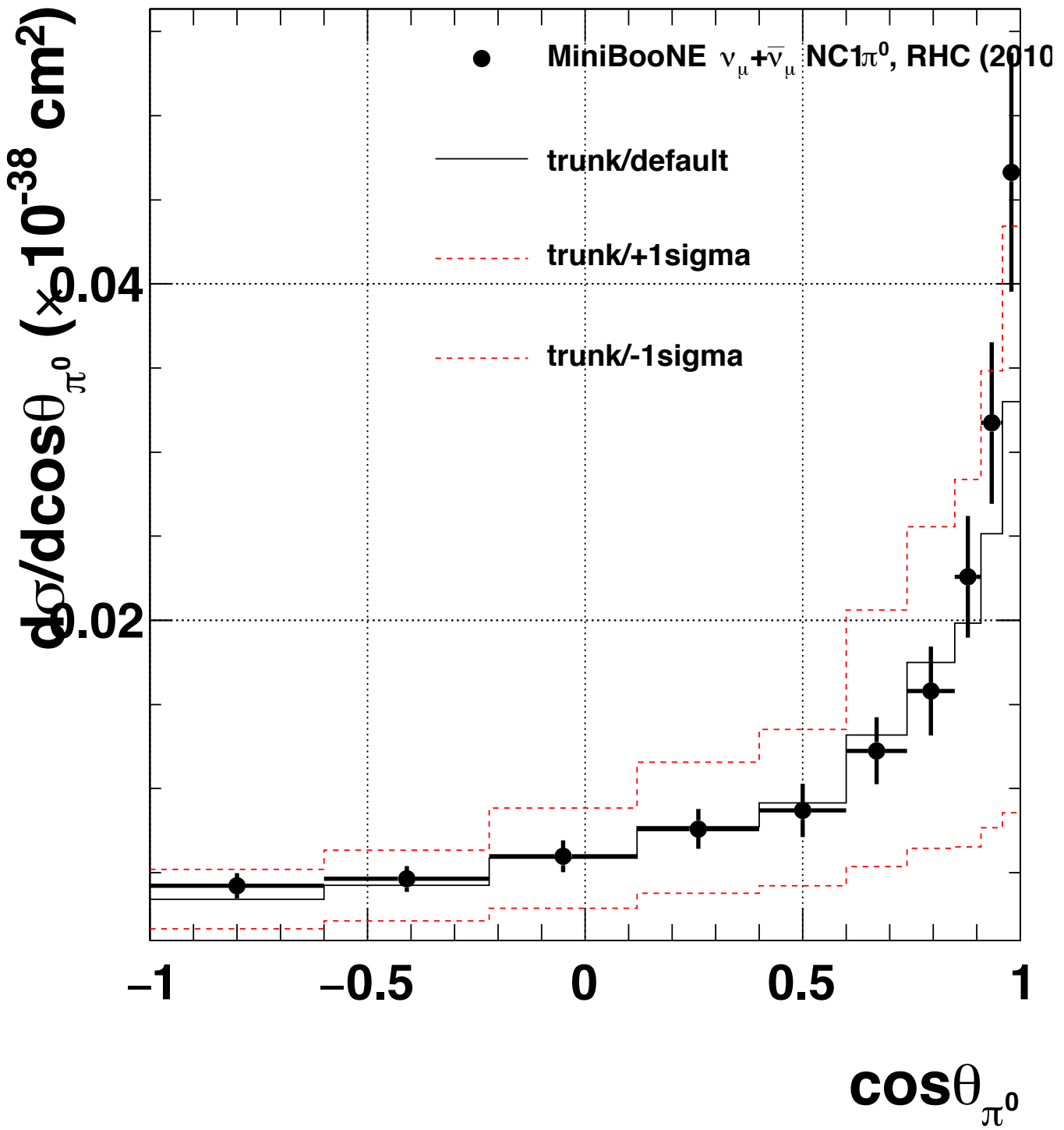


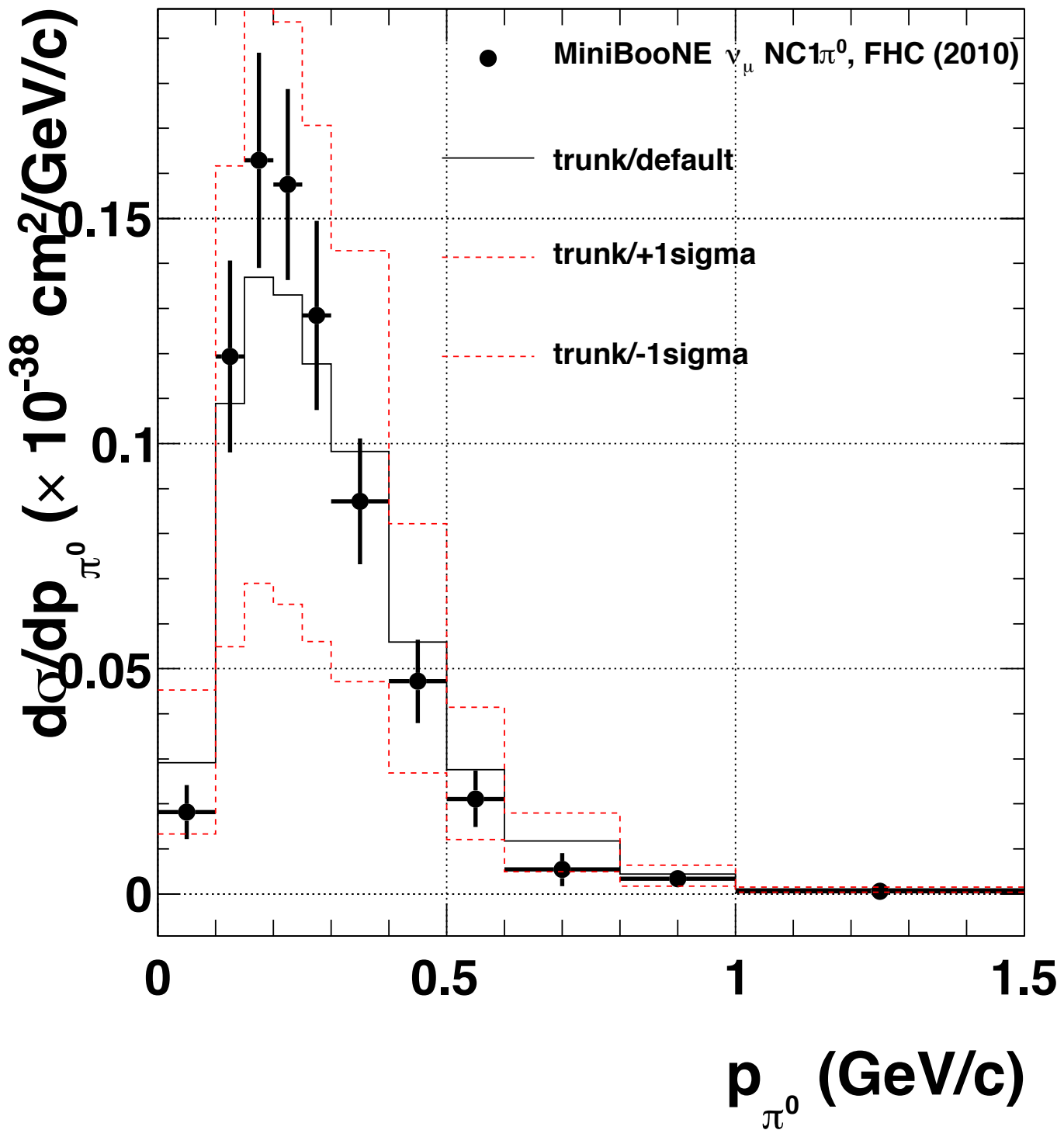


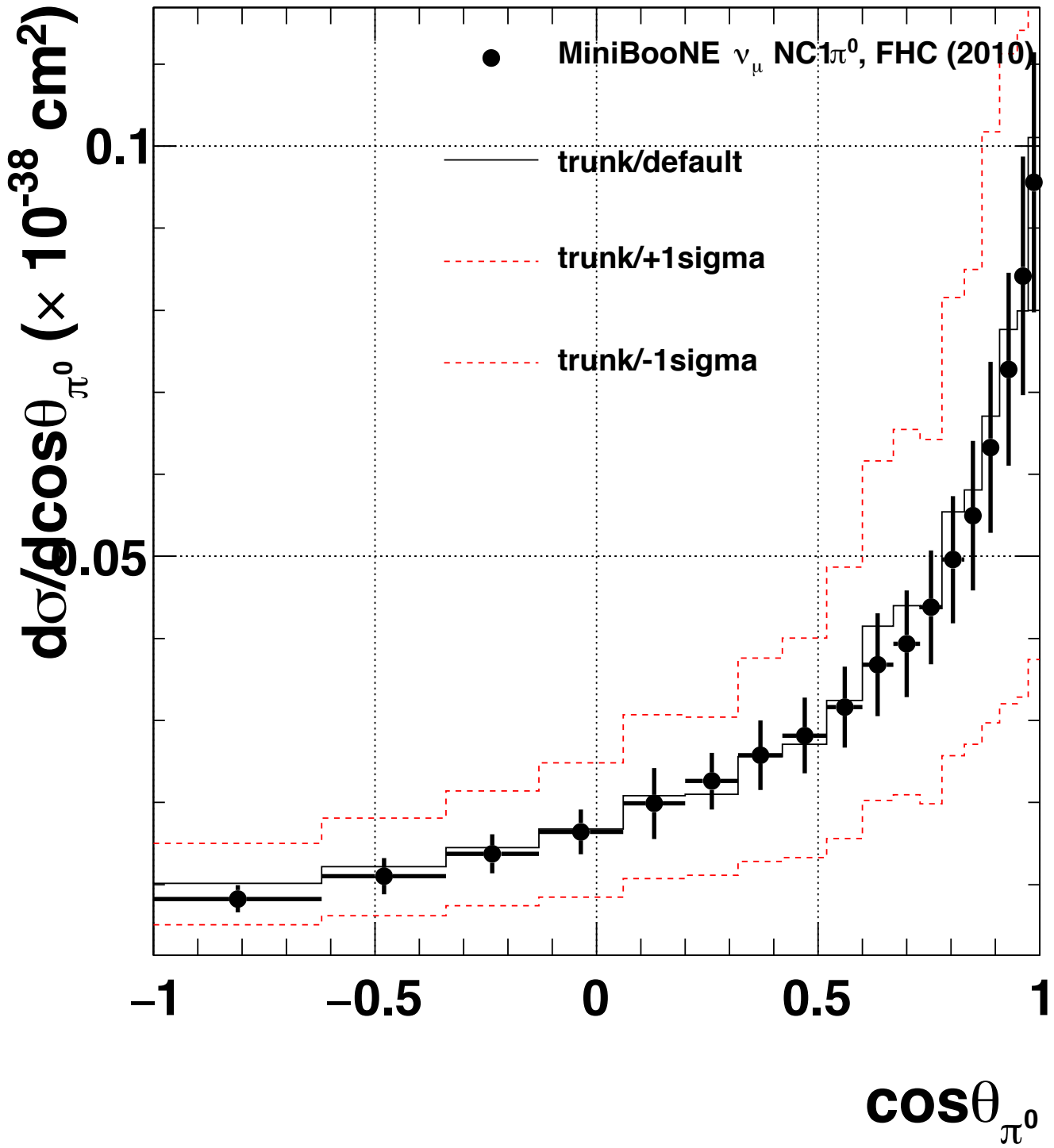


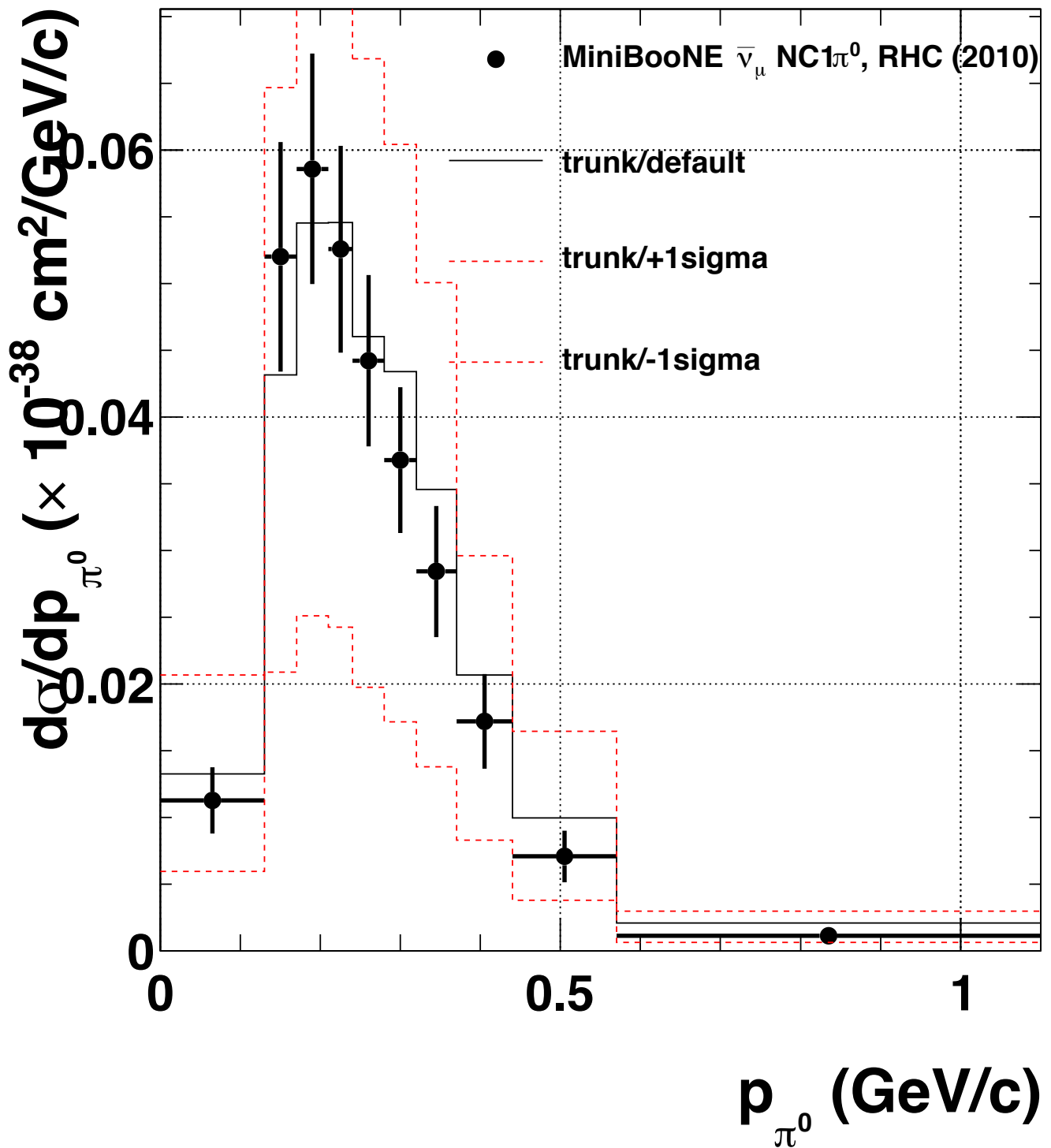


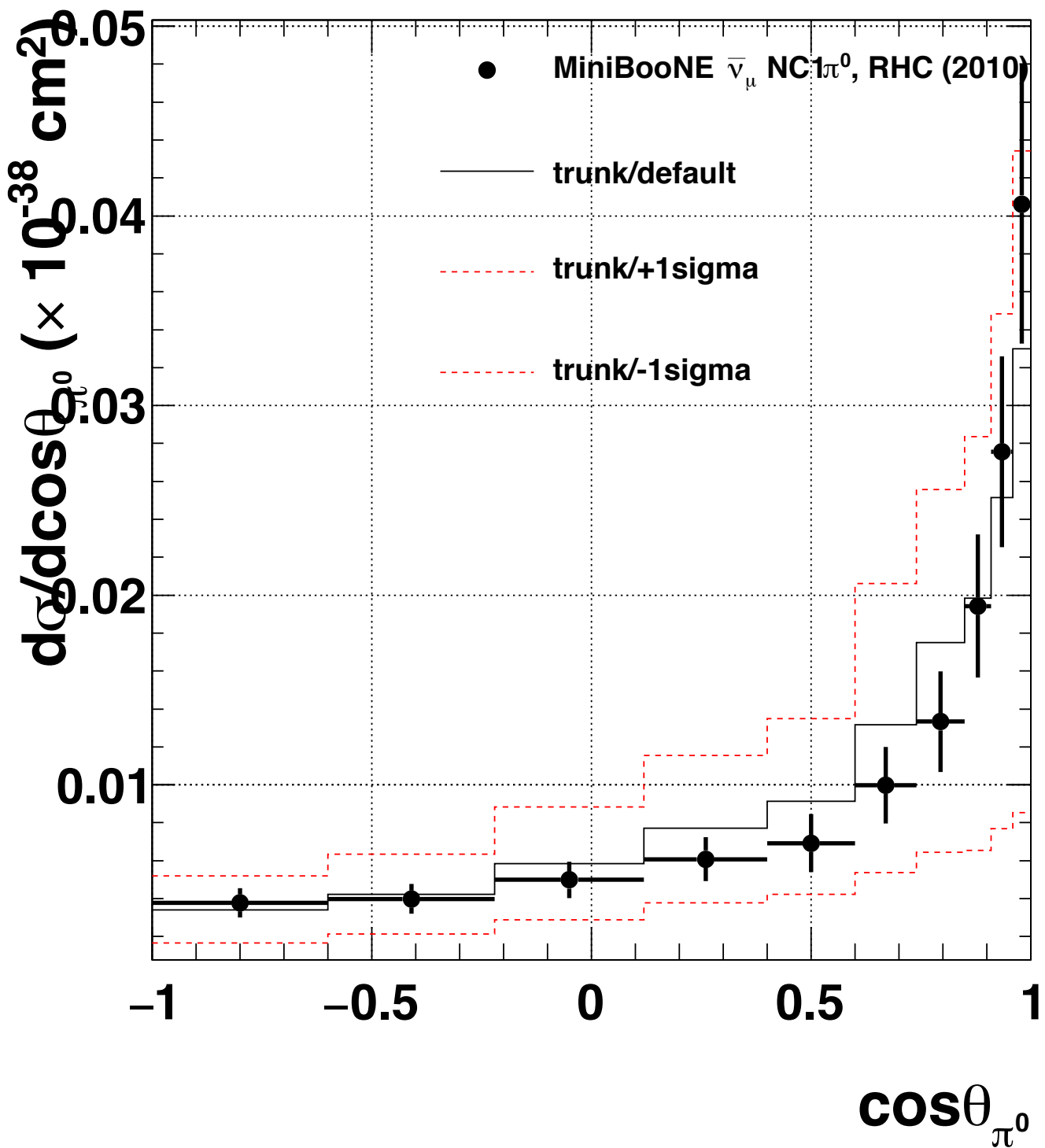












B Applying VALOR systematics to MC templates: Full specification

Table 1: LBNF FHC numuCC1trkQE

Table 2: LBNF FHC numuCC2trkQE

Table 3: LBNF FHC numuCC1piC

Table 4: LBNF FHC numuCC1pi0

Table 5: LBNF FHC $\nu\mu CC1piC1pi0$

Table 6: LBNF FHC $\nu\mu$ CCoth

Table 7: LBNF FHC nueCCincl

Table 8: LBNF FHC numuCCinclWSgn

Table 9: LBNF FHC NCincl

Table 10: LBNF RHC numuCC1trkQE

Table 11: LBNF RHC numuCC2trkQE

Table 12: LBNF RHC numuCC1piC

Table 13: LBNF RHC numuCC1pi0

Table 14: LBNF RHC numuCC1piC1pi0

Table 15: LBNF RHC numuCCoth

Table 16: LBNF RHC nueCCinc

Table 17: LBNF RHC numuCCinclWSgn

Table 18: LBNF RHC NCinc